ELECTRICAL STRUCTURE OF THE CRUST IN SOUTHEAST TASMANIA

by :

Sjafra Dwipa

Submitted in fullfilment of the requirements
for the degree of
Doctor of Philosophy

University of Tasmania
Hobart, Australia
January, 1993

To
my loving companion in life Baswati
and beautiful children Mira and Huon.

STATEMENT

This thesis contains no material which has been accepted for the award of any other degree or diploma in any University and, to the best of my knowledge and belief, contains no copy or paraphrase of material previously published or written by another person, except where due reference is made.

Sjafra Dwipa
University of Tasmania, Hobart, Australia.
January, 1993.

ACKNOWLEDGEMENTS

This research would not have been possible without assistance from many people. I would like to thank my supervisors Drs. R.J.G. Lewis, W.D. Parkinson and D.E. Leaman for their encouragement and patience.

Dr. Lewis allowed me to use the "Pancake" computer program which provided effective analysis of the TEM data. His broad understanding of geophysics computer programming has been of great assistance. Dr. Parkinson, whose long-term involvement in magnetovariational and magnetotelluric research is well-known, shared his wisdom and lent personal materials relating to the topic. Meetings with him and preparing a paper has greatly influenced my thinking. Dr. Leaman was always available to share his expert knowledge of Tasmanian geology and to advise on relevant field methods. The combined expertise of these three geophysicists has been invaluable and of enormous benefit to me.

Van Jensen, the Geology Department technical officer spent many hours modifying equipment and resolving technical problems for which I thank him sincerely. The help and assistance of Mr. P. Cornish and Mr. A. Gillon in arranging transport for field work and laboratory work are deeply appreciated.

Field work was made much easier with the co-operation of numerous farmers and land-owners who allowed this stranger from Indonesia to set up equipment on their properties, sometimes for weeks on end. Some even moved stock to enable field work to proceed. Others provided transport across their land and all showed interest in the project. My field-work experience in Australia will be long-remembered.

My studies in Australia have been funded by the Australian International Development Assistance Bureau and I have appreciated the interest of Ms. Robin

Bowden from the Tasmanian office. I was seconded by the Vulcanological Survey of Indonesia and my thanks go to my directors for releasing me to study in Australia.

I am indebted to my close friends R. Hermanto and M. Roach for constant discussions throughout this research. S. Sampan, Aung Pwa, Ai Yang and U. Hartono, fellow researchers have been understanding colleagues and very good company.

My stay in Tasmania has been enriched by the friendship of my host family, the Eldridges. They have supported and encouraged me during my research and have been caring friends to me and my family. Very special thanks to Margaret Eldridge who assisted with field work and patiently proof-read this thesis.

Finally, my thanks to my parents, my wife, B. Amalia and two lovely children M.Gerania and H. Tamarra who have put up with my long absences from home and who, hopefully, will enjoy having me back!.

ABSTRACT

In the south-east of Tasmania, Jurassic dolerite forms a partial cover over much of the area. The sedimentary and volcanic rocks in this region are mainly Permian or younger. The topography is largely dominated by the local structure of the dolerite.

Utilizing the magnetotelluric and magnetovariational methods, an investigation was made of the electrical structure along two cross-sections to lower crust / upper mantle depths. In conjunction with this study the potential field and transient electromagnetic methods were used. Two-dimensional gravity and magnetic modellings delineated the geometry and possible structural origin of several rock sequences associated with a basin structure. The use of the transient electromagnetic method placed constraints on the thicknesses and resistivities of the surface layer.

As part of the magnetotelluric analysis package, a new rotation angle and dimensionality calculation method is introduced and tested with different geometrical structures. The results when compared to other conventional and the Mohr circle methods show this new method works well and is simpler and faster.

Two types of anomalies, inland and coastal effect, are revealed from magnetovariational observation. Correction for the ocean were applied to induction vectors at periods of 10 and 60 minutes. The inland anomaly is characterized by corrected in-phase induction vectors at stations to the east of the Huon River, pointing north-west. Those to the west of the river point in a north-east direction, indicating the presence of a gradient anomaly zone which lies along the Huon River. Meanwhile the gradual swing in direction from southeast for observed vector to east and almost perpendicular to the coast-line for corrected vector at the eastern-most station of cross-section II illustrates the remaining effect of the coast. This can be explained by high

conductivity contrasts between the resistive block in the eastern part of Tasmania and the conducting ocean floor.

The results from the one and two-dimensional modelling of magnetotelluric, gravity and magnetic data indicate that the base of the Permo-Triassic cover with its stockwork of massive dolerite intrusions, is probably never less than 500 metres below the surface at the northern cross-section and dips south reaching a depth of about 800 metres on the southern cross-section. The Ordovician limestone, which may be a possible source of hydrocarbon deposits, has a bulk apparent resistivity value of 40 Ohm-m inferred from transient electromagnetic modelling. This rock has a thickness of about 300 metres and its distribution is restricted to the western part of the study area which is consistent with the results of the two-dimensional gravity and magnetic modelling. The dipping discontinuity needed in the models to match the magnetotelluric data, results in a trough-like structure with depth from the surface to the bottom of about 6 kilometres. This structure is reflected by a broad and large gravity anomaly together with slightly negative magnetic anomaly and is believed to be associated with a trough of Cambrian volcanics. This trough has a northwest - southeast direction and becomes wider and has more conductive flanks to the south.

The magnetotelluric results also indicate the presence of a low resistivity layer at middle-lower crustal depths. There is broad but not exact correlation with the position of the Cambrian trough above. In combination with other geophysical evidence gained from the magnetovariational method, i.e. the short corrected induction vectors at all stations at periods of 60 minutes, the layer is inferred to exist beneath the entire study area. The likely cause of the low resistivity associated with this layer is believed to be the presence of free carbon along grain boundaries or fractured rocks which provide a continuous conducting path. Another possible cause is the presence of anomalously high temperatures in the deeper crust expected from previous geothermal measurements.

Errata

"Electrical Structure of the Crust in Southeast Tasmania"

by: Sjafra Dwipa

Geology Department, University of Tasmania, Australia

Site	Written	Corrected	Comment
Pg. iii line 17	... induction vector		The direction of horizontal field that correlates with maximum vertical field first called induction vector and then Parkinson vector. In some resent publications, it called induction arrow.
Pg. 1 line 19	... have made magnetotelluric ...	... have made magnetotellurics ...	
Pg. 2 line 16	... magnetovariational ...		Definition: see page 50, first paragraph
Pg. 2 line 17	... transient electromagnetic		Definition: see page 27, second paragraph
Pg. 9 line 1	... cancealed Y-shaped ...	... concealed Y-shaped ...	
Pg. 13 line 17	... lineaments are clearly exposes ...	... lineaments are clearly exposed ...	
Pg. 13 line 20	This lineament continue ...	This lineament continues ...	
Pg. 21 line 24	... ar this part of Figure II.3 ...	... at this part of Figure II.5 ...	
Pg. 24 line 2	... parallel to magnetotelluric sites ...	... parallel to magnetotelluric cross-section II	
Figs. II.5 and II.6	Magnetics (nT)	Magnetics field (nT)	Broken lines are observed data Solid lines are calculated data
Pg. 31 line 9	... up to 32 channels.	... on up to 32 channels.	32 Channels = 164 milliseconds delay time
Pg. 31 line 14	... about 33 milliseconds.		33 milliseconds = recorded at 21 channels
Pg. 33 line 3	ρa	ρa	
Pg. 48 line 15	... susceptibility value of 0.0 cgs ...	... susceptibility value of 0.005 cgs	
Pg. 55 lines 3 and 4			Detailed explanation of eqn. (IV.3 and IV.4) can be seen in Parkinson (1983, pp 332-333) as mentioned in the thesis.
Pg. 55 line 16	$MR = (RI (A)^2 + RI (B)^2)^{1/2}$	$MR = [(RIA)^2 + (RIB)^2]^{1/2}$	

Site	Written	Corrected	Comment
Fig. IV.12		... (redrawn from Dosso et al. 1985)	
Pg. 69 line 15	... raverse for the TE mode ...	... traverse for the TE mode ...	
Pg. 72 line 1	... period of 60 seconds.	... period of 60 minutes.	
Pg. 85 line 6	... to determine the large value.	... to determine the larger value.	
Pg. 85 line 15	... cartesian coordinate system ...	... Cartesian coordinate system ...	
Pg. 183 line 13	... on northern cross-section ...	... on cross-section I ...	
Pg. 183 line 14	... on southern cross-section ..	... on cross-section II ...	
Pg. 104 line 8	... described in section V.3.2.	... described in section V.3.2.4.	
Pg. 136 line 4	... tentatively be achived ...	... tentatively be achieved ...	
Pg. 136 line 9	This is suitable ...	... This is a reasonable first approximation ...	
Pg. 138 line 25	... at the surface layer ...	... of the surface layer ...	
Pg. 185 line 25	... to to explain ...	... to explain ...	

THESIS CONTENTS.

			Page
Acknowledgements.			i
Abstract.			iii
Thesis contents.			v
List of figures.			viii
list of tables.			xi
Chapter	I.	INTRODUCTION.	1
	I.1.	General.	1
	I.2.	Aim of the study.	6
	I.3.	Regional geological setting.	7
	I.4.	Previous magnetotelluric and magnetovariational studies.	9
	I.4.1.	Magnetotelluric.	9
	I.4.2.	Magnetovariational observations.	9
Chapter	II.	POTENTIAL FIELD METHODS.	12
	II.1.	Introduction.	12
	II.2.	Original data.	12
	II.2.1.	Gravity.	12
	II.2.2.	Magnetic.	13
	II.3.	Overview of gravity and magnetic maps.	13
	II.3.1.	Gravity.	13
	II.3.2.	Magnetic.	15
	II.4.	Rock physical properties.	19
	II.5.	Two dimensional modelling.	20
	II.6.	Interpretation.	21
	II.6.1	Cross-section I.	21
	II.6.2.	Cross-section II.	24
	II.7.	Summary.	26
Chapter	III.	TRANSIENT ELECTROMAGNETIC METHOD.	27
	III.1.	Introduction.	27
	III.2.	Basic theory.	28
	III.3.	Data acquisition.	30
	III.4.	Data analysis.	31
	III.5.	Field results.	35
	III.5.1.	Cross-section I.	35
	III.5.2.	Cross-section II.	36
	III.6.	Discussion.	37
	III.6.1.	Cross-section I.	46
	III.6.2.	Cross-section II.	48
Chapter	IV.	MAGNETOVARIATIONAL METHOD.	49
	IV.1.	Introduction.	49
	IV.2.	The basic method.	50
	IV.3.	Instrumentation and procedure.	52

	IV.4.	Data reduction.	52
	IV.5.	Transfer function and induction vector analysis.	53
	IV.6.	Field results.	56
	IV.7.	Discussion.	66
Chapter	V.	MAGNETOTELLURIC METHOD.	74
	V.1.	Introduction.	74
	V.2.	Origin and propagation of electromagnetic field.	74
	V.3.	The earth's dimensionality.	77
	V.3.1.	The one-dimensional earth.	77
	V.3.2.	The two-dimensional earth.	79
	V.3.2.1.	Impedance tensor.	79
	V.3.2.2.	Coherency.	82
	V.3.2.3.	Reliability.	82
	V.3.2.4.	Principal direction.	83
	V.3.2.5.	New rotation angle and dimensionality method.	85
	V.3.2.6.	The skew and ellipticity.	89
	V.3.2.7.	The resistivity.	90
	V.3.2.8.	The tipper.	91
	V.3.2.9.	Induction arrow.	93
	V.4.	Equipment and survey procedures.	94
	V.4.1.	Introduction.	94
	V.4.2.	Field equipment used.	96
	V.4.2.1.	Equipment design philosophy.	98
	V.4.2.2.	Logistics.	98
	V.4.3	Survey procedure.	99
	V.4.3.1.	The electric field sensor.	99
	V.4.3.2.	The magnetic field sensor.	100
	V.4.4.	Summary.	103
	V.5.	Data analysis.	103
Chapter	VI.	MT SOUNDING RESULTS IN SOUTHEAST TASMANIA.	107
	VI.1.	Introduction.	107
	VI.2.	The cross-section I response.	109
	VI.3	The cross-section II response.	118
	VI.4.	Comparison of rotation angle calculations.	128
	VI.4.1.	Discussion.	133
	VI.5.	Summary.	134
Chapter	VII.	INTERPRETATION OF MT RESULTS IN SOUTH-EAST TASMANIA.	136
	VII.1.	Introduction.	136
	VII.2.	One-dimensional modelling.	136
	VII.2.1.	Cross-section I.	137
	VII.2.2.	Cross-section II.	148
	VII.3.	Two-dimensional modelling.	157
	VII.3.1.	Cross-section I.	157
	VII.3.2.	Cross-section II.	169
	VII.3.3.	Comment and summary of two-dimensional. modelling.	175
	VII.4.	Discussion.	176
	VII.4.1.	Sedimentary basin.	176
	VII.4.2.	Deeper structure.	180
Chapter	VIII.	CONCLUSIONS.	183

REFERENCES. 187
APPENDIXES
II. Gravity and magnetic data.
V. Temperature correction.
VII.1. 1D TE model results without lower crustal conductive layer.
VII.2. Static shift.

LIST OF FIGURES

Figure		Page
I.1	Location map.	3
I.2	Distribution of observation stations.	4
I.3	Geology map of the study area.	8
I.4	Induction vectors around Tasmania.	11
II.1	Residual Bouguer gravity anomaly map of southern Tasmania	14
II.2	Compilation of residual magnetic intensity map.	16
II.3	Compilation of magnetic profiles map at 1000 metres above sea level.	17
II.4	Structural and tectonic interpretation based on gravity and magnetic data showing major tectonic element.	18
II.5	2D gravity and magnetics model, cross-section I.	23
II.6	2D gravity and magnetics model, cross-section II.	25
III.1	Induction of Eddy currents in a subsurface conductor.	29
III.2	Transient electromagnetic measurement.	29
III.3	Transient electromagnetic modelling results from Leslie Vale (LSV).	38
III.4	Transient electromagnetic modelling results from Grove (GRV).	39
III.5	Transient electromagnetic modelling results from Judbury (JDB).	40
III.6	Transient electromagnetic modelling results from Lonnavale (LNV).	41
III.7	Transient electromagnetic modelling results from Woodstock (WST).	42
III.8	Transient electromagnetic modelling results from Franklin (FRS).	43
III.9	Transient electromagnetic modelling results from Peppers Rd (PPR).	44
III.10	Transient electromagnetic modelling results from Tahune (THN).	45
IV.1	A sub storm magnetogram, covering 31 hours, showing the principal features of the storm.	51
IV.2	The open magnetosphere model showing the merging of the field lines in the magneto-tail.	51
IV.3	Inphase and quadrature induction vectors, period 4 minutes.	57
IV.4	Inphase and quadrature induction vectors, period 8 minutes.	58
IV.5	Inphase and quadrature induction vectors, period 10 minutes.	59
IV.6	Inphase and quadrature induction vectors, period 12 minutes.	60
IV.7	Inphase and quadrature induction vectors, period 16 minutes.	61
IV.8	Inphase and quadrature induction vectors, period 20 minutes.	62
IV.9	Inphase and quadrature induction vectors, period 32 minutes.	63
IV.10	Inphase and quadrature induction vectors, period 64 minutes.	64
IV.11	Inphase and quadrature induction vectors,period 128 minutes.	65
IV.12	Geographical location of Tasmania showing bathymetric contours around the island.	67
IV.13	Inphase and quadrature vectors for 10 and 60 minutes periods derived from the analogue model study.	68
IV.14	Observed and corrected induction vectors, period 10 minutes.	71
IV.15	Observed and corrected induction vectors, period 60 minutes.	73
V.1	Propagation of an electromagnetic wave (rectangular vectors E and H) through a homogeneous earth.	76
V.2	Propagation of an electromagnetic wave through a layered earth.	76

Figure		Page
V.3	X - Y and X' - Y' coordinate system.	86
V.4	Block diagram of EDA FM-1000B Fluxgate magnetometer.	95
V.5	The magnetotelluric equipment.	97
V.6	The magnetic sensor head.	102
VI.1	Principal axes show on a residual Bouguer gravity anomaly map.	108
VI.2	App. resistivity, coherency, skew and phase from Leslie Vale (LSV).	111
VI.3.	App. resistivity, coherency, skew and phase from Grove (GRV).	113
VI.4	App. resistivity, coherency, skew and phase from Judbury (JDB).	115
VI.5	App. resistivity, coherency, skew and phase from Lonnavale (LNV).	117
VI.6	App. resistivity, coherency, skew and phase from Oyster Cove (OTC).	119
VI.7	App. resistivity, coherency, skew and phase from Woodstock (WST).	121
VI.8	App. resistivity, coherency, skew and phase from Franklin (FRS).	123
VI.9	App. resistivity, coherency, skew and phase from Peppers Rd. (PPR).	125
VI.10	App. resistivity, coherency, skew and phase from Tahune (THN).	127
VI.11	Plot of average and delta theta from Judbury (JDB).	129
VI.12	Plot of average and delta theta from Grove (GRV).	131
VI.13	Plot of average and delta theta from Tahune (THN).	132
VII.1	1D model results from Leslie Vale (LSV).	139
VII.2	1D model results from Grove (GRV).	140
VII.3	1D model results from Judbury (JDB).	141
VII.4	1D model results from Lonnavale (LNV).	142
VII.5	Model of the base of the crust.	145
VII.6	1D TE mode app. resistivity cross-section I, 34 Km depth.	146
VII.6a	1D TE mode app. resistivity cross-section I, 7 Km depth.	147
VII.7	1D model results from Oyster Cove (OTC).	149
VII.8	1D model results from Woodstock (WST).	150
VII.9	1D model results from Franklin (FRS).	151
VII.10	1D model results from Peppers Rd. (PPR).	152
VII.11	1D model results from Tahune (THN).	153
VII.12	1D TE mode app. resistivity cross-section II, 34 Km depth.	155
VII.12a	1D TE mode app. resistivity cross-section II, 7 Km depth.	156
VII.13	Model 2D cross-section I.	159
VII.13a	Obs. (red) and cal. (green) app. resistivity from LSV and GRV stations (a) E-polarization, (b) H-polarization.	160
VII.13b	Obs. (red) and cal. (green) app. resistivity from JDB and LNV stations (a) E-polarization, (b) H-polarization.	161
VII.14	Model 2D cross-section I.	163
VII.14a	Obs. (red) and cal. (green) app. resistivity from LSV and GRV stations (a) E-polarization, (b) H-polarization.	164
VII.14b	Obs. (red) and cal. (green) app. resistivity from JDB) and LNV stations (a) E-polarization, (b) H-polarization.	165
VII.15	Model 2D cross-section I.	167
VII.15a	Obs. (red) and cal. (green) app. resistivity from LSV and GRV stations (a) E-polarization, (b) H-polarization.	168
VII.15b	Obs. (red) and cal. (green) app. resistivity from JDB and LNV stations (a) E-polarization, (b) H-polarization.	169
VII.16	Model 2D cross-section II.	170
VII.16a	Obs. (red) and cal. (green) app. resistivity from WST, FRS, and PPR (a) E-polarization, (b) H-polarization.	171
VII.17	Model 2D cross-section II.	173

Figure		Page
VII.17a	Obs. (red) and cal. (green) app. resistivity from WST, FRS, and PPR (a) E-polarization, (b) H-polarization.	174
VII.18	Plot of 2D MT and gravity and magnetic model along MT cross-section I	177
VII.19	Plot of 2D MT and gravity and magnetic model along MT cross-section II.	179
VII.20	Minimum and maximum bounds on electronic semiconduction resistivity versus temperature for rocks samples.	182

LIST OF TABLES

Table		Page
I.1	List of stations and geographic coordinates.	5
II.1	Density contrast and susceptibility used for rock type within the study area.	20
III.1	Laboratory resistivity measurements.	46

Chapter I.
INTRODUCTION.

I.1. General.

The magnetotelluric (MT) method is a frequency-domain electromagnetic sounding technique used to establish the electrical conductivity of the earth's sub-surface. This technique utilizes naturally occurring electromagnetic waves as the energy source. The waves are generated by complex interactions between solar plasma ejected by the sun and the earth's magnetosphere. These waves penetrate several hundred kilometres into the earth and induce secondary fields in the earth. The horizontal components of the resultant electric and magnetic fields are measured at the surface of the earth. They are related to each other by a surface impedance that is a function of the conductivity structure of the earth's substrata. The experimental values are matched to model curves to obtain an interpretation.

Interpretations of magnetotelluric data are complicated by noise. However, processing techniques can be used to minimize the scattering effect associated with the data. Initially, records are obtained as a function of time and they must be processed to obtain the apparent resistivity as a function of frequency. A Fourier transform must be used to convert the data from the time domain to the frequency domain.

This passive geophysical method has been used as an exploration tool since the early 1950s. Theoretical efforts coupled with improvements in instrumentation, have made magnetotelluric an effective technique for geological structure investigation. It has gained acceptance as a viable geophysical prospecting tool since

Tikhonov (1950) realized the potential of using natural electromagnetic fields for sounding of the earth's crust. One of the milestones in electromagnetic work was the classic paper of Cagniard (1953) on the theory and interpretation of magnetic and telluric field relationships.

Cagniard only considered a one-dimensional (1-D) earth consisting of horizontal, isotropic, planar layers of arbitrary thickness and resistivity. Swift (1967), Vozoff (1972) and other researchers extended the MT method to two-dimensional (2-D) geometries. These geometries allow conductivity inhomogeneities to exist in the horizontal direction as well as the vertical direction. Recent studies by Ting and Hohmann (1981), Spichak (1985), Zhdanov and Spichak (1989 and Cerv and Pek (1990) have further extended the theory to three-dimensional (3-D) conductivity distributions. As of present, however, the interpretation of 3-D geometry field data is in its infancy. In this study one- and two-dimensional earth geometries are presented and discussed in Chapter V.

From late 1989 to early 1991, a total of 9 temporary magnetotelluric and 14 magnetovariational stations were established in south-east Tasmania and data were obtained. In conjunction with this study, the transient electromagnetic method was carried out in order to place constraints on the thicknesses and resistivities of the surface layers. In addition, two-dimensional modelling of gravity and magnetic data was also done along the magnetotelluric cross-sections in order to delineate the geometry and subsurface geological structure in this study area. Figures I.1 and I.2 show the location and distribution of the observation stations. The names, abbreviations and their geographic coordinates are given in Table I.1.

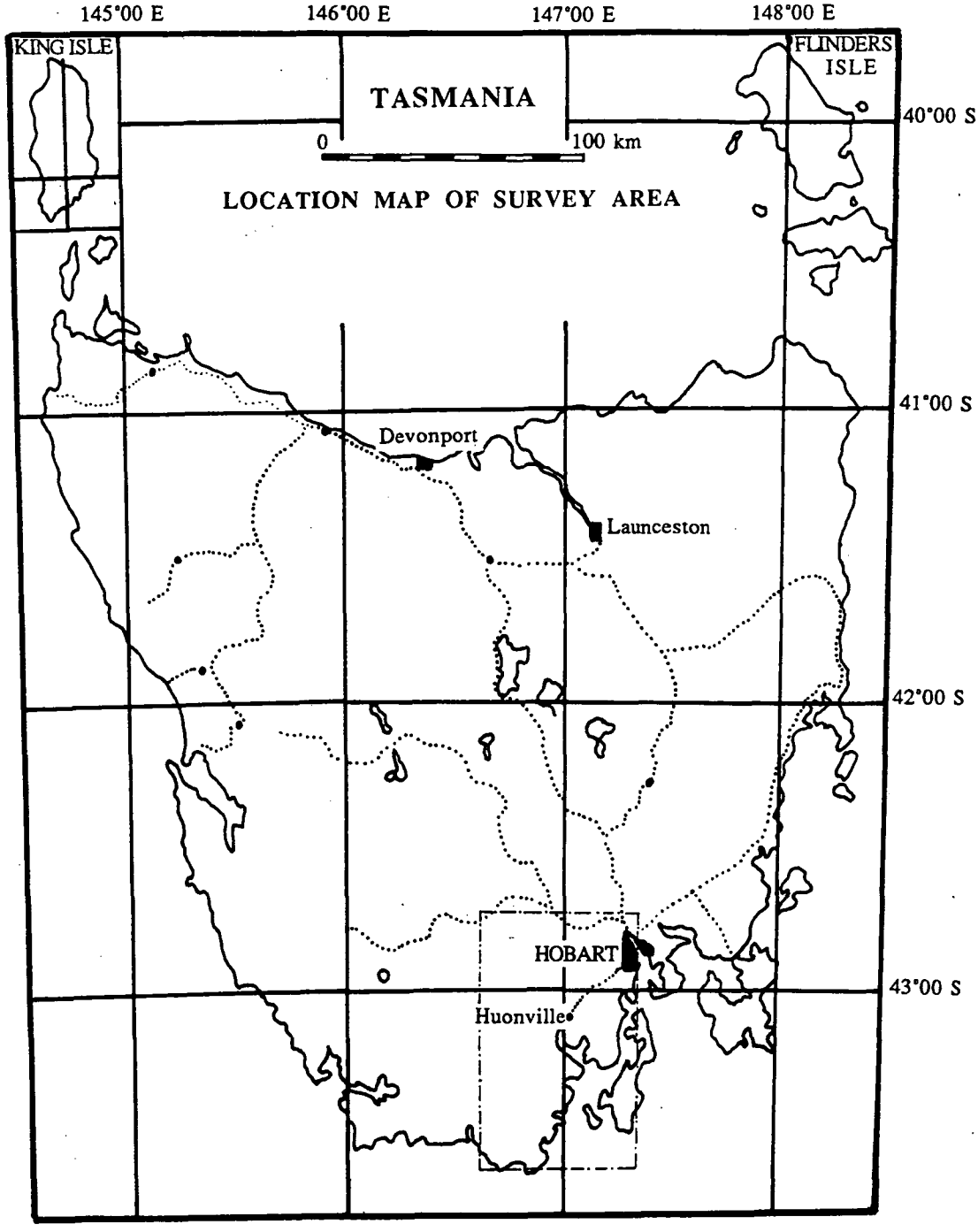

Figure I.1. Location map.

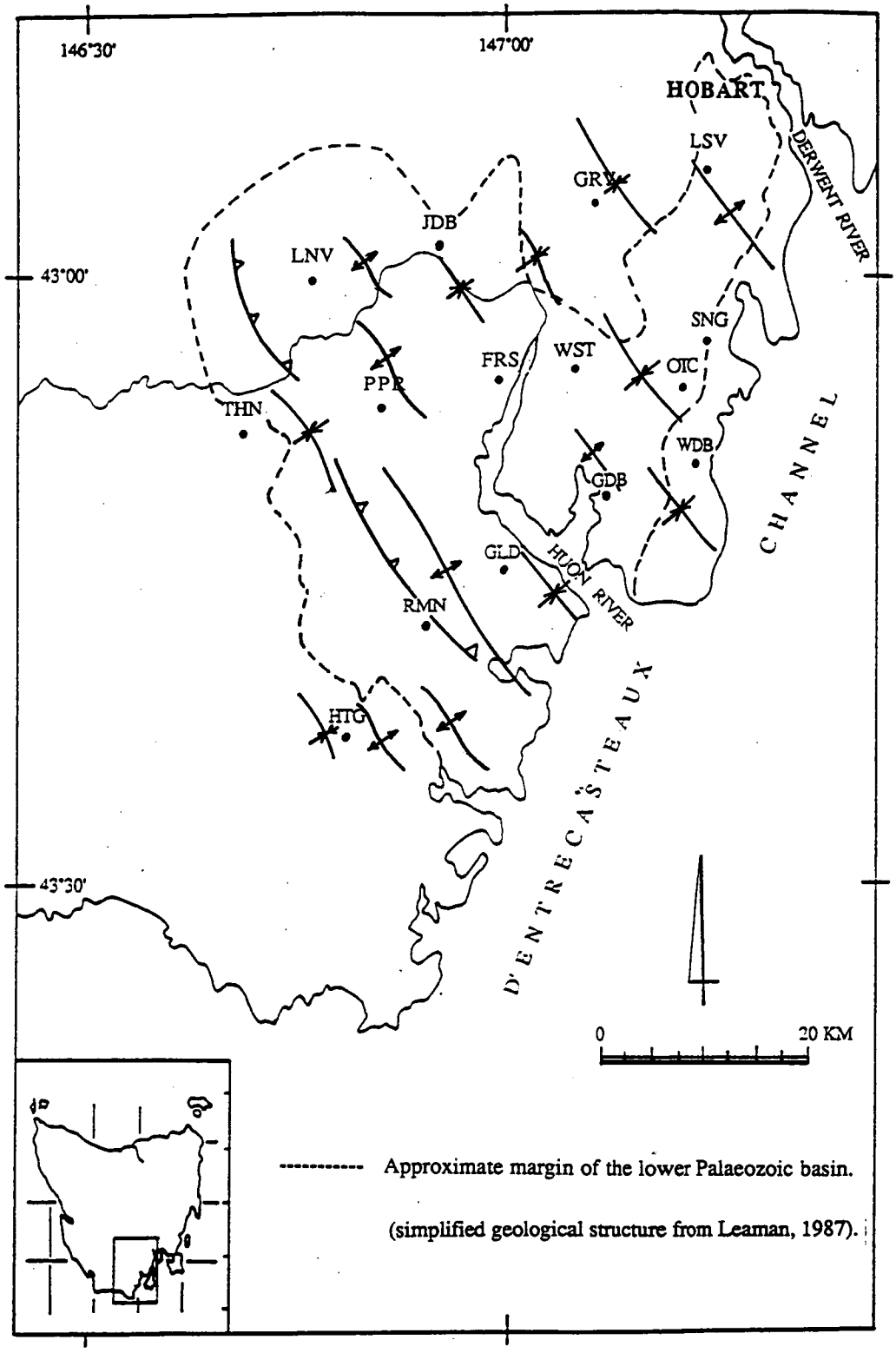

Figure I.2. Distribution of observation stations.

Table I.1

List of stations and geographic coordinates

No	Station	Code	Latitude	Longitude	Method
1	Leslie Vale	LSV	42°56'40"	147°14'20"	MT,MV,TEM
2	Grove	GRV	42°58'00"	147°06'20"	MT,MV,TEM
3	Judbury	JDB	42°59'40"	146°55'10"	MT,MV,TEM
4	Lonnavale	LNV	43°01'30"	146°49'30"	MT,MV,TEM
5	Oyster Cove	OTC	43°07'10"	147°00'00"	MT
6	Woodstock	WST	43°04'30"	147°04'30"	MT,MV,TEM
7	Franklin	FRS	43°04'00"	146°19'20"	MT,MV,TEM
8	Peppers Road	PPR	43°07'30"	146°49'40"	MT,MV,TEM
9	Tahune	THN	43°06'00"	146°43'30"	MT,MV,TEM
10	Snug	SNG	43°04'09"	147°12'21"	MV
11	Woodbridge	WDB	43°09'40"	147°13'10"	MV
12	Gardners Bay	GDB	43°11'22"	147°06'40"	MV
13	Glendevie	GLD	43°15'00"	146°59'10"	MV
14	Raminea	RMN	43°17'40"	146°53'40"	MV
15	Hastings Caves	HTG	43°24'10"	146°50'34"	MV

I.2. Aim Of The Study.

The primary aim of the study was to develop an understanding of the crustal structure of the southeast of Tasmania. In particular, the nature of the pre-Permian geology is very poorly known being obscured by Permo-Triassic and Jurassic dolerite cover. Only two drill holes in southeasten Tasmania, at Glenorchy and woodbridge, have reached the pre-Permian basement. Such knowledge may have economic implications for both mineral and hydrocarbon deposits.

In order to properly fulfil this aim a number of secondary aims emerged:

1. To establish a regional electrical survey in southeast Tasmania by the transient electromagnetic and magnetotelluric methods.
2. To develop the technique of rotation of coordinates in magnetotelluric analysis.
3. To examine magnetic variations to detect correlations between some fixed directions of the horizontal magnetic and vertical magnetic fields by the magnetovariational method. Such correlations are indicative of resistivity contrasts. Correlations of this type have been reported, for example, by Pitcher (1972), Hermanto (1985) and Ingham (1988).
4. To interpret the gravity and magnetic data in terms of major upper crustal structures.

In brief, the problem is to obtain information on the crustal structure of southeast Tasmania: the approach is to use a variety of geophysical techniques and suitable existing geophysical data and where necessary to develop new methods.

A quick glance at the geological structure map (see Figure I.2), will reveal the area is structurally complex. For this reason, the choice of sites was intended to provide traverses of the region across the structure, initially thought to be a sedimentary

basin. Magnetotelluric interpretations have been found to be the simplest in sedimentary areas.

Most of the stations were established along the supposed boundary of the basin (see Figure. I.2). This is important since reliable determinations of the resistivity structure of this region have not previously been obtained.

I.3. Regional Geological Setting.

The region is of high relief which diminishes in height towards the east coast. The higher elevation of the surrounding ranges is due to the erosionally resistant nature of the thick dolerite bodies occurring in this area. These dolerites are tholeiites of mid-Jurassic age (McDougall, 1961; 1962). The regional geology of southeast Tasmania, which illustrates these features, is shown in Figure I.3.

Figure I.3 also indicates that the Jurassic dolerite forms a partial cover over the upper part of the region. The dolerite has intruded all members of the Parmeener Supergroup (Permian and Trassic in age) . Dolerite sheets vary in thickness from 200 m at Cygnet to about 400 m on Mt. Wellington (Leaman, 1972; 1975). Sheets drilled at Woodbridge were about 300 m thick (Farmer and Clarke, 1985).

The middle and lower areas, on the other hand, are mainly blanketed by Permo-Triassic rocks. The Permian sections consist of monotonous mudstone and siltstone sequence with occasional sandstone units, ranging in thickness from about 450 m at Cygnet to 600 m at Hobart. The Triassic section includes Cygnet coal measures, quartz sandstone, quartz and lithic-feldspathic sandstone , and volcanic lithic arenite. These outcrop on the north side of the Wellington Range and exceed 450 m in thickness. All other sections are either faulted, limited or prematurely terminated by dolerite (Leaman, 1987).

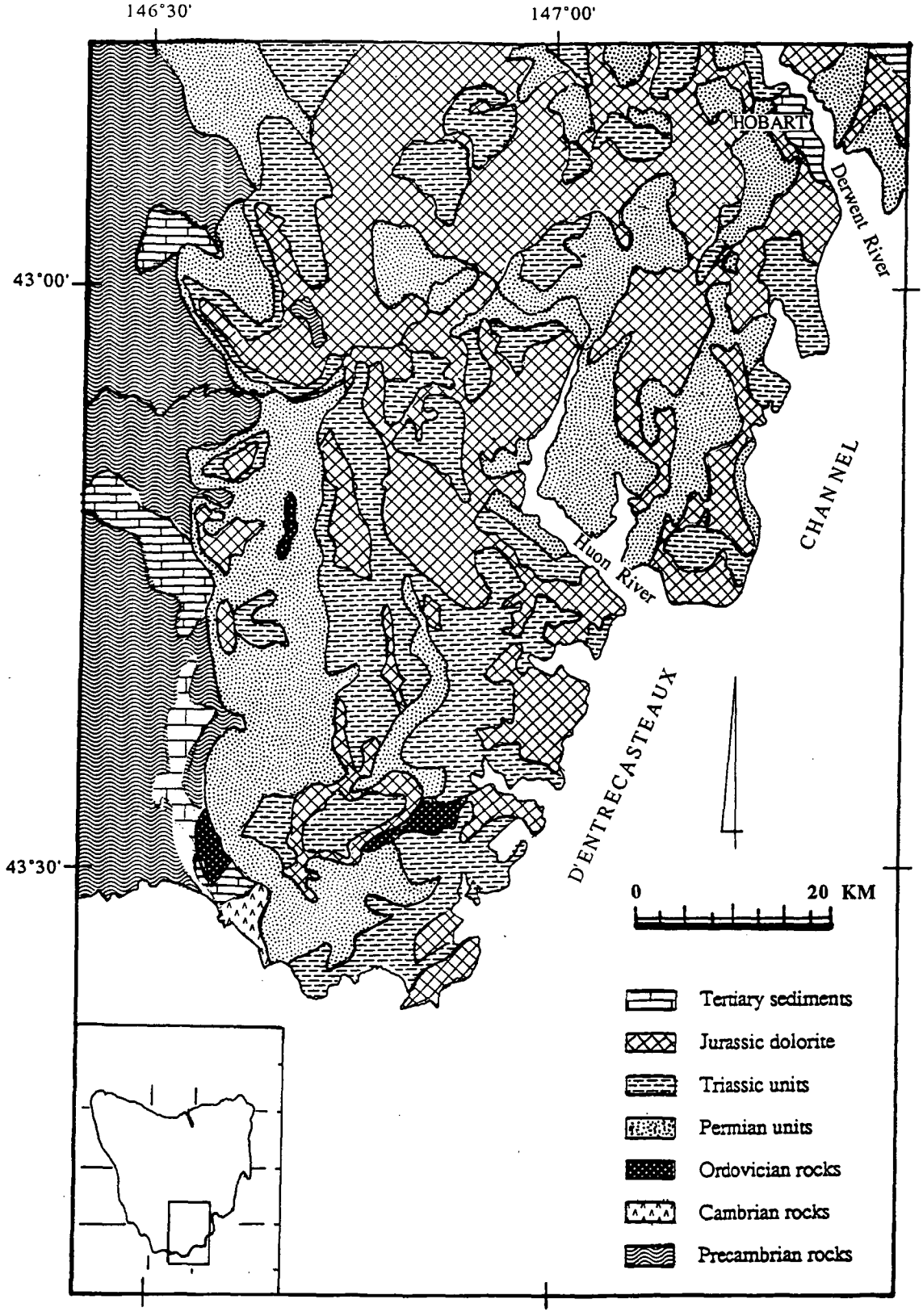

Figure I.3. Geological map of the study area. Simplified from "Geological Map of Tasmania (Mines Department - Tasmania).

The main feature of this region is a cancealed Y-shaped trough-like structure with its major arm extending to the northwest comprising in bulk, Palaeozoic material. The thickness of the trough fill, interpreted from the magnetic and gravity survey in this area, is about 5 to 6 km (Leaman, 1990 ; Leaman and Richardson, 1990). The trough overlaps the margin of Late Precambrian deposition. The Precambrian rocks are also believed to act as the basement for the whole region.

I.4. Previous magnetotelluric and magnetovariational studies.

I.4.1. Magnetotelluric.

The only previous magnetotelluric work in south-east Tasmania was done by Lewis in 1965. This work, the first in Tasmania, was carried out in the Hobart area and studied the conductivity of the crust.

Lewis successfully measured magnetic and electric fields at the Hobart airport and TAU Seismic Vault, University of Tasmania. However, no detailed interpretation was made due to some of the data being affected by geological and artificial noise.

I.4.2. Magnetovariational Observations.

The first magnetovariational observation in south-east Tasmania was done by Parkinson (1962). This observation was conducted in the Hobart area to study the influence of oceans on the geomagnetic field at a coastal station. The result showed that the direction of the induction vector (see Figure I.4), which was determined from bay and similar types of geomagnetic fluctuations at a period of 40 minutes, points to the Southern Ocean. Parkinson concluded that the concentration of induced current along coastlines controls the recording of magnetovariational measurement at a coastal observatory.

The more intensive magnetovariational studies in Tasmania are in the north-east region. They were started by Lilley (1976), see Figure I.4, as a part of his study on geomagnetic variations in south-east Australia. Interesting results from Lilley's study initiated magnetovariational study by other researchers, including Buyung (1980) and Hermanto (1985). Buyung concluded that the reversal in direction of induction vectors on the eastern and western sides of the Tamar River could be due to a zone of high conductivity below the Tamar River. These results led to Hermanto carrying out a more detailed induction study in the north-east of Tasmania. This work illustrated the strong coastal effect on the magnetovariational measurements and identified the conductive anomaly in the Tamar fracture zone. The extension of this zone in south-east Tasmania is probably located to the east of Hobart (Leaman, 1987).

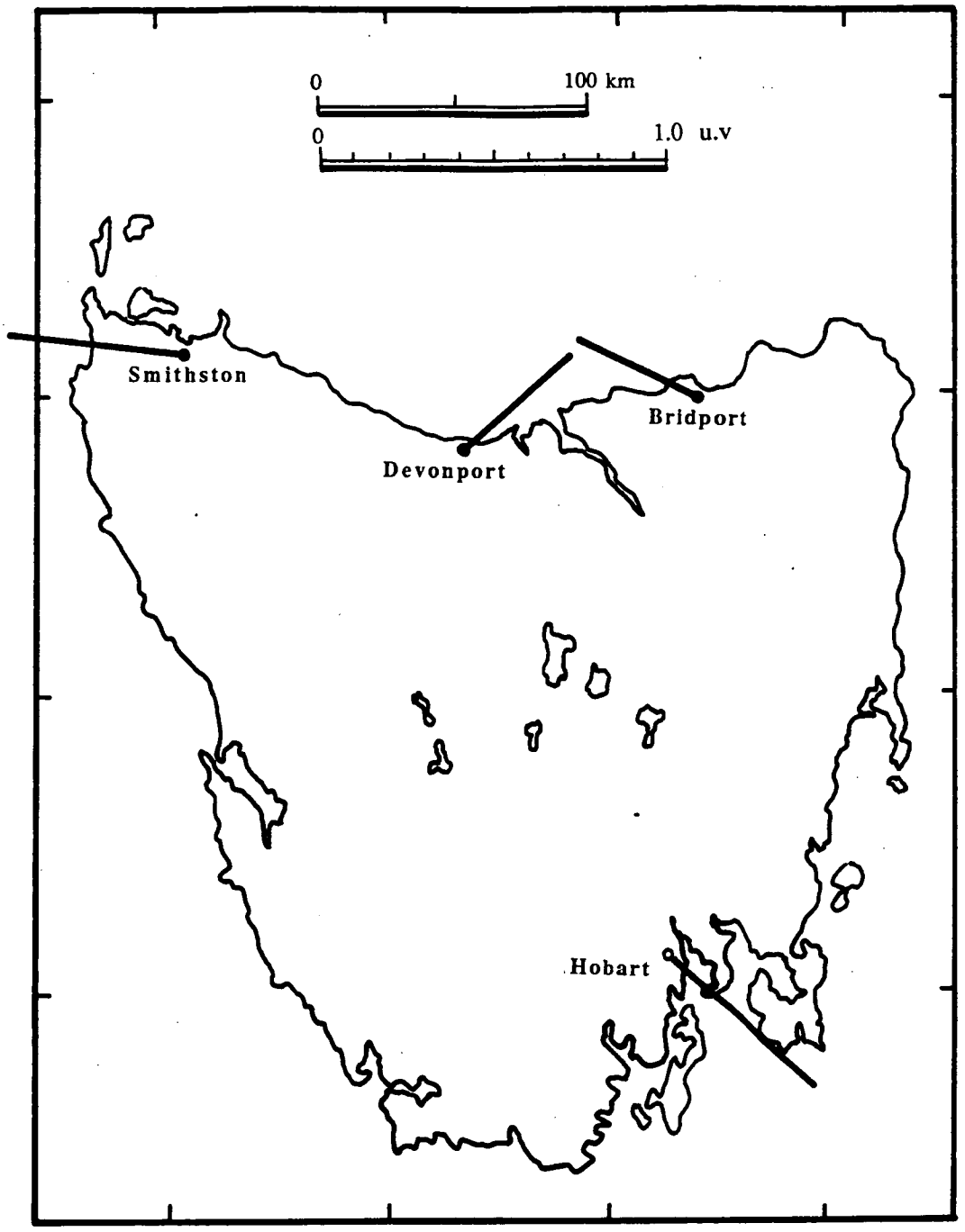

Figure I.4. Induction Vectors around Tasmania. Hobart vector is for 40 minutes period, and Smithton, Devonport and Bridport vectors are for 5 - 20 mintues period.

- ● Lilley (1973 - 1974)
- o Parkinson (1962).

Chapter II.
POTENTIAL FIELD METHODS.

II.1. Introduction.

Potential field methods (gravity and magnetic) have been extensively used in Tasmania for structural assessment (e.g. Leaman, 1992a). Gravity and magnetic surveys are often related and combined in this way since the two fields may assess different facets of the rocks and thus resolve ambiguities inherent in a single approach. Because of their cost effectiveness and their ability to reveal shallow structures and constrain the geometry of dolerite bodies, gravity and magnetic methods have long been used in southeast Tasmania. Using the available data, two-dimensional modelling was carried out during this study in order to delineate the geometry and sub-surface geological structure along the transient electromagnetic and magnetotelluric cross-sections and thus assist interpretation of transient electromagnetic and magnetotelluric data.

II.2. Original Data.

II.2.1. Gravity.

Several gravity surveys have been conducted in the vicinity of the study area, namely, Leaman and Naqvi (1967), and Leaman (1972). However, they were limited by restricted coverage. The gravity data used for interpretation by means of two-dimensional modelling was in the form of a residual Bouguer anomaly gravity map (Figure II.1) of southeast Tasmania compiled by Leaman and Richardson (1989). The gravity data is presently held in the combined TASGRAV and MTREAD data bases of

the Tasmania Mines Department. This data is fully terrain corrected to 20 kilometres and was reduced using a density of 2.67 g/cc.

II.2.2. Magnetics.

The magnetic interpretation was based on a southern Tasmania residual magnetic intensity map (Figure II.2). This aeromagnetic data was surveyed and compiled by Austirex in 1987 using a Caesium vapour magnetometer with an accuracy of 0.01 nT at 20 meters sample spacing. The survey was flown at 1 kilometre above sea level with limited drape flying (150 metres clearance) across the few peaks above this level (Hartz Mountains and Mt. Wellington). The area was covered by two flight line directions. East-west lines were flown at 2.5 kilometres spacing with north-south tie lines at 10 kilometres separation. The survey was carried out originally for Conga Oil, and permission given by the company made the use of this data possible.

II.3. Overview of Gravity and Magnetics Maps.

II.3.1. Gravity.

Figure II.1 is a residual gravity anomaly map of southern Tasmania. The two model cross-sections are shown on this map. As can be seen from Figure II.1 some major lineaments are clearly exposes i.e. the continuation of the Meydina horst and Derwent basin. The most conspicuous feature is the lineament which coincides with the boundary of the Precambrian formations in the south-western of the study area. This lineament continue very clearly to the southeast.

Figure II.1 also indicates anomalies due to localised structures filled with Tertiary sediment in the Hobart-South Arm region marked by negative Bouguer gravity anomalies of about -10 mgals amplitude. This is due to the fact that the Tertiary sediment rocks have a lower density (1.82 - 2.15 g/cc) than the rest of the region. The relatively positive gravity field with amplitude of about +8 mgals is

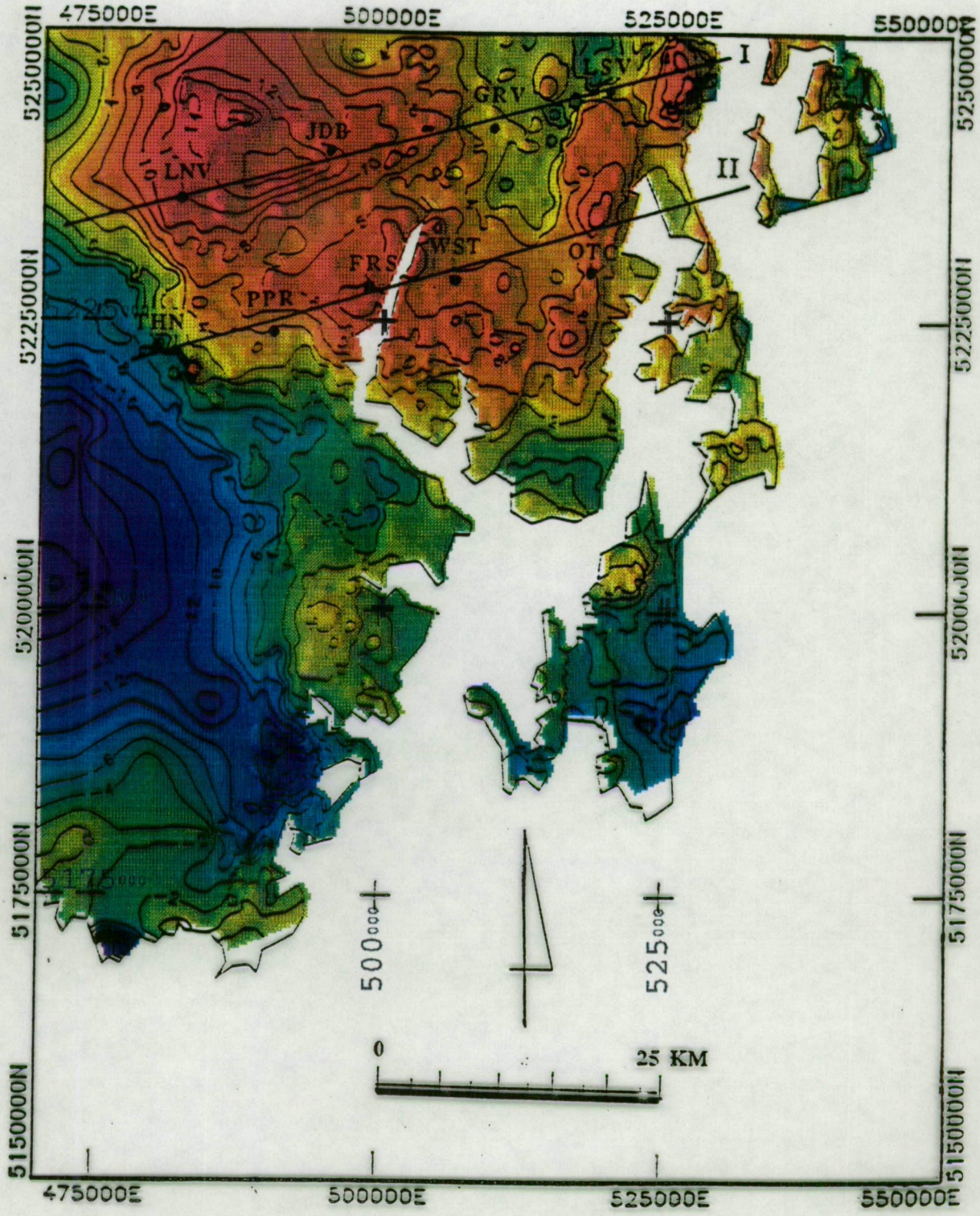

Figure II.1. Residual Bouguer gravity anomaly map of southern Tasmania, MANTLE 91, regional field removed (Leaman and Richardson, 1989). Grid mesh size 250 m, contour interval 2 mGal.

5225000
5200000
5175000
500000
525000

common in the centre of this area. These anomalies, which reflect the denser Pre-Permian rocks and Jurassic dolerite, are scattered throughout the entire Huon and Channel region. This positive anomaly also coincides with the approximate centre and axis of the Huon mobile zone (HMZ) (see figure II.4).

Superimposed on the residual Bouguer anomaly map are the locations at which transient electromagnetic and magnetotelluric recording stations were placed.

II.3.2. Magnetics.

A number of localized ground magnetic and aeromagnetic surveys have been run in this study area, but much of the work is described in unpublished reports. Leaman (1973, 1981) provides a list of references for these surveys.

The magnetic field (Figure II.2) bears little apparent direct relationship to the gravity field (Figure II.1). As can be seen from the magnetic profile map of Figure II.3, there are two main magnetic features associated with this study area. The first is a local magnetic high called the Cygnet anomaly in the middle of the study area. The second is a regional magnetic high along the southwest edge of the area.

The local magnetic high found in the Cygnet area is related to Cretaceous syenites and their effect on intruded dolerite. Previous work by Leaman and Naqvi (1967), and Leaman (1977) has shown that many anomalous spikes occur in this region and are associated with magnetite at intrusion margins and junctions.

Southwest of the Cygnet magnetic anomaly there is a regional magnetic high trending northwest-southeast, which is coincident with the gravity data (see Figure II.1). It is believed that both the magnetic and gravity fields are responding to a deep narrow trough or rift fill containing significantly magnetic and dense Palaeozoic materials.

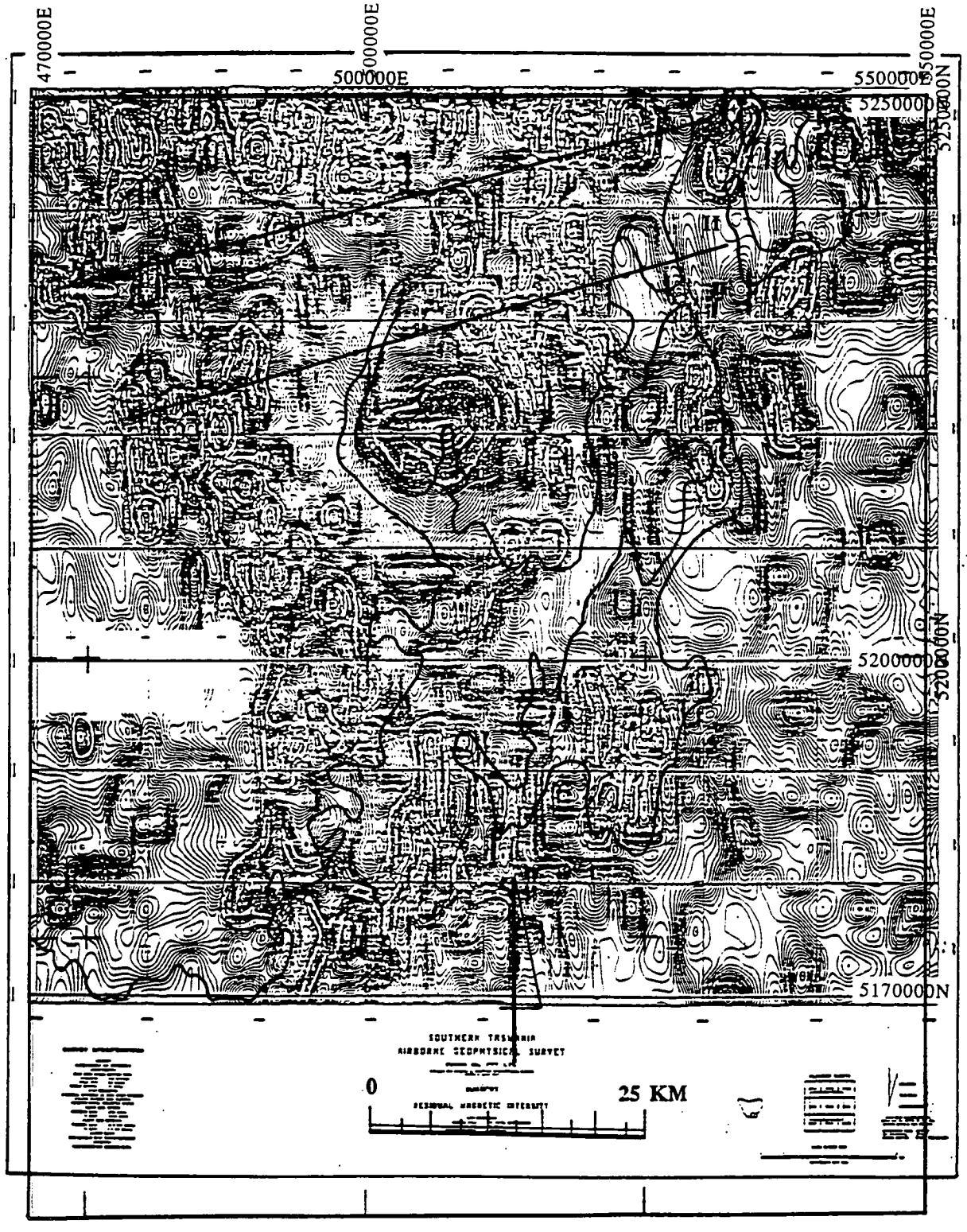

Figure II.2. Compilation of residual magnetic intensity map: aeromagnetic survey at 1000 metres above sea level. Data courtesy of Conga Oil Pty. Ltd.

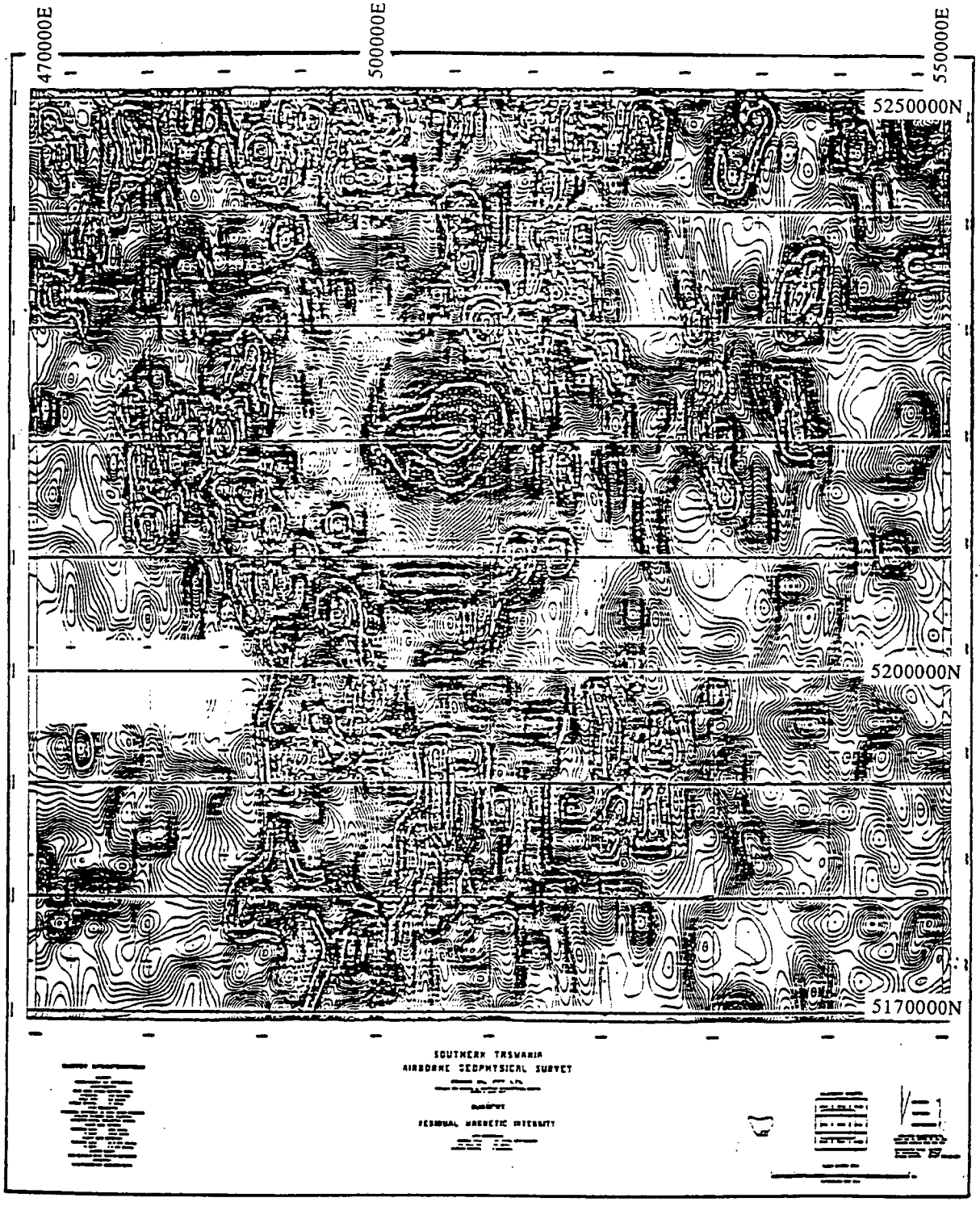

Figure II.2. Compilation of residual magnetic intensity map: aeromagnetic survey at 1000 metres above sea level. Data courtesy of Conga Oil Pty. Ltd.

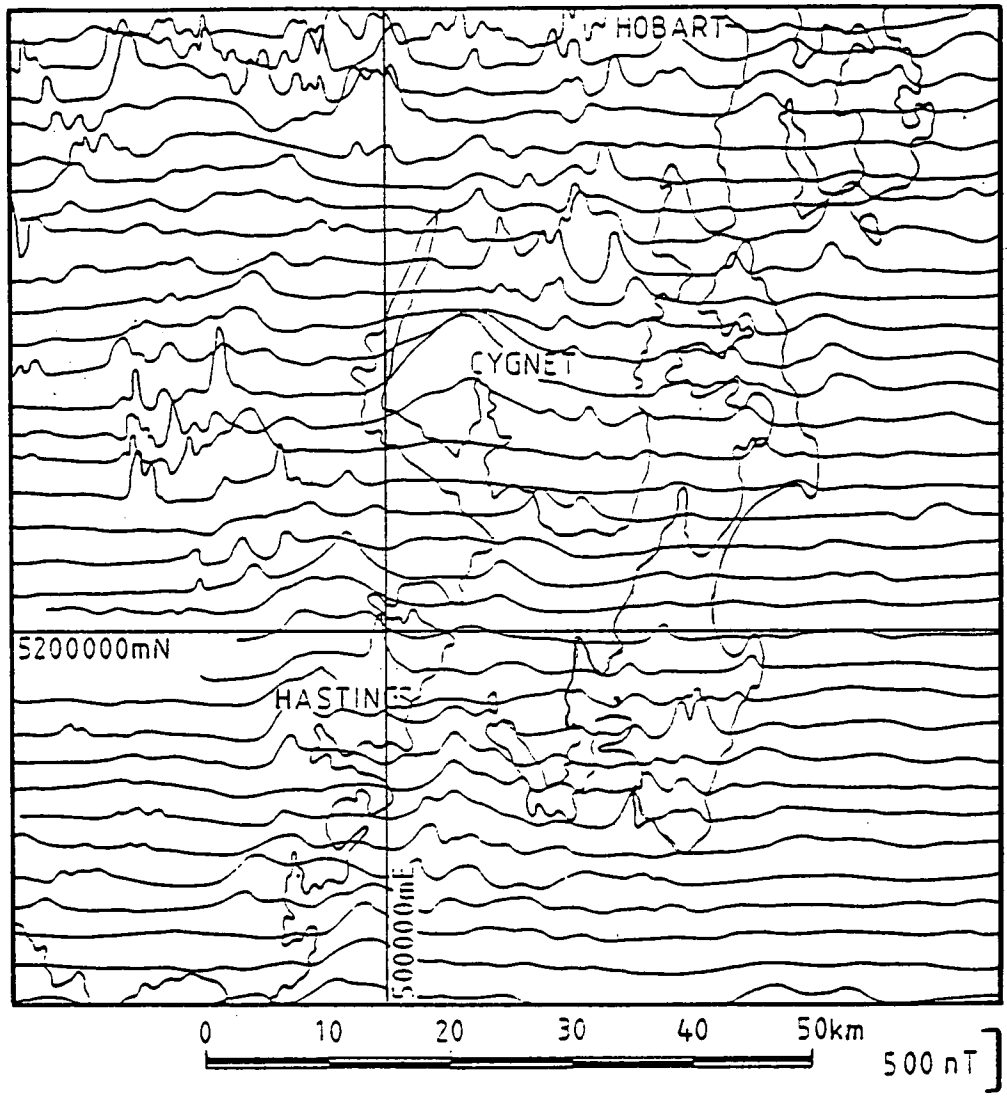

Figure II.3. Compilation of magnetic profiles map at 1000 metres above sea level (after Leaman, 1990).

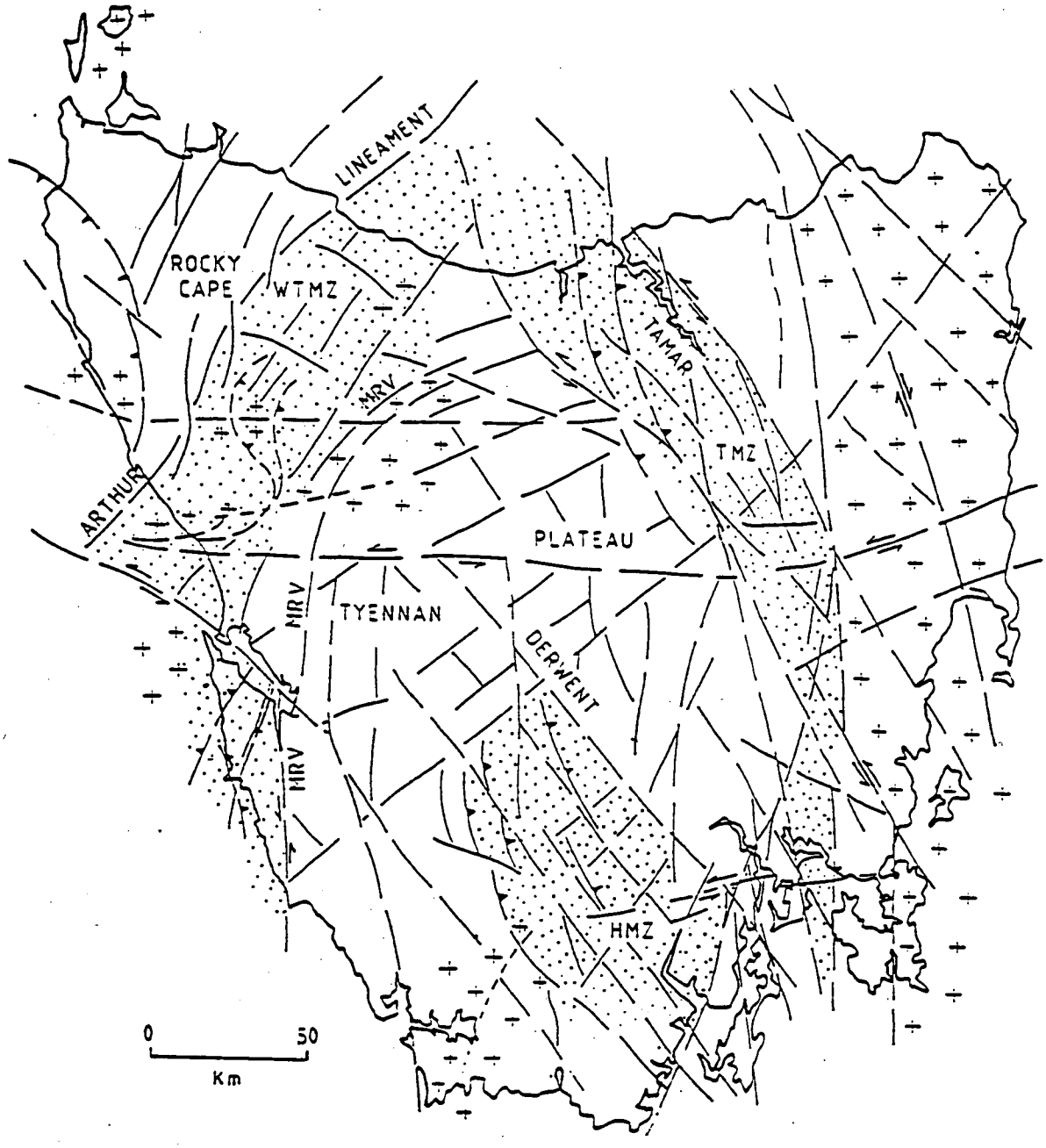

Figure II.4. Structural and tectonic interpretation based on gravity and magnetic data showing major tectonic element (after Leaman and Richardson, 1990).

A summary of major tectonic elements deduced from the residual Bouguer anomaly and aeromagnetic data of Tasmania is given by Leaman and Richardson (1989) and shown in Figure II.4. The most striking geological feature shown here are the western Tasmania mobile zone (WTMZ) in western Tasmania, the Tamar mobile zone (TMZ) in eastern Tasmania and the Huon mobile zone (HMZ) in southeast Tasmania.

II.4. Rock Physical Properties.

Rock physical properties, density and susceptibility, of the study area are well constrained. The table below (Table II.1) lists the value, or range of values used for the density contrast and susceptibility of each unit during the modelling process. The rock physical properties data indicated in this table, adapted from Leaman (1987), show which rock unit has significant effects upon the gravity and magnetic anomalies. The gravity anomalies are principally influenced by five rock types: Tertiary sediment, Triassic sediment rocks, Jurassic dolerite and, to lesser extent, Permian sediment rocks and Cambrian volcanics. The magnetic anomalies, on the other hand, correlate with the presence of the Jurassic dolerite.

Table II.1.

Density contrasts and susceptibility used for rock type within the study area

Rock unit	Density contrast with respect to 2.67 (g/cc)	Susceptibility (cgs)
Tertiary		
-sediment	- 0.60	0.0
Jurassic dolerit	0.23 - 0.25	0.004 - 0.005
Triassics	-0.23 - -0.25	0.0
Permian	-0.12 - -0.15	0.0
Ordovician		
-sandstone	0.0 - 0.1	0.0
Cambrian		
-volcanic	0.07 - 0.1	0.001
Precambrian		
-dolomite	0.0 - 0.1	0.0
- other	0 - 0.007	0.0

II.5. Two-Dimensional Modelling.

Two-dimensional forward modelling of gravity and magnetic data was carried out for two east-west sections crossing the study area, almost parallel to the magnetotellurics cross-sections, using program MODEL2D Version 2.4 written by M. Roach. The program uses algorithms for the response of an arbitrarily shaped, two-dimensional polygon as developed by Talwani and Ewing (1960) and Talwani (1965). All modelling was conducted using gravity data continued to a constant altitude of 1000 metres (consistent with the magnetic data). This was necessary because of the large variation in terrain clearance in the raw magnetic data caused by the rugged topography. The important features of the major magnetic anomalies are

preserved in the continued dataset and must be matched gravimetrically against the same reference levels.

Appendices II.1 and II.2 list the Fourier transform filtered gravity data of cross-sections I and II. Upward continuation of gravity data is a straightforward operation, as the surfaces are held in field-free space (Telford et al., 1976) and this approach has also been tested and used by Leaman (1986a, 1986b).

Areas in which the major part is covered predominantly by igneous Jurassic dolerite, such as southeast Tasmania, usually have complex magnetic variations. Basement features are often masked by higher frequency magnetic effects that originate near the surface. Upward continuation at high level observation reduces these effects, as well as reducing topographic effects (Leaman D.E., pers. comm.).

The topography profile along cross-sections I and II was obtained from Tasmania 1:100.000 topographic map sheet index: Tyenna, Derwent, Huon and D'Entrecasteaux, published by the Lands Department. The surface geological units which were modelled along these cross-sections were based on the Tasmania Geological Survey maps 1:250.000 (Leaman, 1972, Farmer, 1985).

II.6. Interpretation.

II.6.1. Cross-section I.

Figure II.5 is a two-dimensional model combining gravity and magnetic fields almost parallel to magnetotelluric sites (LNV, JDB, GRV, and LSV). The magnetic profile carries a significant non-dolerite component to the magnetic field. This is reflected in the long wavelength feature superimposed along 10 to 20 kilometres and the solution reflects the style of the probable source. The observed gravity field at this part of Figure II.3 drastically increases and forms a dome shape after reaching the maximum values of +16 mGal at 16 kilometres (see Appendix II.1). This pattern of the gravity field suggests that this section has different rock properties compared to surrounding rock. A body 28 kilometres long and 5 kilometres thick and narrowing at

depth is placed to provide a broad positive signature. In this trough-like structure, a magnetic susceptibility of 0.001 cgs and density contrast of 0.1 g/cc has been used. These are the characteristics of Cambrian volcanic rocks (Leaman, 1987). The depth of this body from the surface is about 900 metres. Attempts to change this depth result in higher rms error for both gravity and magnetic calculations. Some spikes on the observed magnetic field were also found in this section. The two small spikes are believed to be associated with the Jurassic dolerite bodies that crop out to the west of Lonnavale.

One of the conspicuous features in this cross-section is a narrow magnetic high near 30 kilometres (see Figure II.4). This anomaly has the highest value of +175 nT at 29.5 kilometres and two minimum values of -120 nT at 25.5 kilometres and -185 nT at 33 kilometres respectively (see Appendix II.1). The major contribution to this magnetic anomaly is the strongly magnetic Jurassic dolerite, which blankets much of the study area. The Jurassic dolerite is modelled as intruding the Permian and Ordovician rocks. The vertical extent of the dolerite is proportional to its width. The extent of the dolerite shown here has a susceptibility of 0.004 cgs, but in some places, the dolerite may contain granophyre (Dr. D. Leaman, personal communication, 1992) which has susceptibility of 0.01 cgs. Consequently the thickness of the dolerite decreases and intrudes the formation below with pipe-like shape.

The gradient of the observed gravity profile varies smoothly along the eastern part of this traverse. The general eastward decreasing gravity trend may be attributed to the thickening of the Permo-Triassic rocks, with secondary effect due to the underlying Precambrian sequences. The thickness of Triassic and Permian rocks at this section is about 400 and 800 metres respectively and takes into account the topography of this area. The thickness of the Permian rock decreases at the most eastern end of the traverse to about 500 metres as suggested by Leaman (1990).

Figure II.5. 2D GRAVITY AND MAGNETICS MODEL

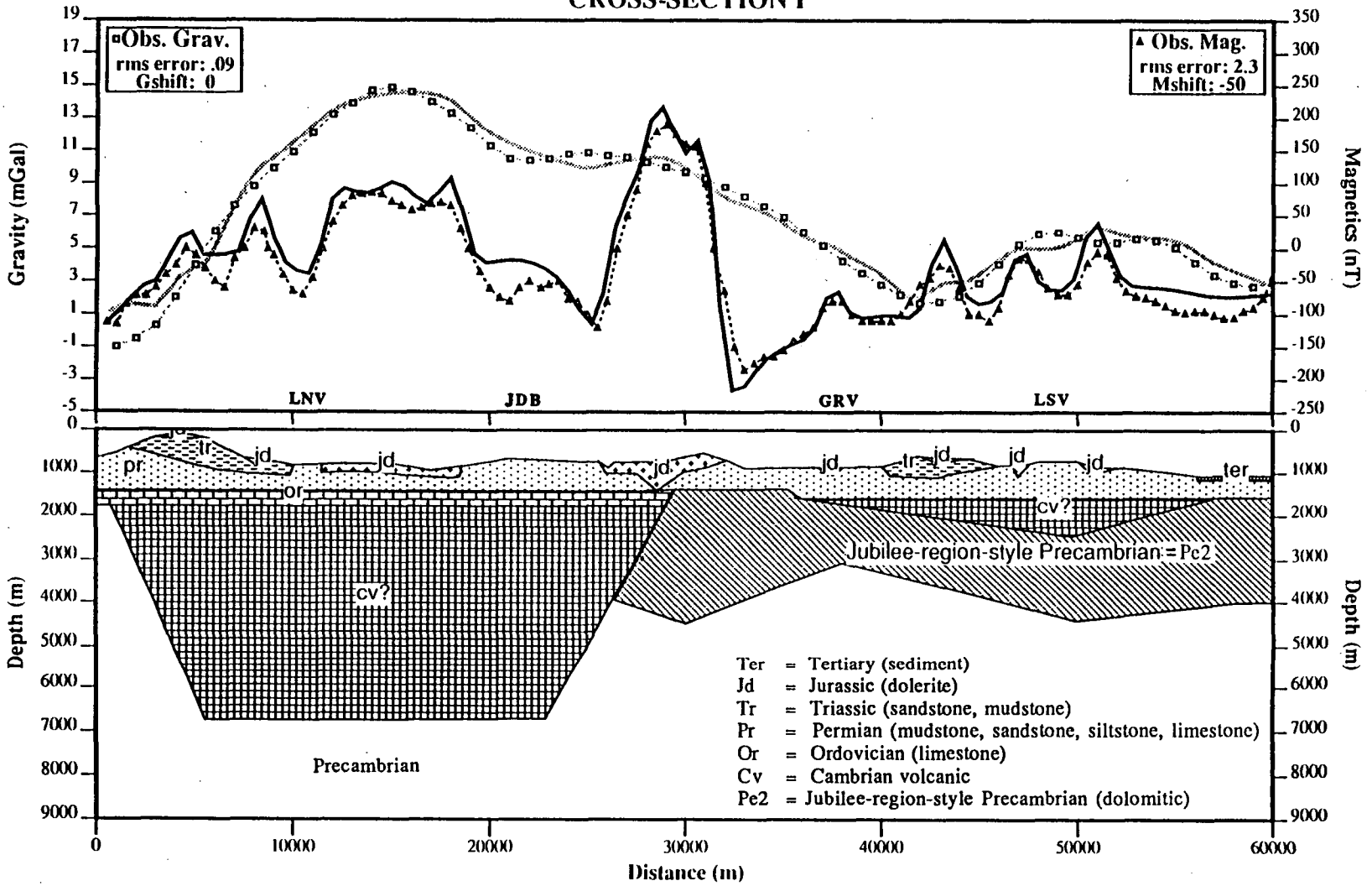

Model File:LINE1L.MOD Obs. Gravity:GRAVINEW.OBS Obs. Magnetic:MAGCRS1.OBS Date:01-04-1993 Time:15:48:45

II.6.2. Cross-section II.

Figure II.6 shows the observed and calculated gravity and magnetic cross-section II almost parallel to magnetotelluric sites (THN, PPR, FRS, WST). As can be seen here the observed gravity profile is slightly different compared to cross-section I. The gravity profile begins with the negative anomaly of -7 mGal (see Appendix II.2) at the western edge of the cross-section and drastically increases at 8 kilometres to form a relatively large positive anomaly at 30 kilometres with maximum value of 9.5 mGal increasing toward the east of the traverse. The characteristic mentioned which is accompanied by a waving pattern of the gravity profile demonstrates that the denser basement extends irregularly east. The broad and large gravity anomaly together with slightly negative magnetic anomaly at the middle of the cross-section may be due to a large Cambrian volcanic body which has a thickness of about 5 kilometres and a base of from 20 - 33 kilometres.

The phenomena shown by magnetic anomalies in cross-section I are also displayed here. Unlike the spikes found in cross-section I, the spikes created by dolerite bodies in cross-section II are larger. At the eastern part of the cross-section, the amplitude of the observed magnetic field is about 400 nT. The susceptibility value used here is 0.005 cgs. Attempts to use susceptibilities less than this imply a greater depth extent with consequent effects on the calculated gravity profile and results in larger rms error. It is suggested that some of this dolerite is more magnetic than in other sections. A reduction in the magnetic value before the large magnetic anomalies at 8 and 48 kilometres indicates that it may be associated with a deep fault.

Figure II.6. 2D GRAVITY AND MAGNETICS MODEL

CROSS-SECTION II

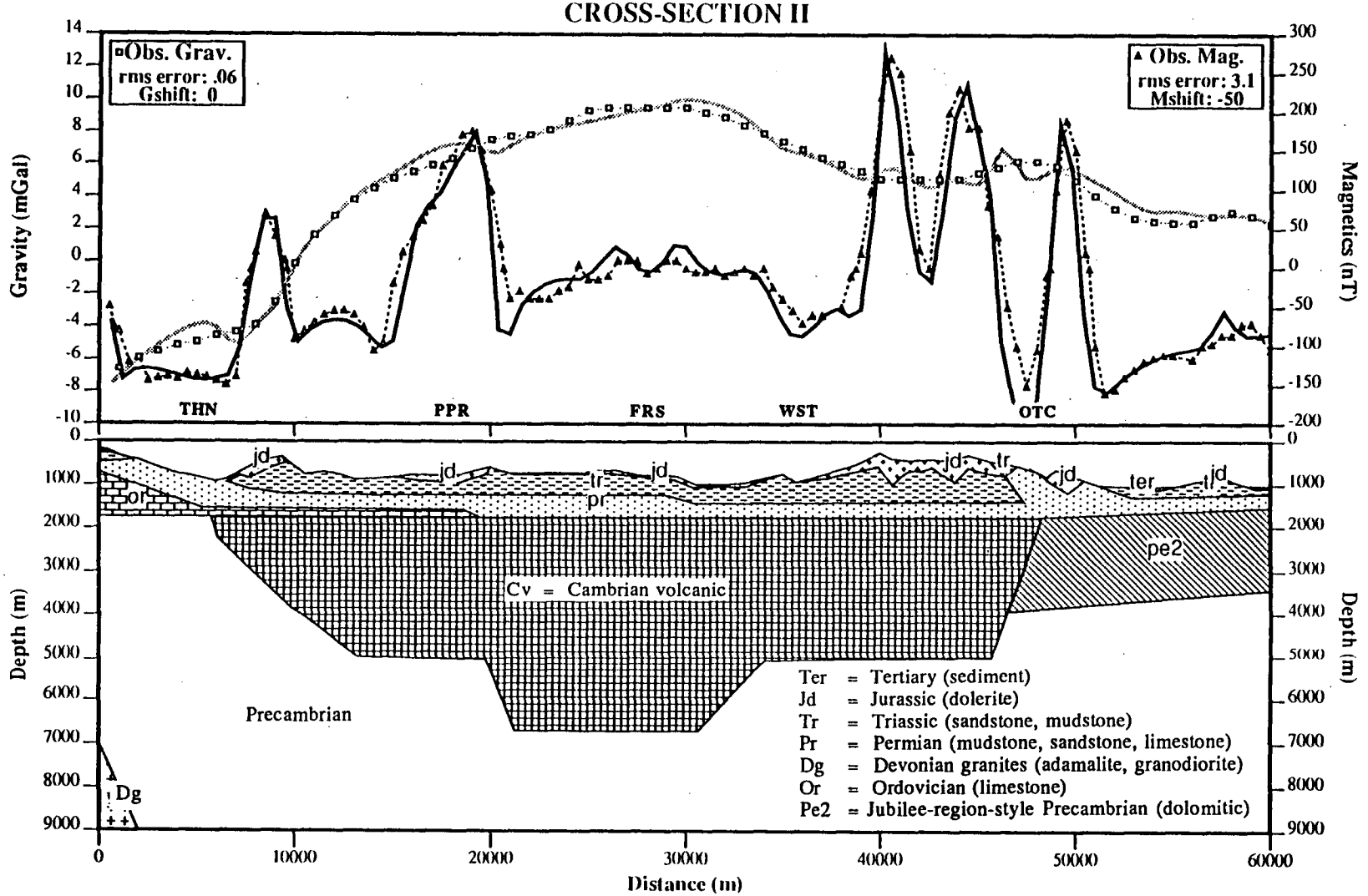

Model File:LINE2G.MOD Obs. Gravity:GRAV2NEW.OBS Obs. Magnetic:MAGCRS2.OBS Date:01-04-1993 Time:15:50:41

III.7. Summary.

Some important information can be drawn from the two-dimensional potential field modelling results: the entire region of these cross-sections is blanketed by Permo-Triassic rocks intruded by Jurassic dolerite; a major unconformity exists at the base of the Permo-Triassic (Parmeener Super group) cover; a drop in the magnetic value before the large anomaly is an indication of a deep fault; a trough like structure with Cambrian Volcanic fill is found at the western part of cross-section I and at the middle part of cross-section II, suggesting that this structure has a northwest - southeast direction and is wider to the south.

Chapter III.
TRANSIENT ELECTROMAGNETIC METHOD.

III.1. Introduction.

Inductive electromagnetic geophysical exploration methods employing a time-varying artificial primary field as a power source, have been used for many years for probing the earth's shallow crust. An alternating or a step function current, when driven into a coil or through a wire grounded at both ends, will produce an oscillating magnetic field. Any conducting material within the region of the magnetic field will have generated within it induced currents, which will tend to flow in paths normal to the direction of the applied magnetic field. These induced, or eddy currents, will in turn generate a secondary magnetic field which will oppose the primary exciting field inside the conductor (see Figure III.1).

Any electromagnetic system operates in the frequency domain involving continuous transmission at a fixed frequency. Time domain electromagnetic systems, in which pulses are transmitted and the transient decay of any resultant secondary field is recorded during the interval between the pulses, have been developed in the last few decades . The name commonly applied to such systems is Transient Electromagnetic or TEM for short. The application of the TEM systems in geophysical exploration on the ground has been reported by many authors.

Recently, there has been considerable activity in the theoretical investigation of TEM systems for mapping the conductivity of the sea-floor (Cheesman et al., 1987;

Cheesman, 1989 and Cheesman et al., 1990). The applications of such tools are numerous and include assessing off-shore placer mineral deposits, mapping quarternary geology and, in deep water, studying the physical properties of mid-ocean ridge hydrothermal regimes and associated massive sulphide deposits.

III.2. Basic Theory.

Comprehensive review articles by Ward (1967), Keller (1971) and Buselli et al. (1985) outline many advances in the instrumentation and theory of the transient electromagnetic method, and the application of this method is discussed by Palacky (1983). When a step function current is applied to a coil or along a wire, a transient electromagnetic field is generated. The response of conducting ground to such a pulse, resulting from abruptly switching off the primary field, is to generate a secondary field which reduces the rate of decay of the total field. The resultant decaying transient field is sampled at discrete time intervals after the cessation of the current in the primary loop, that is, when the primary field is turned off (see Figure III.2). The transient measurements are averaged over many cycles to enhance the signal to noise and finally the average voltage level in each time window is recorded, which allows the transient decay to be recorded and analysed. Variations in the amplitude and decay rate of the transient field allow interpretations of the conductivity as a function of depth to be made.

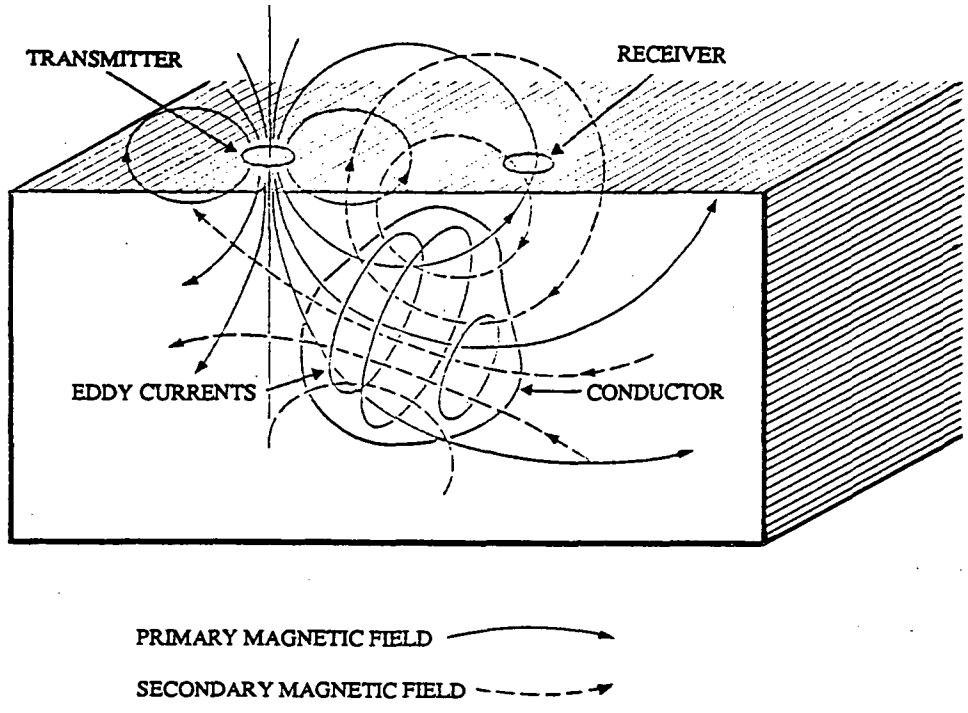

Figure III.1. Induction of Eddy currents in a subsurface conductor (from Geox Sirotem).

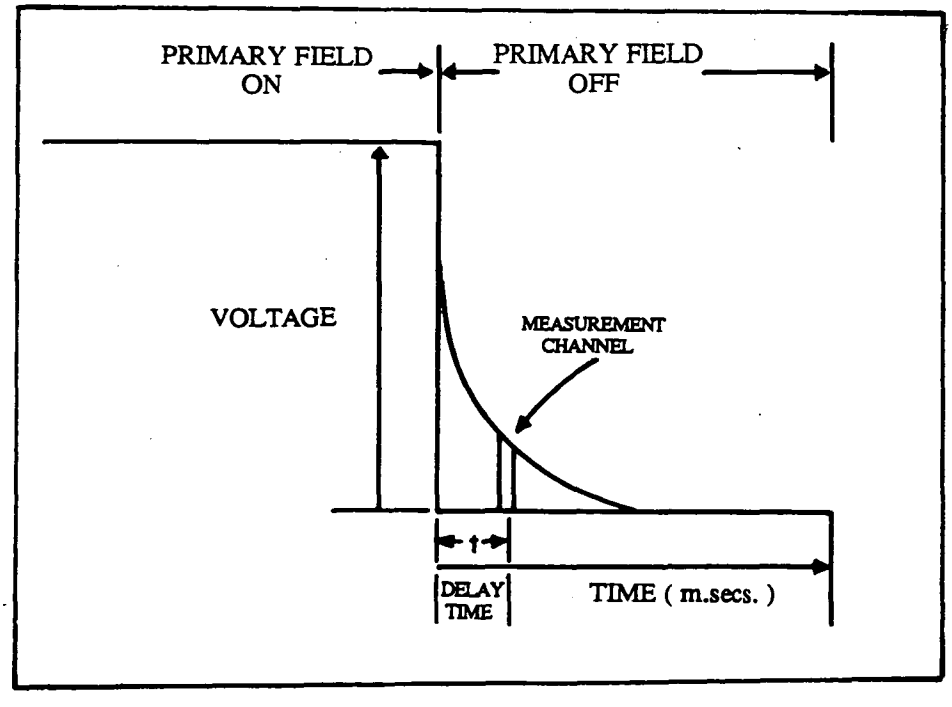

Figure III.2. Transient electromagnetic measurement (from Geox Sirotem).

III.3. Data Acquisition.

The instrument used for this study was a SIROTEM MK1 transient electromagnetic system. SIROTEM was developed as a portable transient electromagnetic system for use in areas of highly conductive overburden, such as occur widely in Australia (Buselli and O'Neill, 1977), from earlier instruments invented in the USSR and North America. For a concise history of the development of transient electromagnetic instruments, see Spies (1980).

The transient electromagnetic systems record data in the time domain, and SIROTEM can record up to 32 channels of data for delay time from 0.4 msec. to approximately 160 msec. after the cessation of the transmitter current. SIROTEM produces, at each survey station, a hard copy of the transient voltages in nanoVolts/Ampere and can also produce apparent resistivity of the equivalent half-space at each delay time.

There are a number of different loop configurations possible for transient electromagnetic measurements, some being better than others for specific geological situations. The coincident loop configuration was chosen as it has the highest signal levels of any configuration because the receiver is in the place of strongest transmission, and therefore best when transmission field is attenuated such as is caused by conductive overburden (Buselli et al. 1985). With coincident loops, if present, the superparamagnetic response causes the ground to appear to be more conductive and at late times the apparent resistivity values are lower than expected. In Tasmania problems with a superparamagnetic ground response are minimal.

The name coincident loop implies that the source of the primary signal is from a loop which is in the same geometrical position as the loop which receives the secondary signal. This can be achieved by a square loop of, in this study, 100 m side length, comprising two insulated single copper wires with one conductor acting as the

transmitting loop and the other as receiving loop. The transmitter loop was displaced 4 m from the receiver loop to avoid any possible superparamagnetic response of the ground. Comprehensive discussion of these superparamagnetic responses may be found in Buselli (1982) and Lee (1984).

Eight stations were established in south-east Tasmania for the transient electromagnetic sounding measurements (see Figure I.2 and Table I.1) in order to place constraints on the thicknesses and resistivities of the surface layers, and to examine the magnetotelluric data for signs of static shifts (see Appendix VII.2). Initially, the transient voltage of each station was recorded up to 32 channels. However, in all eight transient electromagnetic soundings, the last delay-time readings were corrupted by noise. The instrument includes electronic circuitry used to filter out noise (power lines, VLF radio transmissions, sferics) but high noise levels will vitiate interpretation. To this end, selection was made prior to modelling. The noisy data were not used. The data taken into the model were selected up to about 33 milliseconds.

Time domain measurements enable data to be presented as an apparent resistivity versus time pseudosection which is similar to the method of presentation of induced polarization data. Alternatively, as adopted in this study, data can be presented as a single set of transient events. The name commonly applied to such a technique is Transient Electromagnetic Sounding or TS. From the single set of transient events resistivity-thickness can be inferred.

III.4. Data Analysis.

During this study data analysis was mainly carried out using Olivetti M260 IBM compatible PC. In order to convert the transient voltage into the apparent resistivity and calculate the resistivity layer model, an inversion computer programme written in FORTRAN ["PANCAKE"] was used. In the PANCAKE program, voltage

calculation and apparent resistivity transforms include the effect of ramp-function current waveform. Details of the appropriate calculations for uniform half-space, layered half-spaces, and apparent resistivities used here are given in Raiche (1984), Lee and Lewis (1974) and Spies and Raiche (1980). A brief definition of the most commonly used parameters such as voltage response and apparent resistivity are given below.

The voltage response was discussed by Lee and Lewis (1974). The method is based on calculations for a circular loop, and discussed in Spies and Raiche (1980) and Raiche (1984). Accordingly, the voltage response (V), at time t, of a homogeneous half-space (conductivity = σ, magnetic permeability = μ) for coincident Tx - Rx loops of area A, excited by a step current I is as follows:

$$V = \frac{2\mu\sqrt{A}}{t} I\, y(x) \qquad \text{(III.1)}$$

Here, y is a function of the dimensionless parameter $x = \sigma\mu A / 4\pi t$. It is known that the voltage induced in a square loop differs from that produced in a circular loop by less than 1% for $x = < 6$ (Spies and Raiche, 1980).

Making use of the well-known step function response of Lee and Lewis (1974), equation (III.2), to determine y and from which x can be determined, the apparent conductivity σ_a can then be expressed (Spies and Raiche, 1980) as:

$$\sigma_a = \frac{4\pi t x}{\mu A} . \qquad \text{(III.2)}$$

In practice, as an aid to preselection and interpretation, it is convenient to define an apparent resistivity; that is the resistivity of an equivalent half-space which would give the same Z (t), mutual impedance, as that observed, Z_0 (t). No simple expression exists for the apparent resistivity and it will generally change with time.

It is found by a scheme in which the value of $\sigma 1$ is varied to calculate the following equations and to make S (t) / S_0 (see equation IV.13 and IV.14) approach 1 via an iterative procedure. The apparent resistivity ρa is defined as $\rho_a = 1/\sigma 1$, where $\sigma 1$ is the final value of conductivity found at the end of the procedure (Raiche and Spies (1981) and Raiche (1984). For the coincident loops, the mutual impedance for half-space may be written:

$$Z(t) = \frac{2\sqrt{\pi}\, a\mu_0}{t} \int_0^\infty \frac{F(t)}{\alpha} J_1^2(\xi)\, d\xi \qquad \text{(III.3)}$$

where

$F(t) = g(\xi\sqrt{\tau'}) - g(\xi\sqrt{\tau})$

$g(y) = y \exp(-y^2) - \sqrt{\pi}\, \mathrm{erfc}(y)(0.5 + y^2)$

$\tau' = (t - t_0)/\mu_0 \sigma 1 a^2$

$\alpha = t_0 / t$

$J_1(\xi)$ is the Bessel function of the first kind of order one.

ξ is the Hankel transform variable.

erfc is the complementary error function.

a is the radius of loop.

From this we have

$$S_0 = \frac{t}{2\sqrt{\pi}\, a\mu_0} Z_0(t) \qquad \text{(III.4)}$$

$$S(t) = \int_0^\infty \frac{F(t)}{\alpha} J_1^2(\xi)\, d\xi \qquad \text{(III.5)}$$

Apparent resistivities are thus calculated from the mutual impedance data via the iterative procedure which takes a first-order approximation value for the apparent resistivity and successively improves it until the error between the true value S_0 and the estimated S, as given by equation (III.4) and (III.5) above is sufficiently small. The first guess estimate comes from a series inversion of (III.3) and equation 4 of Spies and Raiche (1980).

The equations outlined in the previous section can be used to generate model curves of apparent resistivity for varying model layer parameters and loop configurations. Such model curves can be used to interpret field data in forward modelling. However, this is a tedious process for any but the simplest models and PANCAKE modifies a first guess to match the field data in some sense, usually to minimize the sum of squares of errors. This is the process of inversion or solving the inverse problem. For the inversions in PANCAKE a linearized least-squares inversion routine, similar to that described in Jupp and Vozoff (1975) was used to optimize the model parameters of layer resistivities and thicknesses to match the measured data.

The inversion of field data to best fit layered models was used for interpretation. Basically a starting layered model specifies the number of layers above basement. The starting resistivity values and thicknesses are input into the program as an initial model together with a set of TEM observations (i.e. voltage versus time). The program adjusts the model parameters to obtain a least squares fit to the observation.

When fitting layered models to data, there is always the question of how many layers to use. In this study, a 2 layer inversion model was made as the initial assumption of the geoelectric structures. In choosing the number of layers to be modelled, the standard errors (mean and root mean square), and the parameter called the average predicted residual error (APRE) were calculated following the method of

Raiche et al. (1985). APRE is one of the most useful statistics in finding the most parsimonious model consistent with the data. For a detailed calculation see Raiche et al. (1985). For APRE values less than 15 per-cent the model is considered to be in keeping with the data.

III.5. Field Results.

The theory put forward in the previous sections has been used to calculate the apparent resistivity as a function of time in a 100 m per side of coincident loop for a number of different layered models. These results were plotted against time ranging from 0.4 to 33 milliseconds which is the typical range used in this study.

As shown in Figure I.2, in this study the presentation of the data can be divided into two cross-sections. Cross-section I includes stations: LSV, GRV, JDB, LNV while cross-section II is composed of stations: WST, FRS, PPR and THN. (see Table I.1 for abbreviations).

The transient electromagnetic results may be merged with the magnetotelluric results using the method of Sternberg et al. (1988) to examine the magnetotelluric data for signs of static shifts. This is done in Appendix VII.2. It is appears that static shift corrections are not important here.

III.5.1. Cross-section I.

The plot of each sounding model may be identified from Figures III.3 to III.6. The average predicted residual (APRE) values are generally low. At stations LSV, JDB and LNV the APRE values are 9.3, 9.8 and 8.5 per cent respectively but for station GRV the APRE value is 10.4 per cent. The standard errors, mean and root mean square errors (RMS), are also very low. The highest standard error calculated at this cross-section, RMS 9.8 per cent, is also found at station GRV. For other

stations the standard errors either mean or RMS are generally less than 9 per cent. In order to get the best fit for stations LSV, GRV and JDB models were done putting resistivity decreasing with depth. The values of the standard errors and the APRE above indicate that a two-layer model is a good representation of the data. Attempts to fit three-layer and four-layer models to data set produced considerably worse statistics.

III.5.2 Cross-section II.

As can be seen from Figure I.2, this cross-section is almost parallel with cross-section I. The plot of each sounding model is shown from Figures III.7 to III.10. A similar situation to that at cross-section I is found at this cross-section survey, as the APRE values are low in most cases. In fact they are lower than cross-section I as the highest APRE value is 12 per cent which is calculated at station THN. At stations WST, FRK, and PPR the APRE values are 11, 6.8 and 7.2 per cent respectively. The standard errors from most stations are quite low but THN station has a standard error slightly higher than at cross-section I. The highest mean error calculated is 10.2 per cent at station WST while the highest RMS value of 7.7 per cent is calculated at THN. For other stations the standard error values are less than 8 per cent. However the mean error is as low as 1.79 per cent and RMS error of 2.73 per cent is found at station FRS. In this cross-section, to get the best fit for stations WST and FRS, models were done inserting resistivity increasing with depth, while PPR and THN stations data was modelled with resistivity decreasing with depth. By judging the values of the APRE and standard errors described above, that fall within criterion set in section IV.4, we have confirmation that a two-layer model is the appropriate representation of the data.

III.6. Discussion.

This study has placed constraints on the thicknesses and apparent resistivities of the surface layers, which provide valuable aid in interpretation of magnetotelluric data as discussed in Chapter V.

No rock resistivity laboratory measurements were conducted for the interpretation of the SIROTEM results. Instead the results of resistivity measurements by Leaman 1971, 1973 were used. A list of the resistivities and rock units is shown in Table III.1.

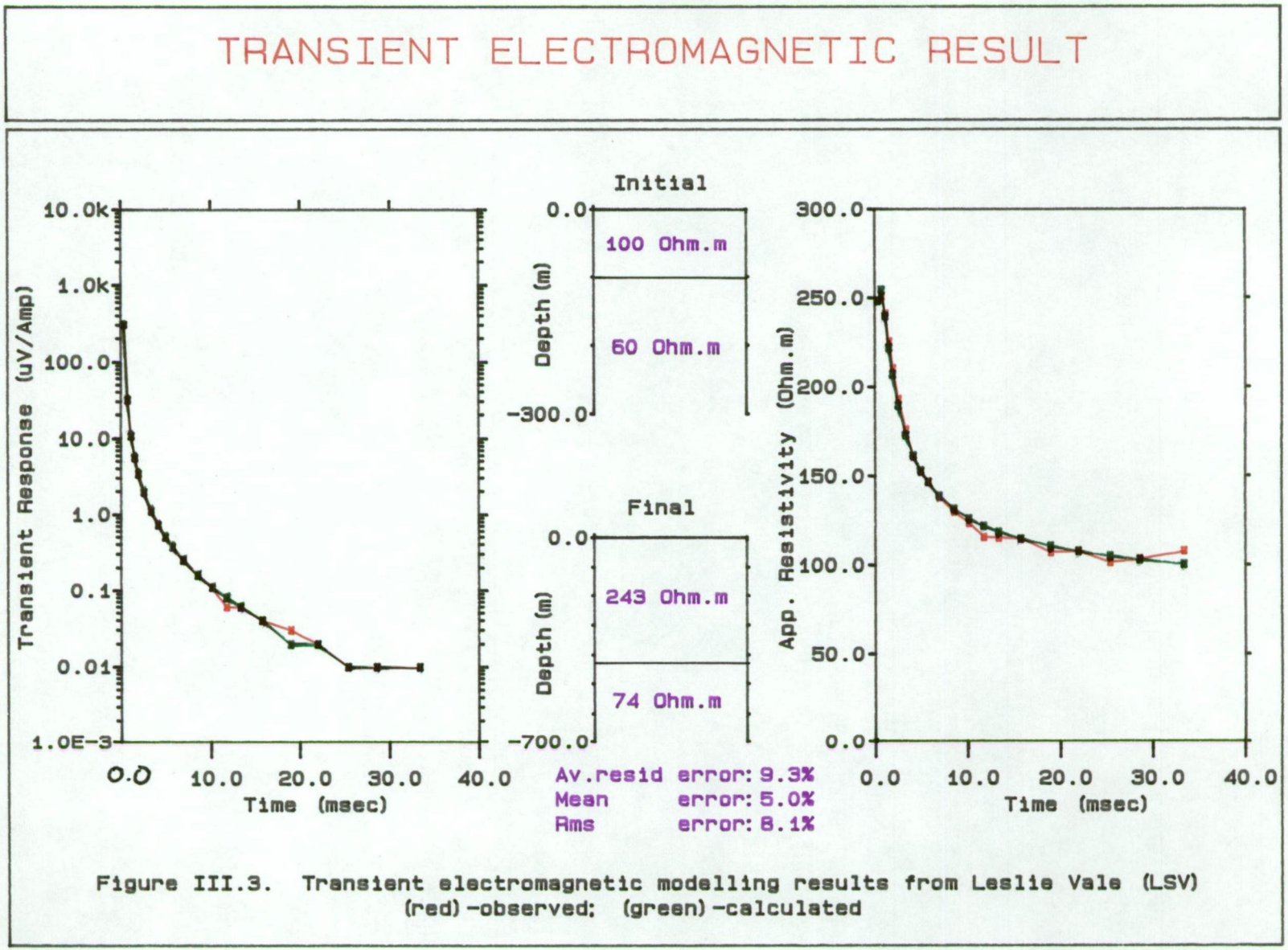

Figure III.3. Transient electromagnetic modelling results from Leslie Vale (LSV)
(red)-observed; (green)-calculated

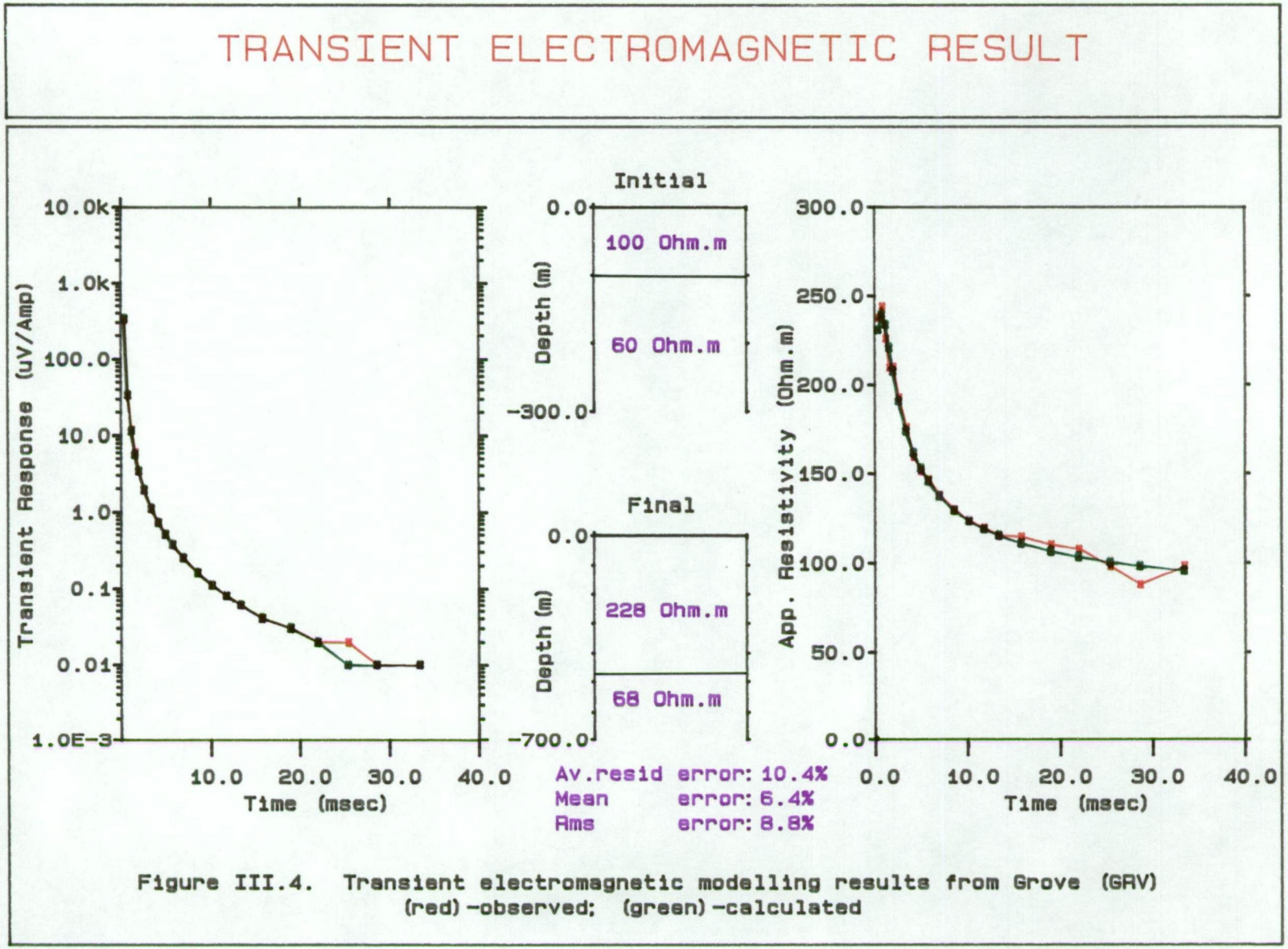

Figure III.4. Transient electromagnetic modelling results from Grove (GRV)
(red) -observed; (green) -calculated

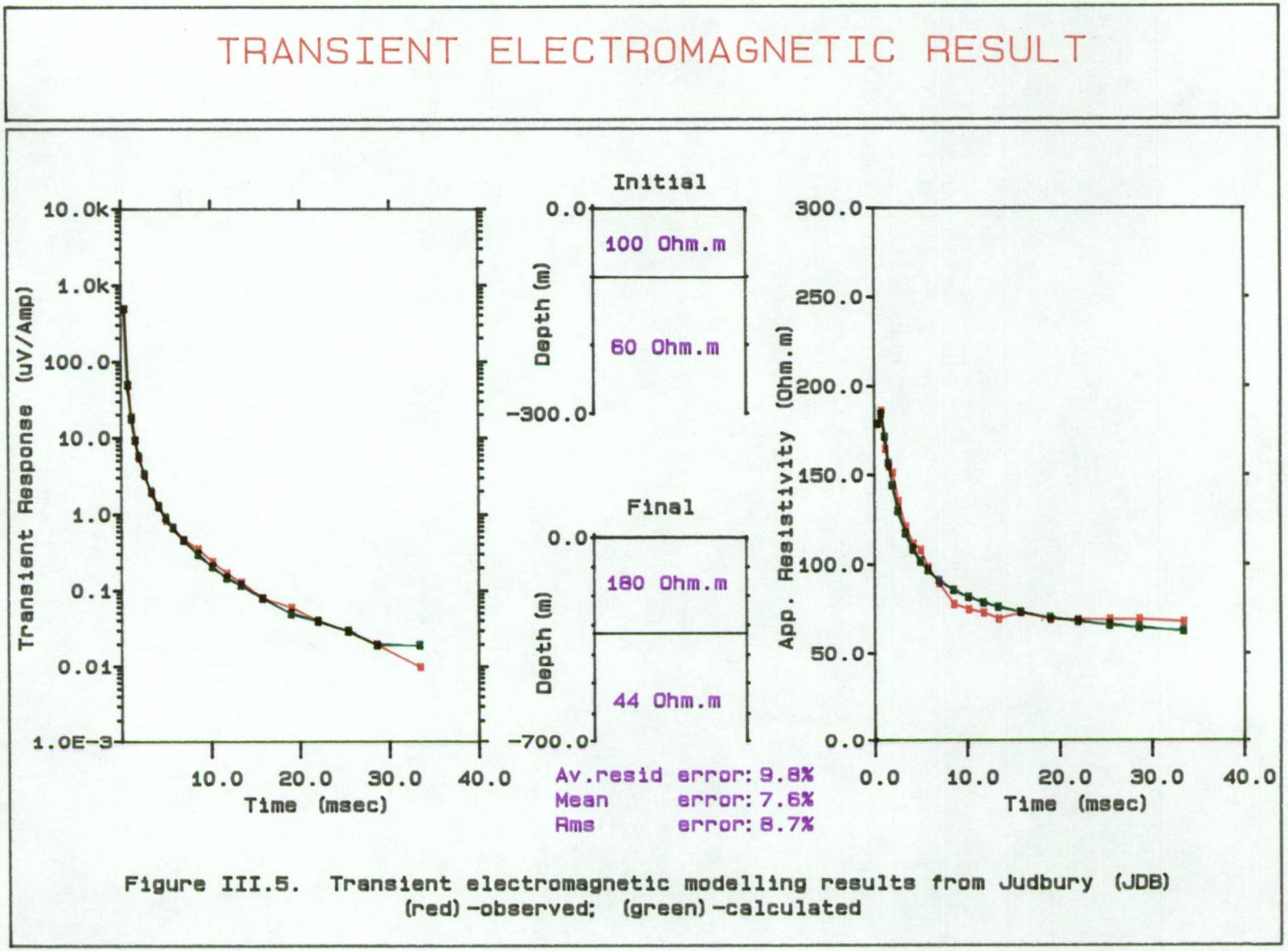

Figure III.5. Transient electromagnetic modelling results from Judbury (JDB)
(red) -observed; (green) -calculated

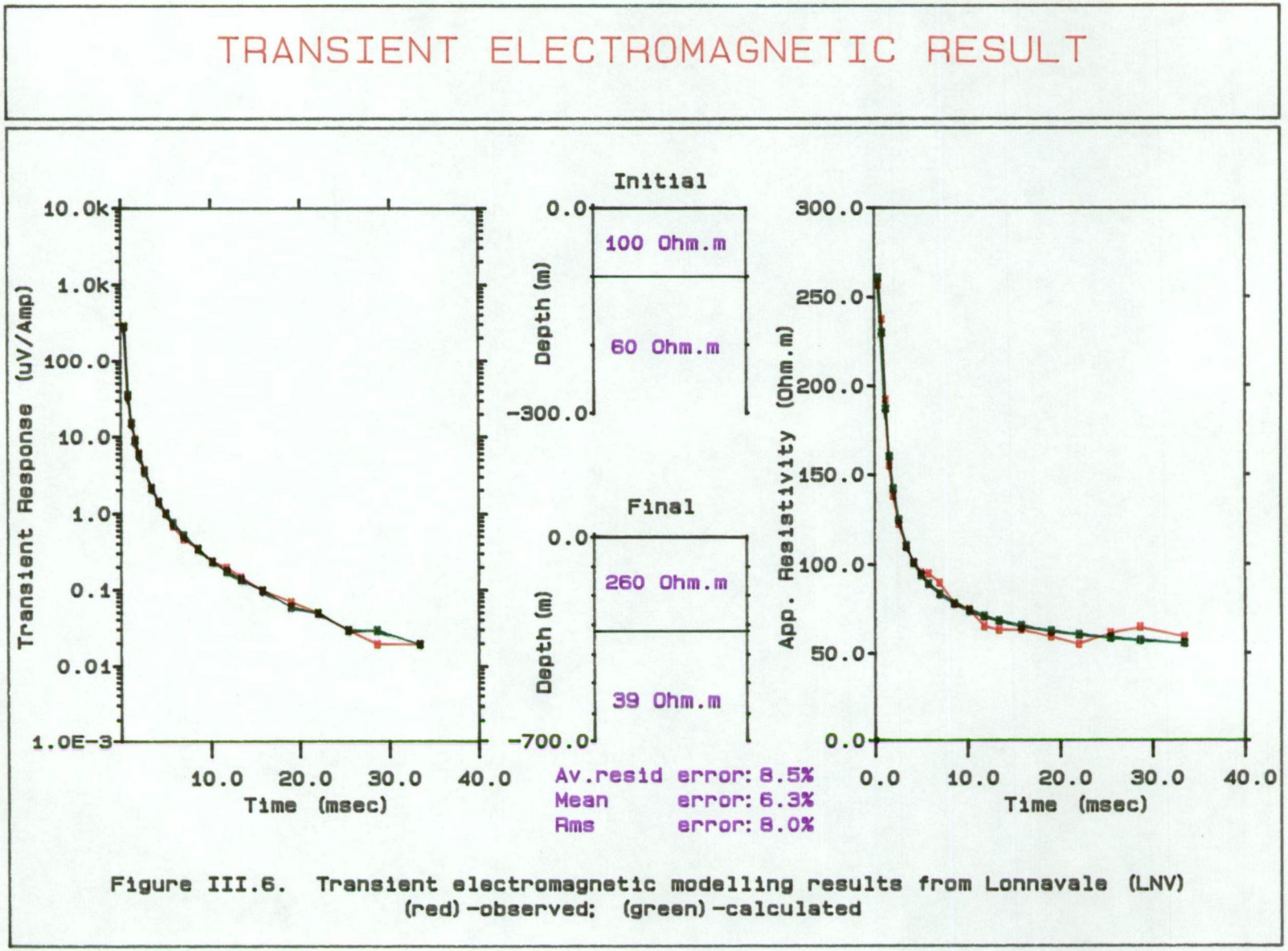

Figure III.6. Transient electromagnetic modelling results from Lonnavale (LNV)
(red)-observed; (green)-calculated

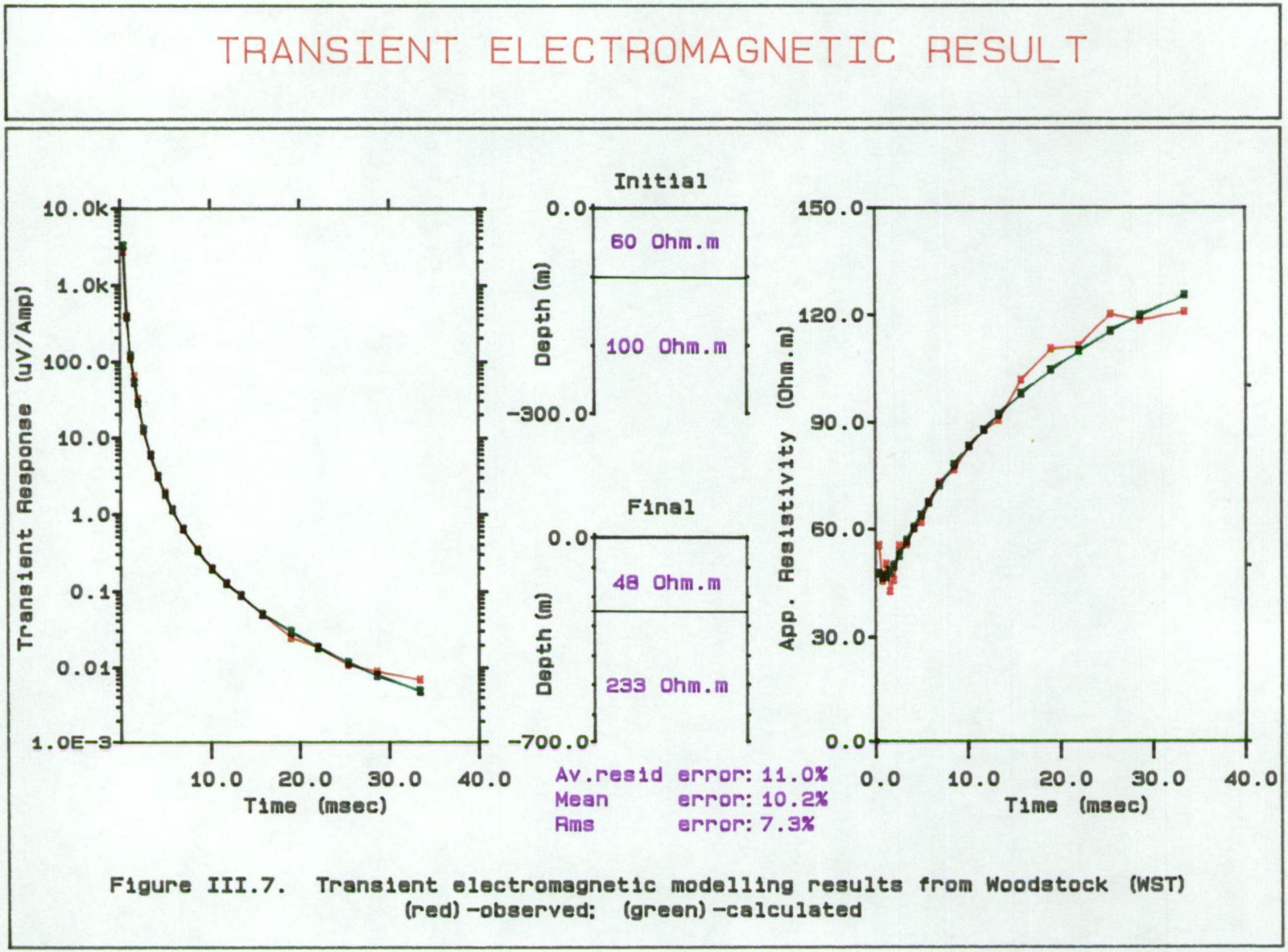

Figure III.7. Transient electromagnetic modelling results from Woodstock (WST) (red)-observed; (green)-calculated

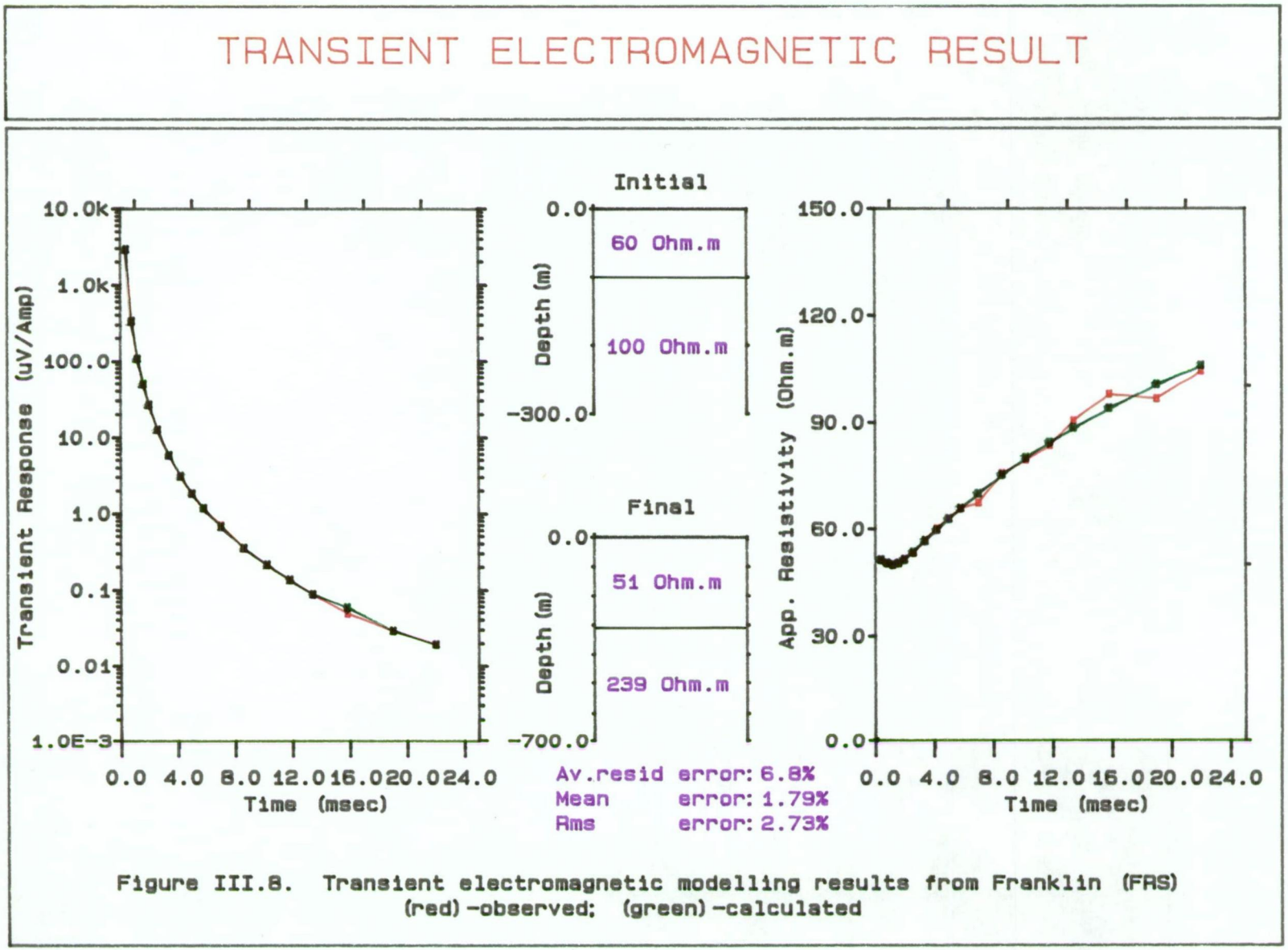

Figure III.8. Transient electromagnetic modelling results from Franklin (FRS)
(red) -observed; (green) -calculated

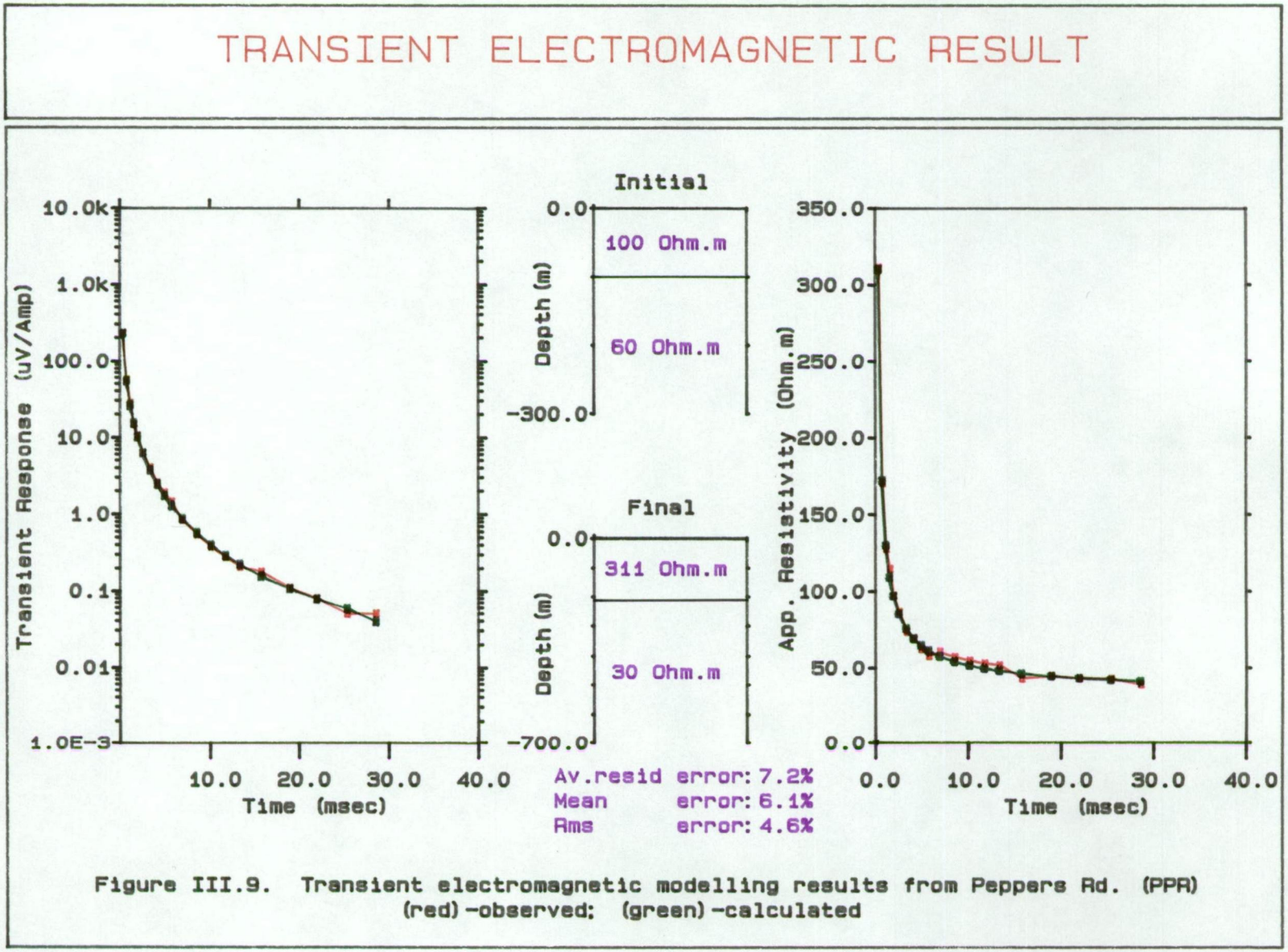

Figure III.9. Transient electromagnetic modelling results from Peppers Rd. (PPR)
(red)-observed; (green)-calculated

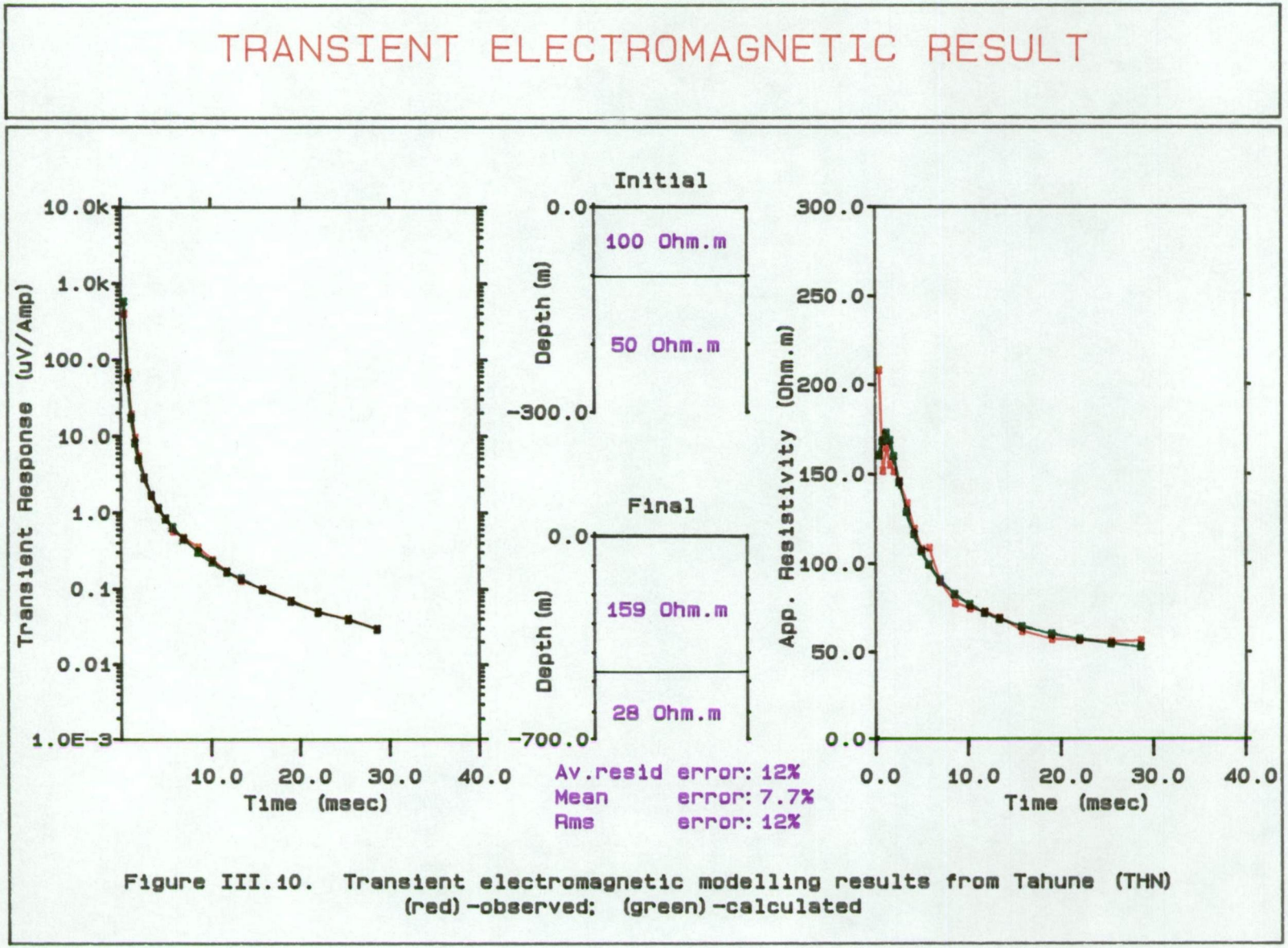

Figure III.10. Transient electromagnetic modelling results from Tahune (THN)
(red)-observed; (green)-calculated

Table III.1.

Laboratory resistivity measurements (after Leaman, 1971,1973)

Rock unit	Resistivity (Ohm-m)	
	Dry	Wet
Quaternary		
- alluvials	10 - 150	1 - 20
Tertiary		
- sediment	10 - 30	< 1 - 10
Jurassic		
- dolerite	> 5000	30 - 1000
Triassic		
- sandstone,siltstone,mudstone	50 - 500	15 - 100
Permian		
-mudstone,sandstone,limestone	100 - 5000	5 - 100
Ordovician		
- limestone	500 - 1500	30 - 500
Cambrian		
- volcanics	50 - 300	10 - 100
Precambrian	100 - 5000	-------

III.6.1. Cross-section I.

The results of the crosss-section I transient electromagnetic survey clearly show at shorter periods a large response which is probably attributable to the resistive first layer which is recorded over the length of the cross-section. At longer periods the apparent resistivity curve decays considerably implying a conductive lower layer. The apparent resistivity of the survey area was determined using the method described in Section III.4. At LSV station, calculation of apparent resistivity indicates that the

surficial layer has a resistivity of about 243 Ohm-m which is in good agreement with the laboratory apparent resistivity measurement (see Table III.1) reported by Leaman (1971). The two-dimensional modelling result of magnetic and gravity fields (see Chapter II)) indicated that this layer may be Permian rock. The depth of penetration calculated indicates that this resistive layer is quite thick (see Figure III.4). This deduction is again supported by a two-dimensional model calculated from gravity and magnetic data. Underlaying this rock unit is a more conductive layer with the apparent resistivity value of 74 Ohm-m which is believed to be Cambrian volcanic rock. At GRV station (Figure III.5), the response is similar to the result obtained at LSV station. However the surface apparent resistivity would appear to be somewhat lower than that at LSV,but still in the range of the resistivity value of Permian rock listed in Table III.1. The underlying rock at GRV station which has a resistivity value of 68 Ohm-m is also believed to be Cambrian volcanic rock. The JDB station is situated about 15 kilometres to the west of GRV. The lowest resistivity value for Permian rocks along cross-section I was found at JDB station being 180 Ohm-m (Figure III.6). The resistivity value and the thickness of this rock unit are in accordance with the listed data of Table III.1 and the result of a two-dimensional model of gravity and magnetic fields. Unlike stations LSV and GRV, at JDB the Permian rocks are underlain by a more conductive layer. The value contrast in resistivity suggests that these layers constitute different rock units. There is no information which can be drawn from the transient electromagnetic survey regarding the contact between these two rock units because of an absence of transient electromagnetic recording between GRV and JDB stations. On the other hand, the potential field method successfully reveals this contact which is at about 8 kilometres to the east of JDB along cross-section I and at 600 metres depth (see Figure II.5). The density contrast and magnetic susceptibility characteristics coupled with resistivity value of this rock suggest it belongs to the Ordovician rock unit. At the western-most station, LNV, the highest resistivity value for Permian rock, 260 Ohm-m, with 325 metres thickness was

found. As at JDB station it it would appear that LNV station indicates Permian rock underlain by Ordovician rock unit.

III.6.2. Cross-section II.

A plot of each sounding model along cross-section II displays a slightly different characteristic from the sounding models along cross-section I. At two stations, WST and FRS, larger transient responses than cross-section I, at early sample times were recorded. At later sample time the signal decreased sharply. It may be inferred from the results that there is a surficial layer of moderate conductivity in this area. Transient electromagnetic data recorded at late sample times highlight anomalies from more resistive bedrock beneath a surficial conducting layer. At WST station, calculation of apparent resistivity indicates that the surficial layer has a resistivity of about 48 Ohm-m which is in the range of resistivity values of wet Permian to Triassic rocks. The density contrast and magnetic susceptibility values contribute important information to this discrepancy where the rock does not crop out. It is known from cross-section II of two-dimensional modelling of gravity and magnetic field results that this rock has a magnetic susceptibility value of 0.0 cgs and density contrast of -0.23 g/cc, thus confirming that the top layer at WST station is Triassic rock. Underlaying this rock unit is a more resistive layer which is believed to be Permian rock. Results from FRS station sounding in general were identical to those at WST and did not contribute any additional information of significance. In contrast to two previous stations, at PPR the Triassic rock underlies the more resistive layer. It is believed that this layer is Jurassic dolerite which has a thickness of about 200 metres. At THN station, the sounding model was similar to the soundings in cross-section I. Here the Permian rock has a thickness of 450 metres. The more conductive bedrock, 28 Ohm-m, encountered here may be the same layer found at station LNV in cross-section I which suggests that the distribution of this Ordovician rock is restricted to the western part of the study area.

Chapter IV.
MAGNETOVARIATIONAL METHOD.

IV.1. Introduction.

The magnetovariational profiling method provides information about the conductivity structure of the earth by distinguishing the magnetic fields produced by the current concentrations induced in high conductivity regions. In a uniform or horizontally stratified earth the external and internal horizontal magnetic fields tend to add and the external and internal vertical magnetic fields nearly cancel. When there is a lateral variation in conductivity the concentration of current in the high conductivity region modifies the horizontal field and produces a significant vertical magnetic field. The assumption of the magnetovariational technique is that the horizontal field due to the current concentration is insignificant and that the vertical magnetic field in the absence of the current concentration is zero. Then the measured horizontal magnetic field can be regarded as "normal" and the measured vertical field can be regarded as "anomalous". The relationship between anomalous and normal fields then defines a transfer function that is characteristic of the lateral variation in conductivity. Determining the transfer functions over a range of frequencies, with a corresponding range of skin depths, allows the depth of conductivity variations to be assessed.

IV.2. The Basic Method.

The magnetovariational profiling method is a way of determining the electrical conductivity distribution of the subsurface from measurements of natural transient magnetic fields on the surface. The principal difference between this method and the magnetotelluric method is that the magnetotelluric method determines conductivity as a function of depth while the magnetovariational method observes lateral conductivity inhomogeneities. Like the magnetotelluric method, this method utilises the naturally varying magnetic field which originates outside the earth. The geomagnetic variations found to be most suitable as a source field are those which are associated with substorms and similar types of disturbance.

The basic features of a magnetic storm are shown in Figure IV.1. Magnetic storms typically occur about once or twice a month. However much more frequent intervals of disturbance occur without all the manifestations of a storm and in which the strongest disturbance is confined to latitudes near the auroral zone. These are known as sub-storms. A sudden increase in solar wind pressure causes the merging of field lines in the earth's magneto-tail. The subsequent pattern of current flow, together with the field aligned currents produced by merging, causes the resultant substorm (Figure. IV.2) (Roederer, 1977)).

Electric fields which are generated by such variations cause eddy currents to flow in the conducting part of the earth. These variations which penetrate into the earth, depending on the conductivity of the medium and the period of the variations, are used as a tool in probing the lateral conductivity contrast.

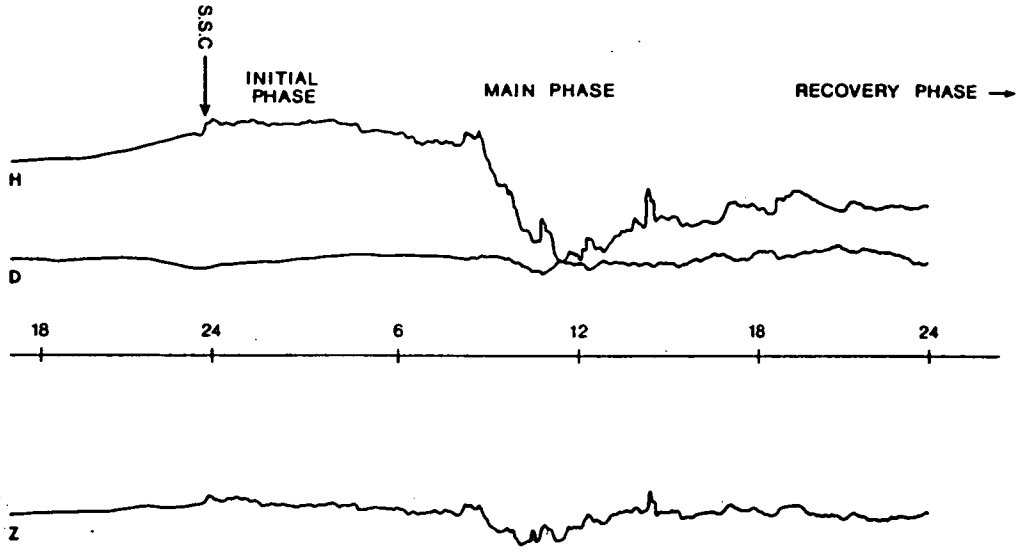

Figure IV.1. A sub storm magnetogram, covering 31 hours, showing the principal features of the storm (after Parkinson, 1983).

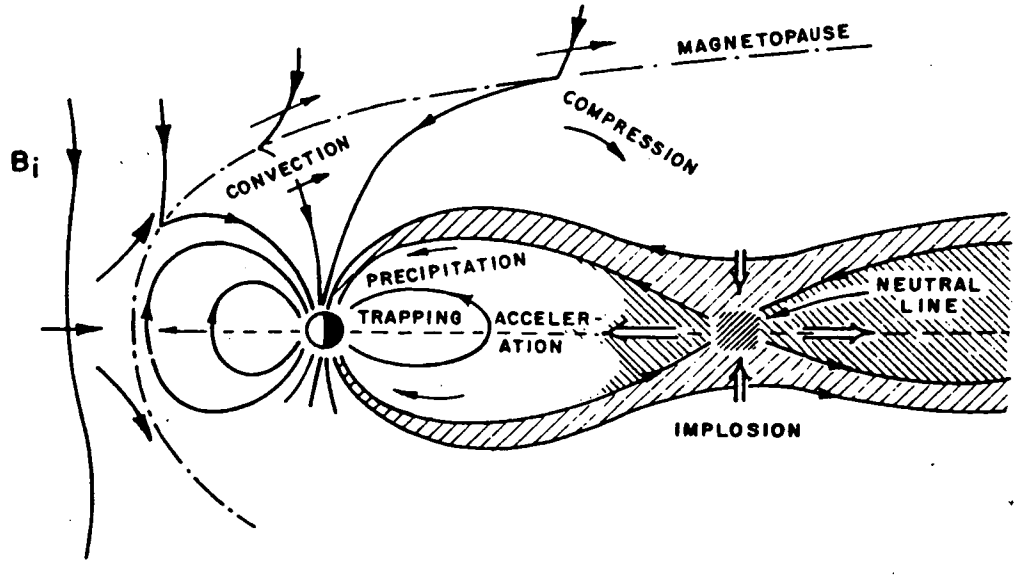

Figure IV.2. The open magnetosphere model showing the merging of field lines in the magneto-tail. This is one explanation for the initiation of substorm (after Roederer, 1977).

IV.3. Instrumentation and Procedure.

A successful magnetovariational survey is critically dependent on good instrumentation with the ability to record changes in the earth's magnetic field accurately. To this end, two three-component EDA FM100B fluxgate magnetometers were utilised for acquisition of 14 stations (see Figure I.1) of magnetovariational data in southeast Tasmania. These instruments are the same as those used for recording magnetotelluric data (see Chapter V.4). Most of the magnetovariational data were then collected together with the magnetotelluric data except for stations SNG,WDB, GDB, GLD, RMN and HTG. At these stations the data were collected with 30 second reading interval only.

Since the purpose of this magnetovariational observation is to study local subsurface conductivity distribution, the spacing of stations should be dense, with stations close together at approximately 10 km. The location of the stations was selected with care. They were distanced from man-made sources of magnetic variation fields to avoid data being contaminated and creating artificial anomalies.

IV.4. Data Reduction.

Since disturbances in the earth's magnetic field occur rarely, much of the collected data is unsuitable for analysis. Therefore the data must be scanned to find events which are large enough and in sufficient quantity to be analysed. This is done with the aid of program MTY3. This program reads the field cassette tapes and it displays the raw data on the computer screen. This analysis is only concerned with events that consist of three components, i.e. X (northward component), Y (eastward component), and Z (upward component) of the magnetic field and not the additional data containing two telluric field components. The process of linear interpolation was employed to remove unusable data and misreadings. This process links the points

adjacent to the data which is to be eliminated. Data from between 50 and 75 events were chosen for further analysis. These events contain slightly less than 512, 256, 128, and 64 consecutive readings. For a 30 second reading rate, for example, these numbers correspond to interval periods of approximately 240, 120, 60, 30 minutes respectively.

The next step of analysis involves the transformation of the time domain data into the frequency domain. The program PCMT23 (modified from programs EMMTEE3, TASIGMA1 and TASIGMA2) uses the fast Fourier transform algorithm which converts the time domain data selected from the above analysis (PCMT1) into the frequency domain. It also calculates every Fourier coefficient at various periods up to the 12th harmonic of data length. The final output of this program is the transfer functions which are used to determine the orientation and length of the induction vector. The computaion of A and B transfer functions will be discussed below.

IV.5. Transfer Function and Induction Vector Analysis.

The direction of horizontal field that correlates with maximum vertical field was first examined by Parkinson (1959,1962). This analysis was extended by the transfer function method of Schmucker (1970) in which the magnetic components are related by complex coefficients A and B. Additional work was done by Everett and Hyndman (1967) who proposed an induction ellipse which gives a measure of the two-dimensionality of the conductivity structure. A detailed review and unifying framework for the induction arrow presentation of magnetovariational results is given by Gregory and Lanzerotti (1980) and an important note about the phase required for quadrature induction arrow presentation is given by Lilley and Arora (1982).

Parkinson (1959) observed that geomagnetic variation with a period less than one hour tended to be confined to some preferred plane inclined at an angle θ with the horizontal. The projection of the normal to this plane in the horizontal direction may be plotted as a vector and is referred to as the Parkinson vector. The Parkinson vector, more recently described as the induction vector, is a fundamental and well established concept in the magnetovariational method (Parkinson, 1959, 1962, 1964, Everett and Hyndman, 1967, Schmucker, 1970).

The induction vector is a 2-D vector (A,B) where A and B are transfer functions describing the behaviour of the vertical component as a function of horizontal components. In this study the transfer functions at each station for various periods were calculated with the aid of program PCMT23 and based on the least-square method of Everett and Hyndman (1967).

A and B are defined by

$$Z = AX + BY \qquad \text{(IV.1)}$$

where:

X is the Fourier coefficient of the magnetic north component

Y is the Fourier coefficient of the magnetic east component

Z is the best estimate of the corresponding Fourier coefficient of the vertical component.

A and B are therefore frequency dependant complex numbers.

Moreover Parkinson (1983, pp. 332-333) calculates the A and B transfer functions using the following equation:

$$|\delta_j|^2 = (Z - AX - BY)(Z^* - A^*X^* - B^*Y^*) \qquad \text{(IV.2)}$$

where

δ_j is the difference between the LHS and RHS of equation (IV.1)

* denotes the complex conjugate.

After differentiating and minimizing $\Sigma \mid \delta_j \mid^2$ with respect to the in-phase and quadrature components of A and B this gives

$$A = \frac{\mid (X^*Z \times Y^*Y) \mid - \mid (Y^*Z \times X^*Y) \mid}{\mid (X^*X \times YY^*) \mid - \mid (XY^* \times X^*Y) \mid} \qquad \text{(IV.3)}$$

$$B = \frac{\mid (X^*X \times Y^*Z) \mid - \mid (XY^* \times X^*Z) \mid}{\mid (X^*X \times YY^*) \mid - \mid (XY^* \times X^*Y) \mid} \qquad \text{(IV.4)}$$

Parkinson (1983) mentioned that if there is a lateral change in the conductivity structure then the magnetic fields tend to follow the sloping interface near the lateral change, because there is a tendency for a time varying magnetic field to avoid a conductor. A point near the lateral change would experience a field with a vertical component correlated with horizontal component parallel to the gradient of conductivity. A map of induction vectors often indicates quite clearly the direction of gradient conductivity.

A and B can be used to determine separate real (in-phase) and quadrature (out-of-phase) induction vectors.

The real vector has azimuth and magnitude given by:

$$AR = \arctan Rl(B) / Rl(A) \qquad \text{(IV.5)}$$

$$MR = (Rl(A)^2 + Rl(B)^2)^{1/2} \qquad \text{(IV.6)}$$

The quadrature vector has azimuth and magnitude

$$AQ = \arctan Im(B) / Im(A) \qquad \text{(IV.7)}$$

$$MQ = (Im(A)^2 + Im(B)^2)^{1/2} \qquad \text{(IV.8)}$$

where the azimuth of the real and quadrature vectors, indicates the horizontal correlating positively with upward vertical change measured clockwise from magnetic north. The magnitude of the vectors indicates the ratio of vertical to horizontal components.

IV.6. Field Results.

The azimuth and magnitude of the induction vectors were calculated from equations IV.5, IV.6, IV.7 and IV.8 at periods of 4, 8,10,12, 16, 20, 32, 64 and 128 minutes. The vectors were plotted in Figures IV.3 to IV.11 with respect to true north. In-phase and quadrature vectors are denoted by solid and broken lines respectively. Since the magnetic declination or variation of the area is about 13.5° to the east of north for the Epoch 1970.0 (Journal ASEG, vol. 10, no.1, p. 139, 1979), all of the azimuth values have had 13.5° added to the east.

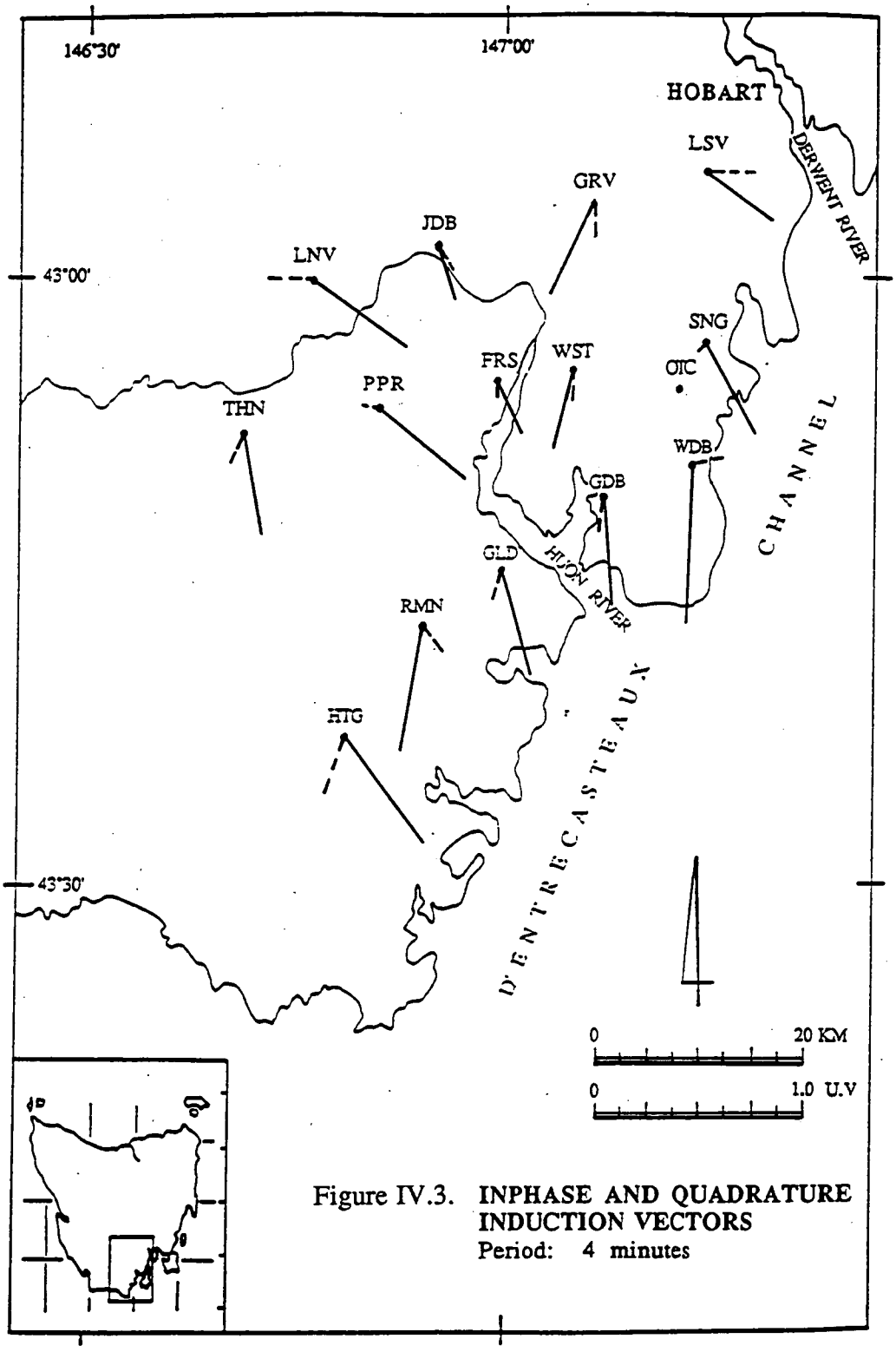

Figure IV.3. **INPHASE AND QUADRATURE INDUCTION VECTORS**
Period: 4 minutes

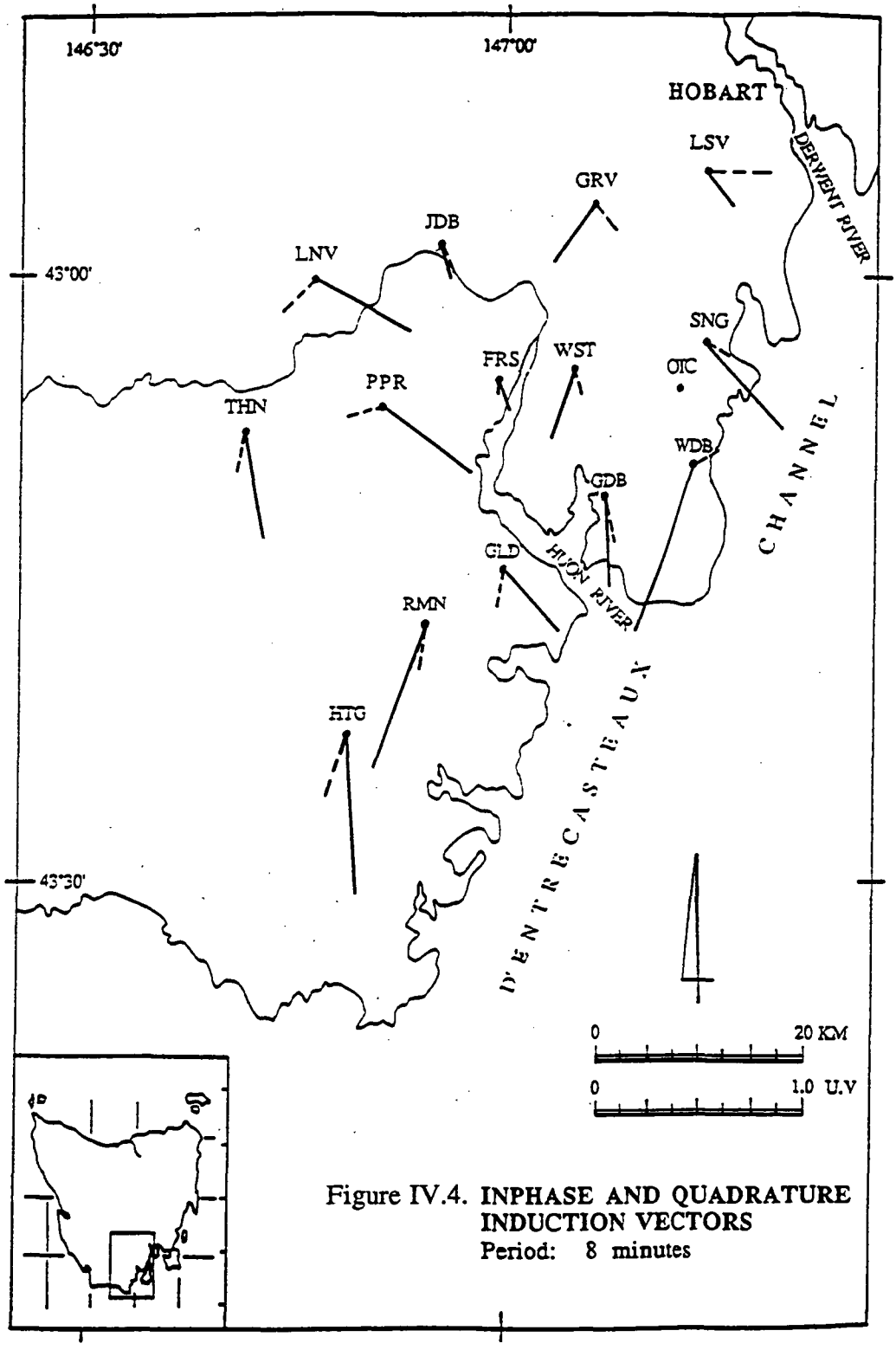

Figure IV.4. **INPHASE AND QUADRATURE INDUCTION VECTORS**
Period: 8 minutes

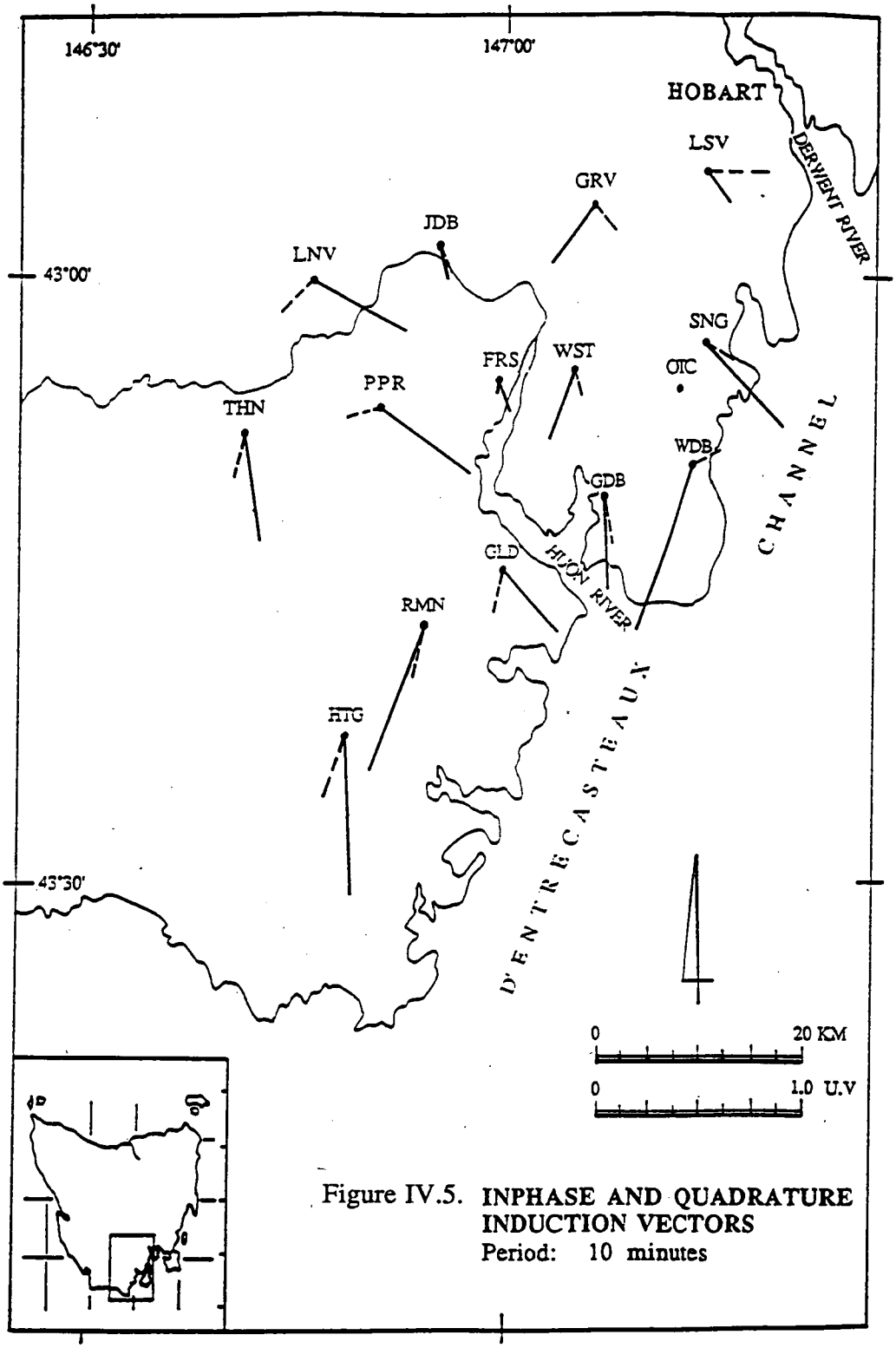

Figure IV.5. **INPHASE AND QUADRATURE INDUCTION VECTORS**
Period: 10 minutes

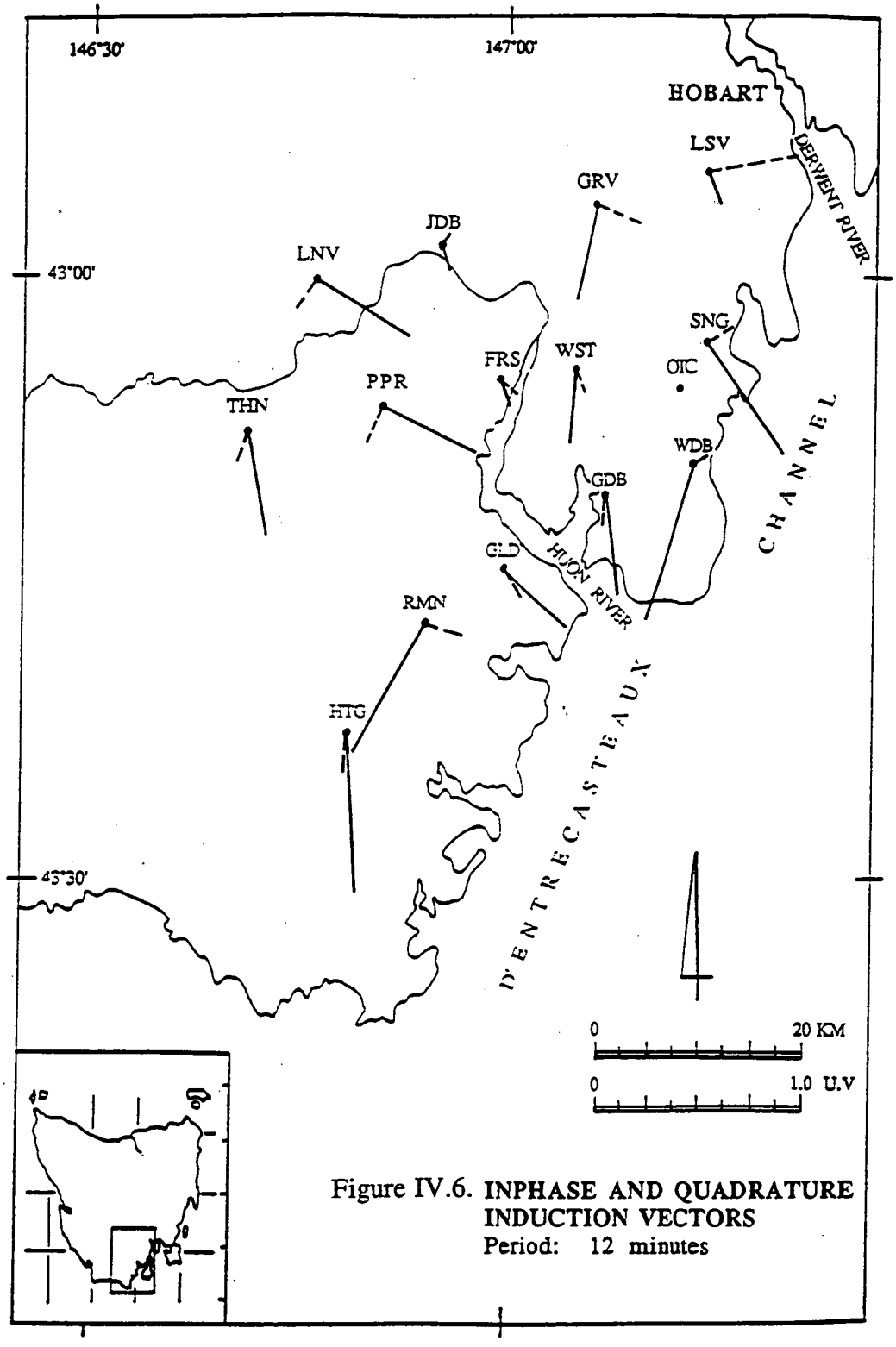

Figure IV.6. **INPHASE AND QUADRATURE INDUCTION VECTORS**
Period: 12 minutes

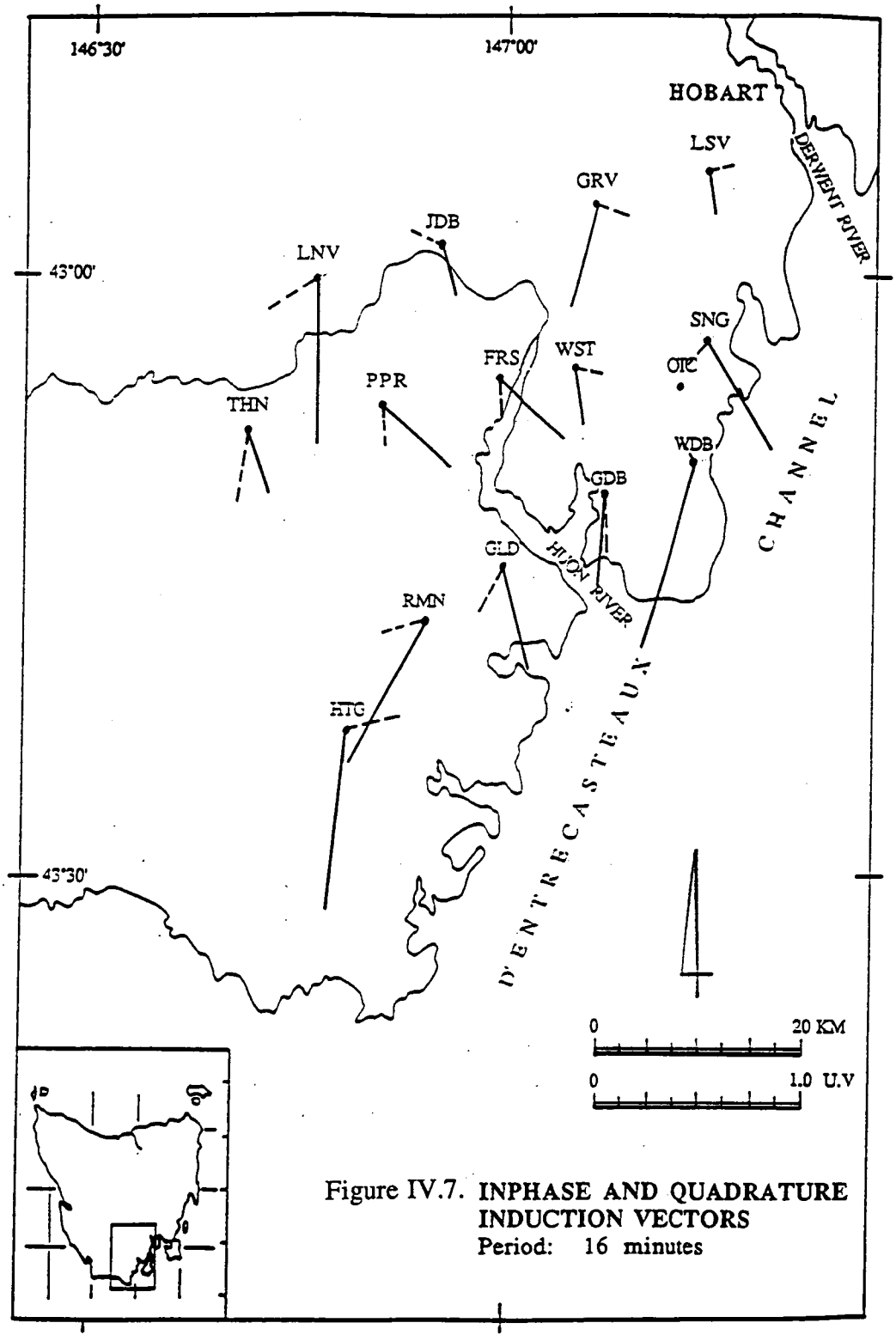

Figure IV.7. **INPHASE AND QUADRATURE INDUCTION VECTORS**
Period: 16 minutes

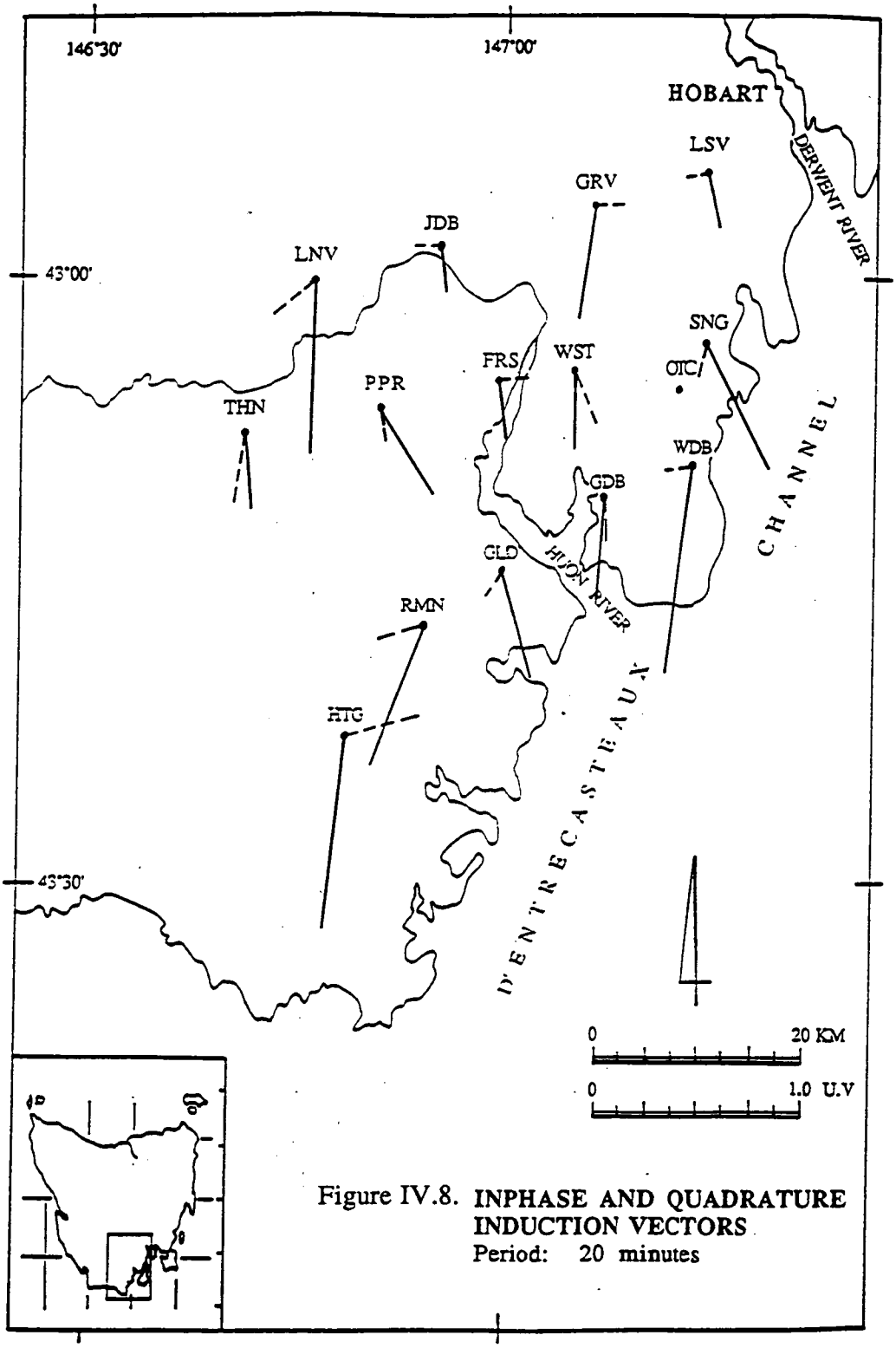

Figure IV.8. **INPHASE AND QUADRATURE INDUCTION VECTORS**
Period: 20 minutes

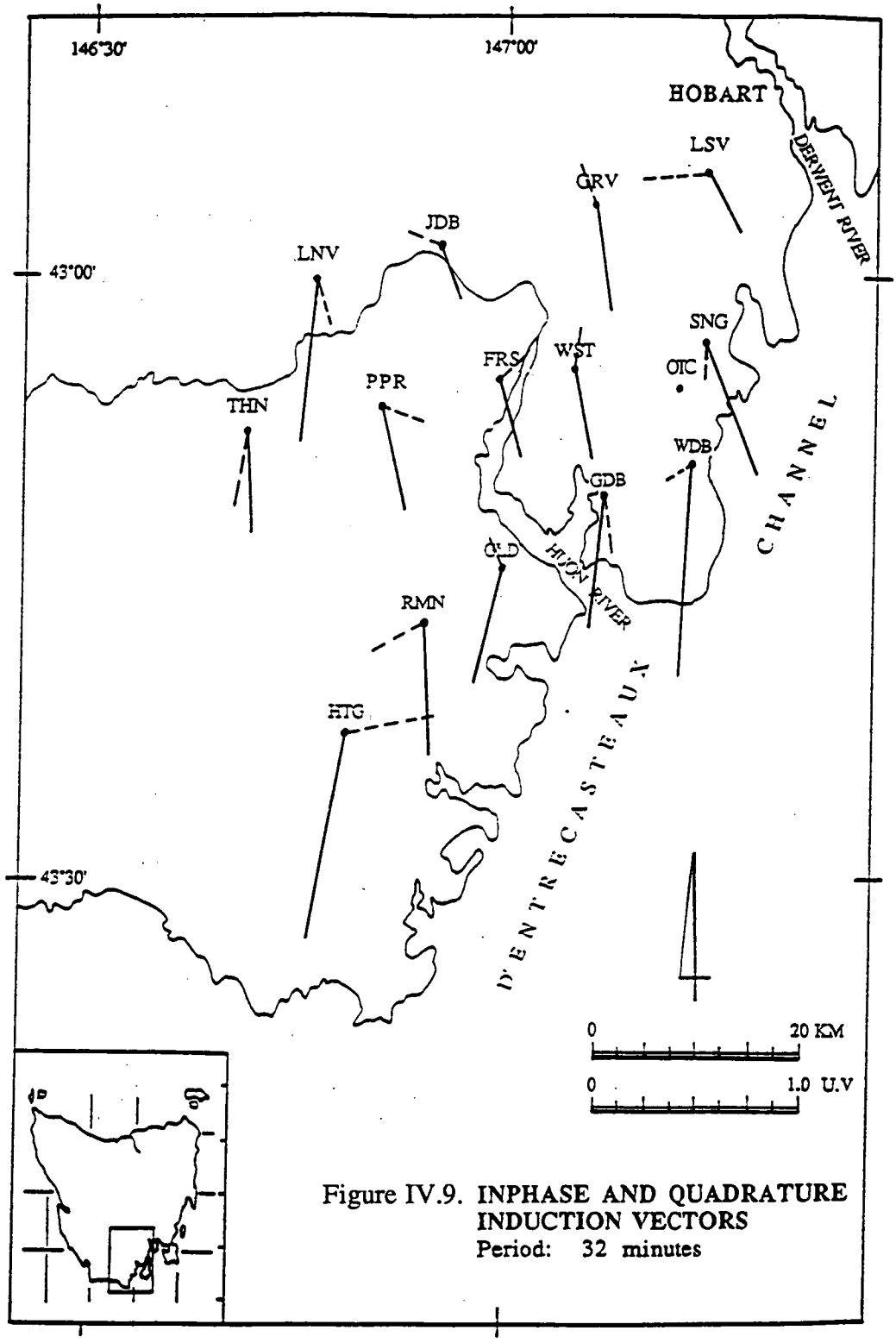

Figure IV.9. **INPHASE AND QUADRATURE INDUCTION VECTORS**
Period: 32 minutes

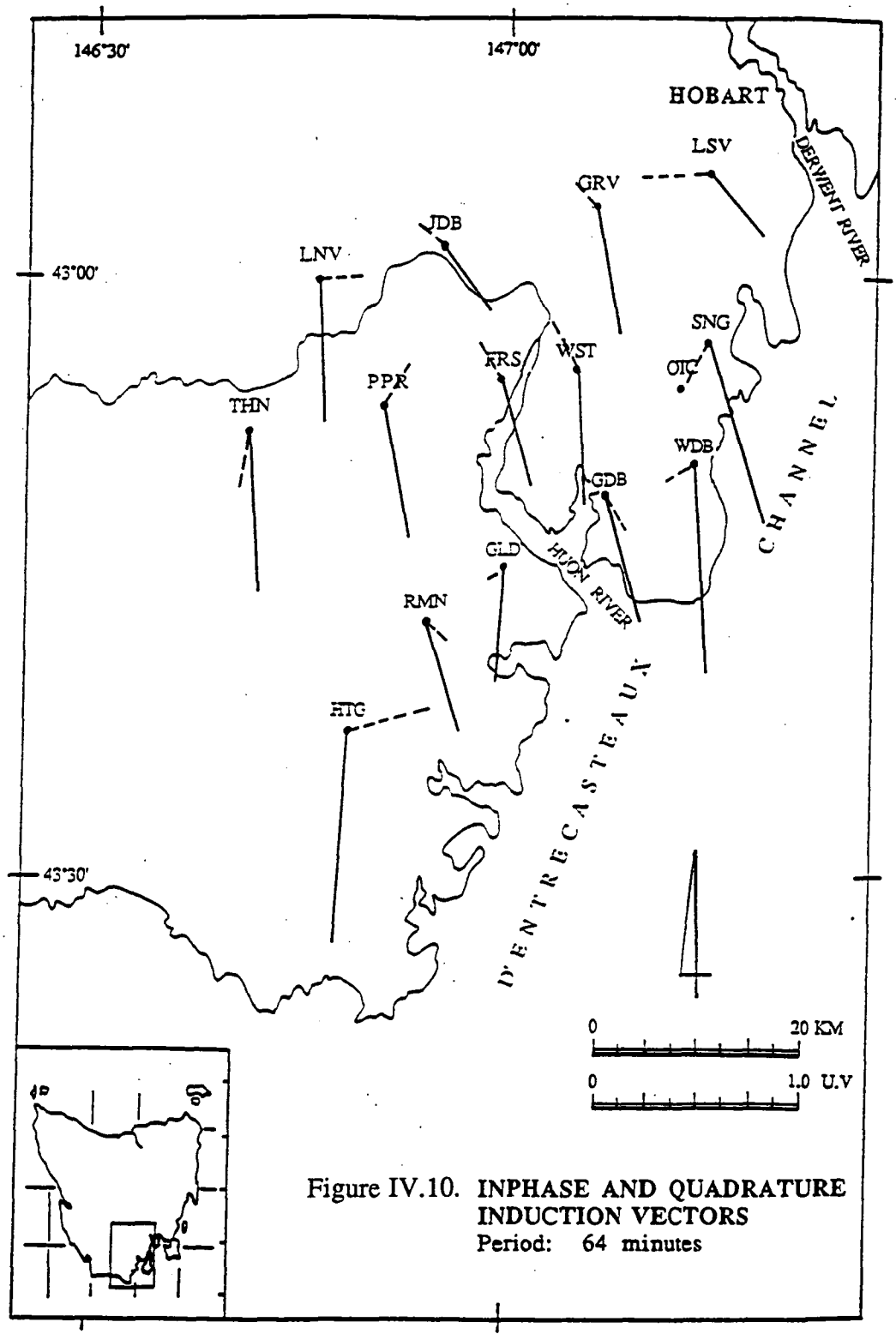

Figure IV.10. **INPHASE AND QUADRATURE INDUCTION VECTORS**
Period: 64 minutes

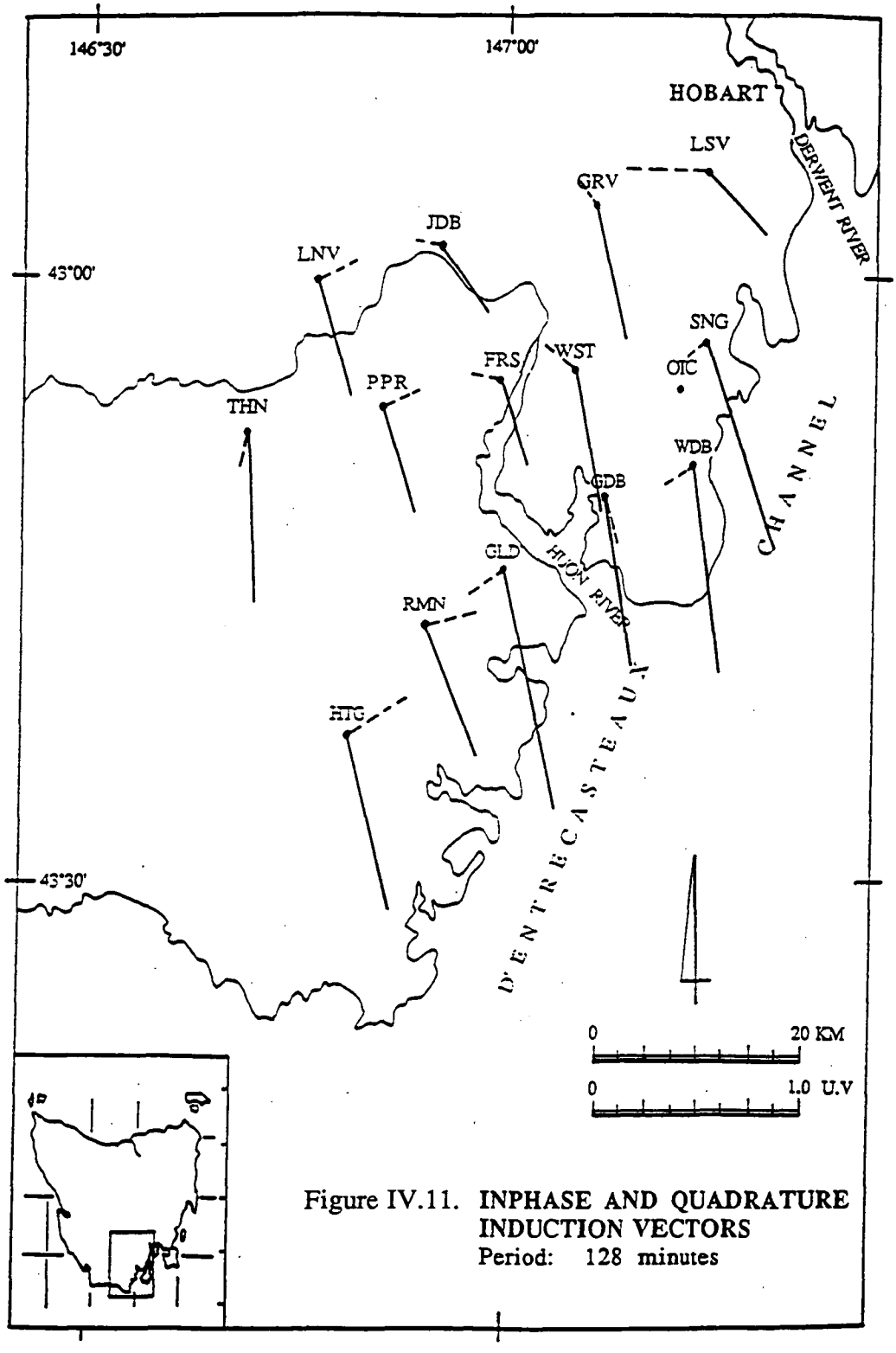

Figure IV.11. **INPHASE AND QUADRATURE INDUCTION VECTORS**
Period: 128 minutes

Some of the obvious characteristics of the in-phase and quadrature induction vectors can be summarised by inspecting Figures IV.3 to IV.11. Generally, the trends of the in-phase and quadrature vectors at period less than 20 minutes are very scattered especially the quadrature vectors. The scattering in orientation at short period is probably influenced by either a local anomaly or ocean effect. For periods longer than 20 minutes, however, the direction of the quadrature vectors remains scattered. Meanwhile the in-phase vectors pointing to south-southeast and south-southwest direction, become uniform to the southeast direction at periods longer than 64 minutes. The length of the vectors, especially the in-phase vectors, tends to increase with increasing period and appears to be at maximum at period 128 minutes. The lengths of the vectors coupled with the almost uniformity of the vectors' orientation at periods longer than 64 minutes indicates the strong effect of the ocean.

IV.7. Discussion.

As Tasmania is surrounded by deep ocean and Bass Strait (see Figure IV.12), the influence of these oceans will be considerable in any induction problem. The effect of the induced currents in the ocean on the magnetic field recorded at stations located near the coastline has been the subject of several experimental (Parkinson, 1962; Parkinson and Jones, 1979; Everett and Hyndman, 1967; Honkura, 1978) and theoretical (Ashour, 1965; Rikitake, 1961 and Roden, 1964) studies. The coastal effect for Tasmanian inland stations has been modelled at the University of Victoria, Canada, by Dosso et al. (1985). As can be seen in Figure IV.13, Dosso's analogue model study, the behaviour of the in-phase and quadrature vectors in the southern region, demonstrates the effect of the ocean on the in-phase vector for all periods and quadrature vector for longer periods. However, the removal of these effects from the field measurements may be part of the interpretation of a conductivity anomaly.

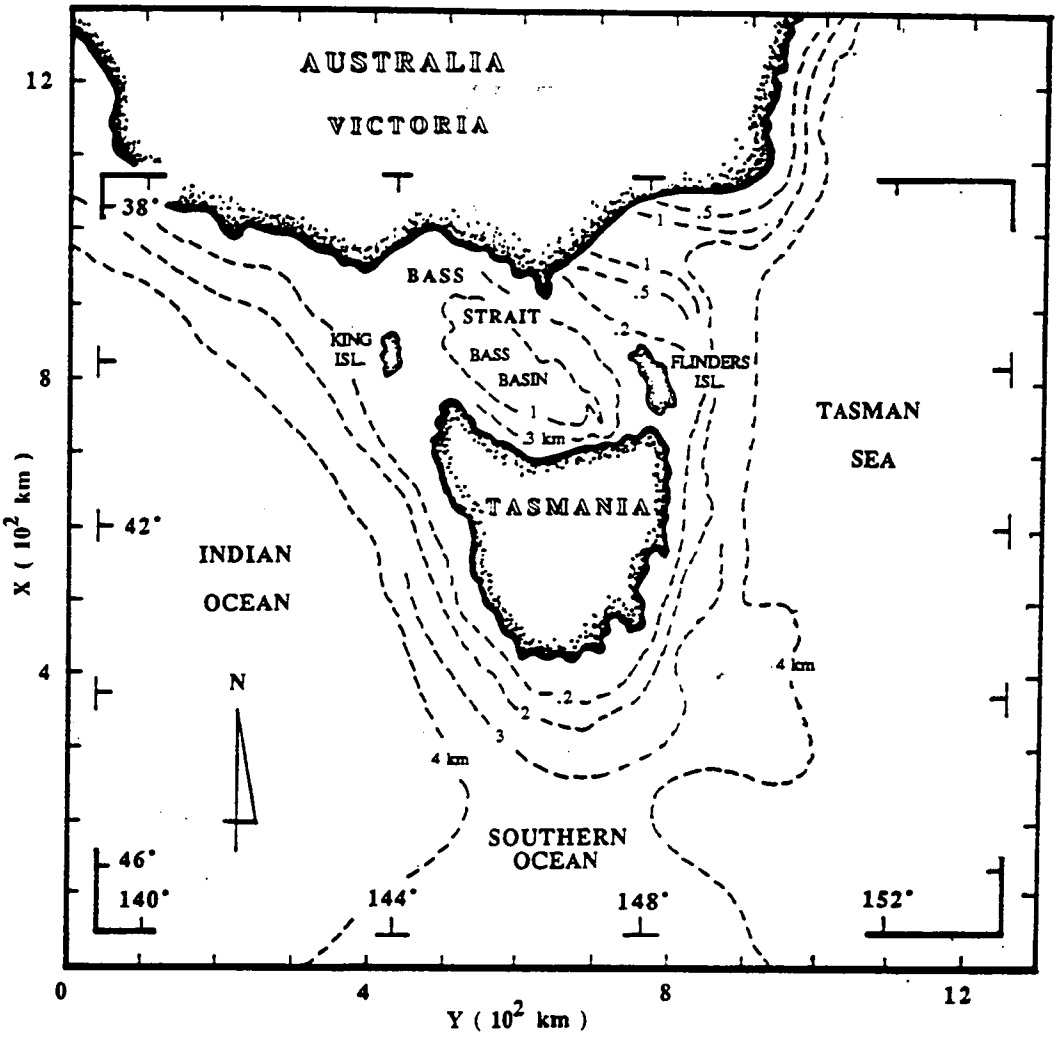

Figure IV.12. Geographical location of Tasmania showing bathymetric contours around the island.

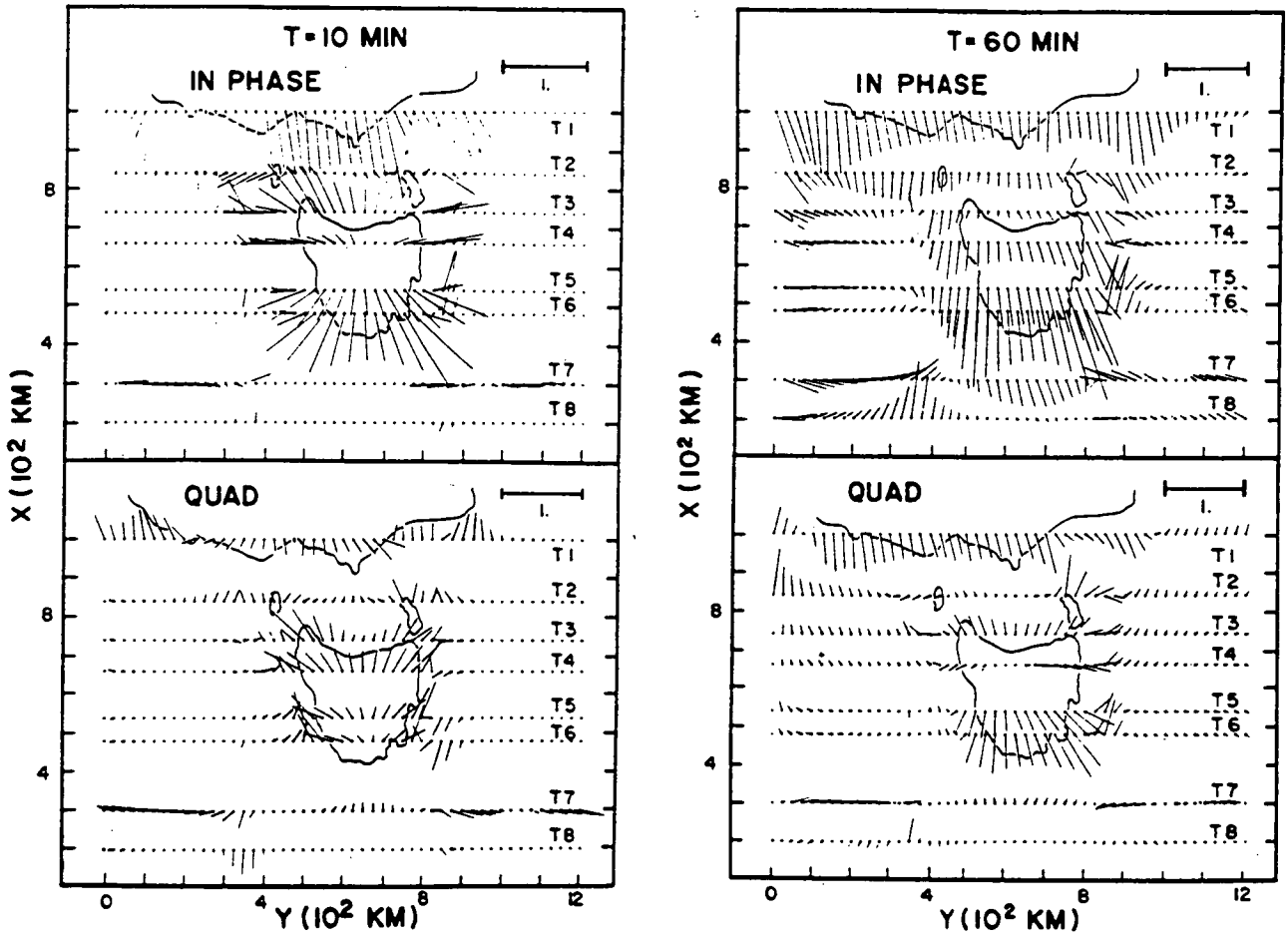

Figure IV.13. In-phase and quadrature vectors for 10 and 60 minutes periods derived from the analogue model study (after Parkinson, 1988).

The field results presented in section IV.6 take no account of the effect of the oceans surrounding Tasmania. To produce a more meaningful result and make use of the analogue model results (Figure IV.13), the correction for 10 and 60 minutes induction vectors was made by using the method described in Parkinson et al. (1988).

Parkinson et al. (1988) mention that for a two-dimensional body with the correct orientation of axes, equation (IV.1) becomes

$$Z = BY \qquad \text{(IV.9)}$$

The vertical component due to the induction in the oceans alone (Z_1) and the vertical component due to the conductor as well as the oceans (Z_2) are defined as

$$Z_1 = B_1 (Y_0 + Y_1) \qquad \text{IV.10)}$$

and

$$Z_2 = B_2 (Y_0 + Y_1 + Y_2) \qquad \text{(IV.11)}$$

where :

B_1 is the length of the vector derived from the analogue model along the raverse for the TE mode and perpendicular to the traverse for the TM mode.

B_2 is the length of the vector derived from the survey area along the traverse for the TE mode and perpendicular to the traverse for the TM mode.

Y_0 is the primary horizontal field taken from the two-dimensional model.

Y_1 is the induced horizontal field due to the oceans.

Y_2 is the induced horizontal field due to the conductor under the survey area.

The required transfer function, for interpretation, is the ratio of $(Z_2 - Z_1)$ to $(Y_0 + Y_2)$. Combining equations (IV.10) and (IV.11):

$$Z_2 - Z_1 = (B_2 - B_1)(Y_0 + Y_2) + (B_2 - B_1) Y_1 \qquad \text{(IV.12)}$$

Since the Y_1 obtained from the analogue model is small, the last term in equation (IV.12) can be neglected and the equation (IV.12) can be re-written to give

$$Z_2 - Z_1 = [B_2 - B_1 / (p + 1)] (Y_0 + Y_2) \qquad \text{(IV.13)}$$

where

$p = Y_2/Y_0$

The required transfer function is enclosed in square brackets.

Figure IV.14 is the corrected in-phase vectors at 10 minutes along which the two-dimensional modelling magnetotelluric data was made. As can be seen from Figures IV.3 to IV.11 the quadrature vectors in the study area are small and erratic, therefore the correction only applies to the in-phase vectors. Plot of the in-phase vectors in Figure IV.14 exhibits how the oceans influence the vertical component in the magnetovariational method. It is apparent from this figure that the corrected vectors have a different direction from that of observed vectors. For example, the corrected vector at SNG is shorter than the observed vector and pointing east, almost perpendicular to the coast line. This sign could be considered as due to an excess coast effect. This effect is probably either due to the conductivity contrast between the rocks beneath the continents and ocean (Parkinson and Jones, 1979). On the other hand, at others stations the corrected vectors point in northeast and northwest directions. The most interesting feature is the corrected vectors at GRV and WST to the east of the Huon river, which point in different directions from those in the west, i.e. LNV and PPR. The convergence of these directions at this period suggests that the better conductor lies along the Houn river at shallow depth.

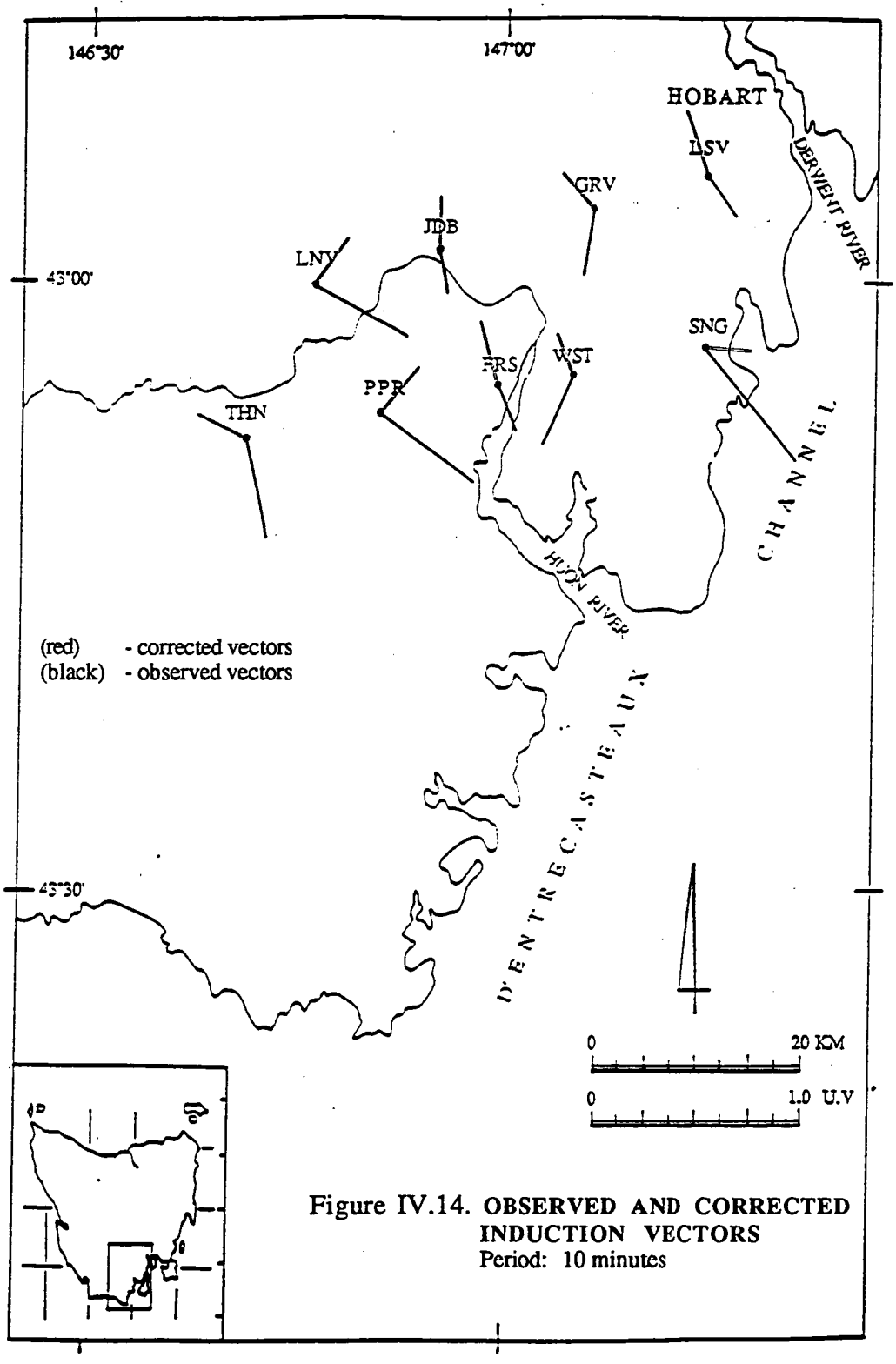

Figure IV.14. **OBSERVED AND CORRECTED INDUCTION VECTORS**
Period: 10 minutes

Figure IV.15 shows the corrected in-phase vectors at period of 60 seconds. Generally, the orientation of the corrected vectors at almost all of the stations at this period is distributed uniformly to the southwest direction. The length of the corrected vectors is much less than that of the observed vectors at all stations. The very short corrected vectors obtained at this period suggest that the deep conductor, described in Chapter VII, is more or less uniform over the whole area.

To obtain more specific information about particular stations it is now necessary to examine the magnetotelluric results.

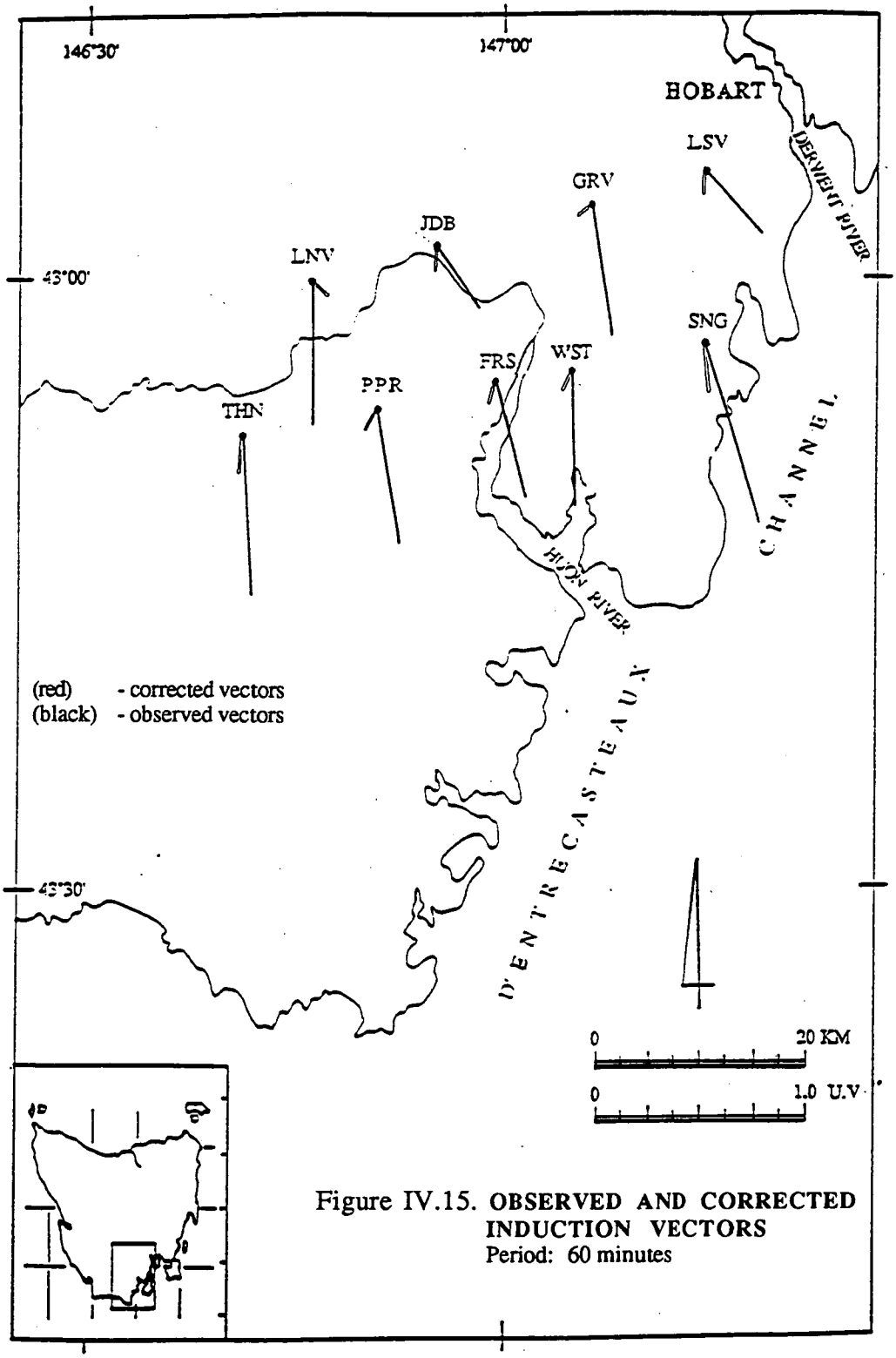

Figure IV.15. **OBSERVED AND CORRECTED INDUCTION VECTORS**
Period: 60 minutes

Chapter V.
MAGNETOTELLURIC METHOD.

V.1. Introduction.

The magnetotelluric method is now being used widely for determining the electrical substructure of the earth. In practice, this is done by recording two horizontal, orthogonal components of the earth's magnetic field and two mutually perpendicular components of the earth's electric field (tellurics). Magnetotelluric sounding theory is frequently expressed in terms of concepts drawn from wave propagation theory and transmission line analogies. Before discussion about the specification of the model (section V.3), the source and transmission of the electromagnetic field utilized must be reviewed.

V.2. Origin and Propagation of Electromagnetic Field.

The magnetotelluric method is a passive geophysical technique that utilizes the naturally occurring fluctuations of the earth's geomagnetic field as its signal sources. The frequencies of electromagnetic fields typically used are between 10^{-5} and 10^{2} Hz. Fields recorded above 1 Hz are generally produced by worldwide thunderstorm activity or cultural noise; fields below 1 Hz are generally produced by current flow in the ionized layers surrounding the earth (Keller and Frischknecht, 1966; Parkinson, 1983). Whatever the source, it is assumed that the incident electromagnetic fields are in the form of vertically propagating plane waves, with orthogonal electric (E) and magnetic (H) components. Horizontal variation in these fields, due to limited spatial dimensions of the source, must be small over a lateral

distance comparable to skin depth (discussed below) in the earth, at the frequency concerned (Word et al., 1971). Figure V.1 and V.2 show the propagation of electromagnetic waves through a homogeneous and layered earth respectively with significant attenuation occurring within the conductive layers.

Upon striking the earth's surface, most of the incident energy of the electromagnetic fields is reflected. The small portion of energy transmitted travels vertically downward. As the wave propagates into the earth, the amplitude of E and H fields is reduced. The depth at which the fields have fallen to 1/e (37%) of their values at the surface is called the skin depth (δ). The skin depth for a plane wave in an homogeneous medium is given by:

$$\delta = \left(\frac{2.\rho}{\omega\mu} \right)^{1/2} \qquad (V.1)$$

where δ is in metres, ω is the angular frequency of an electromagnetic wave in radians/sec., ρ is the resistivity in Ohm-m of the medium through which the wave is diffusing, and μ is the magnetic permeability of the medium in Henrys/m (H/m) (Cagniard, 1953). The magnetic permeability is generally taken to be that of free space: $\mu_0 = 4\pi \times 10^{-7}$ H/m. Equation (V.1) relates the frequency of the propagating field to its depth of penetration. Therefore, the skin depth is often used as a criterion for the depth of investigation.

If the electromagnetic fields encounter any conductivity contrast, the following boundary conditions are imposed (Swift, 1967; Rankin, 1962):

1. The electric field tangential to the interface is continuous.
2. The magnetic field tangential to the interface is continuous.
3. The difference in the current density across (normal to) the interface is equal to the time rate of change of the surface charge density on the interface. The surface charge density is usually considered to be constant and the normal current density to be continuous.
4. The magnetic flux normal to the interface is continuous.

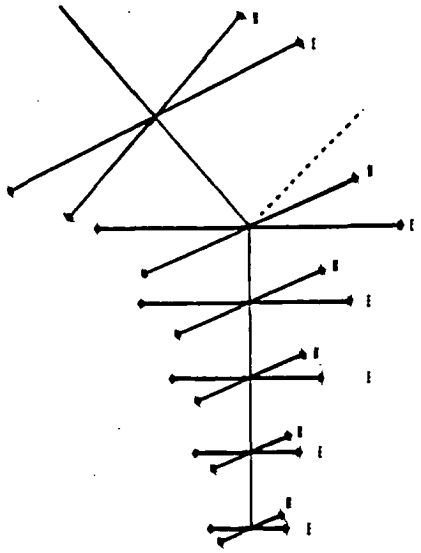

Figure V.1.
Propagation of an electromagnetic wave (rectangular vectors E and H) through a homogeneous earth. (After Waeselynck, 1974)

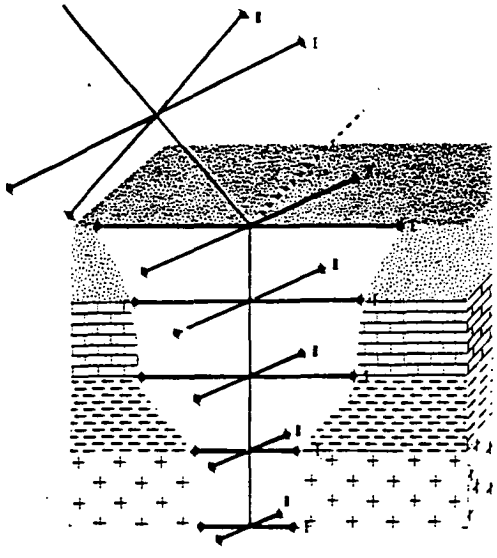

Figure V.2.
Propagation of an electromagnetic wave through a layered earth. (After Waeselynck, 1974).

For the last condition, it is generally assumed that the magnetic permeability within the earth is homogeneous. Therefore, the boundary condition is equivalent to the magnetic field across the interface being continuous.

V.3. The Earth's Dimensionality.

Dimensionality of the earth must be determined for proper interpretation of magnetotelluric data. Three-dimensional earth geometries interpreted using 1- or 2-D techniques will lead, in many cases, to erroneous results. The same is true for 2-D geometries interpreted using 1-D theory. In the following pages a summary of 1- and 2-D magnetotelluric theory is presented. The identification of the electric and magnetic fields as vector quantities is assumed, and no symbols are used to mark them as such. Furthermore, a coordinate system at the earth's surface with the x axis being positive north; y, positive east; and z, positive down, is assumed.

V.3.1. The one-dimensional earth.

For a 1-D earth or one where we consider the conductivity to vary only with depth, with the electric field propagating perpendicular to the magnetic field, we define a quantity called the impedance as:

$$Z_{xy} = \frac{E_x}{H_y} \qquad (V.2)$$

where Z_{xy} is the impedance in Ohms, E_x is the Fourier transform of the electric field along the x axis in volts/meter (V/m), and H_y is the magnetic field along the y axis in amperes/m (A/m). The impedance can be thought of as a complex scalar transfer function. For particular frequency, it linearly relates an electric field component to its orthogonal magnetic component, i.e.:

$$E_x = Z_{xy} H_y \qquad (V.3)$$

or

$$E_y = Z_{yx} H_x \qquad (V.4)$$

Furthermore, because of the symmetry, the impedance for a layered earth does not depend on the orientation of the measuring axes at the earth's surface. So in this case $Z_{xy} = - Z_{yx}$.

The apparent resistivity of the earth is related to the characteristic impedance through the relation:

$$\rho_{xy} = .2\, T\, |Z_{xy}|^2 \qquad (V.5)$$

where ρ_{xy} is in Ohm-meters, T is the period of the electromagnetic wave in seconds, and Z_{xy} the impedance in (millivolts/km)/nanoteslas. The quantity is real, being dependent on the ratios of the amplitudes of the E and H fields. Since the impedance in a 1-D case is invariant for all orientations of the measuring axes, so is the apparent resistivity.

The impedance phase is derived from the characteristic impedance through the relation:

$$\theta_{xy} = \arctan\left(\frac{\text{im } Z_{xy}}{\text{re } Z_{xy}}\right) \qquad (V.6)$$

where θ is in degrees and im Z_{xy} and re Z_{xy} represent the imaginary and real parts of the complex impedance. The phase represents the lag of the magnetic field with respect to the electric field. In homogeneous earth, the phase lag is -45° for all frequencies. In layered earth, the phase varies with the conductivity of the earth's layers encountered. The phase decreases toward 0° if the impedance increases with period. Phases out of the range of 90° to -90° are not possible in a 1-D earth (Hermance, 1973).

V.3.2. The two-dimensional earth.

So far the discussion has been limited to the electromagnetic response of a horizontally layered earth in which each horizontal layer is homogeneous and isotropic. However, this model is not sufficient to describe many real earth situations. In many cases, the earth has lateral changes in conductivity or the layers may be anisotropic in the horizontal plane. The anisotropy may be due to the banded nature of the rocks or to geological structures. Lateral changes in conductivity may be due to faults, continent-ocean contacts, grabens filled with conducting sediment, etc.

V.3.2.1. The impedance tensor.

If the earth's structure is 2-D, defined as one where the conductivity varies in two directions, one of which is vertical, the coupling of the electric and magnetic fields is more complicated than for a layered earth. For example, near a lateral conductivity contrast, the electric fields may be strongly distorted (Hermance, 1973). In this case, the electric field is generally locally polarized at some angle other than 90° to the regional magnetic field. Therefore, each component of the electric field is coupled to both components of the magnetic field (Hermance, 1973). This can be represented by the following equations:

$$E_x = Z_{xx} H_x + Z_{xy} H_y \qquad (V.7)$$

$$E_y = Z_{yx} H_x + Z_{yy} H_y \qquad (V.8)$$

These equations can be written in matrix notation as

$$\begin{vmatrix} E_x \\ E_y \end{vmatrix} = \begin{vmatrix} Z_{xx} & Z_{xy} \\ Z_{yx} & Z_{yy} \end{vmatrix} \begin{vmatrix} H_x \\ H_y \end{vmatrix} \qquad (V.9)$$

or

$$|E| = |Z|\,|H| \tag{V.10}$$

where

$$|Z| = \begin{vmatrix} Z_{xx} & Z_{xy} \\ Z_{yx} & Z_{yy} \end{vmatrix} \tag{V.11}$$

The dyadic Z is termed the impedance tensor. The elements of Z represent coupling coefficients. They are complex, because the electric and magnetic fields are not in temporal phase. Their values are dependent on frequency, and on both the geometry and electrical properties of the conductive inhomogeneity. The elements of the impedance tensor are found by solving equation (V.7) and (V.8).

If the pair H_x and H_y are used, four equations can be developed from equation (V.7) and (V.8):

$$\overline{E_x H_x^*} = Z_{xx}\,\overline{H_x\,H_x^*} + Z_{xy}\,\overline{H_y\,H_x^*} \tag{V.12}$$

$$\overline{E_x H_y^*} = Z_{xx}\,\overline{H_x\,H_y^*} + Z_{xy}\,\overline{H_y\,H_y^*} \tag{V.13}$$

$$\overline{E_y H_x^*} = Z_{yx}\,\overline{H_x\,H_x^*} + Z_{yy}\,\overline{H_y\,H_x^*} \tag{V.14}$$

$$\overline{E_y H_y^*} = Z_{yx}\,\overline{H_x\,H_y^*} + Z_{yy}\,\overline{H_y\,H_y^*} \tag{V.15}$$

The bar represents the band average of the auto-power (i.e., $H_x\ H^*_x$) and the crosspower (i.e., $E_x\ H^*_y$) spectra of the fields beneath. The auto-power and crosspowers spectra are the Fourier transforms of the auto-correlations and cross correlations of the fields in the time domain.

Band averaging takes advantage of the fact that the impedance values vary slowly with frequency. The equations (V.12) - (V.15), therefore can be computed at far fewer frequencies than there are Fourier transform values (frequency values) of the field components (Vozoff, 1972). The auto-power and crosspowers may be taken as averages over some finite bandwidth. This is usually accomplished by passing averaging windows of constant Q through the resultant auto-power and crosspower spectra (Gamble et al., 1979). Q is a term used to describe the sharpness of a filter. It represents the ratio of the midpoint frequency to the bandpass.

It is interesting to note the behaviour of the impedance elements in relation to the earth's geometry as the tensor is rotated. For a one-dimensional earth, these are invariants. In other words for all θ

$$Z_{xy} - Z_{yx} = 0 \qquad \text{(V.16)}$$

$$Z_{xx} = Z_{yy} = 0 \qquad \text{(V.17)}$$

For a two-dimensional earth the impedance values vary with the angle of rotation. For all θ

$$Z_{xy} - Z_{yx} = \text{constant} \qquad \text{(V.18)}$$

$$Z_{xx} + Z_{yy} = 0 \qquad \text{(V.19)}$$

For a three-dimensional earth, the impedance elements also vary with the angle of rotation. For all θ

$$Z_{xy} - Z_{yx} = \text{constant} \qquad \text{(V.20)}$$

$$Z_{xx} + Z_{yy} = \text{constant} \qquad \text{(V.21)}$$

Therefore, the behaviour of the elements of the impedance tensor as they are rotated can test the dimensionality of the earth over which the data were collected.

V.3.2.2. Coherency.

To test the degree of independence of the pair of the measured fields H_x, H_y, E_x, E_y, the ordinary coherency of the fields is calculated (Reddy and Rankin, 1974; Reddy et al., 1976). The ordinary coherency of two functions X and Y is defined in terms of their spectra as

$$\text{coh}\ (X, Y) = \frac{\left| (X\ Y^*) \right|}{\left| (X\ X^*)\ (Y\ Y^*) \right|^{1/2}} \qquad \text{(V.22)}$$

where ( ) indicates a sum either over events or frequency bands, and the variables with the superscript * are complex conjugates. For example, the coherency of H_x and H_y is

$$\text{coh}\ (H_x, H_y) = \frac{\left| (H_x\ H^*_y) \right|}{\left| (H_x\ H^*_x)\ (H_y\ H^*_y) \right|^{1/2}} \qquad \text{(V.23)}$$

If the coherency is equal to 1, the functions are linearly dependent, and if equal to zero they are completely independent (uncorrelated).

V.3.2.3. Reliability.

After the estimates of the elements of the impedance tensor have been achieved, their reliability is tested. The coherency between the predicted and observed electric fields is calculated. This is referred to as the E predictability. The predicted value of the coherency between E_x and $E_x^{\text{predicted}}$ is calculated (Swift, 1967) as

$$\text{coh}\left(E_x, E_x^{\text{pred.}}\right) = \frac{|H_x| Z_{xx} \text{coh}(H_x E_x) + |H_y| Z_{xy} \text{coh}(H_y E_x)}{\left[|Z_{xx}|^2 |H_x|^2 + |Z_{xy}|^2 |H_y|^2 + 2|H_x||H_y| \text{Re}(Z_{xx} Z_{xy} \text{coh}\, H_x H_y)\right]^{\frac{1}{2}}} \quad \text{(V.24)}$$

Similarly, the coherency between E_y and $E_y^{\text{predicted}}$ can be estimated from:

$$\text{coh}\left(E_y, E_y^{\text{pred.}}\right) = \frac{|H_x| Z_{yx} \text{coh}(H_x E_y) + |H_y| Z_{yy} \text{coh}(H_y E_y)}{\left[|Z_{yx}|^2 |H_x|^2 + |Z_{yy}|^2 |H_y|^2 + 2|H_x||H_y| \text{Re}(Z_{yx} Z_{yy} \text{coh}\, H_x H_y)\right]^{\frac{1}{2}}} \quad \text{(V.25)}$$

The higher the coherency of the E predictabilities, the lower the noise content in the observed E and H fields. With less noise, the impedance tensor elements are less distorted (Boehl et al., 1977). Generally, impedances with a predictability of 0.9 or above are highly acceptable for interpretation. In this study, E predictabilities as low as 0.8 were used.

V.3.2.4. Principal direction.

Once the elements of Z have been calculated, they are rotated into the principal directions. In the principal directions, the measuring axes are parallel and perpendicular to the strike of a 2-D conductivity inhomogeneity. For a strictly 2-D geometry, with the measuring axes in the principal directions, Maxwell's equations separate into two modes. One mode, E parallel to strike, depends only on H perpendicular to strike, and the other mode, E perpendicular to strike depends only on H parallel to strike (Hermance, 1973).

Equations (V.7) and (V.8) become

$$E'_x = Z'_{xy} H'_y \tag{V.26}$$

$$E'_y = Z'_{yx} H'_x \tag{V.27}$$

where the prime indicates an orientation of the measuring axes in the principal directions. In this orientation, Z_{xx} and Z_{yy} are 0. Generally, however, the measuring axes are not in the principal directions. In this case, the principal directions are found by mathematically rotating the impedance tensor. The rotation is accomplished by the following equation:

$$Z' = \beta Z \beta^T \tag{V.28}$$

where

$$\beta = \begin{bmatrix} \cos\theta & \sin\theta \\ -\sin\theta & \cos\theta \end{bmatrix} \tag{V.29}$$

β^T is the transpose of β, and θ is the angle of rotation. For a truly two-dimensional earth, the tensor is rotated until the off-diagonal elements are both zero.

Generally, however, the earth is imperfectly two-dimensional. With rotation of the impedance tensor, the magnitude of $Z_{xx}^2 + Z_{yy}^2$ only passes through a non-zero minimum. In this case the principal directions are usually defined as either the minimum of

$$\left| Z'^2_{xx} + Z'^2_{yy} \right| \tag{V.30}$$

or the maximum of

$$\left| Z'^2_{xy} + Z'^2_{yx} \right| . \tag{V.31}$$

The rotation angle , θ, thus

$$4\,\theta_0 = \arctan \left| \frac{(Z_{xx} - Z_{yy})(Z_{xy} + Z_{yx})^* + (Z_{xx} - Z_{yy})^*(Z_{xy} + Z_{yx})}{|Z_{xx} - Z_{yy}|^2 - |Z_{xy} + Z_{yx}|^2} \right| \quad \text{(V.32)}$$

where * is a complex conjugate, Zxx, Zxy, Zyx and Zyy are unrotated tensor impedances (Madden and Swift 1969, Jupp and Vozoff 1989).

If one wishes to determine which is the major axis, one must calculate $|Z'_{xy}|^2 + |Z'_{yx}|^2$ for θ_0 and $\theta_0 + 45°$ to determine the large value.

The above outline of theory represents general published treatments. In this study we develop a new method of the rotation of coordinates in magnetotelluric analysis (Parkinson et al., 1992) and describe it in some detail in the following section.

V.3.2.5. A New Rotation Angle and Dimensionality Calculation Method.

This section discusses an alternative treatment that has some interesting features. The magnetic and electric field vectors are expressed in terms of some cartesian coordinate systems (see Figure V.3), usually magnetic north (X) and east (Y). Let OX,OY be the axes relative to which measured values are obtained (it is assumed that the electric field coordinates have already been rotated into coincidence with those of the magnetic field) and OX',OY' the axes parallel and perpendicular to the strike of the structure. θ is the angle, clockwise, through which OX must be rotated to coincide with OX'. Then the field coordinates relative to OX,OY can be expressed by

$$F_x = F'_x \cos\theta - F'_y \sin\theta \qquad (V.33)$$

$$F_y = F'_x \sin\theta + F'_y \cos\theta \qquad (V.34)$$

where primes indicate coordinates relative to OX',OY'.

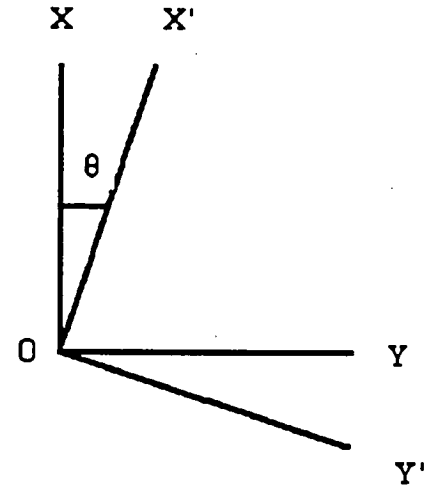

Figure V.3. X - Y and X' - Y' coordinate system.

Substitution of similar expressions for the coordinates of E and H into (V.33 and V.34) leads to

$$E'_x = H'_x [Z_{xx} \cos^2\theta + (Z_{xy}+Z_{yx}) \sin\theta \cos\theta + Z_{yy} \sin^2\theta] + H'_y [Z_{xy} \cos^2\theta - (Z_{xx}-Z_{yy}) \sin\theta \cos\theta - Z_{yx} \sin^2\theta] \qquad (V.35$$

$$E'y = H'_x [Z_{yx} \cos^2\theta - (Z_{xx}-Z_{yy}) \sin\theta \cos\theta - Zxy \sin^2\theta] + H'_y [Z_{yy} \cos^2\theta - (Z_{xy}+Z_{yx}) \sin\theta \cos\theta + Z_{xx} \sin^2\theta] \qquad (V.36)$$

the elements of the rotated tensor being the expressions in square brackets. The required rotation angle is the one that makes both Z'_{xx} and Z'_{yy} vanish. Consider first Z'_{xx}. It will be zero if

$$Z'_{xx} \cos^2\theta + (Z_{xy}+Z_{yx}) \sin\theta \cos\theta + Z_{yy} \sin^2\theta = 0 \qquad (V.37)$$

Dividing by $\cos^2\theta$ leads to a quadratic equation in tan θ with solutions

$$\tan\theta_x = \frac{\left(-S + \sqrt{S^2 - 4Z_{xx}Z_{yy}}\right)}{2Z_{yy}} \qquad (V.38)$$

$$\tan\theta_x = \frac{\left(-S - \sqrt{S^2 - 4Z_{xx}Z_{yy}}\right)}{2Z_{yy}} \qquad (V.39)$$

where $S = Z_{xy} + Z_{yx}$. A similar treatment of Z'_{yy} leads to

$$\tan\theta_y = \frac{\left(S - \sqrt{S^2 - 4Z_{xx}Z_{yy}}\right)}{2Z_{xx}} \qquad (V.40)$$

$$\tan\theta_y = \frac{\left(S + \sqrt{S^2 - 4Z_{xx}Z_{yy}}\right)}{2Z_{xx}} \qquad (V.41)$$

Synthetic data was used to calculate these theta and found that for a truly two dimensional structure tan θ becomes real. An examination of these formulae indicates which root should be used. Consider (V.38) in the case where $Z_{xx} = 0$, $Z_{yy} \neq 0$. Clearly $\theta_x = 0$ is the required solution. This is obtained when the square root is taken with the same sign as S. Similarly if $Z_{xx} \neq 0$, $Z_{yy} = 0$, (V.40) gives $\theta_y = 0$ if the square root is in the same quadrant as S. All variables in these equations are complex but the physical angle through which the observed coordinates should be rotated is given by the real part of the tan θ. Average of θ_x in equation (V.38) and θ_y in equation (V.40) determines rotation angle (θ) and should rotate the observed coordinates into the direction of maximum current flow. Calculation of rotation angle (θ) using real and imaginary part separately should be avoided as the term under the square root is not a linear equation.

Parkinson et al. (1992) state that the other roots are not invalid. There is an interesting relation between (V.38) and (V.41). Take the same sign in each and multiply the solutions together (writing R for the square root)

$$\tan \theta_x \tan \theta_y = \frac{(R - S)(R + S)}{(4 Z_{xx} Z_{yy})} = -1 \qquad (V.42)$$

showing that

$$\theta_x - \theta_y = \pi / 2 \qquad (V.43)$$

It can be shown that the angles have opposite signs, so $| \theta_x |$ and $| \theta_y |$ are complementary angles. The sign of S depends on which principal direction corresponds to a higher current flow.

If the structure is completely two-dimensional, then $\theta_x = \pi/2 + \theta_y$. This is obvious from the vanishing of $Z_{xx} + Z_{yy}$, but this is unusual. The difference between θ_x in equation (V.38) and θ_y in equation (V.40) indicates a measure of how closely the structure approximates to two dimensions. The rotation angle (θ) should be plotted only for the difference between θ_x in equation (V.38) and θ_y in equation (V.40) within $\pm$ 20° (Parkinson, personal communication). If the difference is greater than $\pm$ 20° rotation angle (θ) does not mean anything as it may not represent two-dimensionality of the structure. In other words, the closer the difference to zero degrees the better the approximation to two-dimensionality.

The relation between this difference and the skew is critically dependent on the amount of asymmetry, i.e. the ratio of Z'_{xy} to Z'_{yx}. If this is close to one (an approximation to one-dimensionality) very large differences are found for quite small skew. A ratio of 2 in the impedances gives a difference of 10° for a skew of 0.06 whereas for a ratio of 5 the same difference occurs for a skew of 0.1.

The above treatment can be applied to either the real or imaginary parts of the vectors. However, if the imaginary part of the impedance elements is large, it should

be applied with caution, because the real part of E could be strongly affected by the quadrature part of H.

V.3.2.6. The skew and ellipticity.

The commonly used parameter for determining the dimensionality of the earth is the impedance skew. The skew is a measure of how well the diagonal elements of the impedance tensor are minimized. It therefore indicates how well the observed data meet the criterion necessary to assume a 2-D environment. Swift (1967) defines the skew as

$$\text{SKEW} = \frac{Z_{xx} + Z_{yy}}{Z_{xy} - Z_{yx}} \qquad \text{(V.44)}$$

While there is no set acceptable upper value for SKEW, it is generally agreed that the skew must equal zero for the earth to be truly 1- or 2-D. In this study, data with skew values of 0.5 or less are considered to suggest a 1- or 2-D earth.

Another parameter identifying the earth geometry is the ellipticity. The ellipticity (τ) is defined as (Word et al., 1971)

$$\tau = \frac{(Z'_{xx} - Z'_{yy})}{(Z'_{xy} + Z'_{yx})} \qquad \text{(V.45)}$$

where the prime indicates values of the impedance tensor once it has been rotated to the principal directions. In general, the ellipticity is real for a 2-D earth and complex for a 3-D earth (Word et al., 1971). The condition of both the ellipticity at the principal direction and the skew being zero is a necessary and sufficient condition for identification of a 2-D earth (Word et al., 1971).

In three-dimensional basin structures there is no simple correlation between the degree of distortion in earth response function due to three-dimensional structure

and the magnitude of skew or ellipticity (Hermance, 1982). Skew was thus used only in a qualitative manner for this study.

V.3.2.7. The resistivity.

Once the impedance tensor has been rotated into the principal directions, a pair of apparent resistivities can be calculated. They are

$$\rho'_{xy} = .2\,T\,|Z'_{xy}|^2 \qquad (V.46)$$

$$\rho'_{yx} = .2\,T\,|Z'_{yx}|^2 \qquad (V.47)$$

where T is the period in seconds, Z' the impedance in (millivolts/km)/nanotesla, and ρ is in ohm-m. If the strike of the resistivity inhomogeneity is along the x axis, then the resistivity ρ_{xy} applies to the transverse electric mode, and ρ_{yx} to the transverse magnetic mode. The associated phases (θ) are

$$\theta_{xy} = \arctan \frac{\mathrm{Im}\,(Z_{xy})}{\mathrm{Re}\,(Z_{xy})} \qquad (V.48)$$

$$\theta_{yx} = \arctan \frac{\mathrm{Im}\,(Z_{yx})}{\mathrm{Re}\,(Z_{yx})} \qquad (V.49)$$

In this study the apparent resistivities are, in the normal way, plotted on log-log scale against period, and may be compared with the resistivities obtained from a calculated model. The plotted rotated apparent resistivities may yield the same value as the resistivities based on the model under consideration at all periods. The calculation of a one-dimensional model here was based on the algorithm of Schmucker (1970). While a two-dimensional model was calculated using a program based on Jones and Pascoe (1971) and Pascoe and Jones (1972).

V.3.2.8. The tipper.

When the impedance elements have been rotated into the principal directions, the strike and dip with respect to Z_{xy} or Z_{yx} still must be determined. To resolve this ambiguity, a parameter called the tipper is used. The tipper defines the geoelectric axis in the vicinity of magnetotelluric sounding. It makes use of the correlation between the vertical and horizontal components of the magnetic field. In defining the tipper, a linear relation between the magnetic components is assumed

$$H_z = A H_x + B H_y \qquad (V.50)$$

where A and B are complex coupling coefficients. The coefficients are found in a similar fashion to the elements of the impedance tensor. By multiplying equation (III.37) by the complex conjugate of H_x and H_y, two equations are formed:

$$\overline{H_z H_x^*} = A \overline{H_x H_x^*} + B \overline{H_y H_x^*} \qquad (V.51)$$

$$\overline{H_z H_y^*} = A \overline{H_x H_y^*} + B \overline{H_y H_y^*} \qquad (V.52)$$

These equations can be solved for the coefficients A and B. The resultant equations are

$$A = \frac{\overline{H_x H_x^*}\ \overline{H_z H_x^*} - \overline{H_y H_x^*}\ \overline{H_z H_y^*}}{\overline{H_y H_y^*}\ \overline{H_x H_x^*} - \overline{H_y H_x^*}\ \overline{H_x H_y^*}} \qquad (V.53)$$

$$B = \frac{\overline{H_x H_y^*}\ \overline{H_z H_x^*} - \overline{H_x H_x^*}\ \overline{H_z H_y^*}}{\overline{H_y H_x^*}\ \overline{H_x H_y^*} - \overline{H_x H_x^*}\ \overline{H_y H_y^*}} \qquad (V.54)$$

The pair of coefficients can be thought of as operating on the horizontal magnetic field and tipping part of it into the vertical (Vozoff, 1972). The magnitude of the tipper is defined as

$$| T | = | A^2 + B^2 |^{1/2} \qquad \text{(V.55)}$$

The magnitude of T gives the relative strength of H_Z. The phase of the tipper ($T\phi$) is defined as

$$T\phi = \frac{(A_{re}^2 + A_{im}^2) \arctan (A_{im}/A_{re}) + (B_{re}^2 + B_{im}^2) \arctan (B_{im}/B_{re})}{| T |^2} \qquad \text{(V.56)}$$

where im and re represent the imaginary and real parts of the variable they subscript, and | T | is the magnitude of the tipper (Jupp and Vozoff, 1976). Both the tipper phase and magnitude are invariant with rotation.

For a 2-D structure and noise-free data, A and B will have the same phase. The ratio of B to A will be a real number and define an angle from the x-axis to the tipped horizontal component of the magnetic field (Vozoff, 1972). This angle is given by

$$\phi = \arctan \frac{B}{A} \qquad \text{(V.57)}$$

The angle essentially defines the dip direction. By definition of the dip, the strike is found by adding or subtracting 90° to ϕ. ϕ is useful because the phase difference between H_Z and H_ϕ can give the bearing to certain structures such as dikes. The difference between ϕ and the principal axes also gives a qualitative measure of three-dimensionality.

Tipper skew is the angular difference between the horizontal bearing whose component magnetic field is most coherent with $Im(H_Z)$ and the horizontal component most coherent with $Re(H_Z)$. Therefore, tipper skew may be biased by coherent noise

such as lightning (Rokitiyansky, 1982). Tipper skew is zero for two-dimensional structures and is given by Jupp and Vozoff (1976) as:

$$\gamma = 2T^{-2} [\, \mathrm{Re}(A)\,\mathrm{Im}(B) - \mathrm{Im}(A)\,\mathrm{Re}(B) \,] \qquad \text{(V.58)}$$

The reliability of the value of H_z used in tipper skew calculations may be estimated from the coherence between measured and calculated H_z,

$$\mathrm{Coh}\left[H_z^{meas.}, H_z^{calc.} \right] = \frac{A^* \left\langle H_x H_x^* \right\rangle + B^* \left\langle H_x H_y^* \right\rangle}{\left\langle H_z H_x^* \right\rangle^{1/2} \left[AA^* \left\langle H_x H_x^* \right\rangle + BB^* \left\langle H_y H_y^* \right\rangle \right]^{1/2}} \qquad \text{(V.59)}$$

The tipper azimuth is a marginally less stable indicator of strike direction than the principal axes (Jones and Vozoff, 1978).

V.3.2.9. Induction arrow.

The Schmucker induction arrows V_r and V_i (Schmucker, 1970) are related to the inductive transfer functions (tipper coefficient) A and B by:

$$V_r = \left[\mathrm{Re}^2(A(\omega)) + \mathrm{Re}^2(B(\omega)) \right]^{1/2} \arctan \frac{-\mathrm{Re}(B(\omega))}{\mathrm{Re}(A(\omega))}, \qquad \text{(VI.60)}$$

$$V_i = \left[\mathrm{Im}^2(A(\omega)) + \mathrm{Im}^2(B(\omega)) \right]^{1/2} \arctan \frac{-\mathrm{Im}(B(\omega))}{\mathrm{Im}(A(\omega))}. \qquad \text{(VI.61)}$$

The induction arrow definitions preferred in this study (see Chapter IV) follow Parkinson's convention (Parkinson, 1962) which gives results known as Parkinson's arrows. These induction arrows have a more obvious physical meaning

than either tipper or the Schmucker induction arrows and are easier to calculate. They represent the real and imaginary parts of the ratio of H_Z to the total magnetic field component in the plane normal to strike.

V.4. Equipment and Survey Procedures.

V.4.1. Introduction.

Two three-components EDA FM-100B fluxgate magnetometers (called EDA.I and EDA.II) were utilized for the acquisition of the magnetotelluric data at 9 stations in the southeast of Tasmania (See Figure I.2). The magnetotelluric recording system, developed by the Geology Department, is a revision of a previous system which suffered from excessive digitally generated system noise and was hampered by the lack of high frequency data (Bindoff, 1983). The unit is designed to sample both magnetotelluric and magnetovariational data and is fully microprocessor controlled with real time clock sampling initiation. Seven channels are digitally sampled to 12 bit precision using sampling periods from 60 to 0.2 seconds. The processor automatically switches sample periods and anti-aliasing filters to acquire samples at the specified sample period. A record consists of 1024 samples of each channel and is permanently stored on magnetic cassette tapes.

Seven channels are used in slow recording mode to sample the three magnetic components (called Hx,Hy,Hz) two temperatures (internal, external) and two electric components (Ex,Ey) which are necessary for three-dimensional recording. Provision is also made for sampling five channels only if desired. In this fast memory mode internal and external temperatures are not acquired. The main difference in the display of the two modes of recording lies in the capability of the analog to digital converter (ADC) in the recording unit. The ADC converts data of up to seven channels in the slow mode and only five channels in fast mode. Figure V.4 is a block diagram of the instrument.

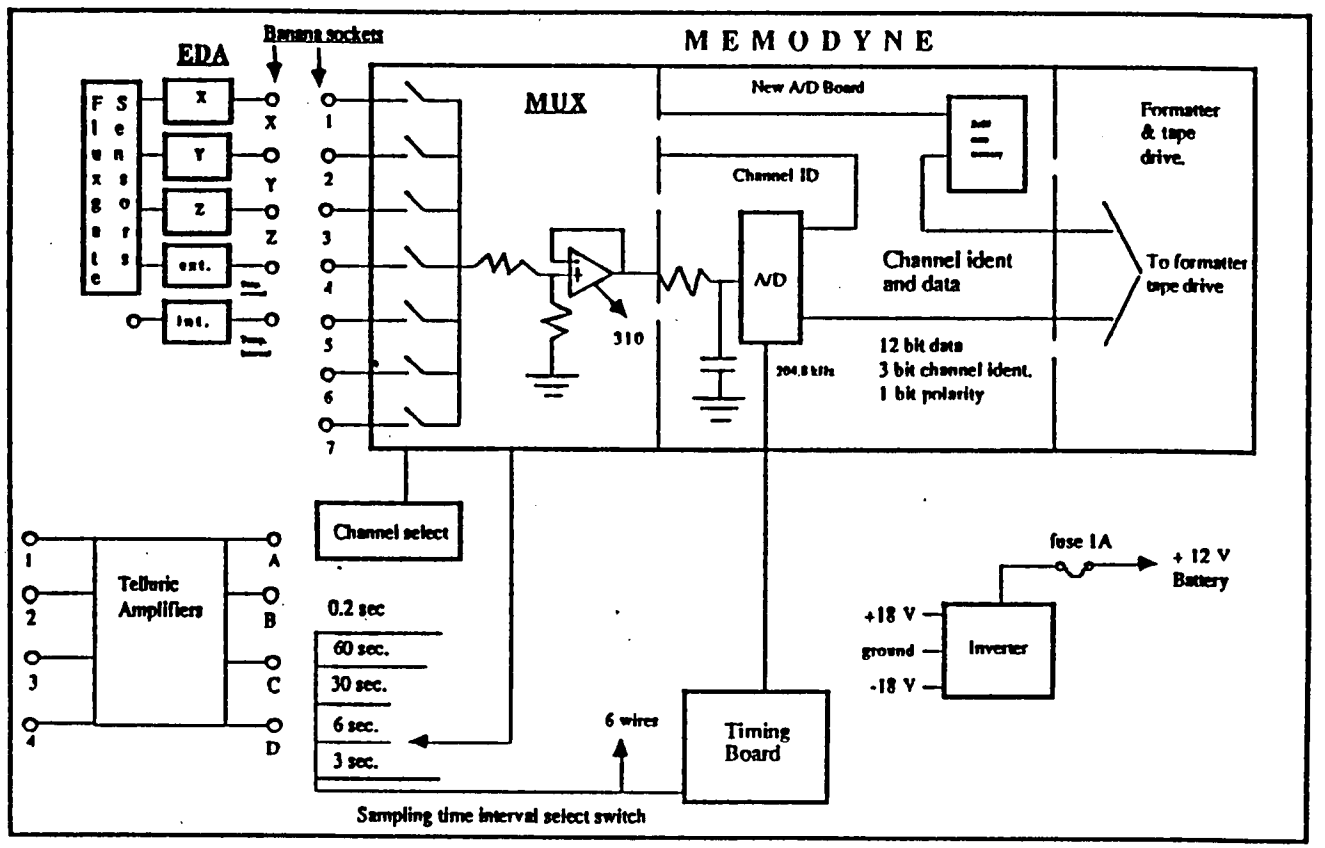

Figure V.4. Block diagram of EDA FM-1000B Fluxgate magnetometer.

V.4.2. Field equipment used.

The field equipment was designed for reliability and ease of operation. Low power and light weight were of particular importance. This was achieved to the extent that simultaneous magnetotelluric recordings by each instrument were made at two sites per month with only one operator.

Data were collected on cassette tapes by a digital Memodyne tape unit then transferred to a floppy disk via a personal computer with the aid of the "READ1" program. The data were then displayed and read and the presence of excessive noise could be determined. This was used to decide if continued site occupation was needed. The recorded data were later stored in binary format on double-density, double-sided floppy disk for further processing.

Each site required the deployment of the following equipment :

* A set of fluxgate magnetometers consisting of three magnetic components and 30 meters interconnecting cable.
* Three electrodes (two remote plus one central), together with a set of two electric field wires, each 200 meters long.
* A recording system consisting of all the signal processing, control circuitry and a Memodyne digital cassette together with a power supply.

The power supply consisted of one 100 amp-hour battery and 37 watt solar cell array. The average recording system power consumption was 4.8 watts. The recording system with batteries occupied a space 75 cm by 40 cm by 25 cm (See Figure V.5).

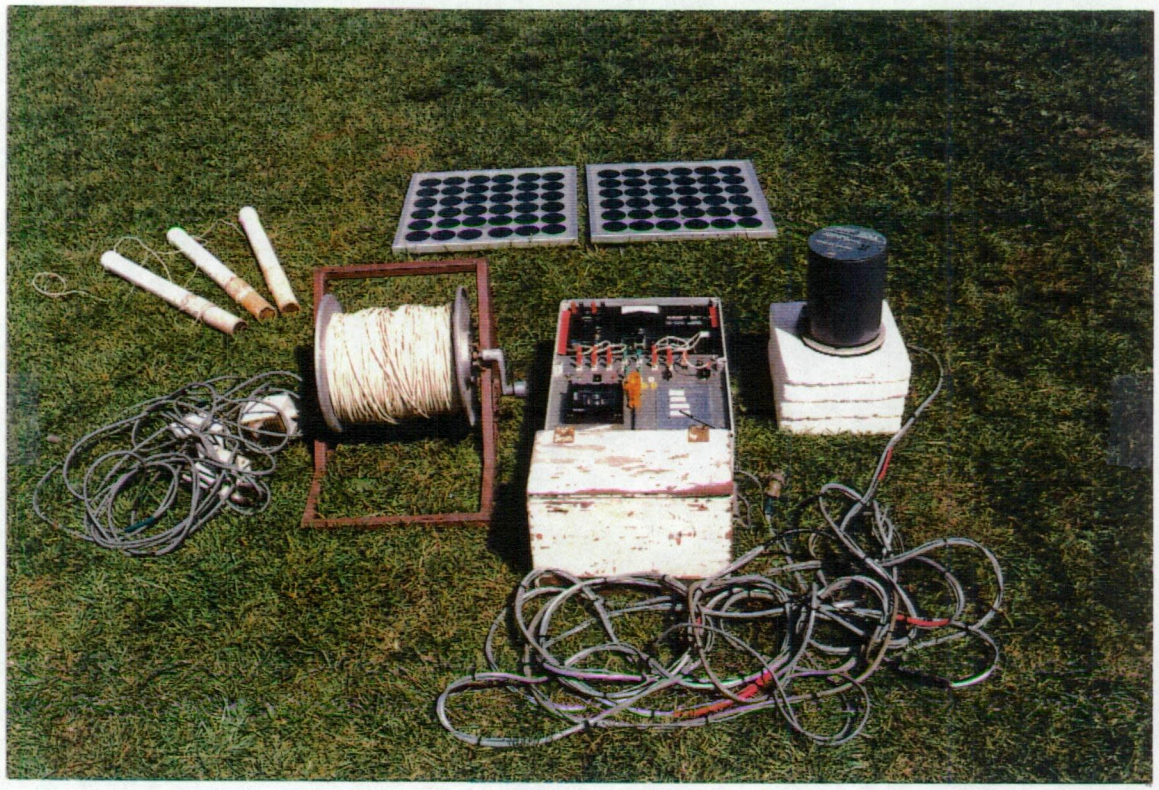

Figure V.5. The magnetotelluric equipment.

V.4.2.1. Equipment design philosophy.

The design of the recording system can be conveniently considered in relation to the electronic circuit designs and the recording playback software. Features to be taken account of for the design of the complete recording system include:

* A requirement for low power consumption in order to obviate the need for a generator power source with the inherent noise and transportation problems.
* Interface facilities to enable data to be transferred to a personal computer.
* An accurate interval timer to ensure a stable data sampling rate.
* Light weight and small physical size.
* A simple and flexible operation, particularly in the field.

V.4.2.2. Logistics.

The deployment of equipment in field situations required planning, particularly when making simultaneous site recordings. In practice both of the magnetometers were operated at 0.2, 0.5, 3, 6 and 30 seconds reading intervals. Consequently, each station had to be occupied for at least 15 days. For example, using a 120 minutes cassette, a recording at 30 seconds takes approximately 10 days to complete. To maintain the continuity of recording, it is necessary to keep the battery fully charged by the aid of a solar panel (See Figure V.5). In Tasmania, to get the maximum sunlight the solar panel is set facing north at a vertical angle of 45 degrees. During winter the battery is changed at least every five days. For shorter reading intervals (0.2, 0.5 and 3 seconds) stations were erected in the afternoon, operated at night and dismantled in the morning.

The two electric lines were laid north-south, east-west (magnetic) from the recording system with the two extreme ends electrically connected to the soil.

Magnetic and electric field sensors were aligned parallel and perpendicular to magnetic north to within ± 1°.

V.4.3. Survey procedure.

To use the magnetotelluric technique for geophysical prospecting, the ratio of the horizontal electric field in the ground to orthogonal horizontal magnetic field, must be measured accurately over a number of frequencies. By selecting an appropriate frequency range, shallow as well as deep structure can be investigated.

When recording the natural electromagnetic field strength, the signal level may vary considerably from day to day, or even from hour to hour. Therefore, the recording system requires a large dynamic range to cope with these changes, and it must be sensitive enough to obtain satisfactory data.

V.4.3.1. The electric field sensors.

The horizontal electric field components were measured with 150 metre long dipoles arranged in an L-shaped array, with one arm in the north - south direction whenever possible at each site and electrically connected to the soil at the extreme ends. The connection points to the ground are implanted non-polarisable Pb-$PbCl_2$ type electrodes.

Non-polarising electrodes were selected because they are more stable over long periods, less sensitive to temperature effects and have low noise characteristics compared with metallic stakes or sheets in the anticipated frequency range (Petiau and Dupis,1980). The electrodes were buried 50 - 60 centimetres below the surface and it was often necessary to wet the ground with salt water around the electrodes to ensure good contact with the soil. If the soil is dry, the circuit resistance through the electrode is increased.

The wires were loosely strung on the ground with rocks or soil placed on them at irregular intervals and pegged at each end. This reduces the risk of wind generated signals (due to wire movement) to a minimum.

The placement of electrodes is important because the surface conductivities may not be uniform on a scale of the same order as the electrode spacing. The sites were tested by four distant electrodes, a short and long line in each of the two directions. The short line should be about half the length of the long line. A site is satisfactory if the signal from the short line is a duplicate at half amplitude of the signal from the long line. If a site is satisfactory only the long lines need be used for magnetotelluric recording. The location of the electrodes must then be surveyed, since the line length must be known to calculate the electric field. An electric field component can be calculated from the relations:

$$E_X = \Delta V_X/\text{length} \qquad \text{(V.62)}$$

Equation (V.62) assumes that the surface is laterally homogeneous in the neighbourhood of the particular site. In inhomogeneous terrains it is more desirable to use an X-shaped electrode configuration to minimise the distortions caused by shallow surface inhomogeneities to the measured electric field (Swift, 1967; Vozoff, 1972).

V.4.3.2. The magnetic field sensor.

The magnetic field varies with time of day, latitude and during storm cycles, and it ranges from a few nanoteslas during quiet times to hundreds of nanoteslas. To measure the magnetic field over this large range, and still maintain the required sensitivity, two three-component EDA FM-100B fluxgate magnetometers with the components oriented magnetic north, east and vertically down were used (see Figure V.6). The EDA fluxgate magnetometers which have a resolution of approximately 1 nanotesla and a frequency response with 3 db from 0 Hz to 0.5 Hz were used.

The magnetometer is sited at approximately 20 meters from the central point and at 45 degrees to the compass points so as to be minimally affected by the electric cables. The device is covered with a grounded aluminium shield when in operation to protect it from stray electric field, rain etc.

The sensing head is located as far away from the recording station and roads as possible. It is attached to a seventy-five centimetre length of aluminium pipe driven into the ground leaving about twenty-five centimetres exposed. To avoid vibration, it is imperative that the aluminium pipe is supported solidly. Once the head is securely fastened to the pipe, it should be carefully levelled using the adjustment screws and level bubbles provided, since tilting the head by one degree can cause a 1000 nanoteslas change in H_x or H_y reading.

In use the magnetometer head is covered by a inverted rubbish bin to reduce long period drifts from temperature effects. Both the sensor head and magnetometer itself are temperature dependent. Temperature corrections (see Appendix V.1) were then applied to the data before any computation was carried out. In addition, the detector temperature and the internal temperature of the recording equipment are recorded on cassette tape along with the 3 magnetic and 2 telluric signals.

The inherent advantages of the fluxgate equipment are its simplicity, reliability, small size and modest power consumption.

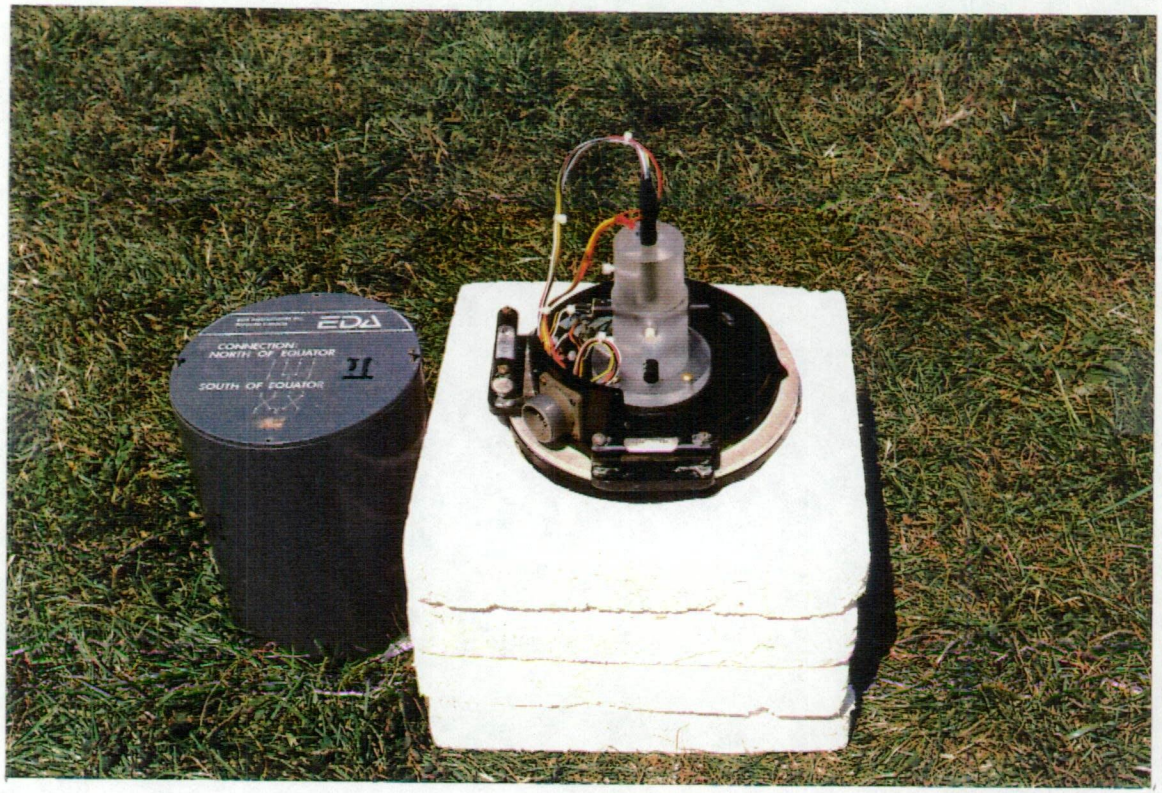

Figure V.6. The magnetic sensor head.

V.4.4. Summary.

In operation the fluxgate magnetometers and electric preamplifier circuit worked well. However, the EDA.I magnetometer showed a tendency to long period DC drifts which may have been due to amplifier drifts. This was soon cured by installing a new set of preamplifiers.

The field equipment used enabled the mounting of a magnetotelluric survey with the minimum of logistic support.

V.5. Data Analysis.

The raw data obtained from measurements of the magnetic micropulsations and telluric voltages are very irregular. The purpose of analysing the data is to transform them into magnetotelluric parameters as discussed in section V.3. which can then be interpreted. During this study, data analysis was mainly carried out using FORTRAN programs : MTY3 and MTYZ45.

Some corrections must be made for any magnetotelluric events chosen from the data, i.e. output of the READ1 program, as discussed in section V.4.2. For example, the errors in data points recorded caused by dropouts in the cassette tape have to be removed. This is done by program MTY3. This step of data analysis allows for the elimination of noise from original data. The program applies linear interpolation on bad data points and the noise is subsequently replaced with interpolated data points. This process needs to be carried out since the Fourier transform of a spike has a broad spectrum and thus would severely distort the frequency spectrum. The instrumental gain, analog to digital converter factor as well as temperature correction , as discussed in section V.4.3.2, are also applied. The output unit of the chosen events here is in nT for the orthogonal horizontal (H_x, H_y) and vertical (H_z) components of the magnetic field and mV for the orthogonal horizontal (E_x, E_y) components of the electric field. In addition, files of set up data, selected events used in the calculation of the magnetotelluric parameters, and tabulated

results were stored in binary format on double-density, double-sided floppy disk files. These files were used as the input of program MTYZ45 in the next step of the analysis and from this point on we will concentrate on applications of program MTYZ45.

Once acceptable and correctly formatted data was obtained the E_x and E_y components of electric fields were rotated to coincide with H_x and H_y axes of the magnetometer (see Figure V.3) using MTYZ45 program. The rotation is carried out using the method described in section V.3.2. This puts all the data sets in a common reference frame. At this step the electric fields data is also converted from mV to mV/km.

Since data are obtained as a function of time, after removing the data that are affected by excessive noise levels, each of the five components must be converted into the frequency domain. This conversion is required because most of the theoretical solutions for interpretation have been developed in the frequency domain. A Fast Fourier Transform (FFT) technique was used on all of the data presented in this thesis. As such, after rotation, the data was transformed to the frequency domain using a standard FFT algorithm routine (RFFTB) available at the Geology Department library. No filter corrections were applied to the data since matched filters were used in all channels and ratiometric relations among the field components are the only concern.

The calculation of the appropriate transfer function of the magnetotelluric impedance tensor (section V.3.2.1) was done using a least squares estimation based on the band-averaged values of the product of the spectral matrix. The spectral matrix contains the auto- and cross-powers of the measured fields. From the spectral matrix and estimated impedance tensor, the standard magnetotelluric parameters were calculated as discussed in section V.3.

Each of the magnetotelluric stations used in this study is analysed with the purpose of identifying the geometry of the earth's subsurface (i.e., 1-D, 2-D, or 3-D) and the noise content of the data. Excessive noise will distort the impedance estimates, resulting in resistivities which have little dependence on the earth's electrical properties. Therefore, each station is analysed in order to identify data which could produce interpretational errors.

The data quality of each station was determined by a wide range of criteria. The different criteria are briefly discussed below. In this discussion, the station numbers correspond to the locations identified on Figure I.2.

The next step in the data analysis was to estimate the dimensionality of the earth at each station. Two magnetotelluric parameters were utilized as criteria to accomplish this: the skew and rotation angle. In addition, a third criterion of comparing the geoelectric strike directions between adjacent stations was used.

The skew criterion was applied as suggested in section V.3. Data at periods where the skew values were less than or equal to 0.5 were considered to be relatively 2-D. Data at periods where the skew was greater than 0.5 were considered to be 3-D. This criterion was applied to trends in the data. Since low skew (actually zero skew) is a necessary, but not a sufficient, condition for two-dimensionality, other tests were applied to the data. Some workers, however, have felt they obtain useful parameters even when the skew exceeds 1.0 (Kurtz and Garland, 1976; Jiracek et al,. 1979).

Stability in the impedance rotation angle was also used as an indicator of a 2-D earth. The geoelectric strike for a 2-D earth is constant with depth; thus the angle of rotation to the principal directions should be constant at all periods. However, if the geoelectric strike varies with depth, then so should the rotation angle as a function

of period. Therefore, a widely varying rotation angle was taken to indicate a 3-D earth.

The geoelectric strike directions were determined from the field data and shown in Figure VI.1. This was done by assigning the values of ρ_{xy} to either the TE or TM mode. If ρ_{xy} was assigned to the TE mode, its corresponding impedance rotation angle defined the strike direction. If ρ_{xy} was assigned to the TM mode, its correspoding impedance rotation defined the dip direction and $\pm 90^{o}$ was added to obtain the geoelectric strike direction. However, noise contamination can cause rotation angles to vary rapidly over a small frequency range. Therefore, only data that were of constant strike ($\pm 10^{o}$) over at least one decade of the sounding spectrum were considered representative of the geoelectric strike.

The next step in the data analysis was to determine the reliability of the impedance. This was accomplished by using the E_x, E_y, and H_z predictabilities (see sections V.3.2.3). In this study, E and H predictabilities of less than 0.8 identified noisy data. Data with these coherencies were not used for computer modelling.

Chapter VI
MAGNETOTELLURIC SOUNDING RESULTS IN SOUTHEAST TASMANIA.

VI.1. Introduction.

Two magnetotelluric cross-sections were established in southeast Tasmania during the period of this study. Both of these cross-sections stretch across the gravity maxima which is known as the Huon Mobile Zone (HMZ) (Leaman and Richardson, 1990). From the two dimensional gravity and magnetic modelling results, discussed in Chapter II, it is now believed that this gravity anomaly represents a trough-like structure filled with Cambrian volcanic rocks extending in a NW - SE direction. The locations of the stations comprising the cross-sections are shown in Figure I.2 and their geographic coordinates are listed in Table I.1.

The analysis of all data was made using the tensor techniques discussed in Chapter V. All data presented in this chapter were based on data which has coherency between the E and E predicted of greater than 0.8 and coherency between H_x and H_y of less than 0.8. Data which fell outside these coherency criteria were regarded as noisy data and were not used for computer modelling.

Figure VI.1 shows the principal axis directions as described in Chapter V for stations along cross-sections I and II respectively. These azimuths are plotted for the average over-all period band analysed. It can be seen that the axes are oriented north-west to south-east which is approximately parallel to the strike of the main geological

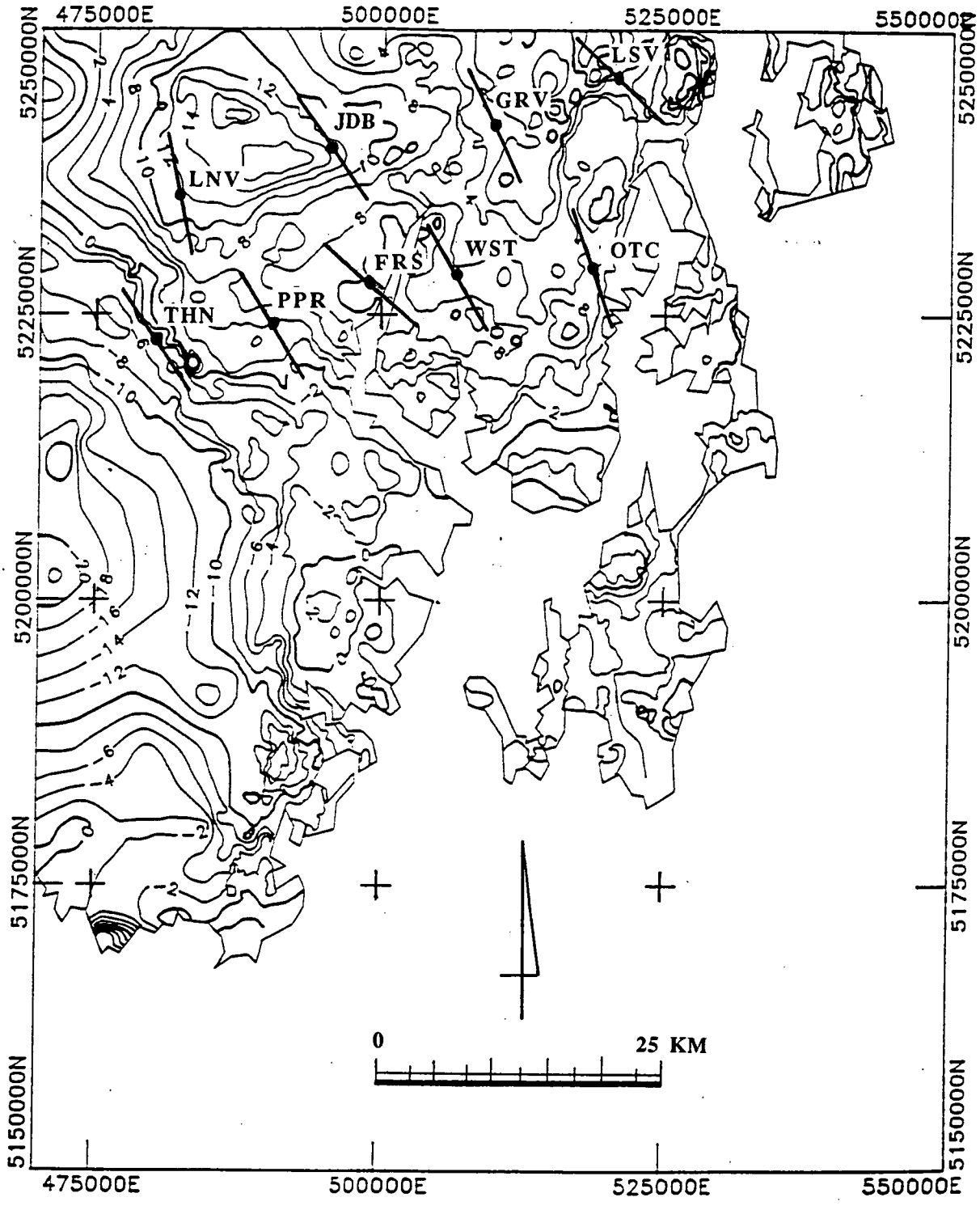

Figure VI.1. Principal axes show on a residual Bouguer gravity anomaly map.

feature (HMZ) in this region. This consistency is remarkable when one considers the geological complexity of the region. The rotation angle defined here is almost the same as the result of the new method discussed in the previous chapter. It is justifiable to assume, then, that JDB which is situated approximately on the middle of the HMZ with data in three decades of period and rotation angle (θ) of 40° is representative of the region. This rotation angle (40° west of magnetic north) was then used to rotate the observed coordinate axis at all sites to their principal axes direction.

Error bars which are plotted on apparent resistivity, coherency, skew and phase, represent quartiles from a series of data where the minimum data calculated is four. If data at a particular period are less than four then the lower and upper limit of the error is determined from the lowest and highest value of those data.

VI.2. The Cross-section I Response.

The total length of this cross-section from Leslie Vale in the east to Lonnavale in the west is approximately 40 kilometres and its orientation is 70° east of north which is almost perpendicular to the main geological feature in the study area. Local surface features are reasonably flat and topographic effects are assumed to have no major effect on apparent resistivities.

Recording periods in the field do not always produce data indicating geomagnetic disturbances because of the irregularity of their occurrence. For example, at JDB such data was obtained from periods of 10 to 10,000 seconds but at LNV only at periods of 10 to 1000 seconds were data affected by significant geomagnetic disturbances. In the following section the magnetotelluric parameters versus period plot obtained for LSV, GRV, JDB and LNV are discussed in some detail.

i) Leslie Vale (LSV).

This location was chosen to determine the apparent resistivity curves over the sedimentary basin of southeastern Tasmania at the eastern edge of the approximate margin of the lower Palaeozoic basin. The data was recorded on sedimentary rocks of Permian age. This rock crops out at 200 metres east of the recording site, and consists of a sequence of pebbly mudstone, pebbly sandstone and limestone. These rocks may be classified as the lower Parmeener super-group rock unit reported by Leaman (1973) and Farmer (1985). The thickness of this rock unit under LSV station is inferred from two-dimensional gravity and magnetic modelling and is believed to be about 600 metres, but the transient electromagnetic modelling result gives a slightly shallower depth of 450 metres with an apparent resistivity value of 243 Ohm-m.

The apparent resistivity curve (Figure VI.2) indicates that the subsurface resistivity properties are reasonably anisotropic as period increases. The resistivity curve for TE and TM modes tends to merge at periods less than 100 seconds. The merging of both the TE and TM tensor resistivity curve is probably due to an isotropic overburden layer. The sharp increase of the TE mode resistivity curve towards longer periods suggests that the resistivity gradually increases with depth.

Skew which is normally used to determine dimensionality of a site is given in Figure VI.2. The skew which is very small especially at shorter periods, may result from one- or two-dimensional structures at shallow depth. The skew factor increases as the periods increase, but does not exceed the value of 0.3, reflecting the lateral inhomogeneity contrast at middle depth where the subsurface structure is no longer isotropic. The relatively small skew as shown here, suggests that this station is approximately two-dimensional. As also can be seen from Figure VI.2 the E_x - E_x predicted and E_y - E_y predicted coherencies of 0.9 are observed at almost all periods. These coherencies indicate that the presence of noise in the data is about 10%.

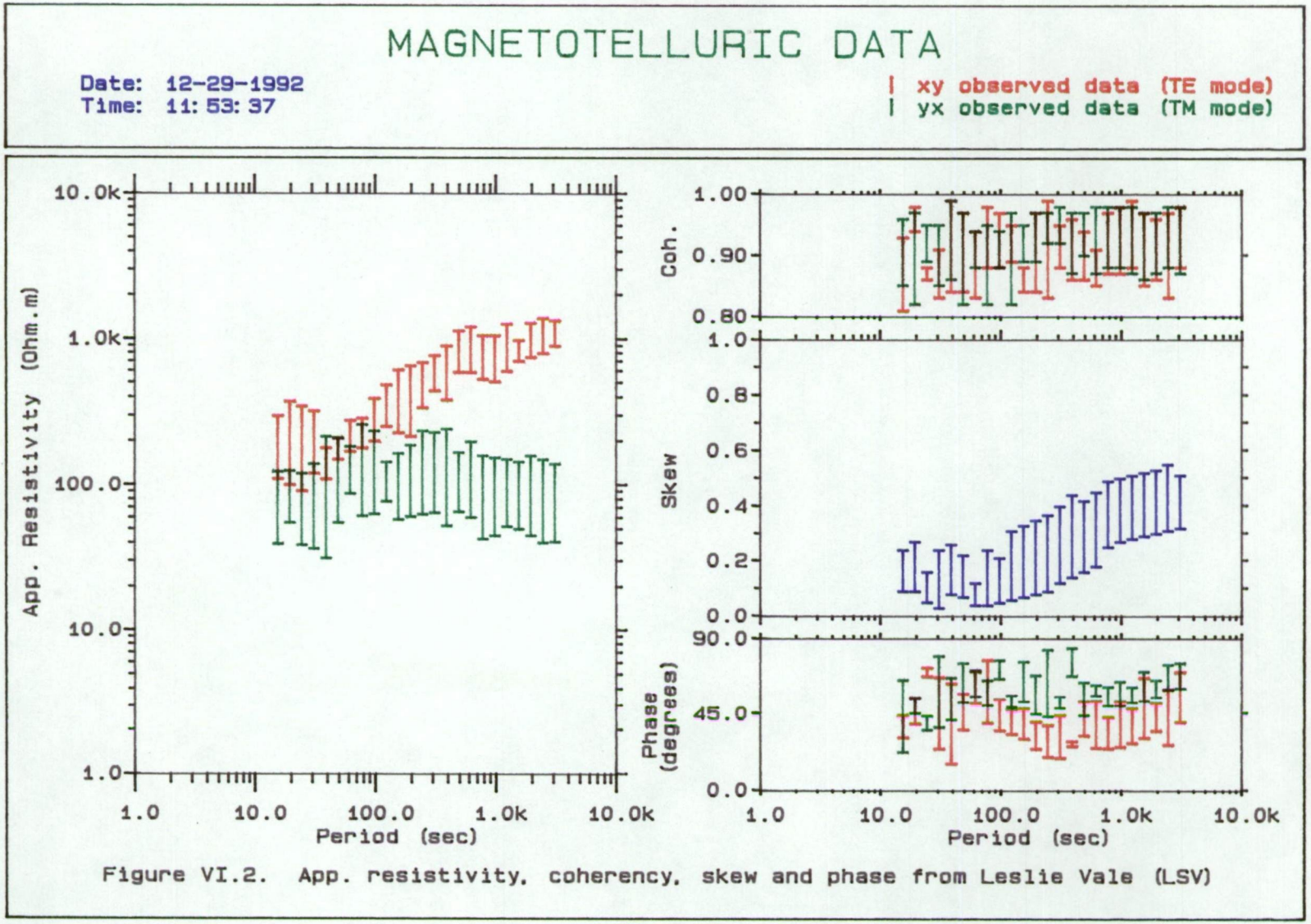

Figure VI.2. App. resistivity, coherency, skew and phase from Leslie Vale (LSV)

ii) Grove (GRV).

This station is located approximately 12 kilometres to the west of station LSV. The recording apparatus was situated on similar rock units as at LSV which is believed to be the lower Parmeener super-group. The thickness of this rock unit is inferred from two-dimensional gravity and magnetic modelling and is less than that at LSV station being about 475 metres. The same thickness is also inferred from the transient electromagnetic modelling result with an apparent resistivity value of 228 Ohm-m.

A plot of apparent resistivity versus period at GRV station (Figure VI.3) indicates that the degree of anisotropy at periods less than 80 seconds is very small. It can be seen here that both the TE and TM modes resistivity curves are very close and almost parallel to each other. The anisotropy ratio ($\rho_{major} / \rho_{minor}$) is between 1 - 2 at short periods and increases to 4 for periods longer than about 100 seconds. As observed at station LSV, the TE modes here also exhibit an increase in apparent resistivity at greater depth.

Skew plot for this station can be seen in Figure VI.3. The skew factor, in general, tends to be small at approximately 0.2 at all periods. According to Swift's (1967) criteria and the anisotropy ratio, this indicates that the geological structures beneath this station can be described as 'weakly' two-dimensional.

Both of the TE and TM modes have quite high predicted coherency (see Figure VI.3). The lowest predicted coherency value is 0.9 observed at period 40 seconds. As the period increases, however, this value increases to 0.95 indicating the data is less affected by noise.

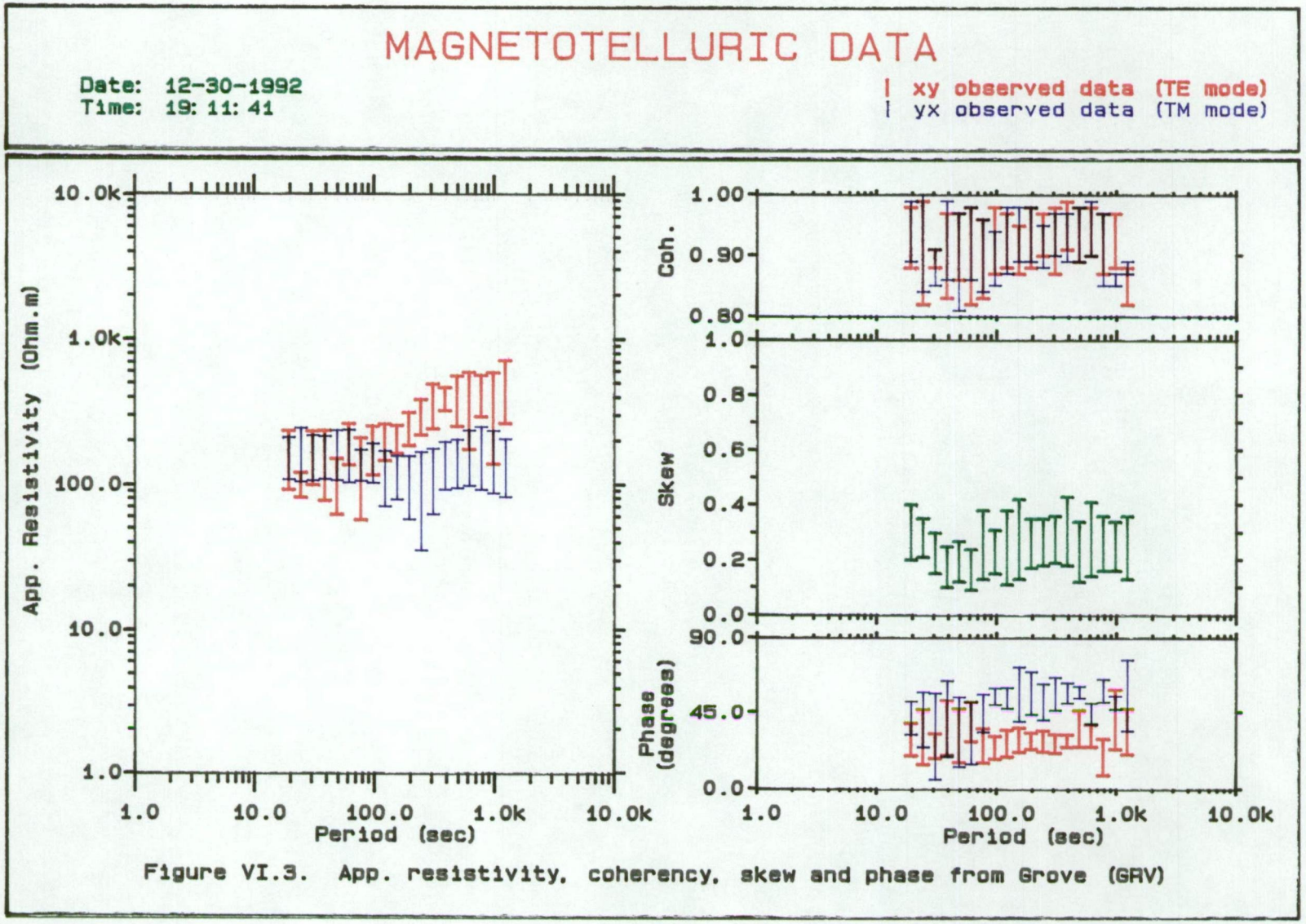

Figure VI.3. App. resistivity, coherency, skew and phase from Grove (GRV)

iii) Judbury (JDB).

Station JDB is situated approximately 16 kilometres to the west of GRV. When this project was designed, a 10 kilometres spacing between stations at every cross-section was initially proposed in order to map the resistivity structure in southeast Tasmania. In reality, however, it is difficult to find locations that can satisfy the survey procedure criteria discussed in the previous chapter, resulting in irregularity of the stations.

The JDB station is located on Parmeener sub-group rock units. Unlike the two stations previously discussed (LSV and GRV) where this rock unit is underlain by Cambrian volcanic rocks, it is believed that the low Parmeener super-group sits on a sequence of marine quartz-sandstone, siltstone and limestone of probably Ordovician age at JDB station. The transient electromagnetic modelling result indicates that the apparent resistivity value for this layer is 44 Ohm-m.

Apparent resistivity curves for the TE and TM modes, can be seen in Figure VI.4. It shows that both the TE and TM curves tend to separate at period 80 seconds which indicates a strong anisotropy beneath this station. This degree of anisotropy suggests that the station may be close to a vertical discontinuity in structure. The TE mode curve appears smoother compared to the same apparent resistivity mode at other stations, but this is probably due to the greater amount of data analysed and the correspondingly greater number of accepted estimates. The apparent resistivity for TE mode appears period independent at period less than 100 seconds. With increasing period, the apparent resistivity decreases from 200 Ohm-m at period 10 seconds to a minimum peak of about 100 Ohm-m at period 40 seconds and increases to about 1000 Ohm-m at longer periods thus suggesting the existence of a conductive layer at depth beneath this station. This is also supported by the short corrected induction vector obtained by the magnetovariational method at this station (see Figure IV.15).

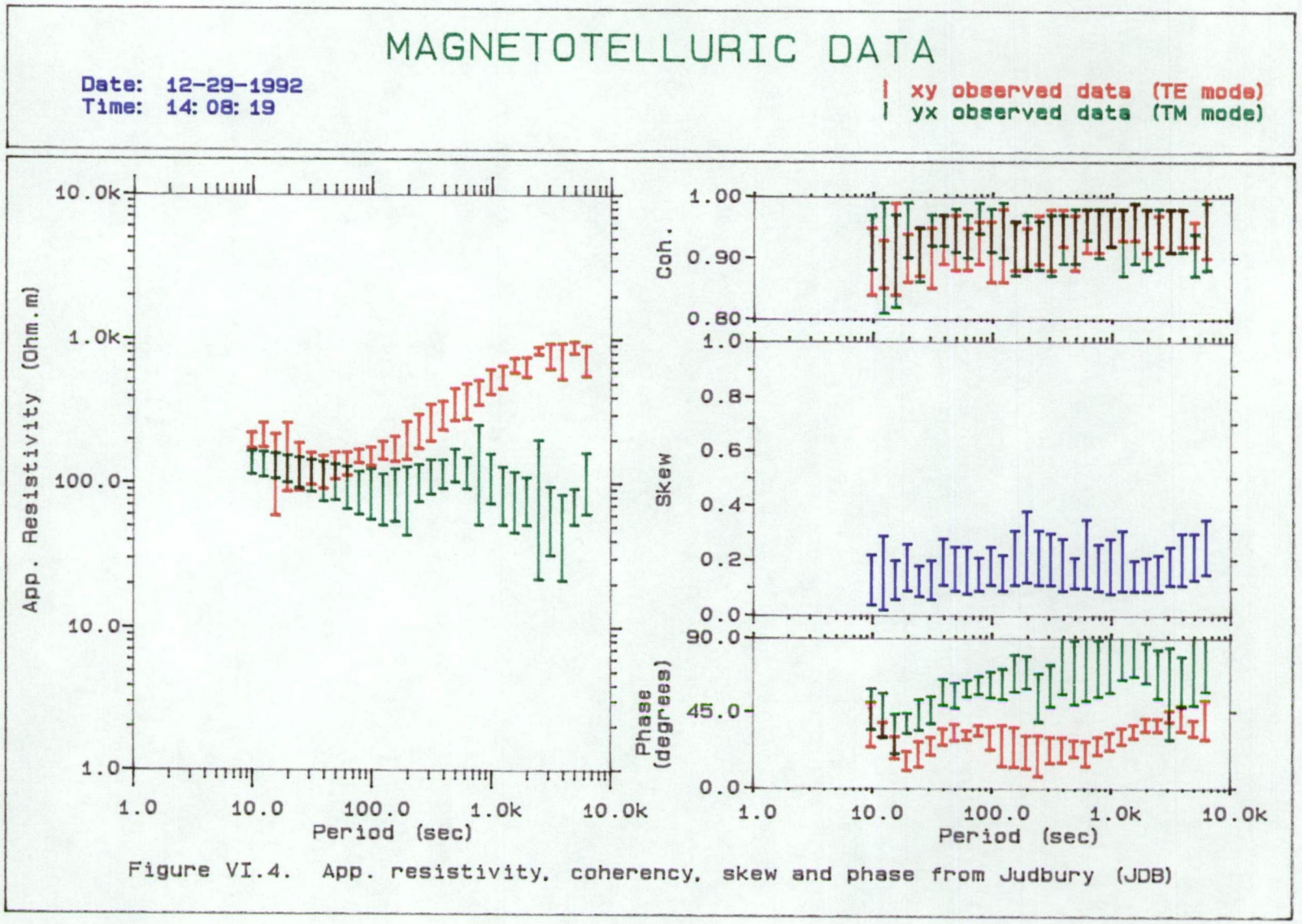

Figure VI.4. App. resistivity, coherency, skew and phase from Judbury (JDB)

For two-dimensional structures skew should be small. This is particularly true for JDB. Skew values of the magnetotelluric impedance tensor here were less than 0.3 for all periods, and less than 0.2 for the majority of periods as shown in Figure VI.4. For this reason, it can be concluded that the subsurface resistivity structure beneath this station cannot be three-dimensional in character. The quality of the data at this station is good. The predicted coherencies of about 0.95 are observed at most periods which indicates the data are almost free of noise.

iv) Lonnavale (LNV).

The Lonnavale station is situated at the western edge of the approximate boundary of the lower Palaeozoic basin. At all stations including LNV along cross-section I, the data were recorded on the Permian rock unit. Underlying this rock is believed to be Ordovician rock which has apparent resistivity value slightly less than that found at LNV being 39 Ohm-m which is inferred from two-dimensional gravity and magnetic and transient electromagnetic modelling results.

The apparent resistivity curves as shown in Figure VI.5, display increasing anisotropy with increasing periods. The TE mode curve, however, has very small variation at periods longer than 100 seconds implying an almost uniform resistivity layer at depth below this station.

Figure VI.5 shows plot of skew from this station. In general the skew factor is extremely low being about 0.1 for the length of the recording period. Based on this skew and apparent resistivity results, it is clear that the structure under this station is most likely two-dimensional.

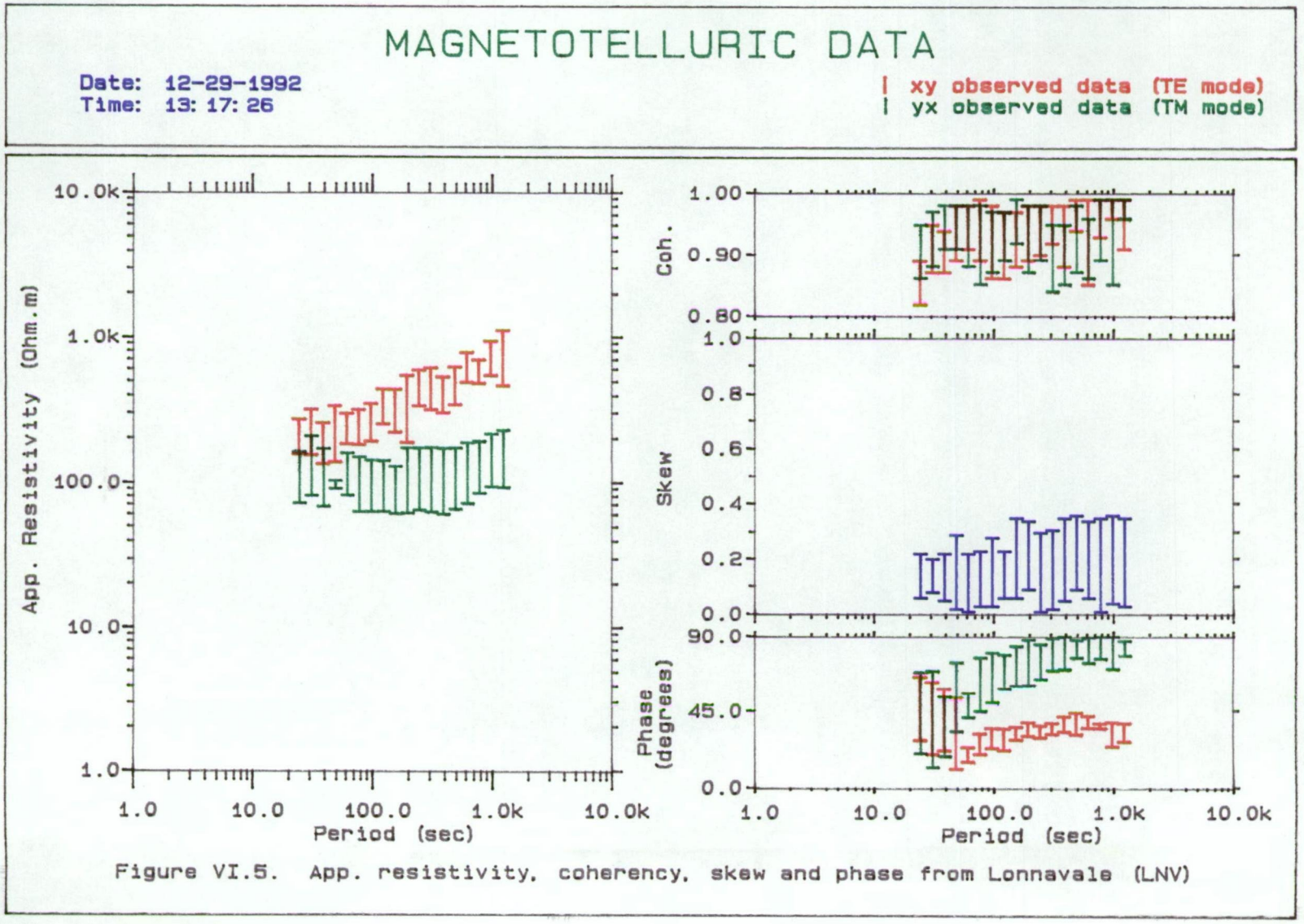

Figure VI.5. App. resistivity, coherency, skew and phase from Lonnavale (LNV)

VI.3. The Cross-section II Response.

Cross-section II is almost parallel to cross-section I. The total length of the cross-section from Oyster Cove in the east to Tahune in the west is approximately 50 kilometres and its orientation is 60° east of north, almost perpendicular to the geological grain in the study area. This section reports the results obtained from stations OTC, WST, PPR, FRS, and THN.

i) Oyster Cove (OTC).

This station is the eastern-most location of the southern cross-section and is situated about 6 kilometres to the south of gravity and magnetics cross-section II. It lies on the lower glacio-marine sequence of pebbly mudstone, pebbly sandstone and minor limestone of Permian age. The thickness and the apparent resistivity of the rock unit beneath this station is unknown. It should be mentioned here that there is no transient electromagnetic measurement taken at OTC. The order of magnitude of the apparent resistivity, however, suggests a relatively resistive structure which is intuitively compatible with the situation of site LSV of cross-section I.

The apparent resistivity curves which are shown in Figure VI.6 indicate that the degree of anisotropy at period 50 seconds is very small. It can be seen here that both the TE and TM modes resistivity curves are very close and almost parallel to each other. The curves then start to split at period greater than 50 seconds which implies that the structure may become more anisotropic at great depth. The anisotropy may be associated with the contact between the Cambrian volcanic and crystalline rock of Precambrian age as inferred from two-dimensional gravity and magnetic modelling and a drillhole at nearby Woodbridge.

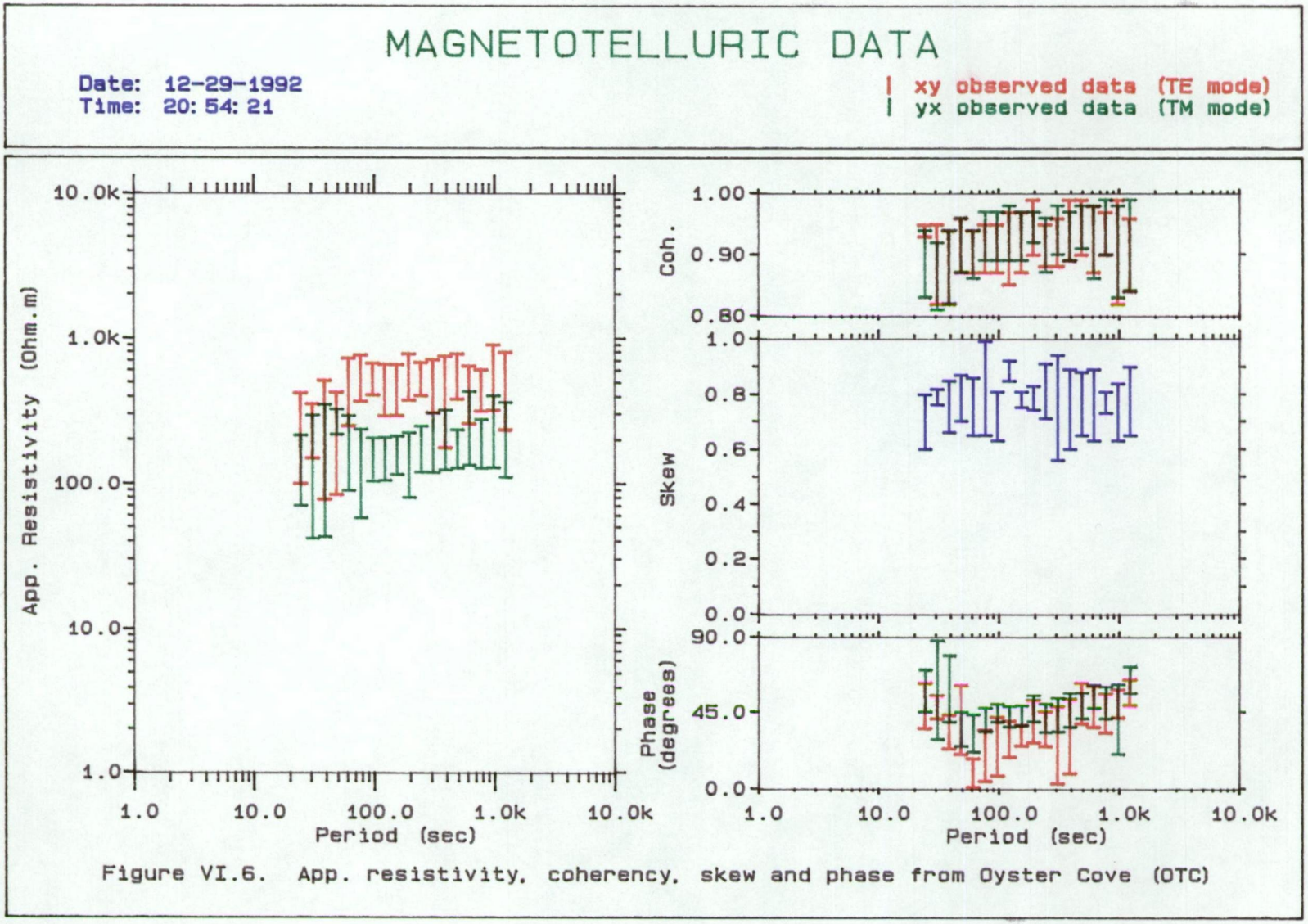

Figure VI.6. App. resistivity, coherency, skew and phase from Oyster Cove (OTC)

The coherencies and skew for all estimates on apparent resistivities are also shown in Figure VI.6. Both coherencies suggest very good data. The skew value becomes larger as period increases, reaching values greater than 0.8 and is the largest encountered. This feature therefore represents general structure which is far from two-dimensional. As the location of this station is close to the coast, the large skew may be associated with the resulting lateral inhomogeneity.

ii) Woodstock (WST).

This station is located approximately 15 kilometres west of OTC. The data was collected on sedimentary rocks of Triassic age. This rock outcrops in the Sandfly Rivulet bank 300 metres to the north of the recording site. It consists of sequences of sandstone, siltstone, mudstone with some carbonaceous materials. These rocks are part of the upper Parmeener super-group (Leaman, 1973; Farmer, 1985). The thickness of this rock unit under this station is assumed from two-dimensional gravity and magnetic modelling and it is believed to be about 350 metres. This thickness agrees with the transient electromagnetic modelling result which also gives the apparent resistivity value of 48 Ohm-m.

Apparent resistivity curves for both TE and TM modes, can be seen in Figure VI.7. For the whole period, both apparent resistivity values are slightly smaller compared to the apparent resistivity on station OTC, therefore suggesting that this station sits on a more conductive body. The resistivity curves for TE and TM modes which tend to separate at almost all periods, indicate a strong anisotropy.

A plot of the dimensionality factor (see Figure VI.7) indicates that the subsurface conductivity structure under this station is probably two-dimensional at middle depth since the average skew value is about 0.5. The predicted coherencies plot shown in Figure VI.6 demonstrates that the quality of the data is reduced at

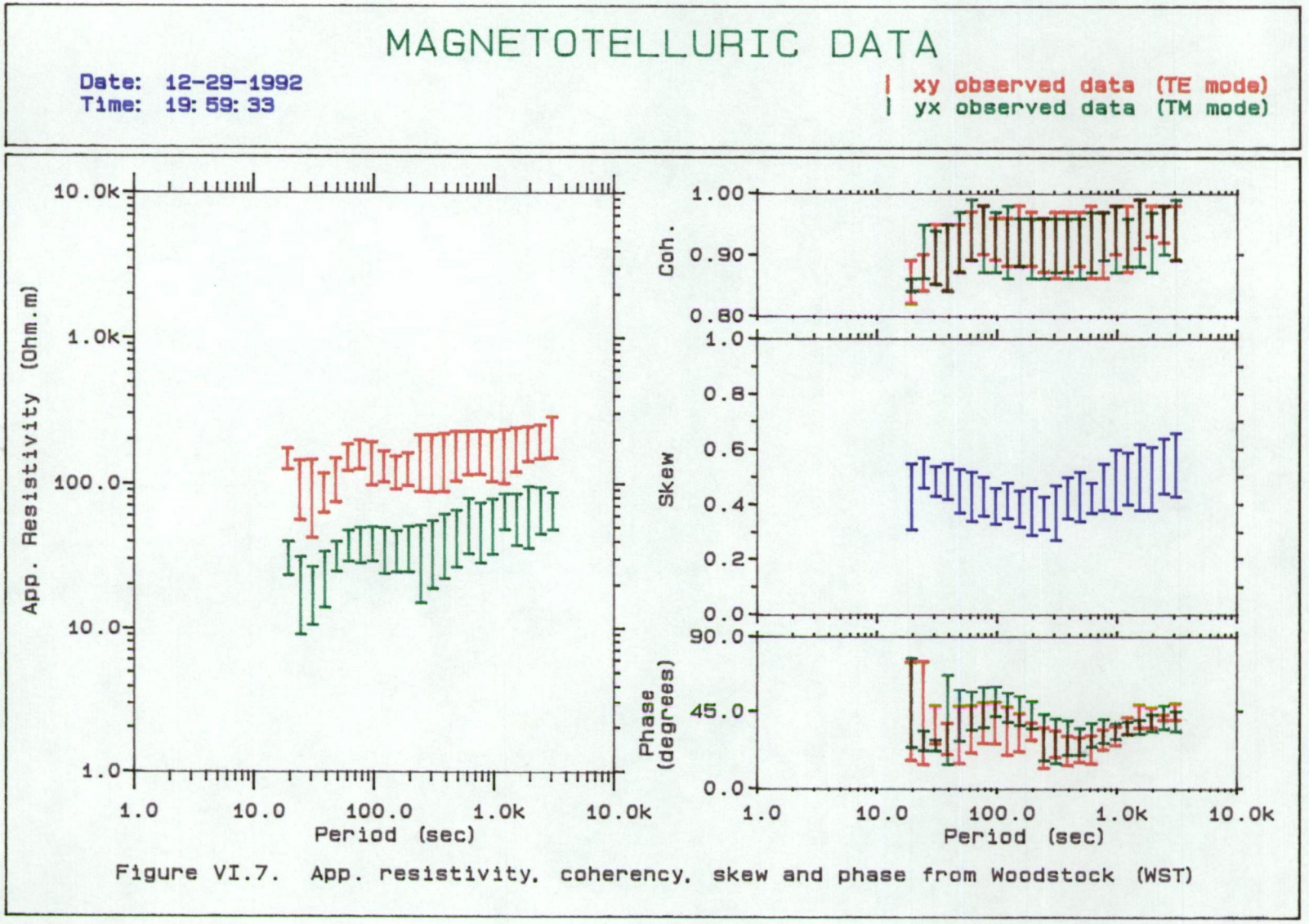

Figure VI.7. App. resistivity, coherency, skew and phase from Woodstock (WST)

periods below 30 seconds to the value of 0.85. Beyond these periods, however, the presence of noise in the data is limited to about or less than 10%.

iii) Franklin (FRS).

Station FRS is located approximately 8 kilometres west of WST. This station which sits on the same rock unit as WST, lies approximately above the middle of the Palaeozoic basin. The thickness of the Triassic rock unit under this station is about 400 metres and has apparent resistivity of 51 Ohm-m. Depth to pre-Permian rocks must be about 800 metres.

Of particular significance is the fact that the apparent resistivity plots for this station (Figure VI.8) are dramatically different from those recorded at stations WST and PPR. Such difference usually indicates major structural boundaries in the vicinity (Vozoff, 1972), and consequently, these stations must be subject to different structural constraints. Several characteristics of the curves will be important in the interpretation. For example, the TE mode apparent resistivity is almost an order of magnitude larger than those at WST and PPR. For this station, a distinct decrease of the TE mode curve is observed at period less than 30 seconds and followed by a slight increase in apparent resistivity from 40 seconds, indicating a conductive zone within the crust.

Figure VI.8 also contains information about data quality and structure dimensionality. As can be seen from Figure VI.8 noise content in the data is moderately small, i.e. 10%. The skew factor is about 0.1 up to periods of 90 seconds and tends to increase at longer periods. In general the skew value is less than 0.3, therefore it can be concluded that the conductivity distribution beneath this station is probably two-dimensional.

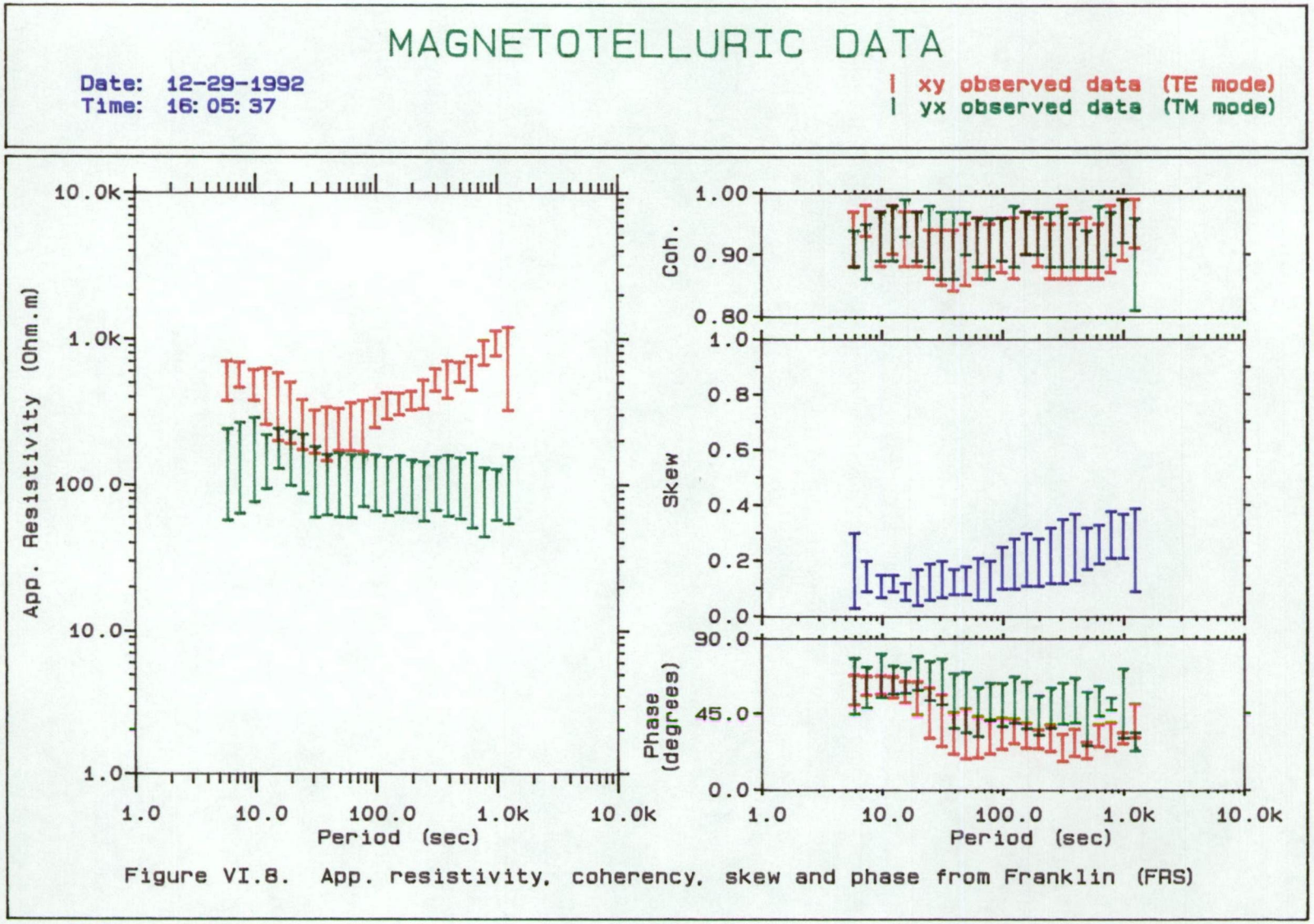

Figure VI.8. App. resistivity, coherency, skew and phase from Franklin (FRS)

iv) Peppers Road (PPR).

This station sits on dolerite of Jurassic age. The thickness of this igneous rock is inferred from two-dimensional gravity and magnetic modelling and is believed to be about 200 metres. The transient electromagnetic modelling result, gives the apparent resistivity value for this rock as 311 Ohm-m and it is believed that the Jurassic rock overlies Triassic rock which has apparent resistivity value of 30 Ohm-m.

In Figure VI.9 both the TE and TM mode apparent resistivities data display increasing anisotropy with increasing period. The values of apparent resistivity, in both TE and TM modes are particularly small compared to the apparent resistivity figures for the FRS station, and lie between 20 and 200 Ohm-m. It is thus indicated that there is a more conductive part of the basin under the PPR. The ratio of the TE and TM modes apparent resistivities at 30 seconds period is almost 10 compared to the ratio of apparent resistivities at the same period at FRS which is about 2, indicating lateral variations at a shallow depth beneath these stations.

Figure VI.9 also displays variation of the dimensionality of the structure underneath this station. The skew tends to decrease until about 20 seconds where it reaches the minimum value of about 0.3 and it begins to gradually increase to nearly 0.6 at period 200 seconds before reducing to 0.4 at longer periods. It indicates that the distribution of conductivity beneath this station may be a two-dimensional structure at least up to middle depth. As can be seen from Figure VI.9, the data possesses a high predicted coherence (self-consistency between telluric and magnetic components) i.e. greater than 0.9

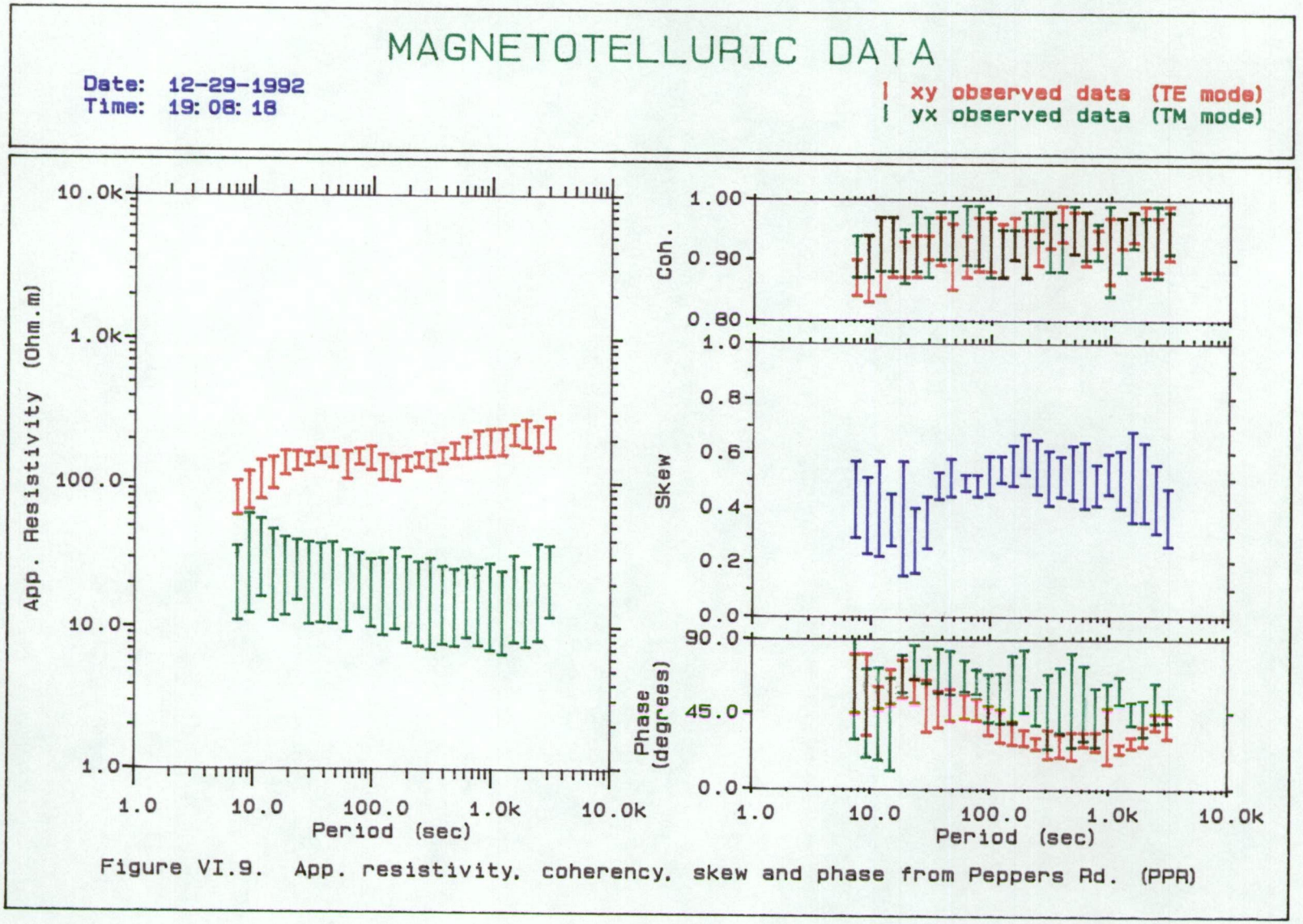

Figure VI.9. App. resistivity, coherency, skew and phase from Peppers Rd. (PPR)

v) Tahune (THN).

This station is the western-most location of cross-section II and is situated approximately 12 kilometres west of PPR. The data was recorded on the lower Parmeener super-group rock unit, the same rock unit as at station LSV, having the apparent resistivity value of 159 Ohm-m. Underlying this rock is believed to be Ordovician rock which has apparent resistivity value of 28 Ohm-m.

The apparent resistivity curves as shown in Figure VI.10 illustrate increasing anisotropy with increasing periods. The smooth rise of the TE mode resistivity curve toward longer periods, for example, suggests that the resistivity gradually increases with depth. In addition, the separation of the TE and TM modes suggests that the station may be close to a vertical discontinuity in structure.

Skew values of magnetotelluric impedance tensor were about 0.5 for a period of 40 seconds, and dramatically increase at longer periods, almost reaching the value of 1.0 as shown in Figure VI.10. The dramatic increase in skew factor toward longer periods indicates the three-dimensional structure beneath this station. This three-dimensional effect may be associated with a buried fault at 800 metres depth and the edge of the granite body which is found at 8 kilometres depth beneath this station as inferred from two-dimensional gravity and magnetic cross-section II.

The predicted coherencies (see Figure VI.10) of just above 0.9 are observed at periods longer than 40 seconds. These coherencies also suggest that the presence of noise in the data is about 10%.

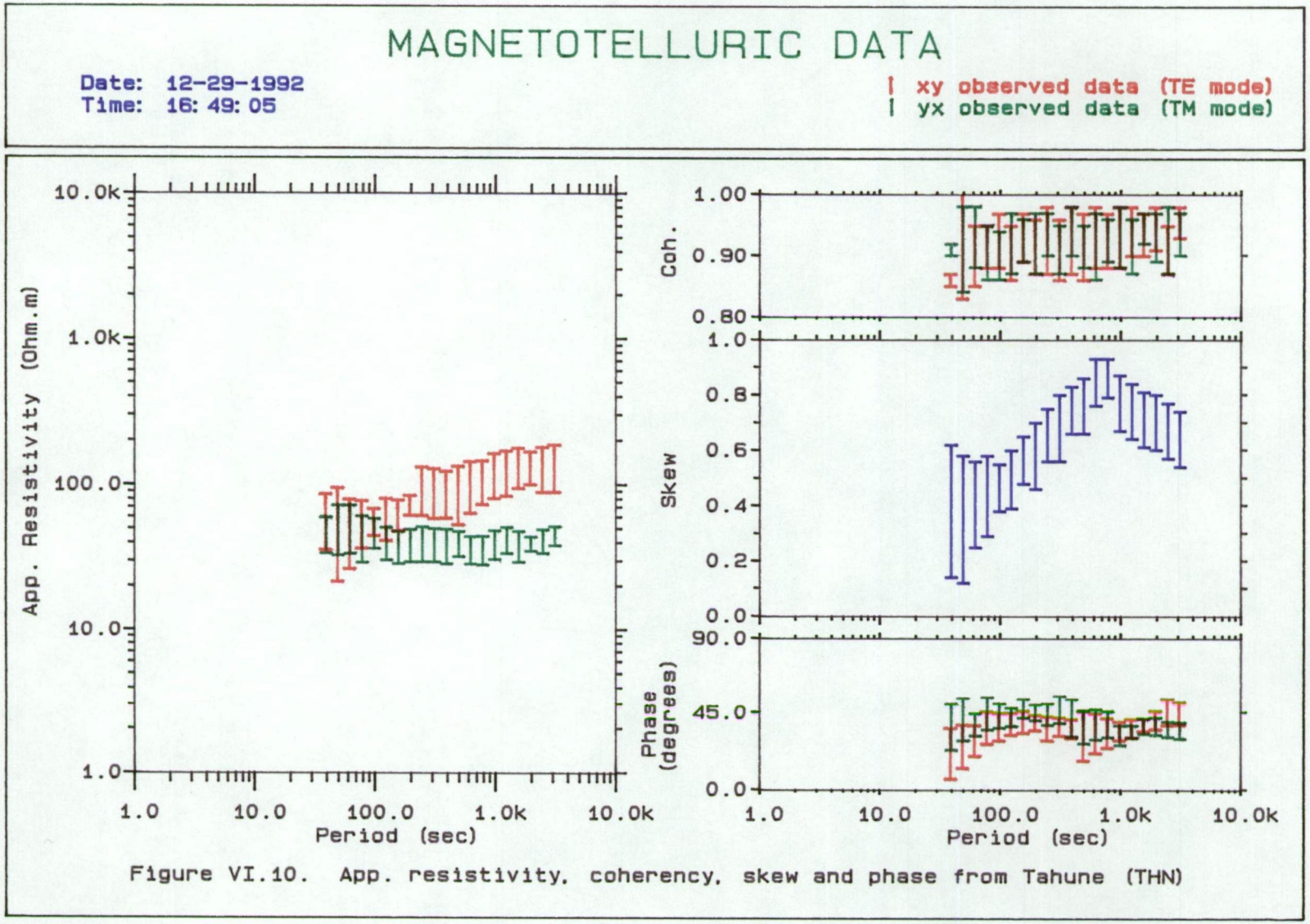

Figure VI.10. App. resistivity, coherency, skew and phase from Tahune (THN)

VI.4. Comparison of rotation angle calculation.

This section reports the results of the new rotation angle and dimensionality calculation method which is discussed in Chapter V.3.2.5. The calculation of rotation angle (θ) analysis was carried out using the PTH2.FOR program based on equations (V.38) to (V.41). The purpose of this analysis was to examine and compare the theoretical approach described in Chapter V.3.2.5 to the conventional method and apply it to the real geological situation.

Although this method was applied to all nine magnetotelluric stations to calculate the rotation angle and examine the dimensionality of the subsurface structure, only three representative stations will be presented here. These are a two-dimensional-like structure (JDB), a weakly two-dimensional structure (GRV) and a possibly three-dimensional structure (THN).

Figure VI.11 shows the result from JDB station. The rotation angle (θ), which is assigned in the analysis as average theta, is plotted on the left hand side of Figure VI.11. The average theta was determined from the average of θ_x and θ_y of equations (V.38 and V.40). The average theta that is shown here is based only on delta theta values within $\pm$ 20 degrees which are plotted on the right-hand side of Figure VI.11. Delta theta was derived from the difference of θ_x and θ_y of equations (V.38) and (V.40). As can be seen from Figure VI.11 both average and delta theta plots are good and very few of these data are scattered. It also shows the advantage of analysing a large population of data. Plot of rotation angle (θ) or average theta indicates slightly scattered data at periods less than 100 seconds with average theta about 50 degrees and at periods greater than 100 seconds most of the average theta lies at about 45 degrees. This angle represents an anticlockwise rotation. The rotation angle defined for this station agrees very well with the approximate strike of the Huon Mobile Zone. Delta theta which can be used as a measure of how closely the structure

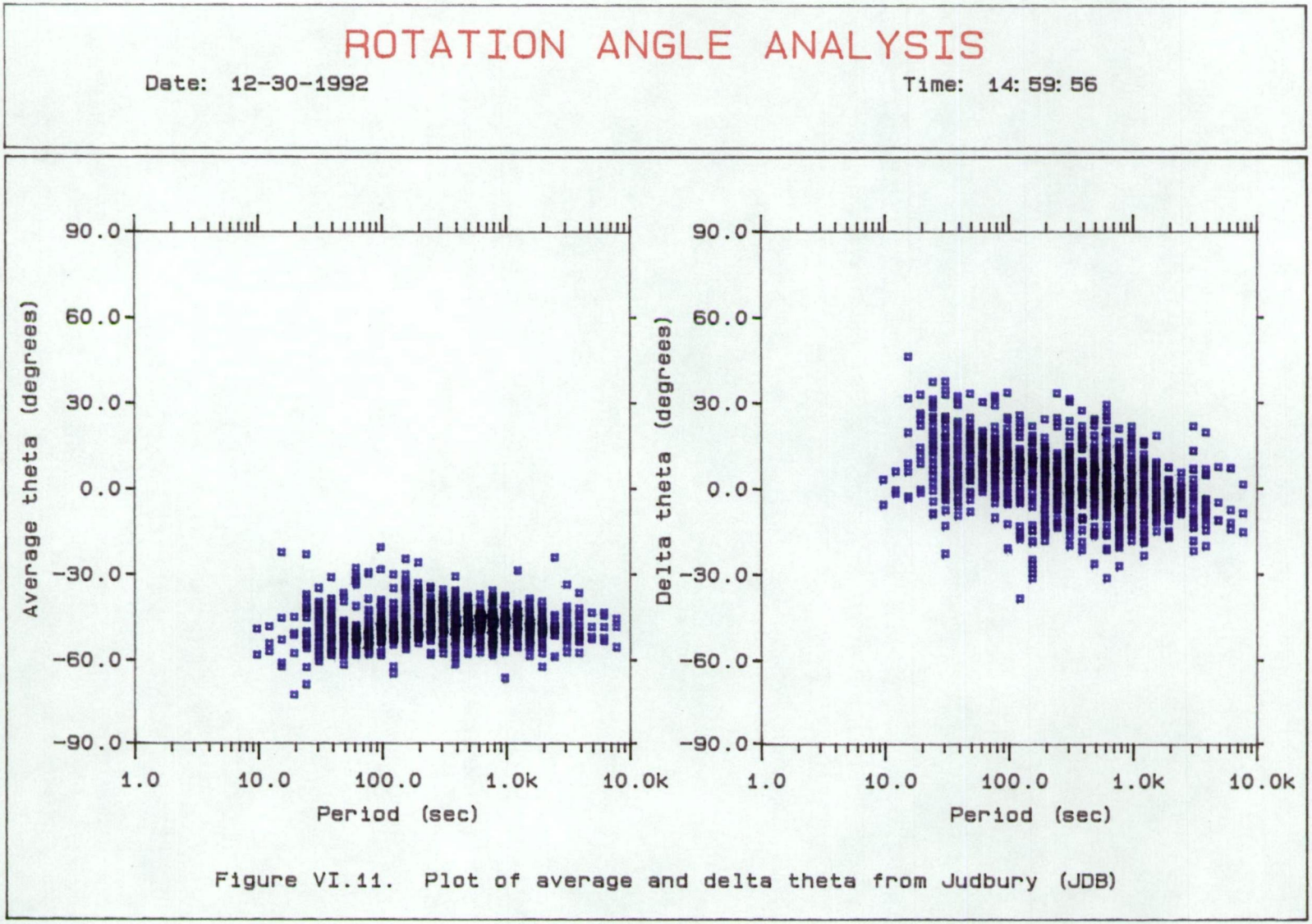

Figure VI.11. Plot of average and delta theta from Judbury (JDB)

approximates to two-dimensions, is plotted on the right-hand side of Figure VI.11. At period less than 100 seconds delta theta is confined to a range of 10 degrees and at longer periods most of delta theta lies very close to zero. Based on the small variation of average theta and almost zero of delta theta it can be concluded that this station is two-dimensional. This result is in good agreement with the result given by skew (see Figure VI.4)

The rotation angle (θ) analysis result from a weakly two-dimensional structure station (GRV) can be seen in Figure VI.12. Rotation angle (θ) or average theta, on the left hand side of Figure VI.12, determined for this station is approximately 45 degrees at periods less than 50 seconds and swings to 40 degrees for the rest of the recording periods. This angle represents anticlockwise rotation and is very similar to the rotation angle found at JDB. This average theta was again plotted based on delta theta values within $\pm$ 20 degrees. Unlike the plot of delta theta at JDB, delta theta here, on the right hand side of Figure VI.12, is very scattered at longer periods. The scattering of the delta theta cannot be attributed to the noise content in the data since the coherency of the data is greater than 0.9. It is most likely that the scattered data reflect irregularities in the structure. Because this phenomenon is also exhibited by the skew (see Figure VI.3) where it tends to increase at longer periods, the structure under this station therefore can be approximated to have two-dimensional structure at middle depth then changing to possible three-dimensional structure at great depth.

Plot of rotation angle (θ) analysis results at a possibly three-dimensional structure station (THN) may be found in Figure VI.13. It shows the average theta plot is remarkably scattered at periods less than 200 seconds where the data lie between +30 and -65 degrees. This angle represents both anticlockwise and clockwise rotations. For periods greater than 200 seconds, however, most of the data is confined to an angle of about -65 degrees. The delta theta plot is also very scattered at

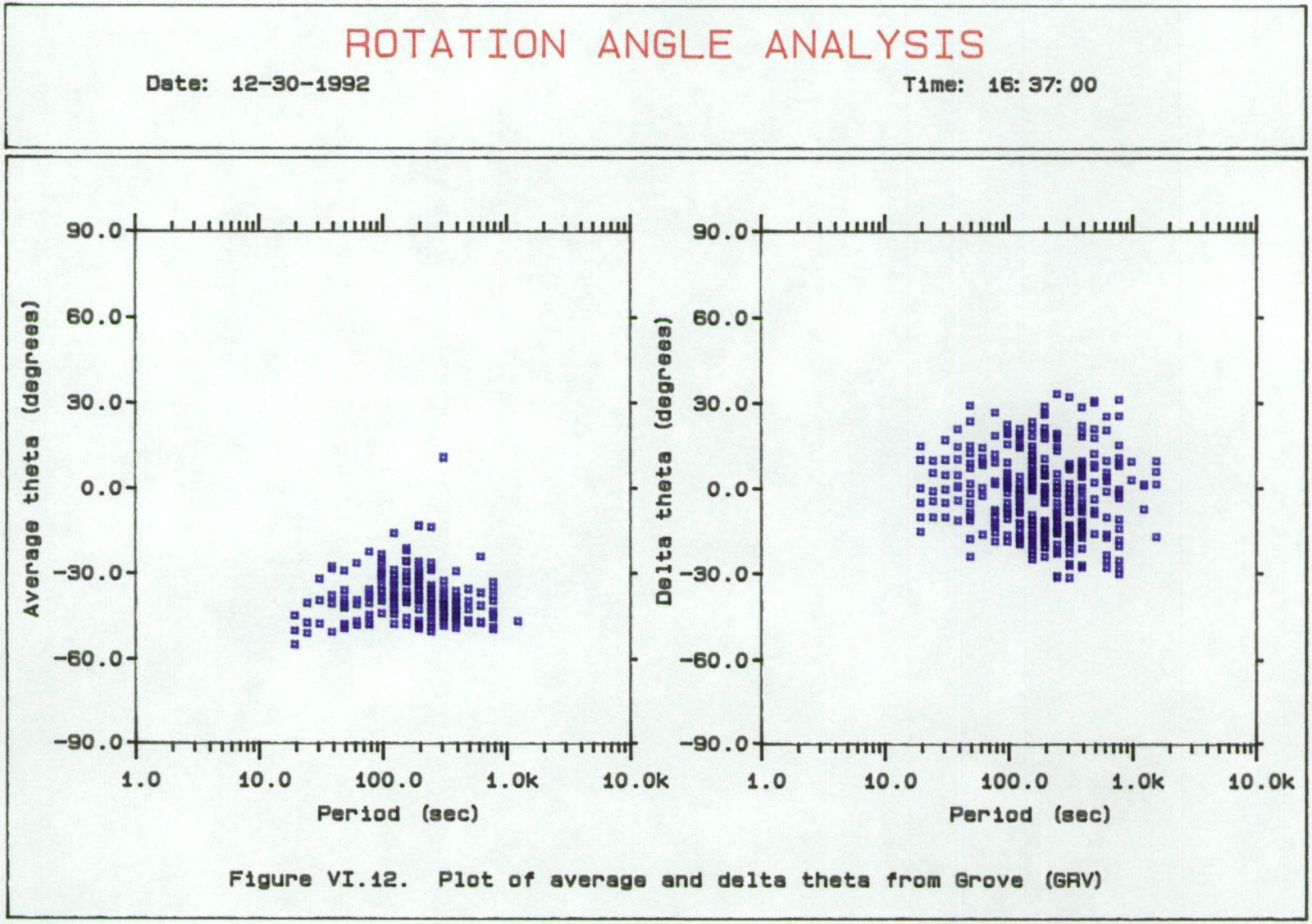

Figure VI.12. Plot of average and delta theta from Grove (GRV)

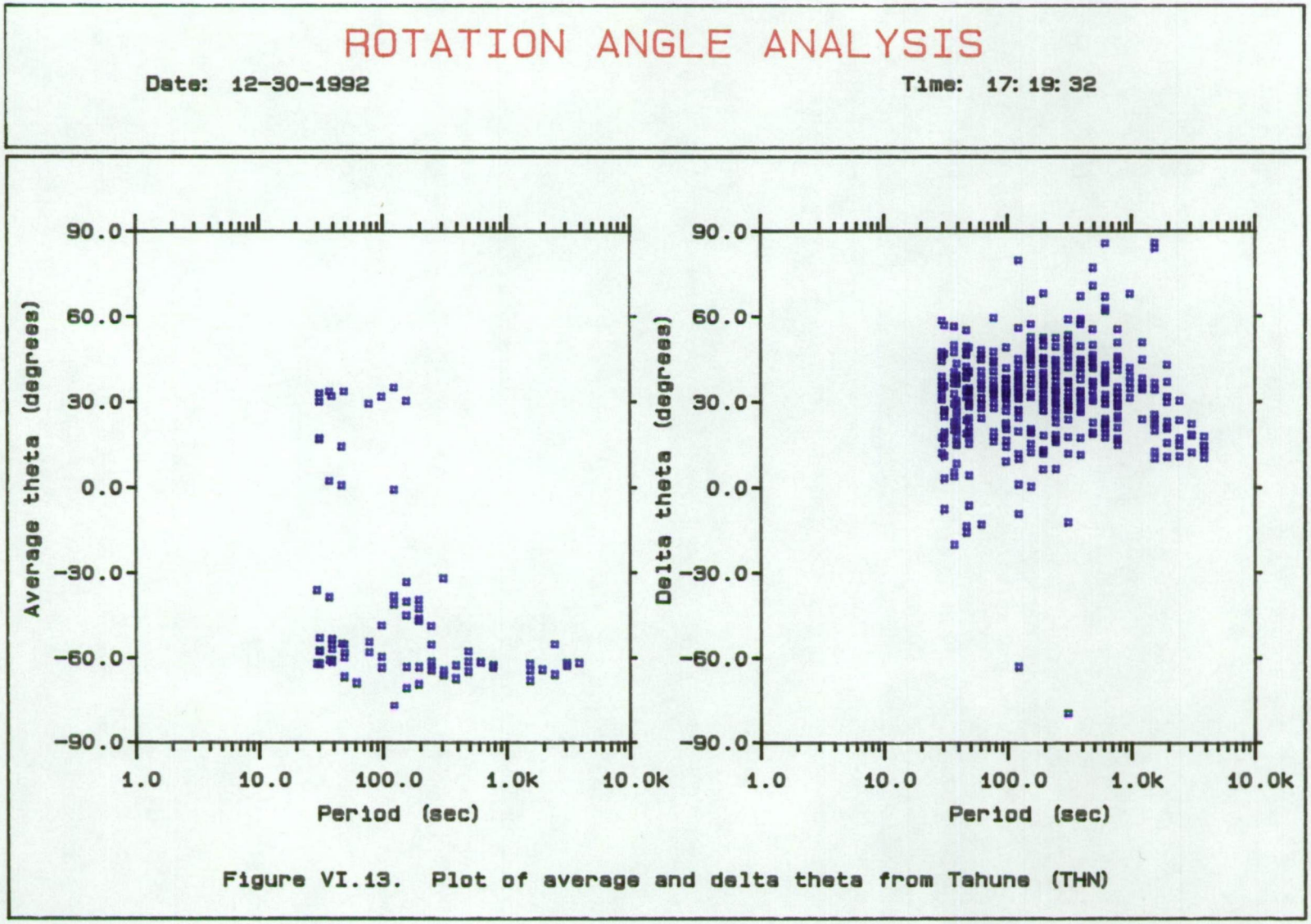

Figure VI.13. Plot of average and delta theta from Tahune (THN)

period less than 200 seconds and gathering at about 30 degrees, which is outside the two-dimensional criteria set in Chapter V.3.2.5. It was expected, as this station is possibly three-dimensional at least at a shallow depth. Delta theta which has a tendency to decrease toward zero at longer periods, indicates a two-dimensional structure at great depth beneath this station . This result is almost the same as the result given by the plot of skew factor for this station (see Figure VI.9).

VI.4.1. Discussion.

The application of the new calculation of rotation angle and dimensionality method into three different geometrical structures in the previous section shows that this method works well and gives results very close to the conventional methods.

The most interesting feature of the results is the characteristic of the rotation angle at JDB and GRV. Figures VI.11 and VI.12 show a slight change of about 5 degrees in rotation angle (θ) or average theta from short to longer period. Interpretation of the change of this rotation angle azimuth indicates different structures. At shallow depth the electromagnetic energy may sense the structure associated with the HMZ. As the penetration of electromagnetic energy becomes deeper it may detect a purely two-dimensional-like structure, probably associated with a conductive body at depth.

This new method of determining rotation angle has also been tested at Conara Junction, northeast Tasmania (Hermanto 1993), on what has long been known as a two-dimensional conductivity structure (Bindoff, 1983; Sayers, 1984; Richardson, 1985). Hermanto found very small delta theta values indicating a good estimate consistent with two-dimensionality. This characteristic of delta theta is very similar to the result found at Judbury (JDB) in southeast Tasmania.

The Conara Junction station is located approximately in the middle of the Tamar Mobile Zone (TMZ). For the stations outside of TMZ and situated on the three-dimensional-like structure beneath, Hermanto (personal communication) finds a very scattered plot of rotation angle and he also finds plot of delta theta no longer confined to ± 20 degrees. This result again shows similarity to the plot of rotation angle and delta theta for THN in southeast Tasmania (see Figure VI.13).

This new method of calculating rotaion angle and dimensionality method was compared with another method. By using Lilley's (1992) Mohr circle method we have calculated the rotation angle at JDB station (Parkinson et al., 1992). The result obtained was very close to the rotation angle (θ) obtained by the proposed method, i.e. it differed by about 8° in a northwest direction. However, the Mohr circle method requires more steps during data analysis and hence is more time consuming.

VI.5. Summary.

The following is a summary of the magnetotelluric results presented and discussed in Chapter VI, by cross-section.

At cross-section I, the characteristics shown by the apparent resistivity curves may indicate an almost isotropic structure at shallow depth beneath stations LSV,GRV,JDB and LNV. The degree of anisotropy tends to increase at greater depth at all stations. The resistivity values exhibit a slightly low value at stations JDB and GRV. The resistivity curves at all stations indicate the existence of a conductive layer at greater depth. The skew and delta theta are small. At JDB station which is situated at the centre of the HMZ, plot of delta theta almost confines to zero degrees for the whole recording period. In general, all stations at cross-section I (LSV,GRV,JDB and LNV) have fairly strong two-dimensional indications.

At cross-section II, the tensor apparent resistivity curves from stations OTC, WST, FRS, PPR and THN show large to moderate anisotropy. The largest degree of anisotropy encountered at this cross-section is at station PPR where the ratio of $\rho_{maximum} / \rho_{minimum}$ at long periods is about two decades. The resistivity values determined at almost all stations of cross-section II are smaller than resistivity values at cross-section I, except at FRS station. The resistivity values tend to decrease toward the stations west and east of FRS. Unlike the skew and delta theta values at cross-section I, here they are very large at OTC and THN. The large skew and delta theta findings at OTC may be associated with the coastline and a buried fault beneath this station. At THN, the large skew and delta theta may be related to granite intrusion found under this station. It can be concluded that only WST,FRS and PPR stations have a good two-dimensional indication at cross-section II, whereas stations OTC and THN are contaminated by local three-dimensional structures.

The new method of calculating rotation angle and dimensionality has been described and applied to three stations in the southeast Tasmania survey, and is proposed as a valid and useful method.

Chapter VII.
INTERPRETATION OF MAGNETOTELLURIC RESULTS IN SOUTHEAST TASMANIA.

VII.1. Introduction.

Geophysical interpretation of magnetotelluric data is designed to give an estimation of the resistivity distribution within the earth. In this study area this can tentatively be achived by the one-dimensional modelling process, but for a more accurate expression of resistivity distribution, two-dimensional modelling is required.

VII.2. One-dimensional Modelling.

Surface impedance values can be used to obtain information about the conductivity structure beneath the area of investigation. The simplest model is one where the conductivity varies only as a function of depth. This is suitable for determining the conductivity of the lower crust and upper mantle.

There are two diagonal apparent resistivity curves calculated in the tensor analysis. They are namely the ρ_{xy} and ρ_{yx} resistivities. The problem now becomes to decide which of the two curves best represents the electrical conductivity structure under the region. Since the anisotropy becomes larger at longer periods, the structure causing the separation most likely lies at some depth in the crust. If it is assumed to be approximately two-dimensional (i.e. resistivity varies with depth and in a NE-SW direction), two cases may be considered: one with currents flowing in the direction parallel to the strike of the structure (TE mode), and one with currents flowing

perpendicular (TM mode). Studies with two-dimensional models (Patrick and Bostick, 1969) have shown that for the station on or off a buried conductor, the higher apparent resistivity curve is more representative. Since the TE mode (ρ_{xy}) in this study gives the higher resistivity, it is therefore used throughout the modelling. The use of TE mode is more relevant because this resistivity is less affected by the lateral inhomogeneity contrast (Swift, 1967) and therefore should represent the gross structural feature of the region. Orange (1981) also showed that the TE mode apparent resistivity values are relatively unaffected by inhomogeneity at near surface in the vicinity of magnetotelluric stations (± 200 metres). Orange (1981) therefore suggests that an interpretation based on the TE mode would produce more reliable models.

The one-dimensional modelling program used for this study was RES1DD written in BASIC based on the Schmucker algorithm (1970). This program is controlled by interactive command and can calculate up to a maximum of 15 layers. To achieve an acceptable layer model from the program, several constraints were applied i.e based on local geology, shallow resistivity determined by the transient electromagnetic method and results from shallow drilling.

VII.2.1. Cross-section I.

The major structural units for cross-section I may be seen in a plot of calculated apparent resistivity versus depth. However, before calculating each data set, appropriate resistivity estimates as a function of depth must be obtained to ensure the starting models are appropriate.

The magnetotelluric data contain no information on apparent resistivity at near-surface layers. To constrain the resistivity and thickness parameters to shallow

depth, data obtained from surface geology and other geophysical methods must be used.

Taking into account the cross-section I models of electrical resistivity proposed in Chapter III for LSV, GRV, JDB and LNV stations (see Figures III.3 to III.6) on the basis of transient electromagnetic results, several models were tested and the resulting apparent resistivity calculated. At least two important facts emerge, namely the approximate depth of first layer and the resistivities of the first and second layers, which become obvious from transient electromagnetic results, and are used throughout the modelling. However, the thickness of the layers was varied during modelling to find the result best fitting the observed and calculated data. In addition, the two-dimensional modelling of gravity and magnetic results also plays an important role and is used to estimate the thickness of the basin.

To assess the electrical structure of southeast Tasmania, one-dimensional modelling was performed. Both the layer resistivities and thicknesses of the basin were variables along with a fixed number of layers preset at 6. The result is given in Figures VII.1 to VII.4 for stations LSV, GRV, JDB and LNV respectively. In general, the best fit calculated to the observed data at every station is quite good. For the first surface layer the variation of the resistivity ranges from 180 to 260 Ohm-m. These resistivity values represent Permian rocks which have a thickness of about 500 metres beneath LSV and GRV stations, becoming shallower at JDB and LNV stations to 350 metres. These thicknesses are based on the transient electromagnetic results. An attempt to model with the same resistivity values having a thickness based on the interpretation of the two-dimensional gravity and magnetic model of cross-section I, (650 metres at LSV, GRV and 600 metres at JDB, LNV), produces a very similar result. It indicates that the effect of a small change in thickness at the surface layer is insignificant.

1D MAGNETOTELLURIC MODEL

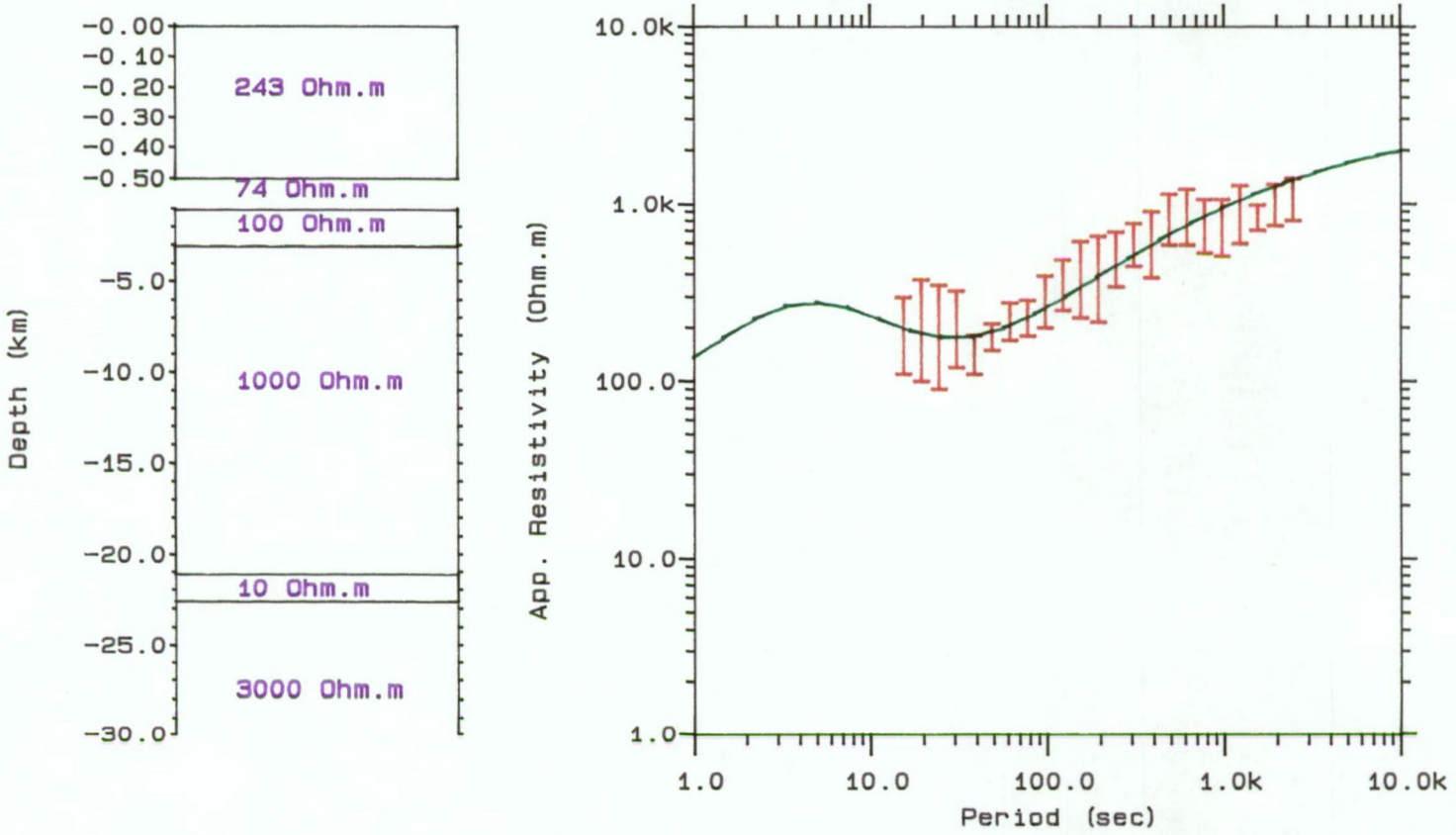

Figure VII.1. 1D model results from Leslie Vale (LSV)
(red)-observed; (green)-calculated

1D MAGNETOTELLURIC MODEL

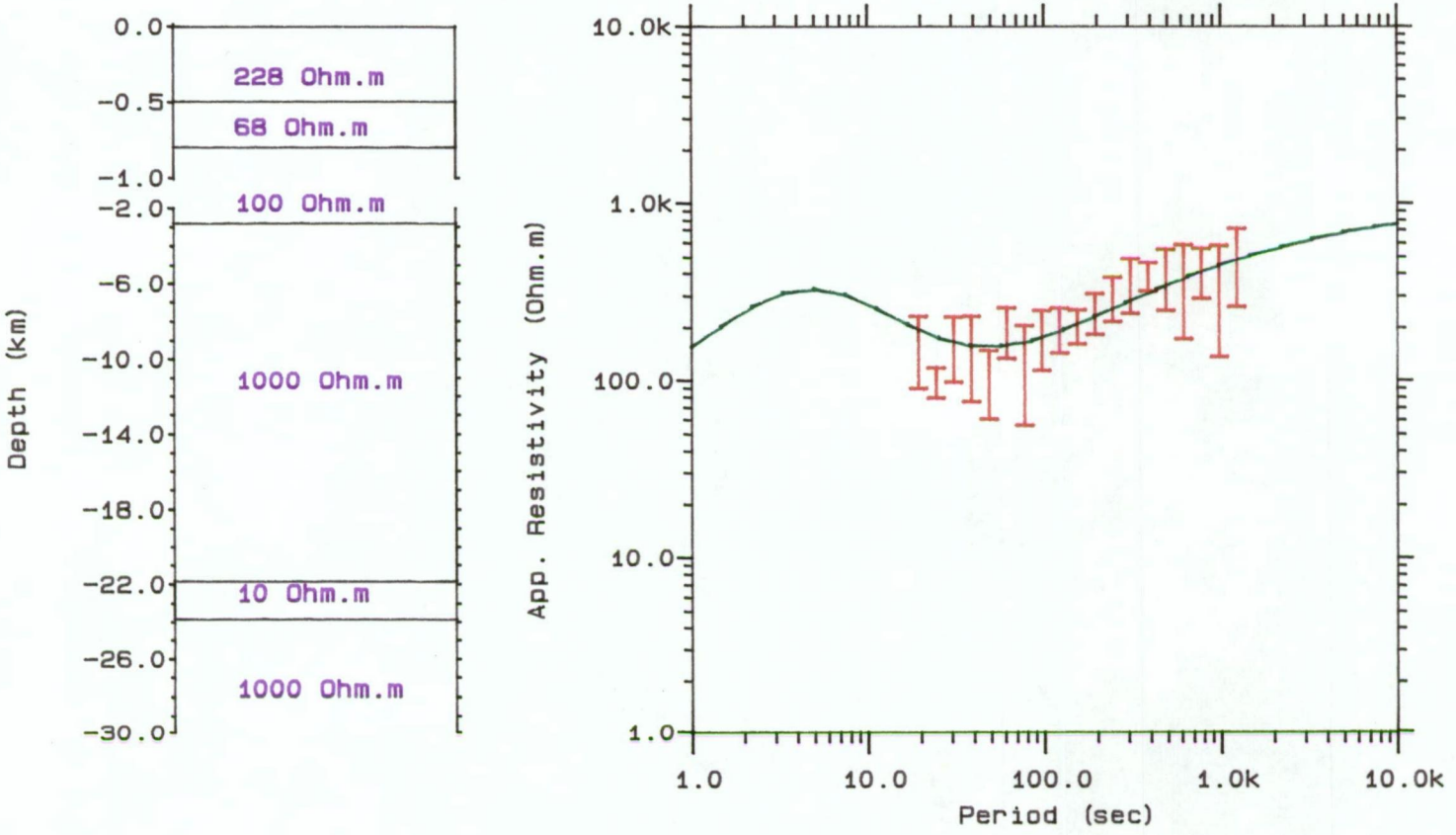

Figure VII.2. 1D model results from Grove (GRV)
(red)-observed; (green)-calculated

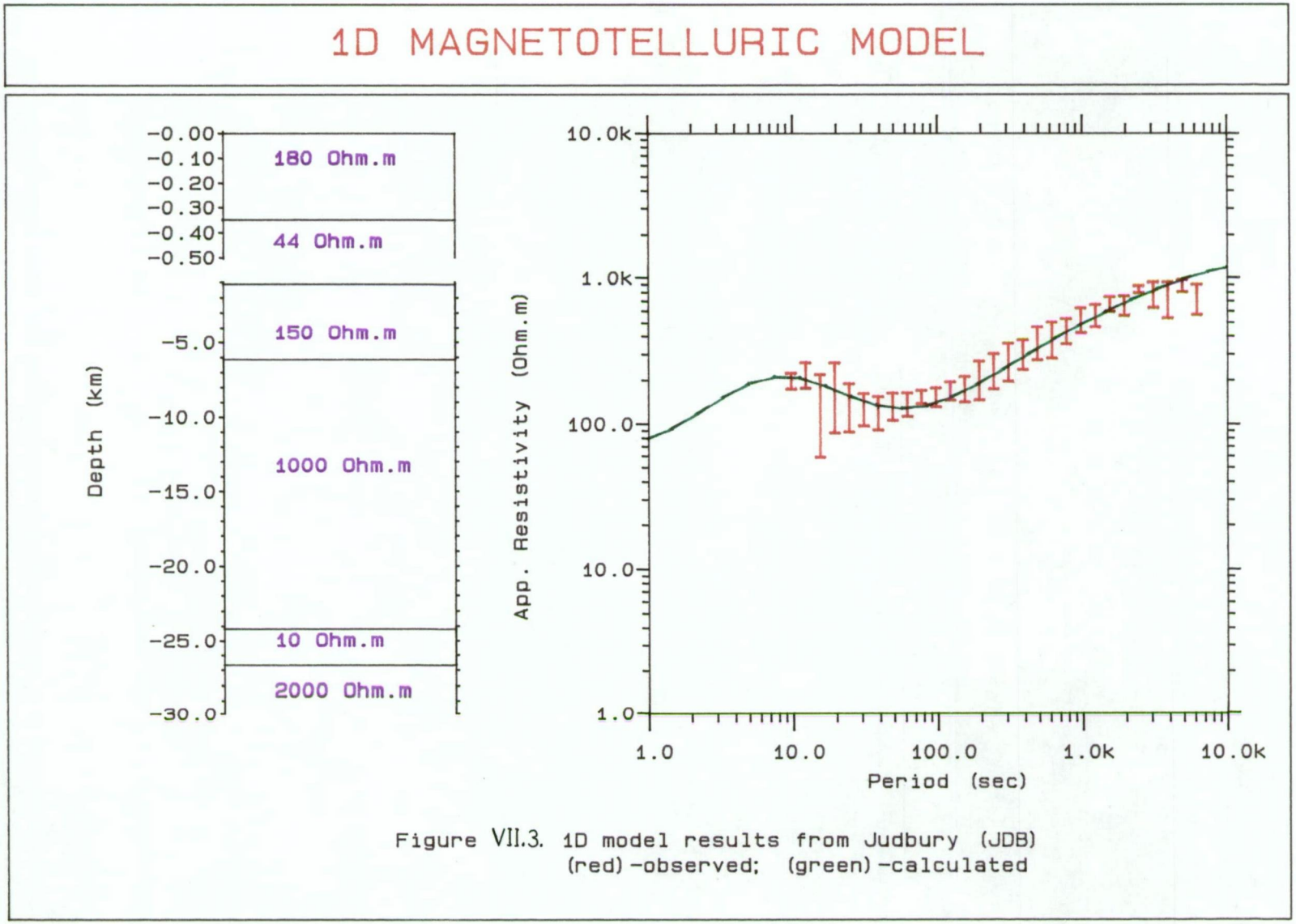

Figure VII.3. 1D model results from Judbury (JDB)
(red) -observed; (green) -calculated

1D MAGNETOTELLURIC MODEL

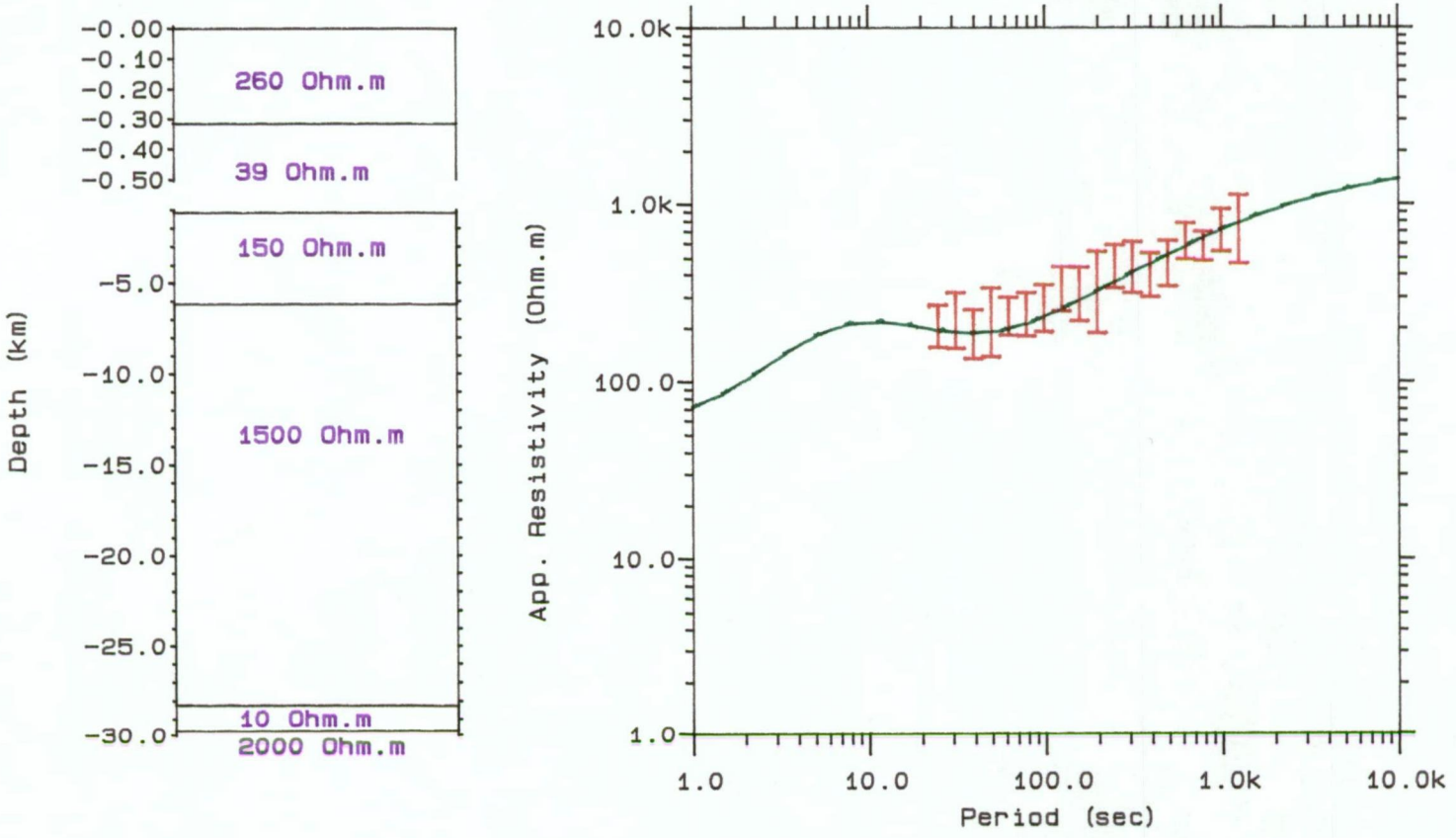

Figure VII.4. 1D model results from Lonnavale (LNV)
(red)-observed; (green)-calculated

The resistivity values to be used for the second layer were again based on the transient electromagnetic results. From now on the thickness information is based merely on the two-dimensional gravity and magnetic modelling results. Two different resistivity layers are inserted. They are namely, a layer with a resistivity value of 68 to 74 Ohm-m which is represented by Cambrian volcanic rocks beneath GRV and LSV, and a layer which has a resistivity value of 39 to 44 Ohm-m for Ordovician rocks at LNV and JDB. The thickness of the 68 to 74 Ohm-m layer varies from 300 metres at GRV to 700 metres at LSV, while the thickness of the 39 to 44 Ohm-m layer is very uniform at LNV and JDB being 300 metres.

A resistive layer is required to fit magnetotelluric data at stations LSV, GRV, JDB and LNV. This third layer has resistivity of 100 Ohm-m with thickness of 2000 metres at both LSV and GRV stations. Based on the result of the two-dimensional gravity and magnetic model the 100 Ohm-m resistivity value seems likely to represent the resistivity value of Jubilee-region-style Precambrian rocks (largely dolomites). Toward the western stations the resistivity and the thickness of this third layer increases gradually and it probably represents a different rock type. This layer possesses resistivity of 150 Ohm-m and thickness of 5000 metres either at JDB or LNV. It is believed that this 150 Ohm-m layer represents Cambrian volcanic rocks.

Another more resistive layer of 1000 to 1500 Ohm-m needs to be inserted underneath the third layer. This represents Precambrian rocks which underlie the sedimentary cover in this region. The thickness of this fourth layer is grading toward the western stations i.e. to the centre of the island. The depth from the surface to the bottom of this layer varies from about 21 kilometres at LSV to 28 kilometres at LNV. This depth agrees with the depth of the Moho in Tasmania (see Figure VII.5) obtained from gravity modelling (Johnson, 1972; Leaman et al., 1980; Leaman and Richardson, 1989).

To fit magnetotelluric observed data at all stations, a very conductive layer is required as the fifth layer. There is no evidence on the surface of the presence of an intra-crustal conducting zone in this region. However inspection of the TE mode apparent resistivity curves shows its existence. A good fit calculated to the observed data is obtained by inserting a layer with a uniform resistivity of 10 Ohm-m. The average thickness of this layer at all stations is about 2 kilometres. Beneath all magnetotelluric stations, this layer is underlain by a 2000 Ohm-m layer which probably represents the upper mantle layer. The one-dimensional model cross-section I may be found in Figures VII.6 and VII.6a for the deep structure and sedimentary basin respectively..

To consider the ambiguity of the presence of a 10 Ohm-m layer, a one-dimensional model was constructed without the conductive layer at depth. The results, which display an unrealistic fit, are shown in Appendix VII.1. The conclusion which can be drawn from this is that the presence of the 10 Ohm-m layer is essential to fit magnetotelluric data and Figures VII.1 to VII.4 are the preferred models to represent the gross one-dimensional electrical structure of this region.

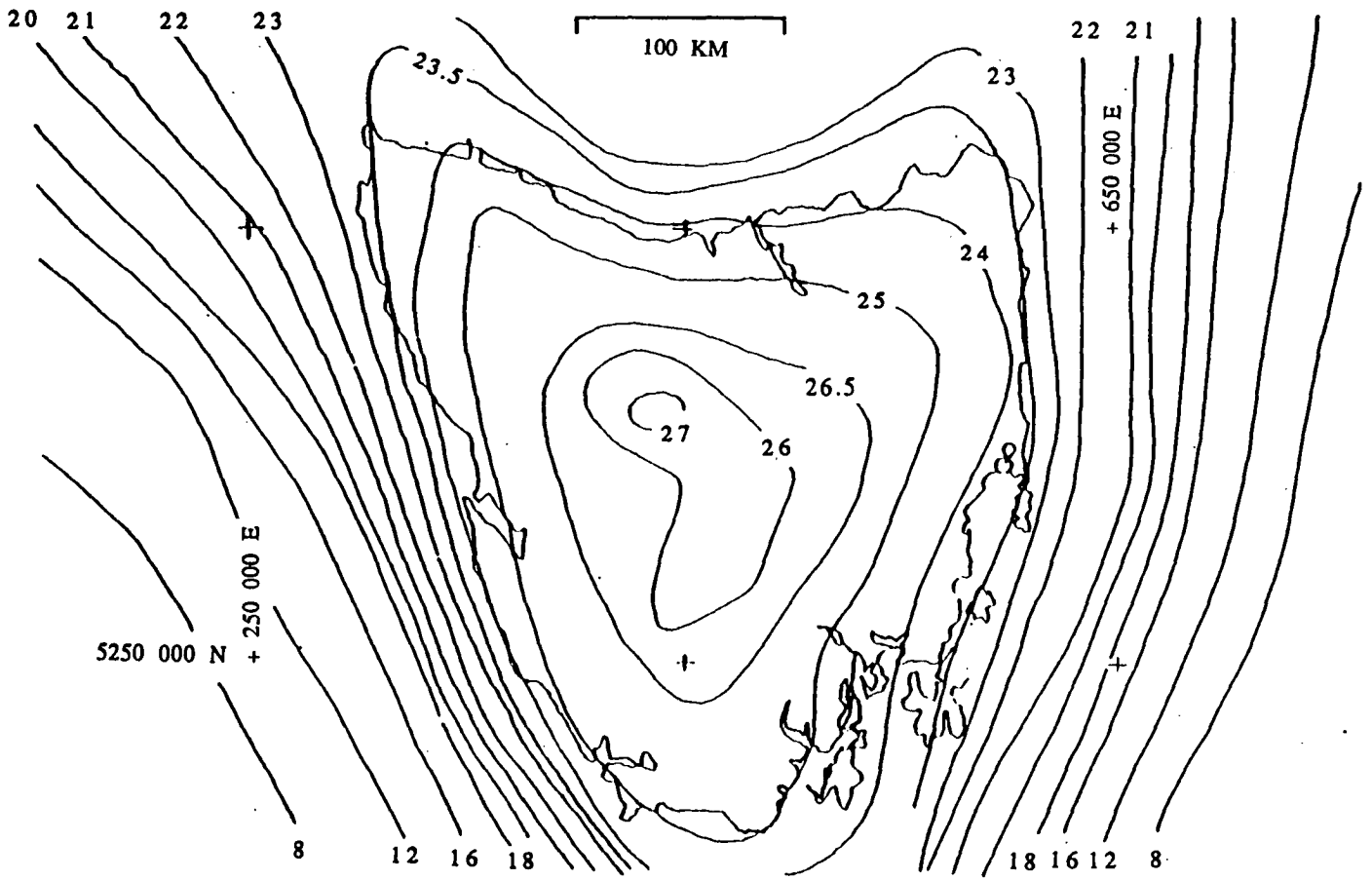

Figure VII.5. Model of the base of the crust. Contours in km below geoid (sea level). (after Leaman and Richardson, 1989).

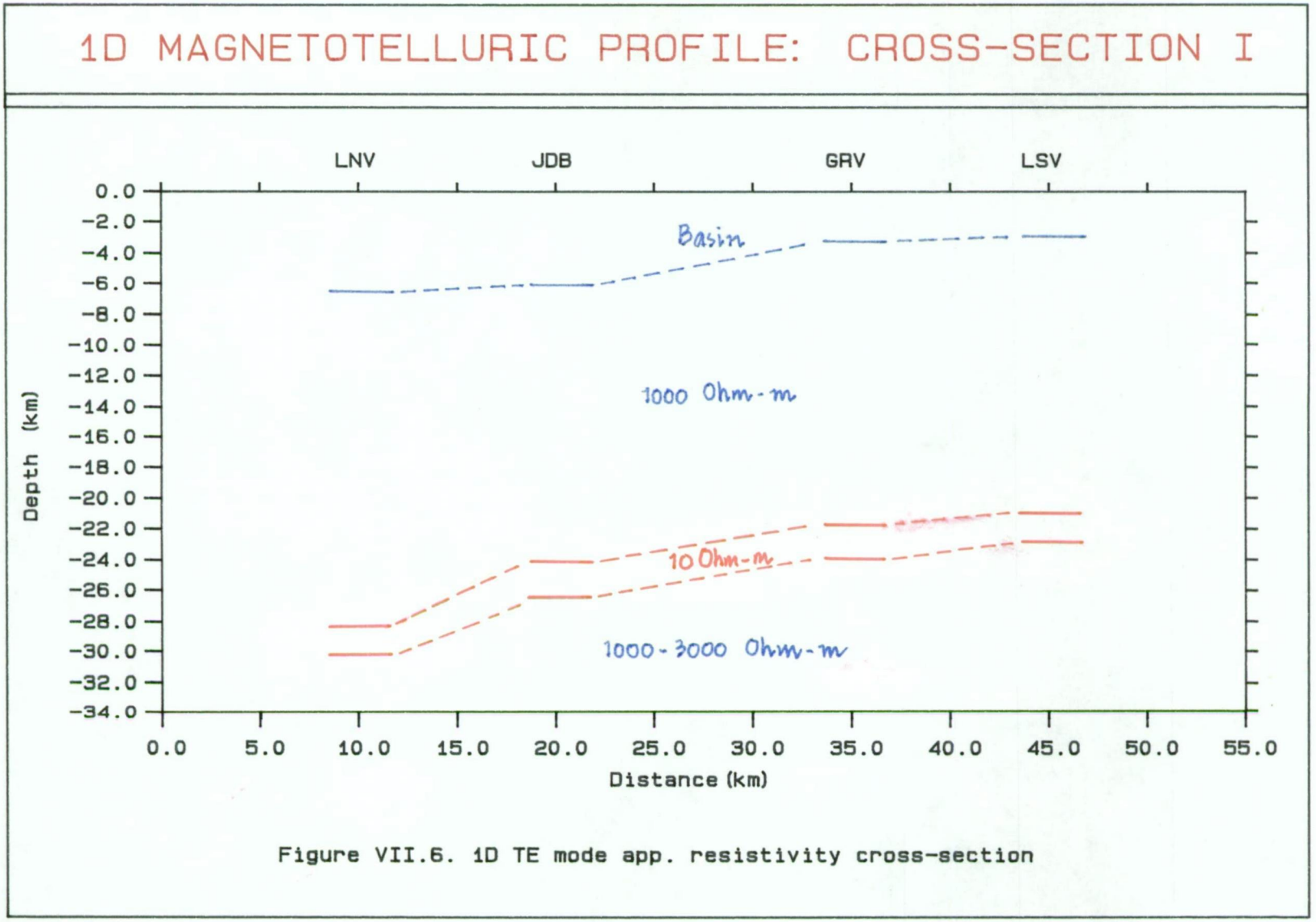

Figure VII.6. 1D TE mode app. resistivity cross-section

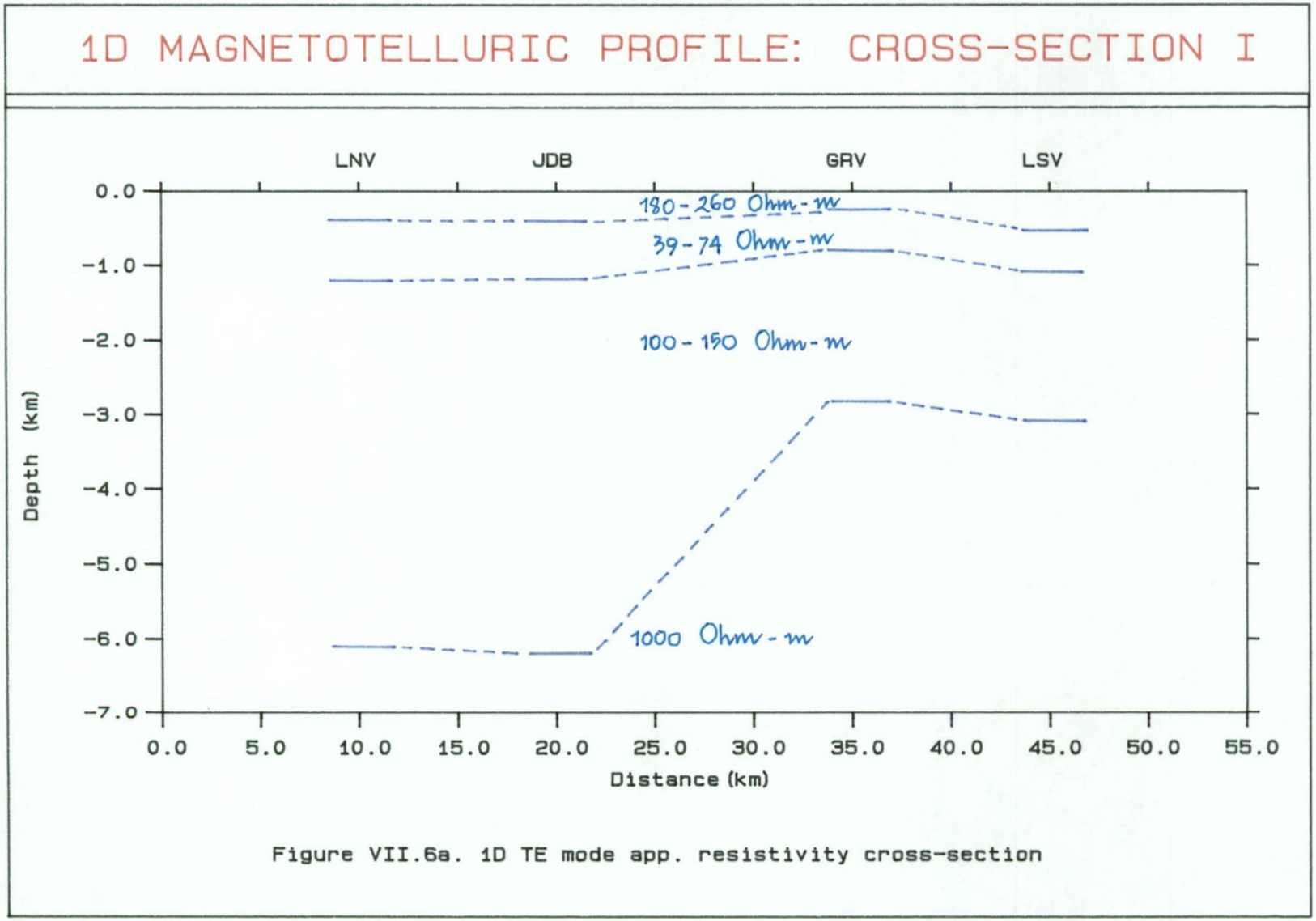

Figure VII.6a. 1D TE mode app. resistivity cross-section

VII.2.2. Cross-section II.

The one-dimensional model of cross-section II is shown in Figures VII.7 to VII.11 for OTC, WST, FRS, PPR and THN stations respectively. As in cross-section I, the construction of one-dimensional models from the magnetotelluric data in this cross-section was aided by the transient electromagnetic and the two-dimensional gravity and magnetic results. The shallowest layer has resistivities in the range of 48 to 51 Ohm-m, except at PPR and THN to the west, where the 51 Ohm-m layer is replaced by layers of 311 and 159 Ohm-m respectively. Based on two-dimensional gravity and magnetic modelling and deep drilling, the 48 to 51 Ohm-m layer at OTC, WST and FRS can be correlated with Triassic mudstone, sandstone and minor limestone, while the 311 and 159 Ohm-m layers represent dolerite rock at PPR and Permian mudstone, sandstone and limestone at THN.

Underlying the shallowest layer is an almost uniform layer beneath OTC, WST and PPR with resistivity about 233 to 239 Ohm-m which represents Permian rocks. At PPR and THN the second layer has a resistivity of 28 and 30 Ohm-m respectively and may be correlated with Triassic rock at PPR and Ordovician rock at THN.

The resistivity layer that represents Cambrian volcanic rocks in the trough-like structure varies from 200 Ohm-m at WST and 500 Ohm-m at FRS to 50 Ohm-m at PPR. The thickness of this layer is about 5 kilometres at FRS and decreases to 4 kilometres at WST and PPR i.e. east and west stations from FRS. The dramatic change in the thickness and resistivity of this layer may indicate a zone of faultings. The 75 Ohm-m layer inserted at OTC represents Jubilee-region-style Precambrian rocks.

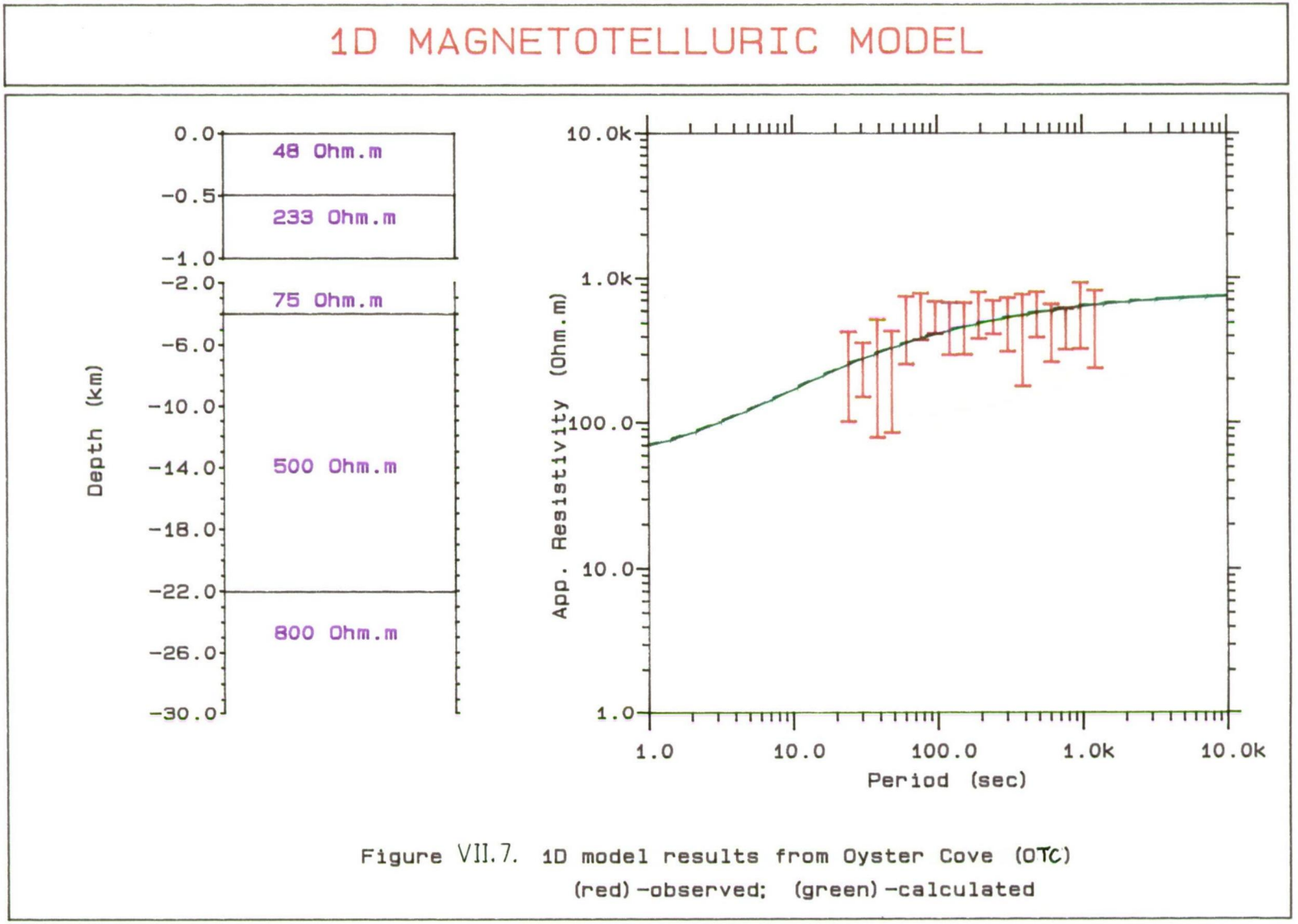

Figure VII.7. 1D model results from Oyster Cove (OTC)
(red)-observed; (green)-calculated

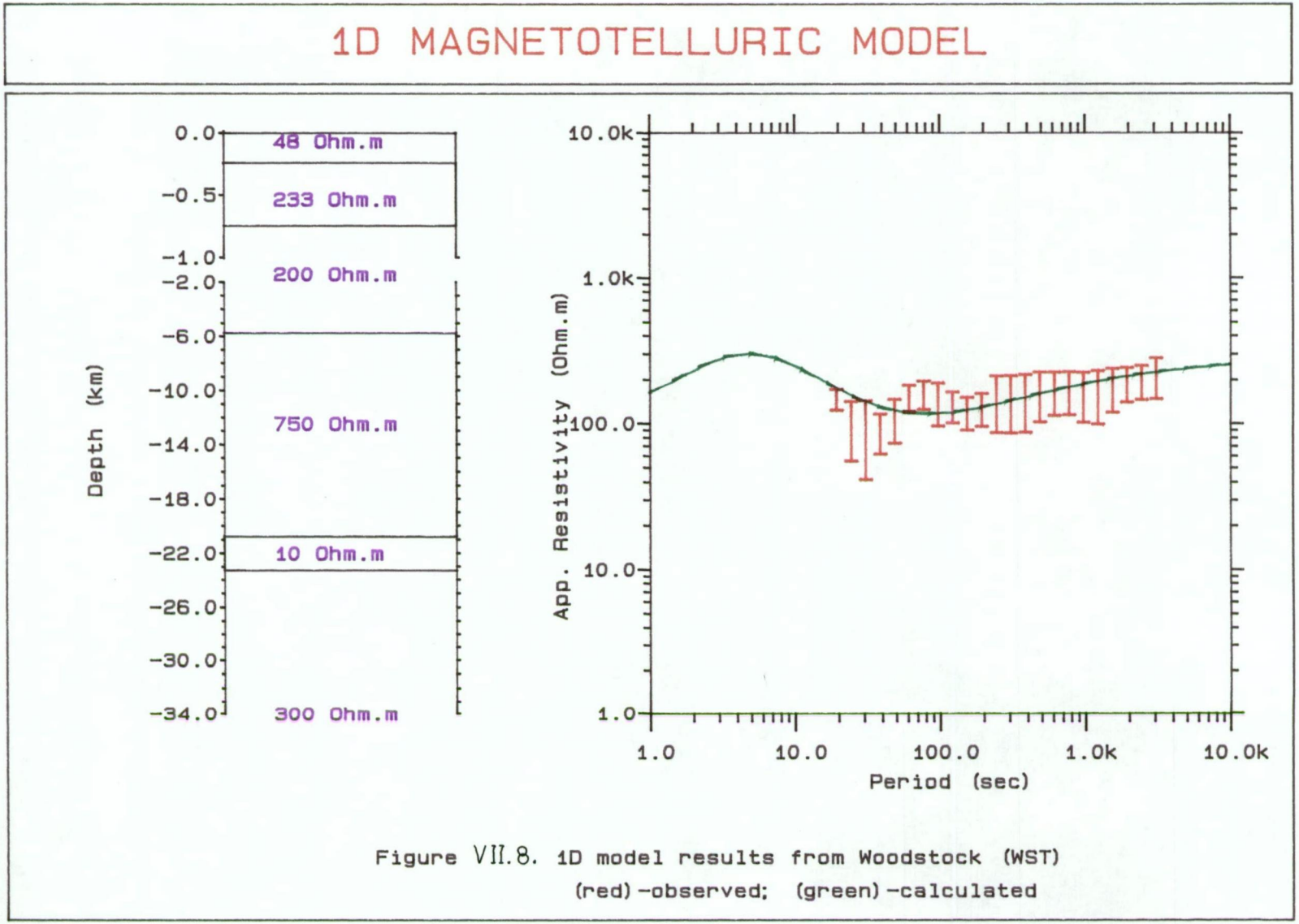

Figure VII.8. 1D model results from Woodstock (WST)
(red)-observed; (green)-calculated

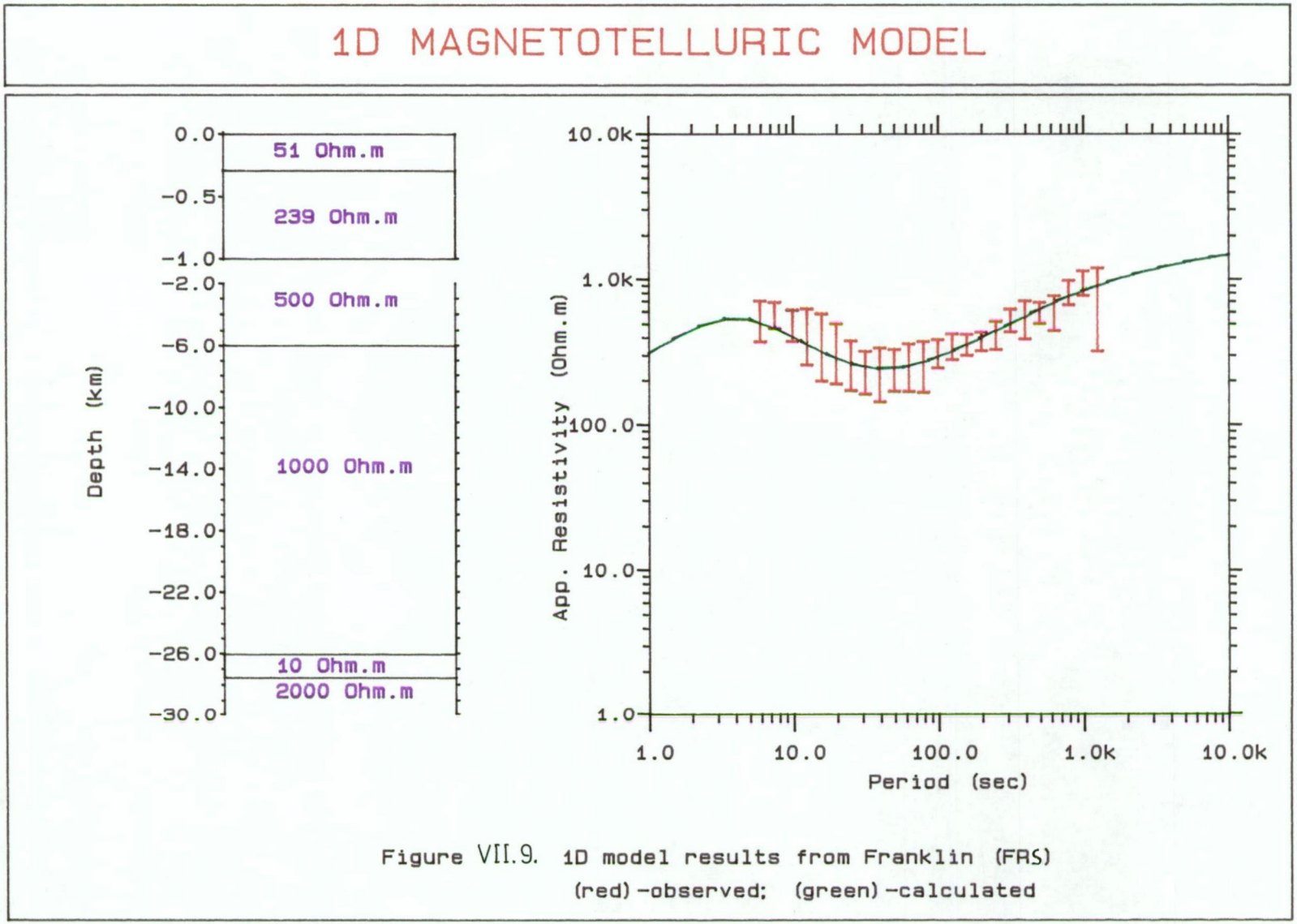

Figure VII.9. 1D model results from Franklin (FRS)
(red)-observed; (green)-calculated

1D MAGNETOTELLURIC MODEL

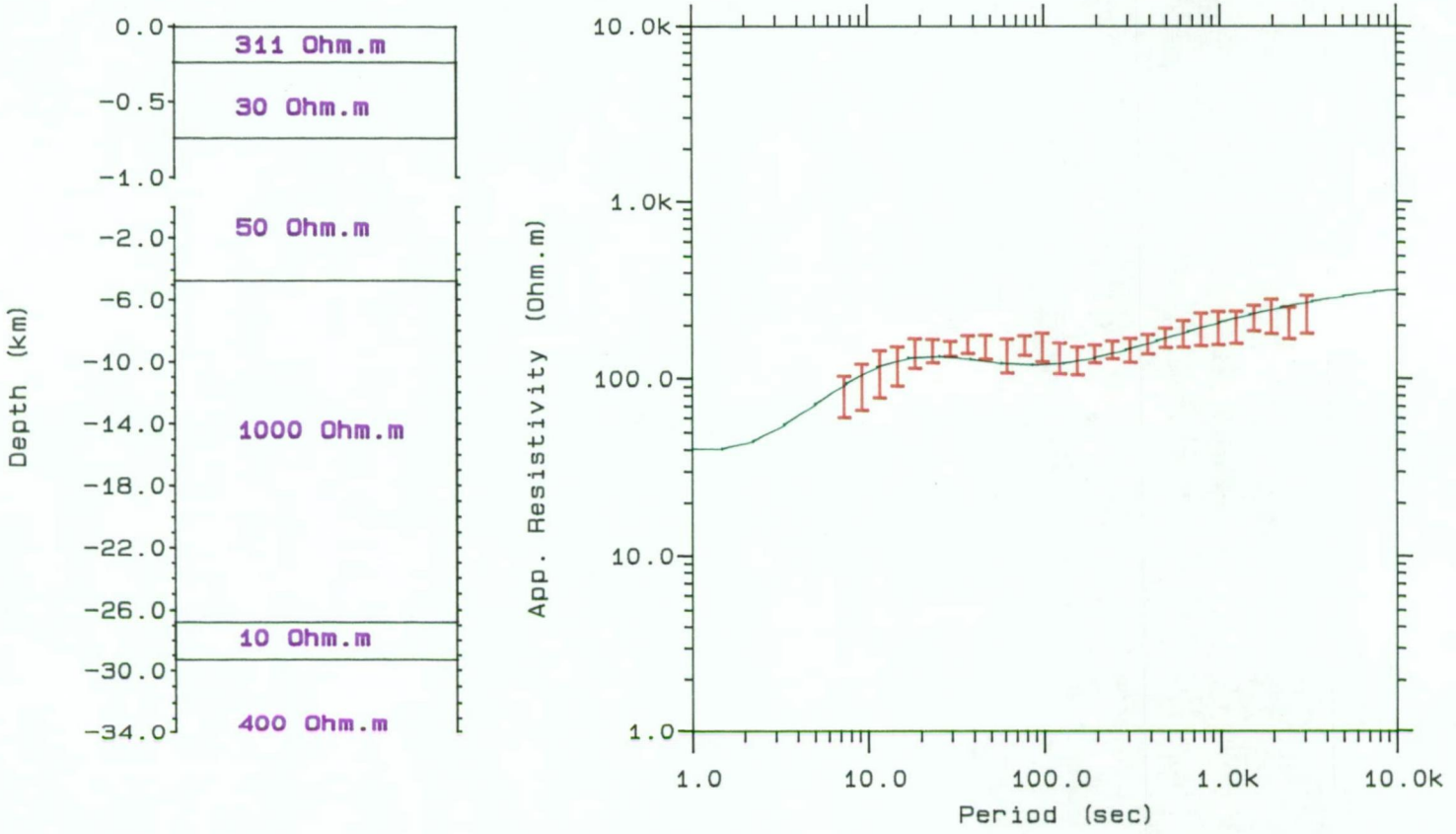

Figure VII.10. 1D model results from Peppers Rd. (PPR)
(red)-observed; (green)-calculated

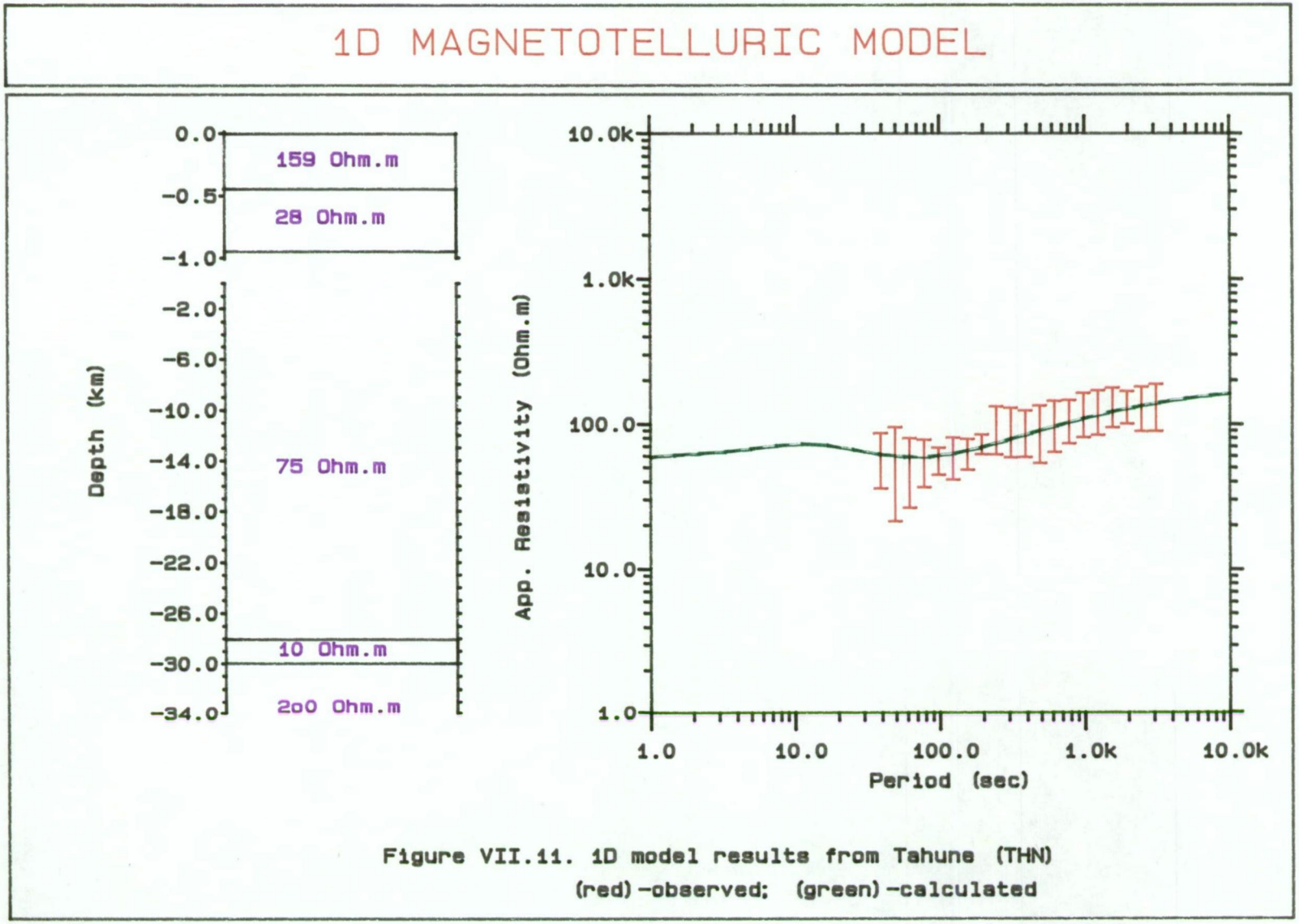

Figure VII.11. 1D model results from Tahuna (THN)
(red)-observed; (green)-calculated

Except for THN, a resistive layer is needed to fit magnetotelluric data at stations OTC, WST, FRS and PPR which underlie the sedimentary cover in this cross-section. This layer has resistivity ranging from 500 to 1000 Ohm-m and its thickness from the suface is similar to the fourth layer of cross-section I which also agrees with the depth of the Moho in this region. Underneath this layer very close to the Moho, a layer with very low resistivity is also required to fit magnetotelluric data at almost all stations. This layer is not resolved at OTC. However at FRS the presence of this conductive layer is very obvious. The one-dimensional model cross-section in this magnetotelluric traverse can be seen in Figures VII.12 and VII.12a for the deep structure and sedimentary basin respectively. .

Based on the one-dimensional model result of cross-section II, the degree of confidence of the model result is very low as the best fit of the observed and calculated data is poor. This may be partly due to the fact that a three dimensional earth was modelled with a one-dimensional modelling program. Nevertheless, the presence of a lower crustal conducting zone seems to continue and be consistent at almost all magnetotelluric stations in this cross-section. This is in agreement with the results obtained by the magnetovariational method, i.e. the short corrected induction vectors at periods of 60 minutes at all stations (see Figure IV.15).

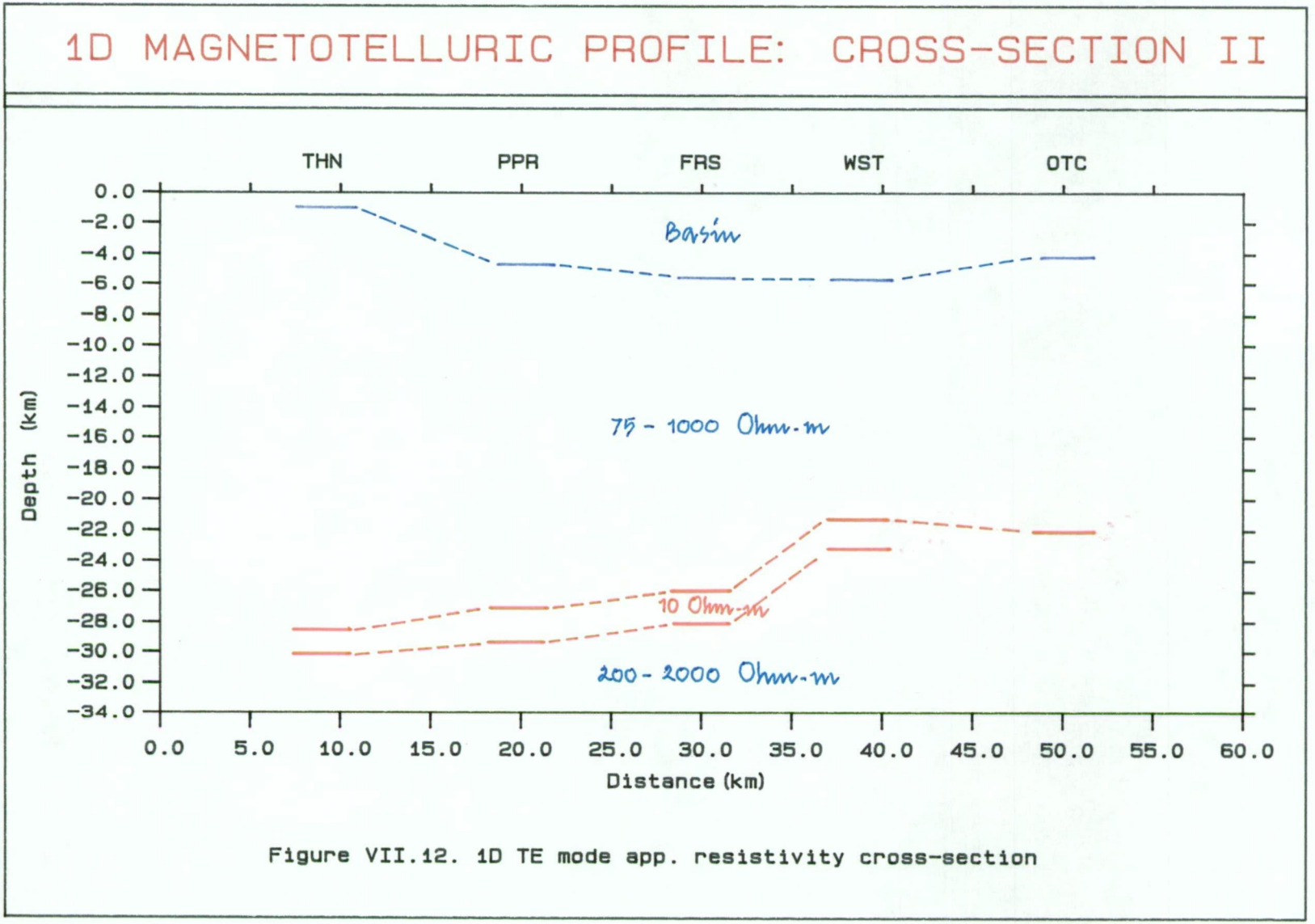

Figure VII.12. 1D TE mode app. resistivity cross-section

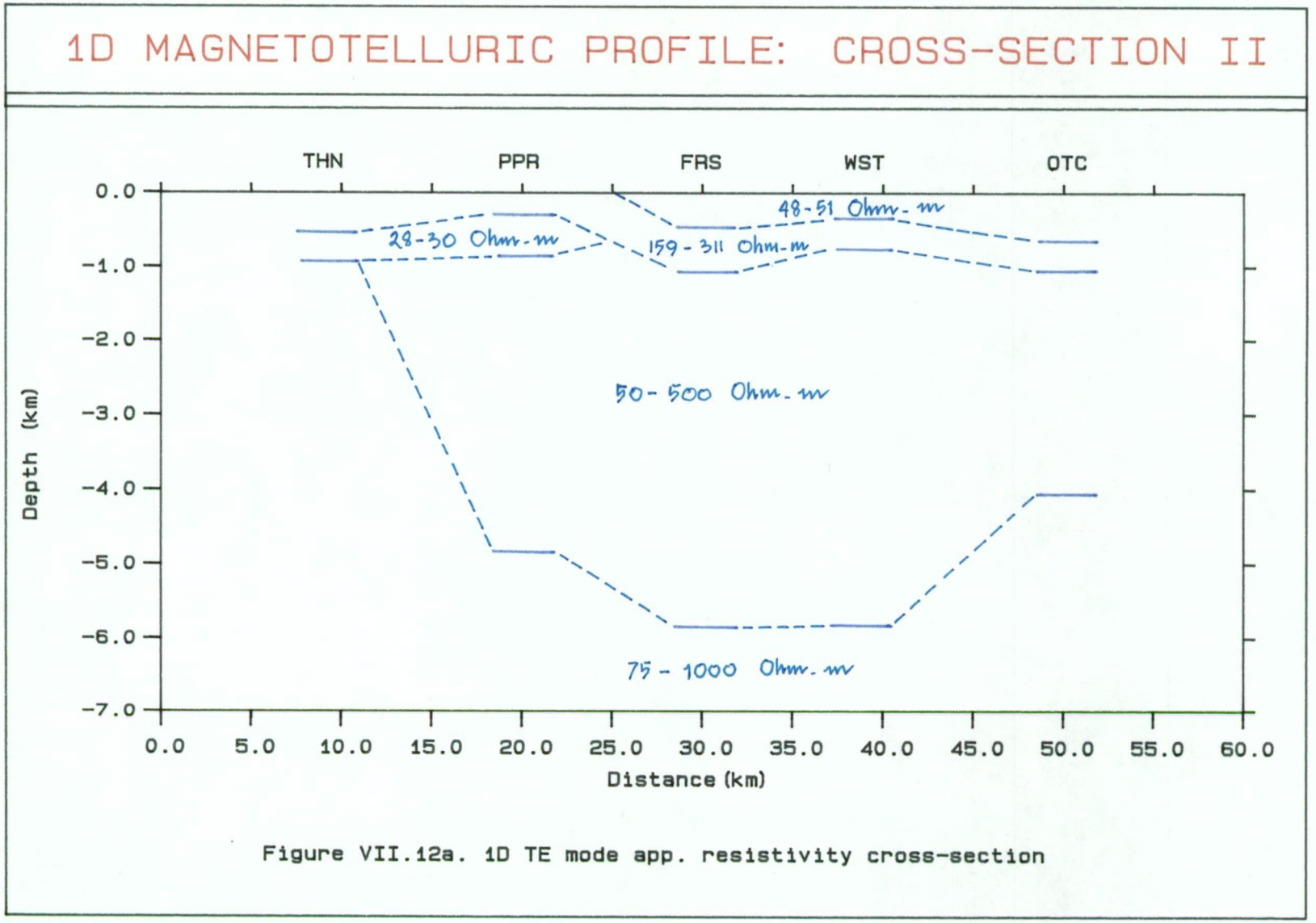

Figure VII.12a. 1D TE mode app. resistivity cross-section

VII.3. Two-dimensional Modelling.

Two-dimensional modelling of magnetotelluric data is more complex than one-dimensional modelling since the apparent resistivity varies with rotation of measurement axes. The aim of two-dimensional modelling is to determine whether the structures obtained from one-dimensional modelling are true representations of the geoelectric distribution in the region.

The response of a two-dimensional model with a conductive layer at the base of the crust will now be examined to see what it can reveal about the conducting structure. The computation of two-dimensional modelling in this experiment was carried out using the JP2DEH1 program. This program is based on the algorithm by Jones and Pascoe (1971) and boundary value routines of Pascoe and Jones (1972) including modifications suggested by Williamson et al. (1974) and Jones and Thomson (1974). For a given period, the program can be used to calculate the resistivity across the structure, for both the E- and H-polarisations.

The configuration of the model is composed of a 41 x 41 element grid, and its response is computed at 14 periods. Up to 1000 iterations are required for each before convergence is obtained for the E-polarisation. Convergence is assumed to have occurred when the maximum change of the fields at any grid point between successive alterations is less than 10^{-6}. In addition, all vertical grid lengths are taken to be small relative to the skin depth to ensure the program uses the maximum number of iterations and gives the most accurate result (Pascoe and Jones, 1972).

VII.3.1. Crosss-section I.

The starting two-dimensional model of cross-section I may be found in Figure VIII.13. This initial model was constructed based on the one-dimensional

results. It must be explained that in regard to the plotting data no air layer is included in this configuration and other two-dimensional configurations. Calculated data curves from the initial model (Figure VII.13) for every station are compared to the observed data curve and plotted in Figures VII.13a for LSV and GRV and VII.13b for JDB and LNV stations respectively. By inspection of these figures it is apparent that the fit obtained between observed data and model curve is not good. The calculated TE modes apparent resistivity curves for example, have too high an apparent resistivity over the whole period range. There are certain factors that could be responsible for this phenomena. The first possibility is that the thickness of the deep conductive layer which is 2.5 kilometres seems too thin in this model. The second is that the resistivity value of the layer which underlies this intra-crustal conducting zone may be too high. However, the calculated TM mode apparent resistivity fits quite well with the observed data at JDB and LNV stations.

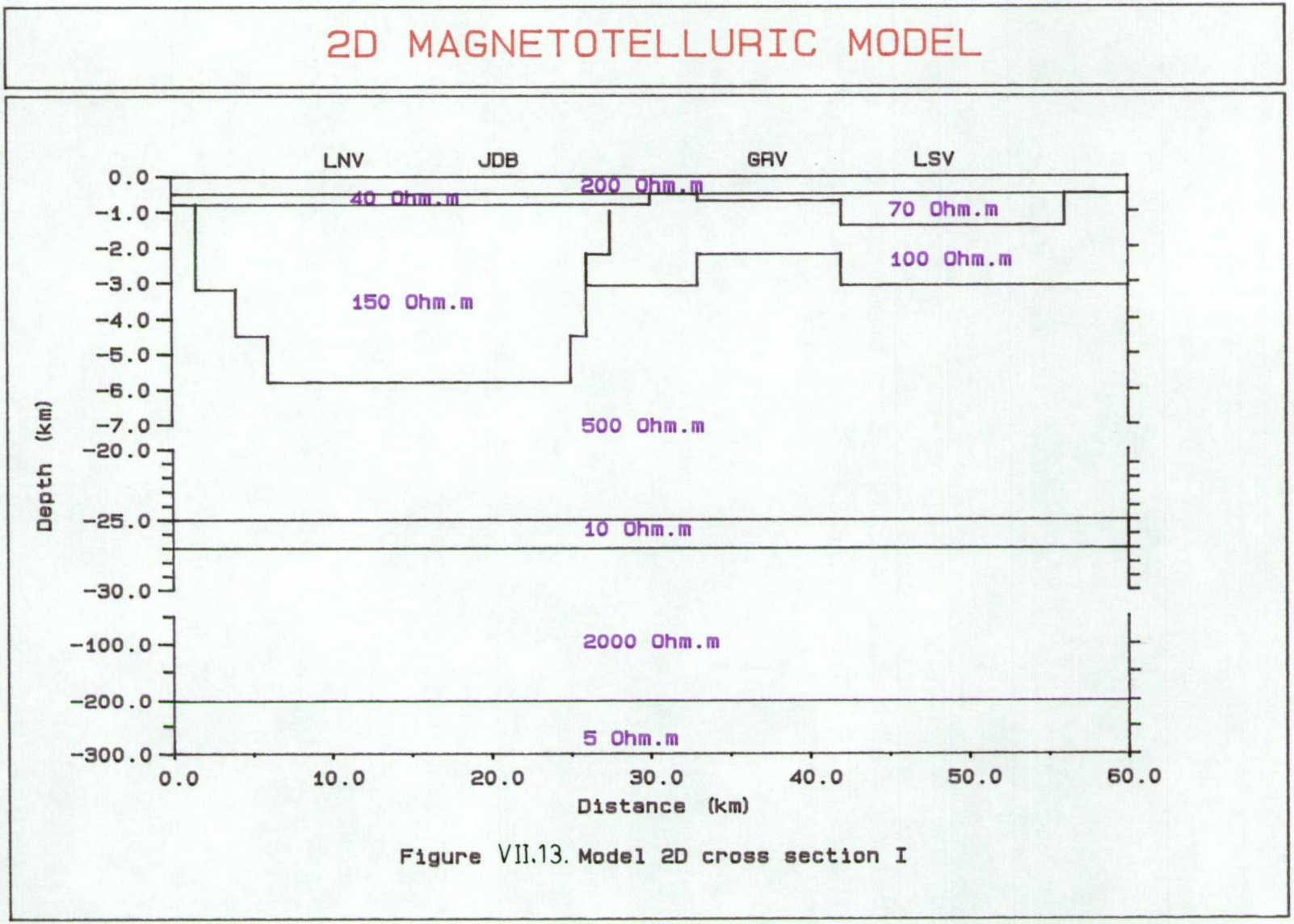

Figure VII.13. Model 2D cross section I

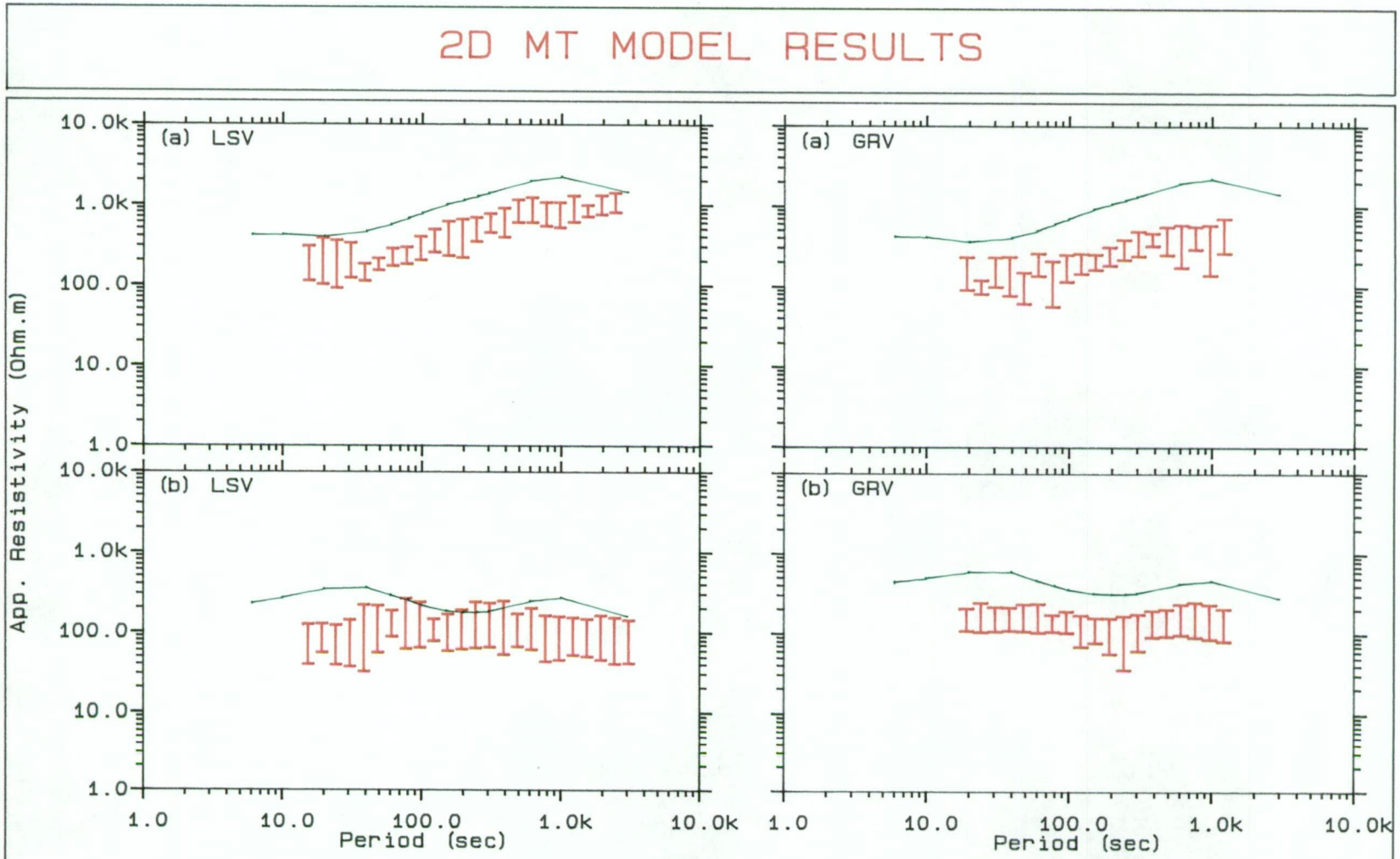

Figure VII.13a. Obs. (red) and cal. (green) app. resistivity from LSV and GRV stations
(a) E-polarization, (b) H-polarization

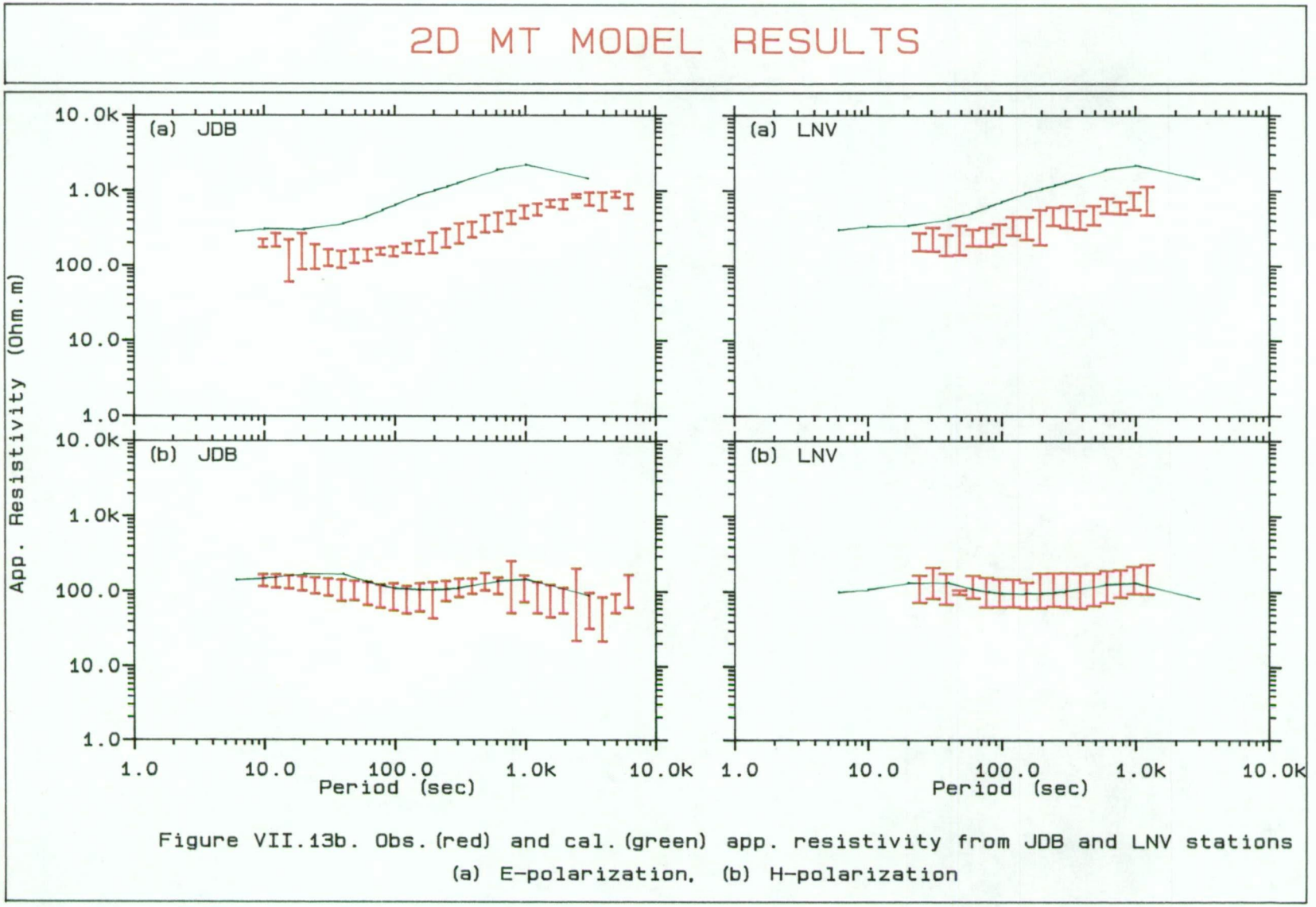

Figure VII.13b. Obs. (red) and cal. (green) app. resistivity from JDB and LNV stations
(a) E-polarization, (b) H-polarization

From the starting model just presented an attempt was made to construct a more realistic model of the electrical structure in the vicinity of the study area. The subsequent models are still based on the one-dimensional result but differ slightly from the model presented in Figure VII.13 in that now allowance has been made for a varying resistivity and thickness within the lower crust and upper mantle. The intra-crustal conducting zone was first modified by varying the resistivity and thickness which only improved the match of the model and observed data at periods of 100 to 200 seconds. This result seems to suggest that to get a better fit for periods longer than 200 seconds the resistive basement layer has to be modified. An attempt was made to run several models by reducing the resistivity values of the resistive layers and also vary their thickness so that their results show a better fit. As a separate run the resistivity and thickness of both the intra-crustal conducting zone and the resistive layers were also modified. The result is shown in Figure VII.14.

For the sake of completeness, the lateral extent of lower crustal layer is to be determined. To consider in quantitative manner a two-dimensional model having the basin characteristics shown in Figure VII.13 but with a deep conducting layer only beneath the deeper part of the basin (see Figure VII.15) further modelling was attempted. The results are shown in Figures VII.15a and VII.15b. These results indicate that the minimum in the observed apparent resistivity curves could not be due to the structure of the sedimentary basin alone. In fact, the basin appears to have an insignificant effect on the longer period data for this model. It therefore confirms that the extent of the deep conductive layer to the east of this model is essential to fit the data at GRV and LSV.

Figure VII.14 is the model configuration that produces the best fit to the observed data at all stations in this cross-section. Results at LSV, GRV, JDB and LNV from this model can be seen in Figures VII.14a and VII.14b. This model has a very uniform top layer with resistivity of 200 Ohm-m. This resistivity value seems

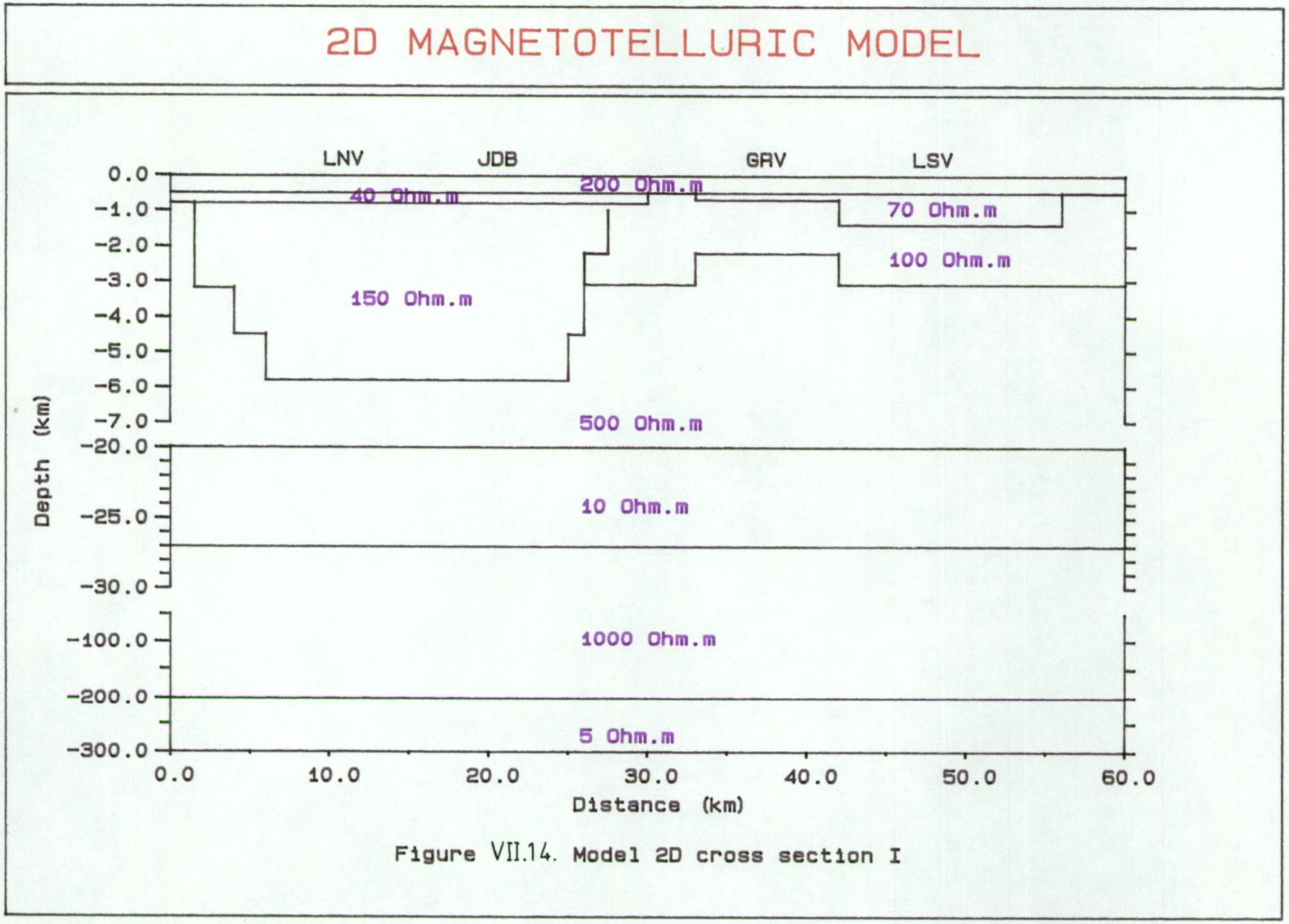

Figure VII.14. Model 2D cross section I

2D MT MODEL RESULTS

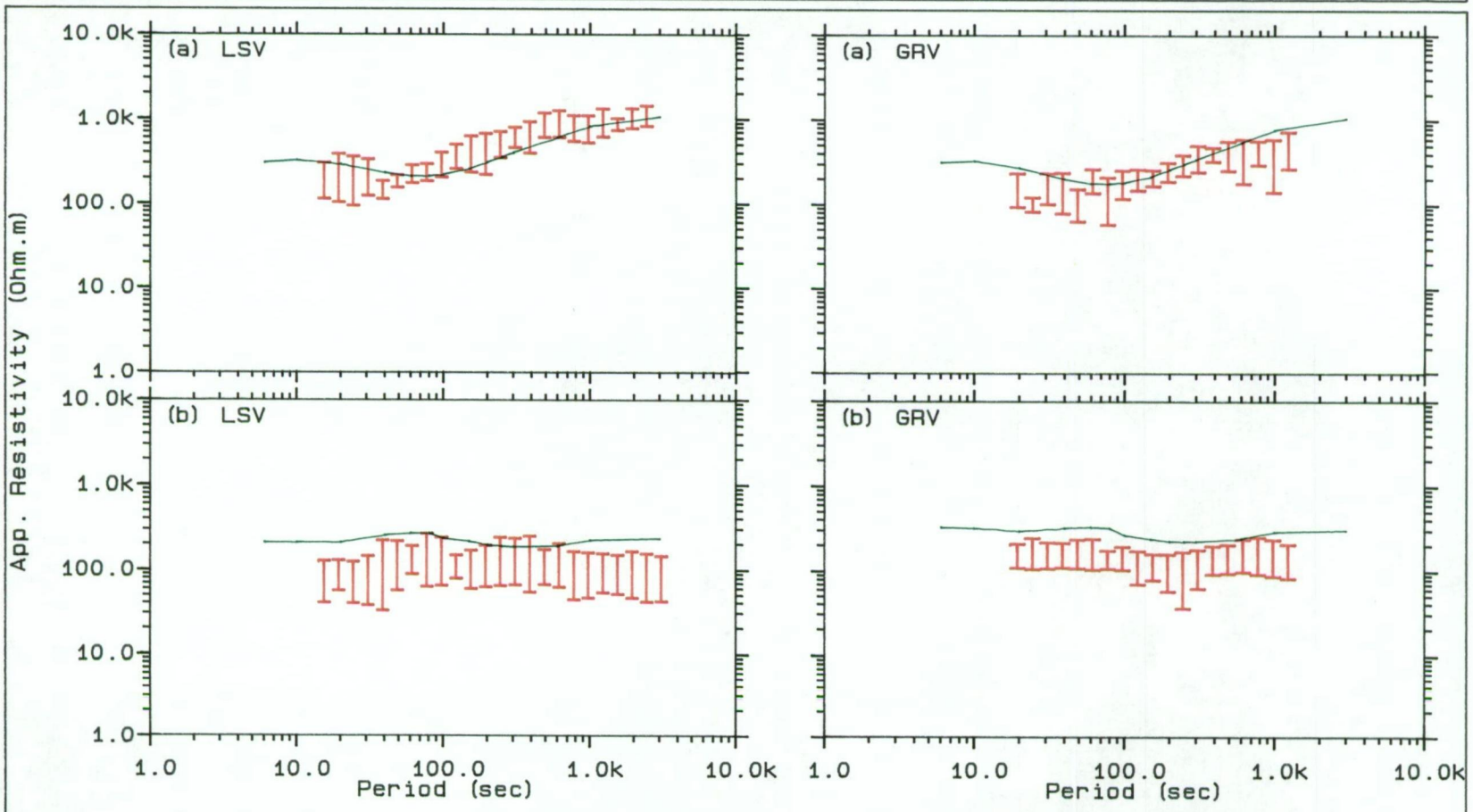

Figure VII.14a. Obs. (red) and cal. (green) app. resistivity from LSV and GRV stations
(a) E-polarization, (b) H-polarization

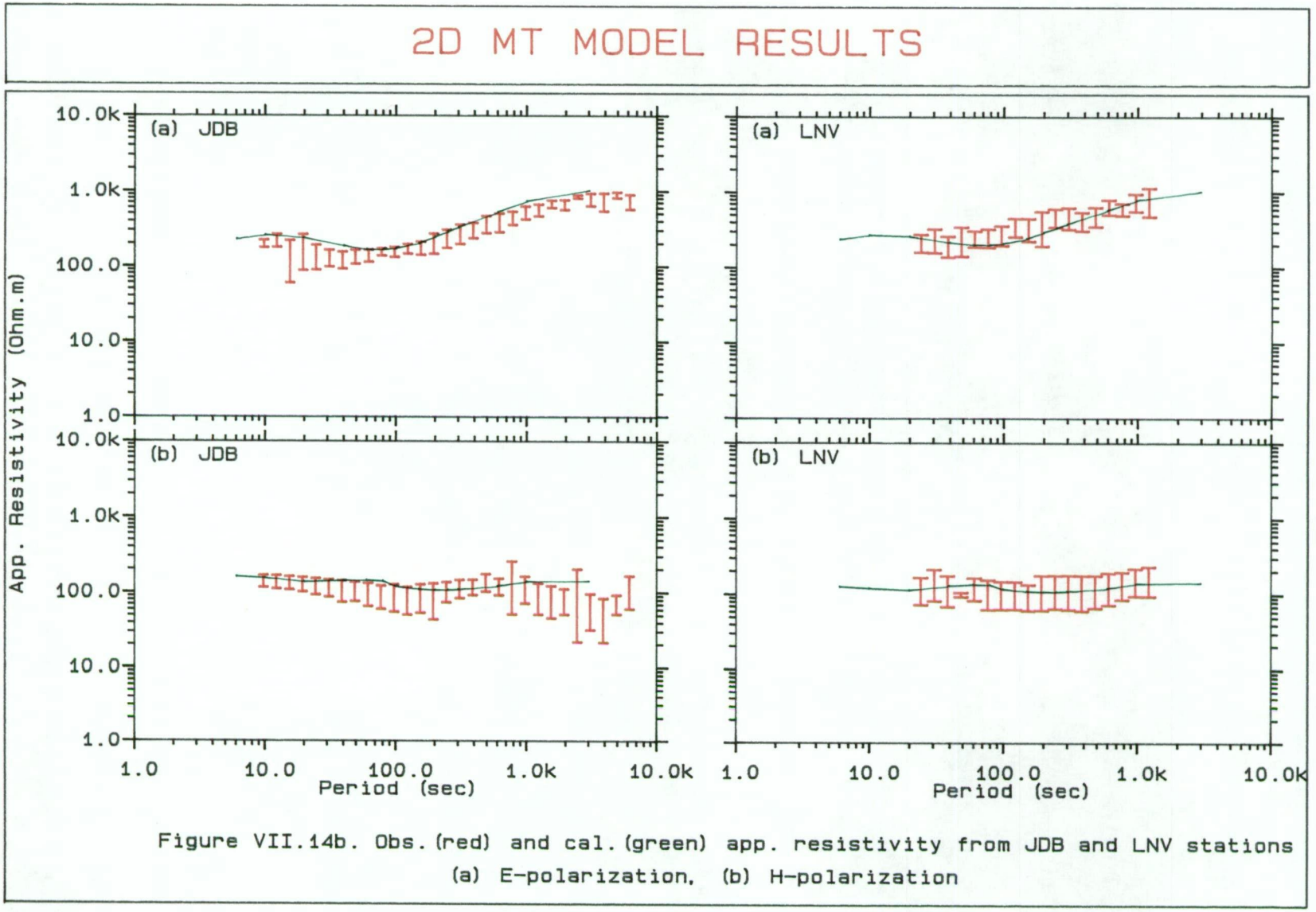

Figure VII.14b. Obs. (red) and cal. (green) app. resistivity from JDB and LNV stations
(a) E-polarization, (b) H-polarization

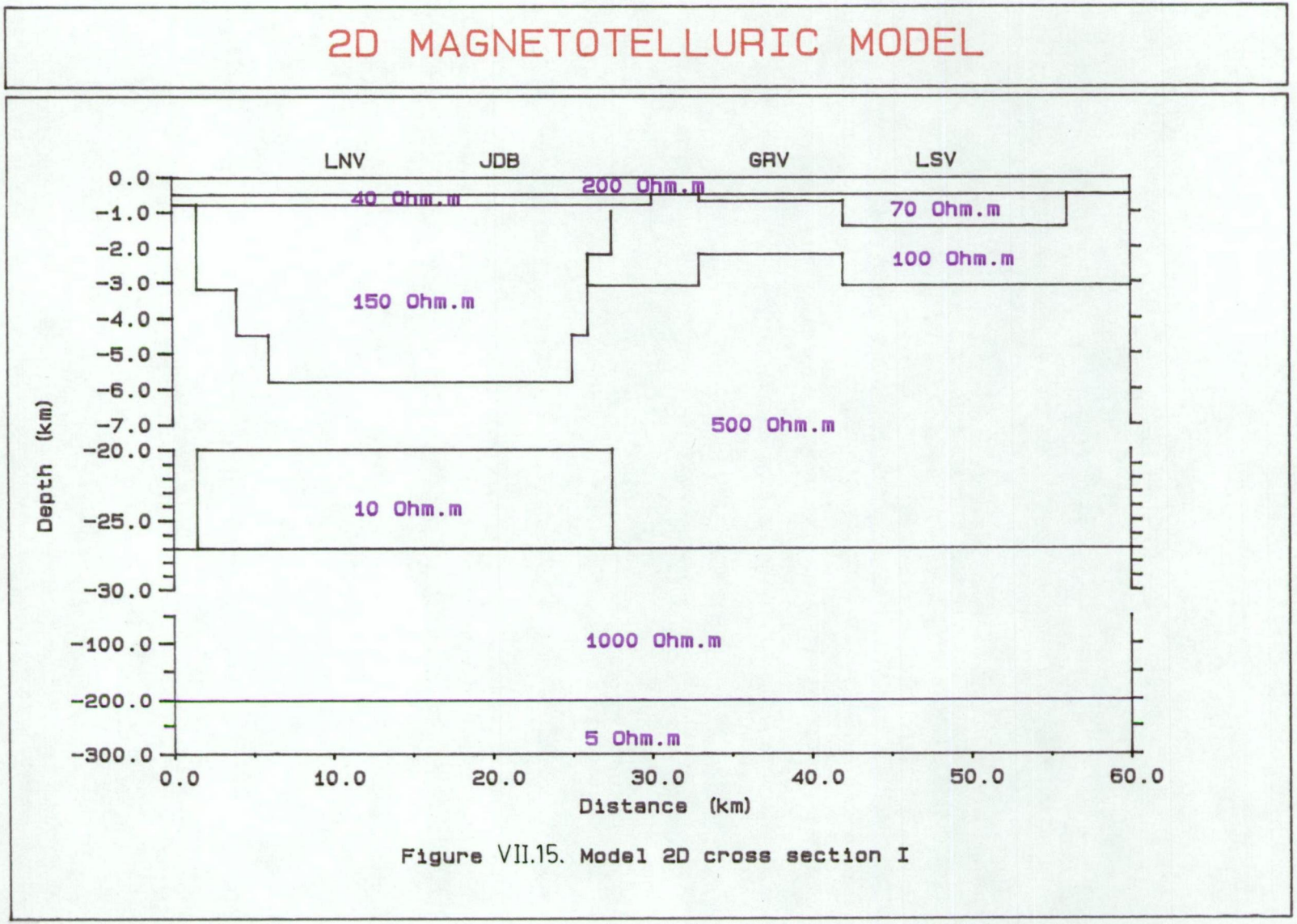

Figure VII.15. Model 2D cross section I

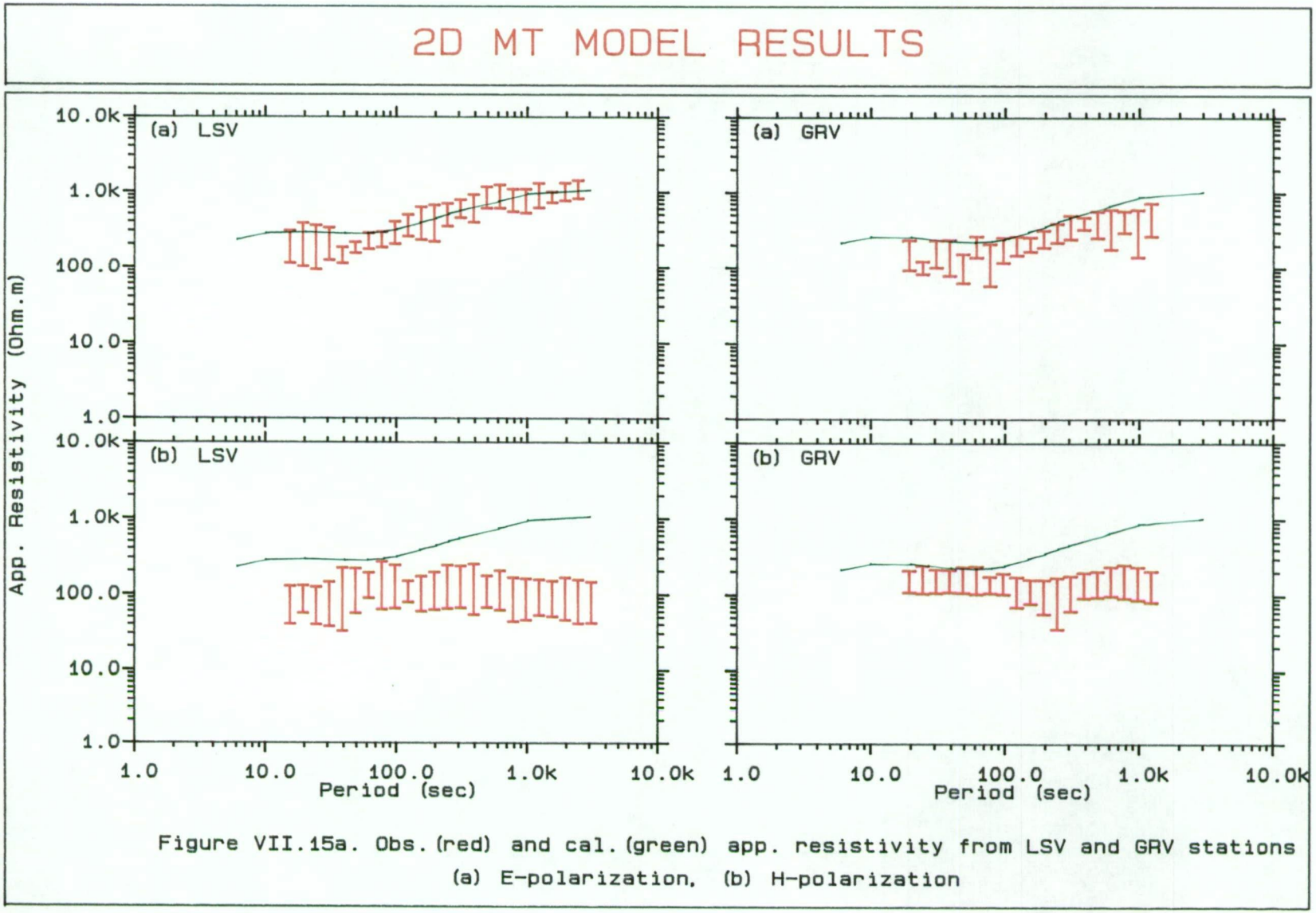

Figure VII.15a. Obs. (red) and cal. (green) app. resistivity from LSV and GRV stations
(a) E-polarization, (b) H-polarization

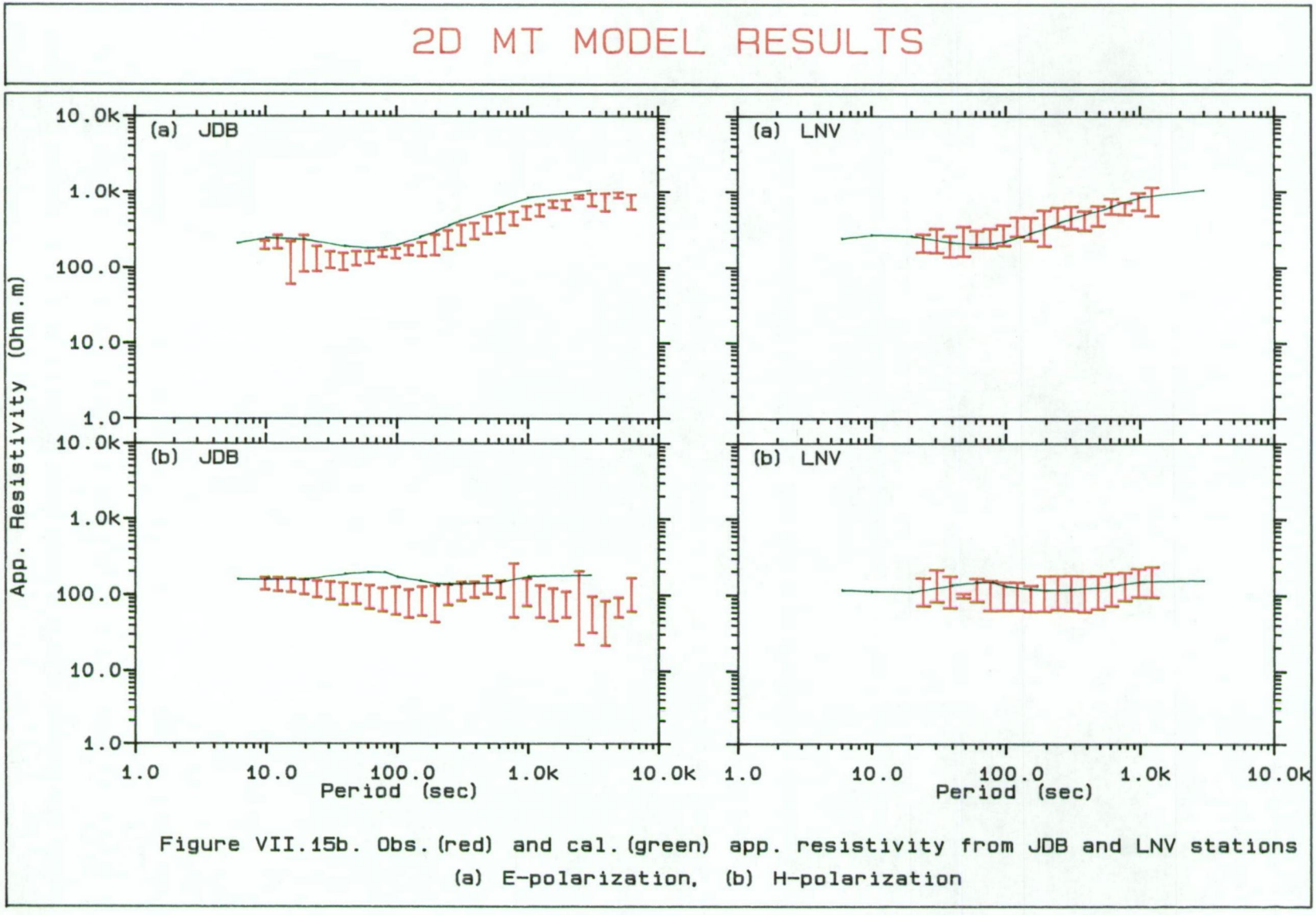

Figure VII.15b. Obs. (red) and cal. (green) app. resistivity from JDB and LNV stations
(a) E-polarization, (b) H-polarization

likely to represent the gross resistivity value of the Permo-Triassic cover which has a thickness of about 600 metres. At either side of the 150 Ohm-m layer, the thick body also dips inward which is consistent with the two-dimensional gravity and magnetic modelling along this magnetotelluric cross-section (see Figure II.5). The intra-crustal layer still has resistivity value of 10 Ohm-m and is thicker than in the previous model. The thickness of the 10 Ohm-m layer is about 7 kilometres and uniform at all stations. This model is the most preferred model compared to 35 other models prepared to represent the two-dimensional structure for this region.

VII.3.2. Cross-section II.

Skew values for the magnetotelluric data at most stations of cross-section II are rather high. Kurtz and Garland (1976) have interpreted magnetotelluric data from eastern Canada having high skew of about 1.0 in many cases. In southeast Tasmania, however, only the stations that have skew less than 0.5 i.e. WST, FRS, and PPR are modelled. Other stations, OTC and THN, have larger skew especially OTC (> 0.8) and are assumed to depart from two-dimensionality.

Figure VII.16 shows a starting two-dimensional configuration for cross-section II. This initial model was created based on the one-dimensional result. However, the resistivity and thickness for the intra-crustal layer were set as in the two-dimensional result of cross-section I i.e. 10 Ohm-m and 7 kilometres at all stations. Calculated data from this model for WST, FRS, and PPR stations each for the TE and TM modes, are plotted with the observed data superimposed and can be seen in Figure VII.16a.

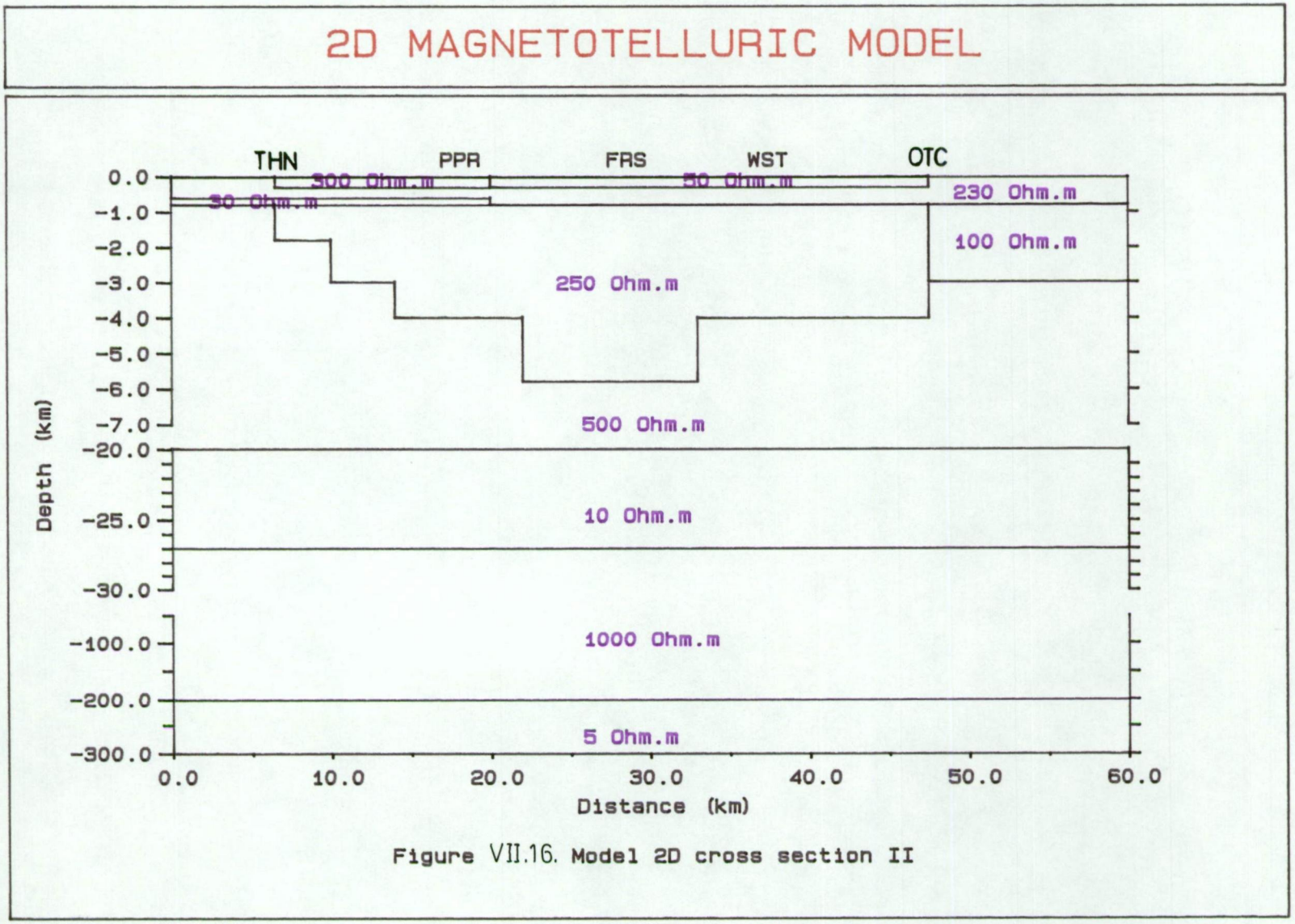

Figure VII.16. Model 2D cross section II

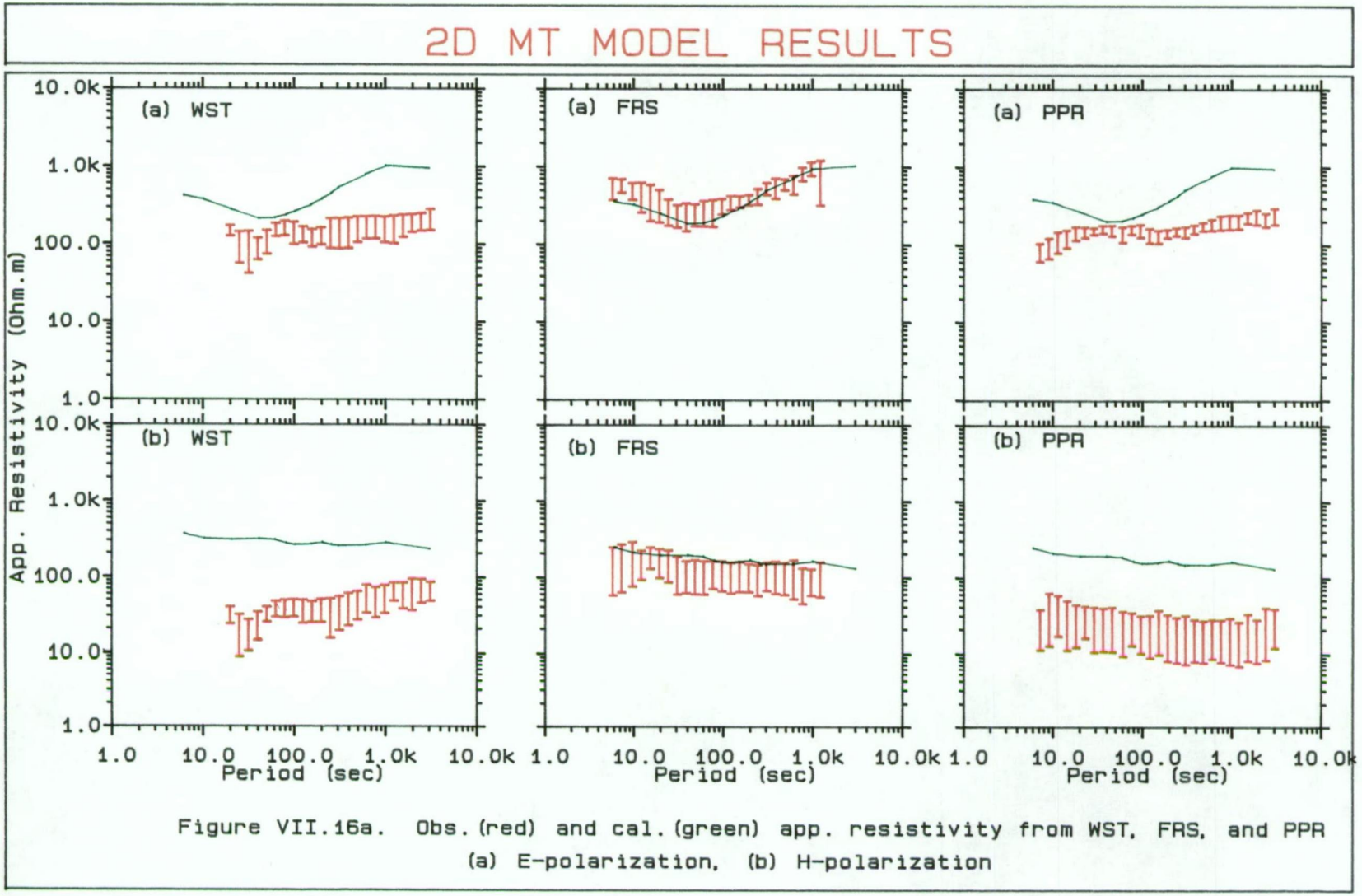

Figure VII.16a. Obs. (red) and cal. (green) app. resistivity from WST, FRS, and PPR (a) E-polarization, (b) H-polarization

It is noticeable from these figures that almost all of the calculated data from magnetotelluric stations do not match their observed data, except for FRS station. At this station the calculated TE and TM modes apparent resistivities data fit quite well to the observed data. For the stations to the east of FRS i.e. WST and to the west i.e PPR, both the calculated TE and TM modes apparent resistivity are too high over the whole period range. It should be mentioned here that this model was tried by placing a 1000 Ohm-m layer to represent the layer that underlies the deep conductive layer and has a uniform bulk resistivity i.e 250 Ohm-m for the basin to be consistent with cross-section I.

Because the above model does not give results that fit the observed data another model which was still based on the one-dimensional result but has different resistivity value for the basin and upper mantle beneath each stations, was then tried. To fit magnetotelluric data at WST and PPR the layer which represents the basin needs to be more conductive than that at FRS. At WST, for example, the 300 Ohm-m is replaced by a 60 Ohm-m layer with thickness of 3.3 kilometres. To the west of FRS, i.e. PPR the 300 Ohm-m layer is substituted by a 50 Ohm-m layer with thickness of 3.3 kilometres. The two-dimensional model configuration and plot of observed and calculated data from this exercise may be found in Figures VII.17 and 17a. In general the best fit model to the observed data at each station is quite good. This model is therefore considered as the best model to represent the electrical structure of cross-section II.

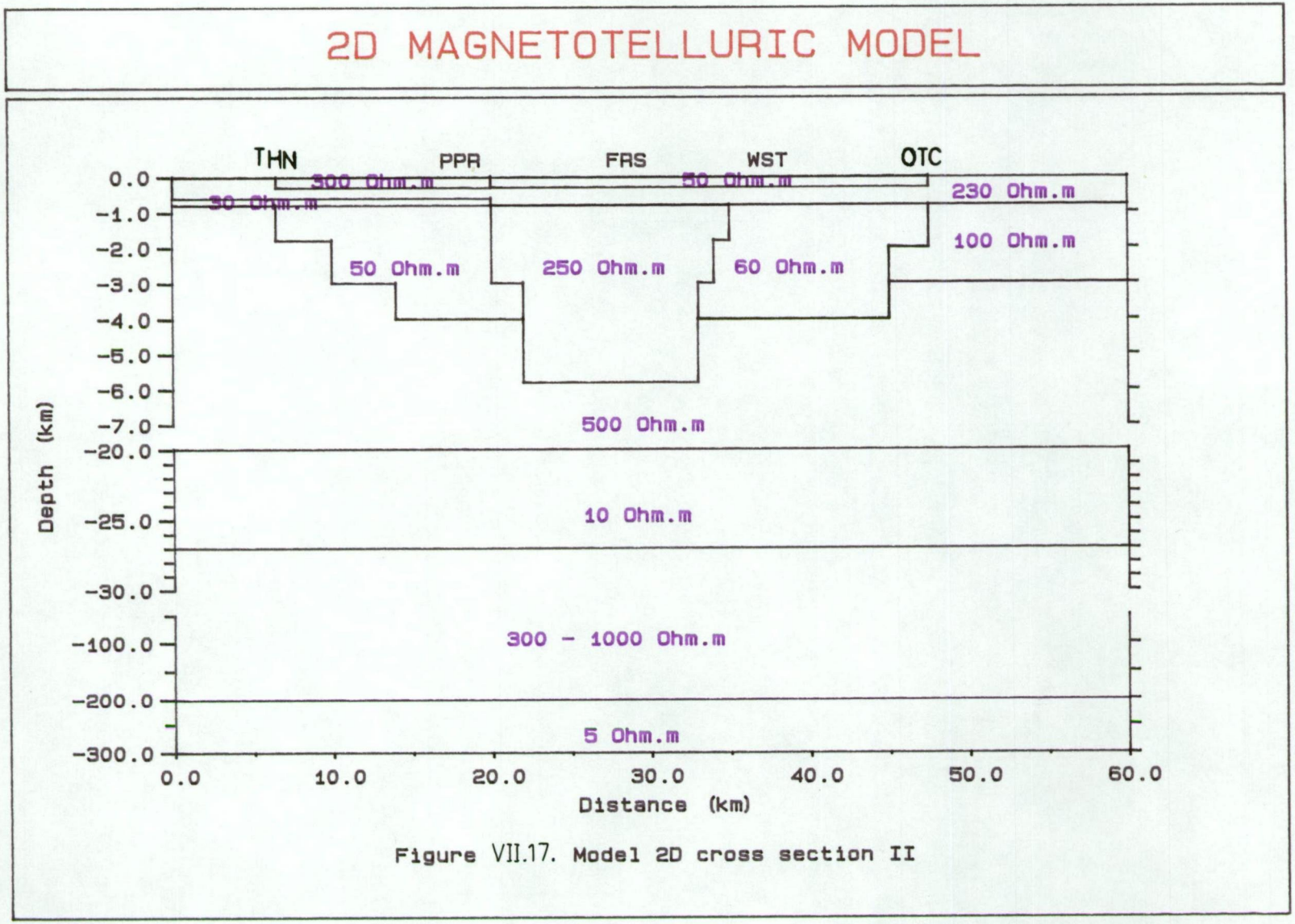

Figure VII.17. Model 2D cross section II

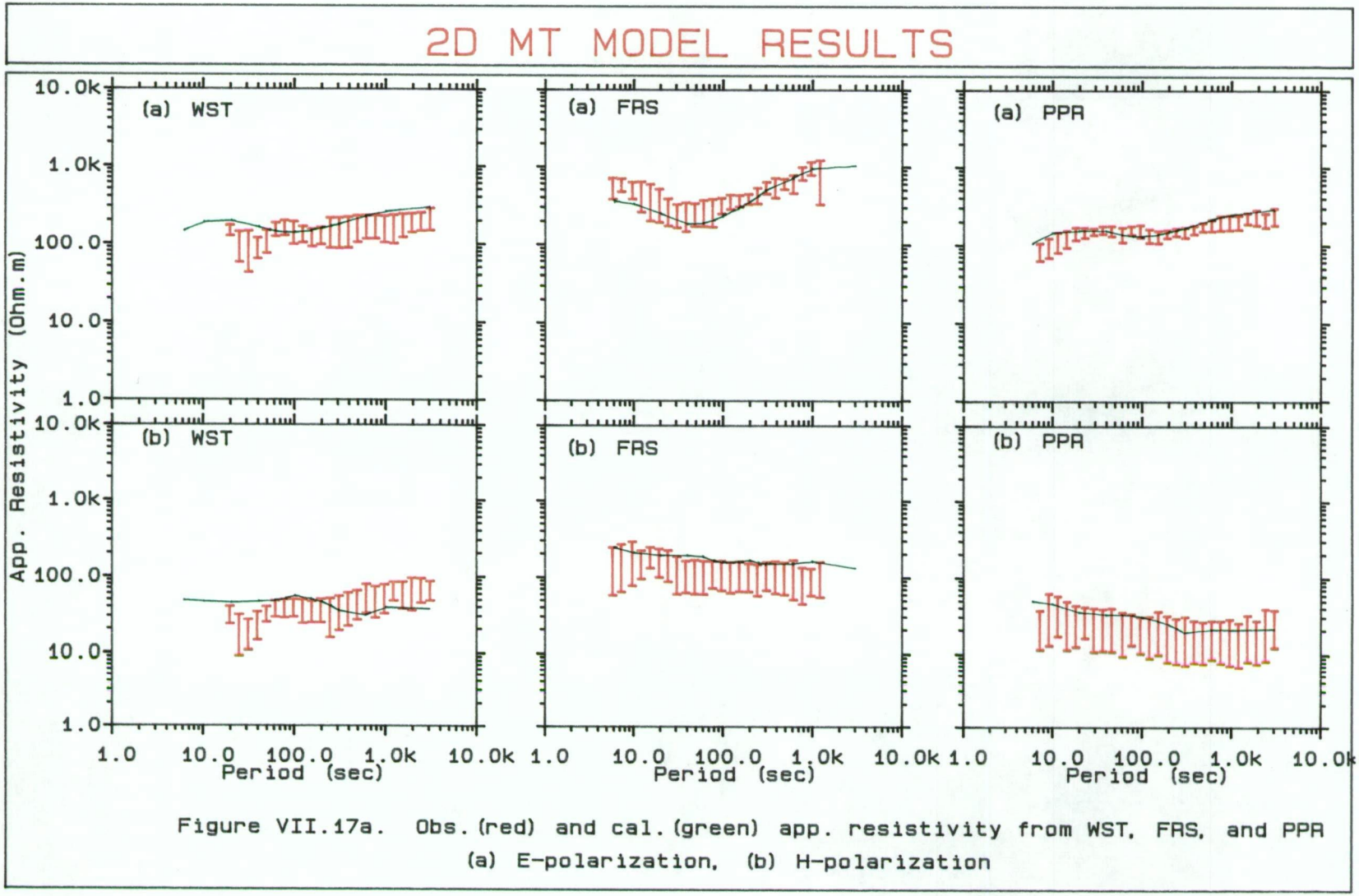

Figure VII.17a. Obs. (red) and cal. (green) app. resistivity from WST, FRS, and PPR
(a) E-polarization, (b) H-polarization

VII.3.3. Comment and summary of two-dimensional modelling.

It should be made clear that no ocean is included in the two-dimensional models presented in the previous sections. However, to see how much effect the ocean has on calculated data, modelling with ocean was carried out and gave unrealistic results especially for the long period data where the calculated resistivity curves have extremely large value compared to the observed data. It is not surprising as the structure may not be perfectly two-dimensional in this region. In addition, if the Tasman sea east of the study area has to be modelled, then the Southern ocean in the west, together with the sea in the south also have to be included, which is impossible with a two-dimensional program. The present distribution density of the stations does not allow use of three-dimensional modelling.

The conclusions from this modelling process are essentially the ones which have been assumed all along. These are that for all stations in cross-section I and WST, FRS and PPR in cross-section II, the TE mode apparent resistivity curves are representative of an equivalent plane-layered earth at almost all period ranges. Furthermore, any masking effects or perturbations to the TE mode due to the surficial basin structure are relatively insignificant in affecting the resolvability of the characteristics of the intra-crustal layer. The same cannot be said of the TM mode apparent resistivity, however, primarily because of the effect on the TM mode of the lateral inhomogeneity contrast caused by faults and granite intrusion. Lastly, the lower crustal layer is a well-resolved feature of the model.

Figures VII.14 and VII.17 from cross-sections I and II are the most preferred models to represent the two-dimensional structure for the study area.

VII.4. Discussion.

Discussion on the resistivity structure beneath cross-section I and cross-section II is divided into two parts: (1) the general sedimentary structure (upper diagram in Figures VII.14 and VII.17) and (2) the deep structure within the crust and upper mantle (middle diagram in Figures VII.14 and VII.17).

VII.4.1. Sedimentary basin.

The gross structure of the sedimentary sequence in the southeast Tasmania basin can be outlined by using calculated resistivities derived from the magnetotelluric models.

The first horizon in resistivity seen by the sounding at cross-section I (Figure VII.14) is the upper Parmeener super-group and at cross-section II (Figure VII.17) is the lower Parmeener super-group rock unit. The base of this Permo-Triassic cover with its stockwork of massive dolerite intrusions, is probably never less than 500 metres at cross-section I and dips toward cross-section II to about 800 metres. The Ordovician limestone, which is assumed to be a possible source of hydrocarbon deposits in this region (Leaman, 1987), underlies the Permo-Triassic rock at the western part of the study area. This rock has a thickness of about 300 metres becoming narrower toward cross-section II.

Figure VII.18 shows two-dimensional magnetotelluric model results superimposed on two-dimensional gravity and magnetic model results at cross-section I (note that the scale depth of magnetotelluric model is modified to be consistent with gravity and magnetic results). This figure also shows some interesting relationship between these two models. The sloping discontinuities needed in the models to match the magnetotelluric data curves, resulting in a trough-like structure, this is consistent

Figure VII.18. Plot of 2D MT and gravity and magnetic model along MT cross-section I.

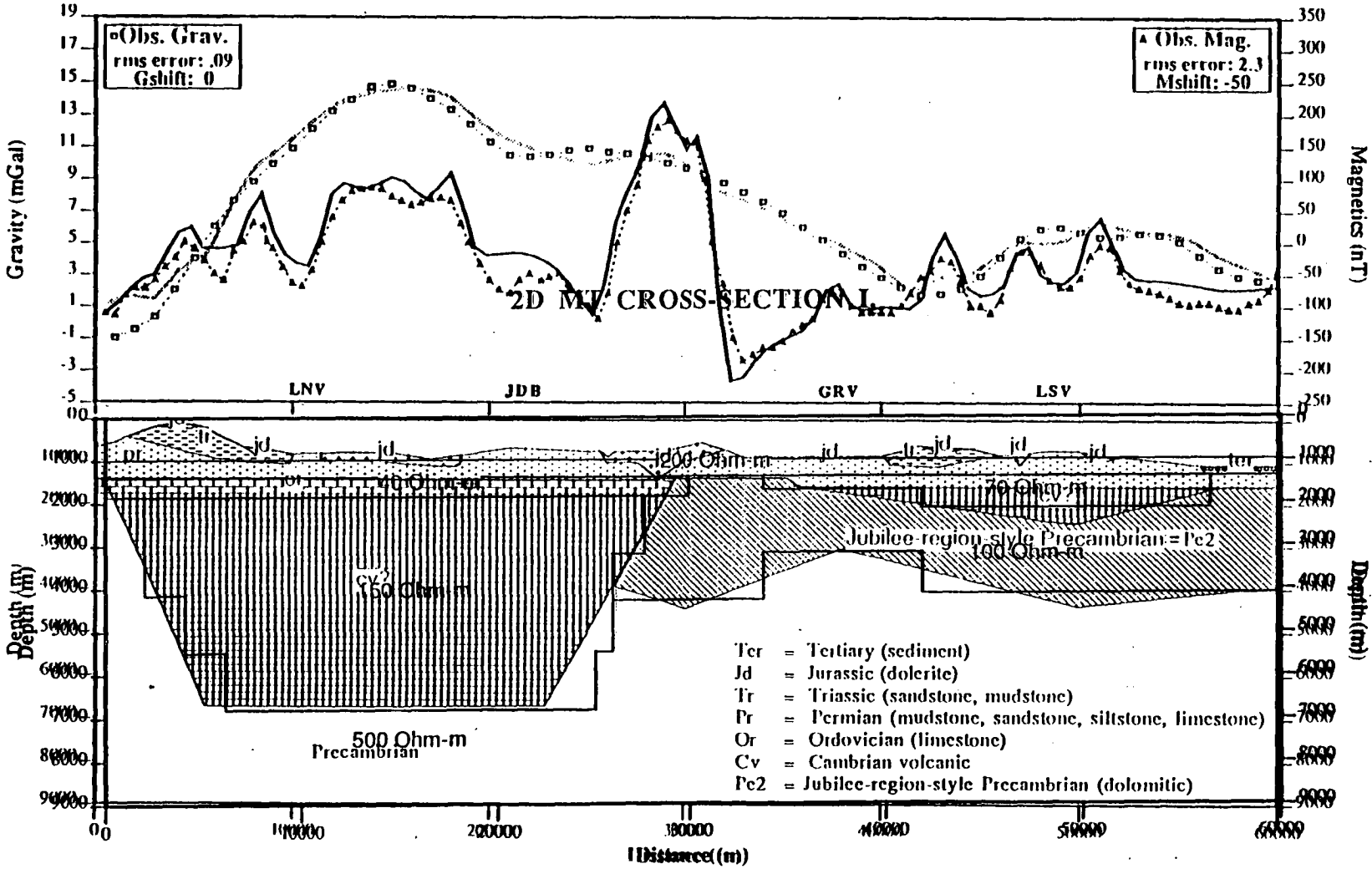

Figure VII.18. Plot of 2D MT and gravity and magnetic model along MT cross-section I.

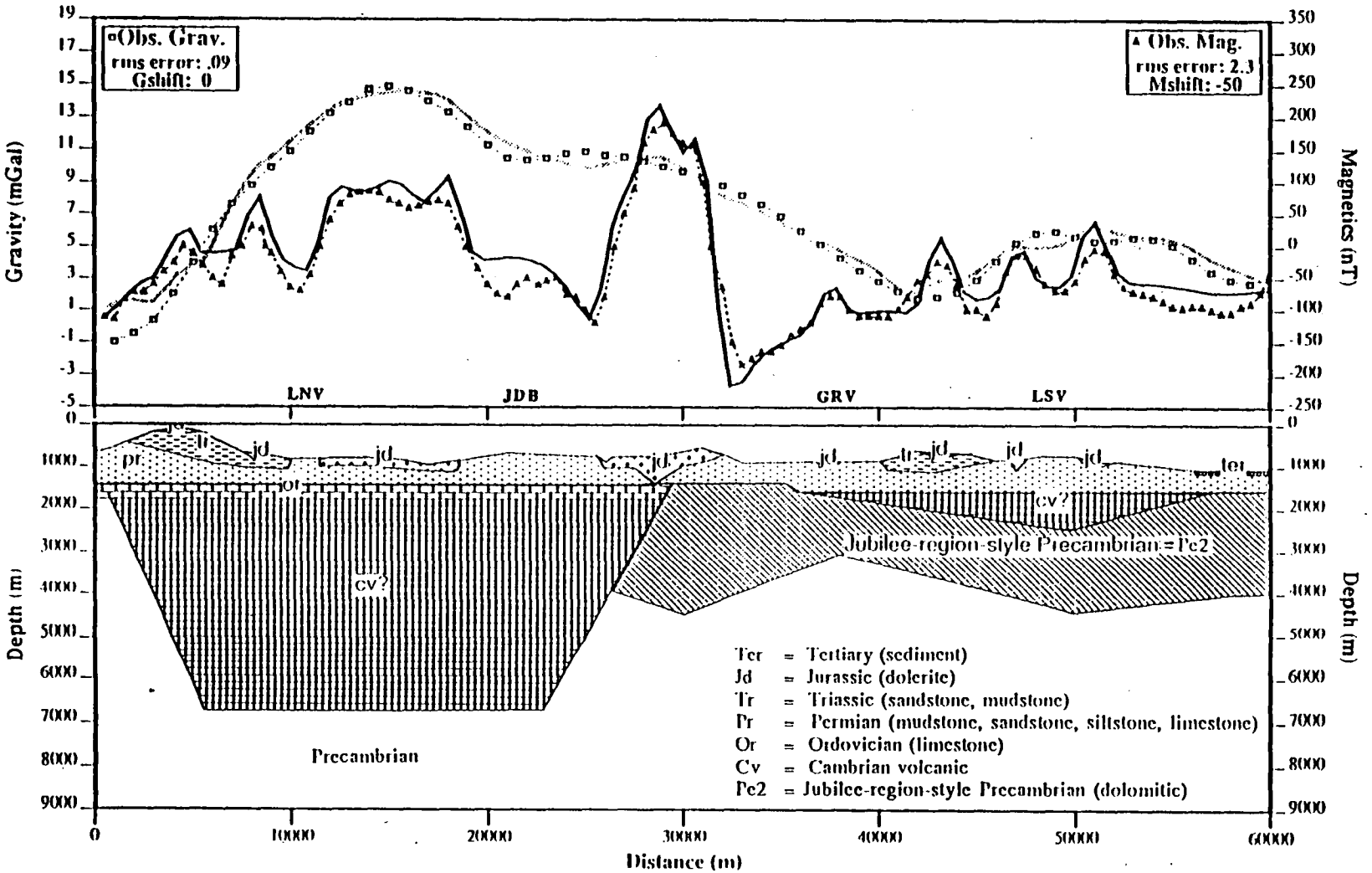

with the shape of the two-dimensional gravity and magnetic modelling. The taper contact at both sides of the body suggest complicated boundaries between differing geological units. The complexity of the contacts between differing resistivity zones is also suggested by two-dimensional gravity and magnetic results. The depth from the surface to the bottom of this trough is about 6 kilometres as shown by these two models. To the east is a large of 100 Ohm-m body seems to be associated with the Precambrian Jubilee dolomitic sequences.

A correlation between the two-dimensional magnetotelluric modelling results and two-dimensional gravity and magnetic model results at cross-section II, may be find in Figure VII.19. At this cross-section the best fit of magnetotelluric data may be obtained by inserting three different resistivity values beneath WST, FRS and PPR. There is no evidence from the two-dimensional gravity and magnetic modelling result along this magnetotelluric traverse concerning these resistivity boundaries. However, it is not impossible that the faulting between WST and FRS, FRS and PPR extends right up at least to the bottom of the Permo-Triassic rocks as can be seen from magnetotelluric model result in Figure VII.19. The high conductivity materials occur on the wide flanks of this cross-section. Such flanks are absent at cross-section I so perhaps a particular facies deposited only on the shallower flanks is responsible for the conductivity or perhaps the cross-section I has some mixture of 50 and 250 Ohm-m materials.

Figure VII.19. Plot of 2D MT and gravity and magnetic model along MT cross-section II.

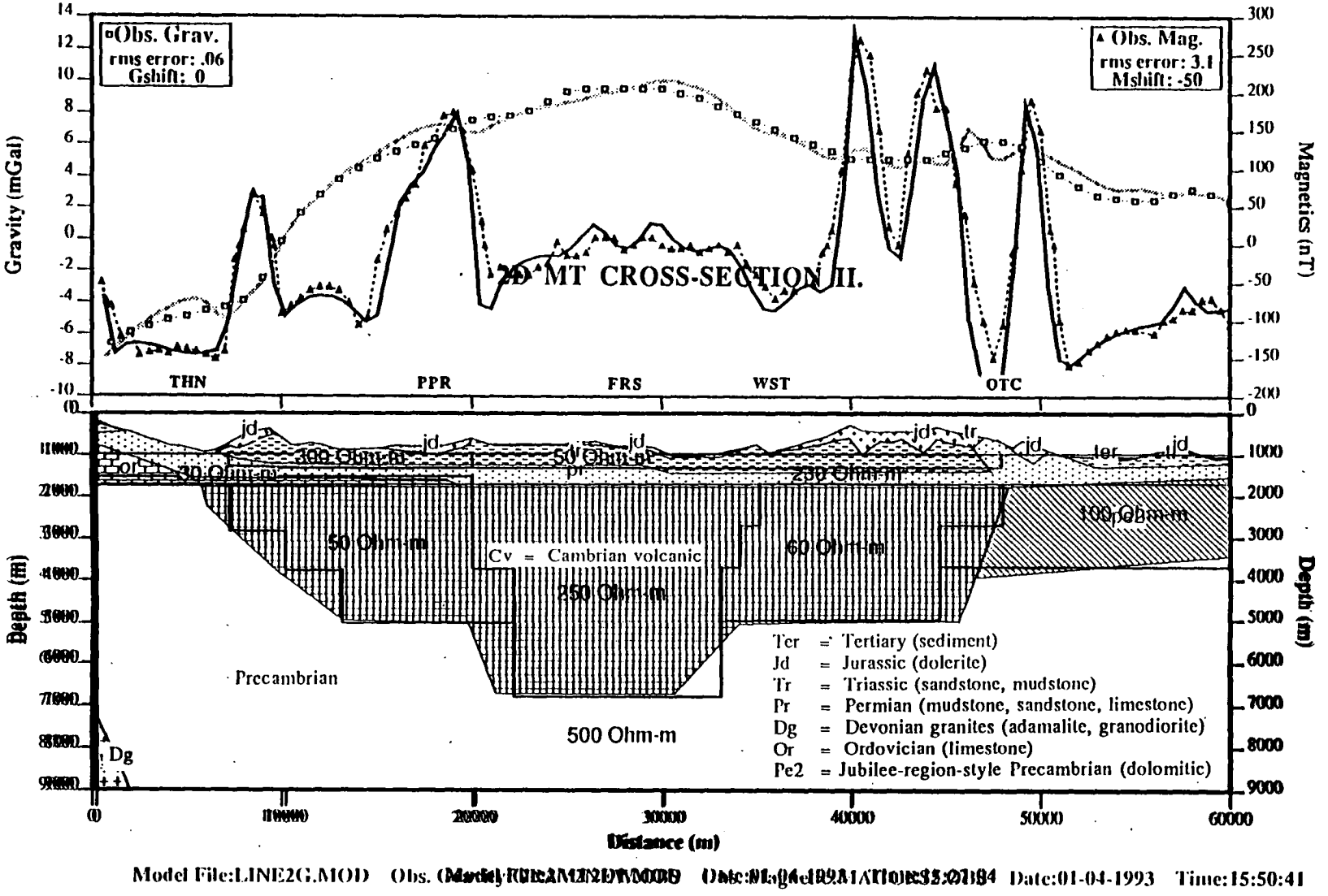

Figure VII.19. Plot of 2D MT and gravity and magnetic model along MT cross-section II.

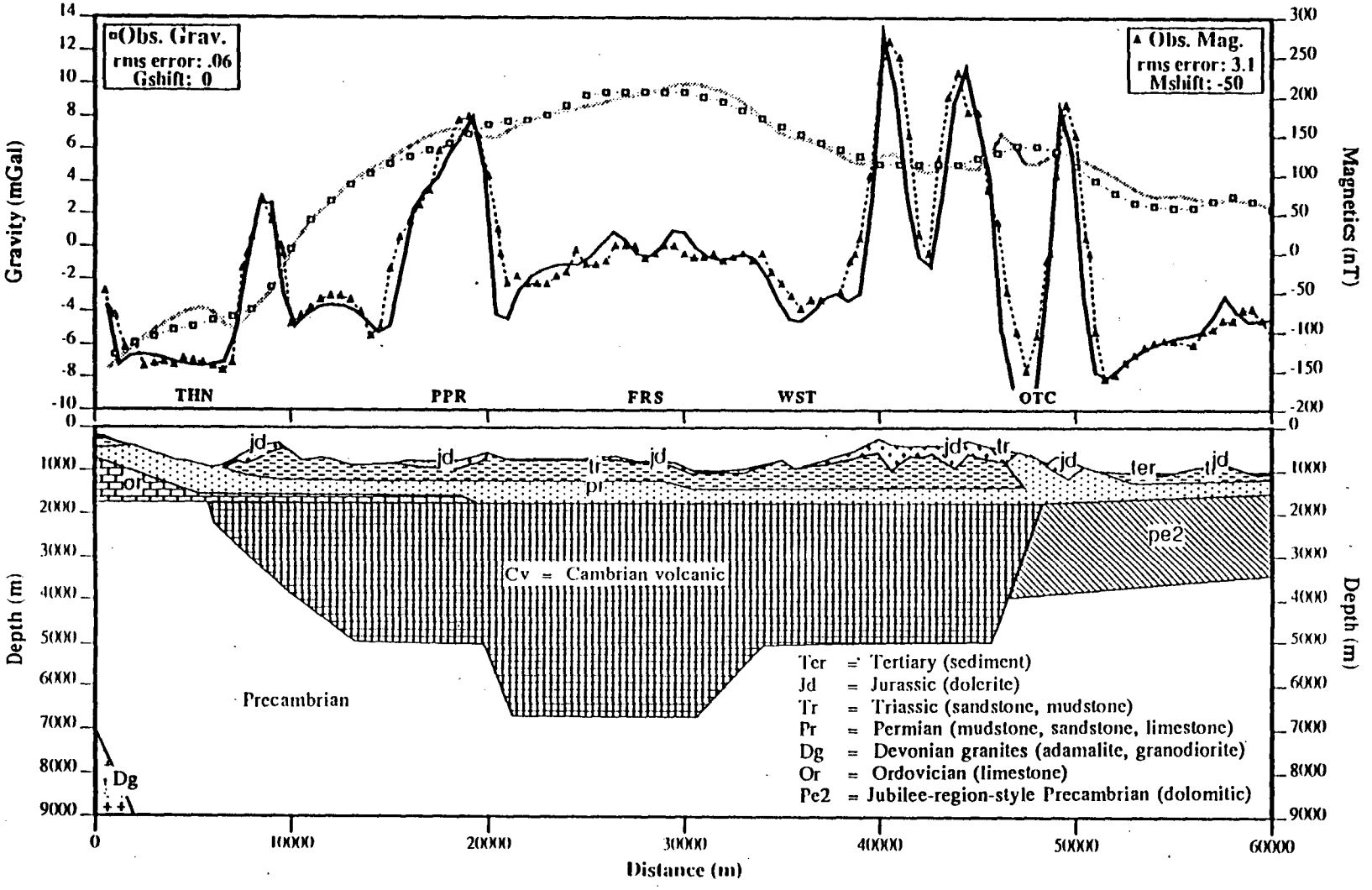

Model File:LINE2G.MOD Obs. Gravity:GRAV2NEW.OBS Obs. Magnetic:MAGCRS2.OBS Date:01-04-1993 Time:15:50:41

VII.4.2. Deeper structure.

The most significant feature of the models is that there is a lower part of the crust which is very conductive with a resistivity of 10 Ohm-m compared to the high value of 500 Ohm-m on top and 1000 Ohm-m under it.

There are a number of factors that could possibly account for the low resistivity of the intra-crustal conducting layer. The presence of free water, free carbon, some hydrated minerals such as serpentine, metallic oxides and sulphides has been known for some time to cause low electrical resistivities of crustal rocks. However, since the last decade following much intensive discussion, it appears that the favoured factor contributing to low electrical resistivity of crustal rocks is the presence of aqueous fluids with a high ionic content (Connerney et al., 1980; Shankland and Ander, 1983; Lee et al., 1983).

Rockmelts at lower crustal depths would of course lower the resistivity considerably, as Schwarz et al. (1984) discussed with reference to their studies in the Andes in Northern Chile. However, in a tectonically non-active region such as southeast Tasmania, the possibility of partial melts occurring at such depths seems to be unlikely.

Similarly the idea that the low resistivity anomaly could be associated with metallic oxides or sulphides can be rejected since very large quantity would be required for this to be a realistic option. In addition the gravity and magnetic anomaly along cross-sections I and II does not support this idea.

The likely cause of the highly conductive zone in the lower crust in this region is, therefore, the presence of free carbon. Although there is no surface evidence for the presence of carbon in the study area, it is not impossible for carbon to

be deposited deep in the crust beneath this region. Carbon in the form of black shales does crop out in western Tasmania (Dr. A. J. Crawford, personal communication, 1992). Duba and Shankland (1982), for example, suggested graphite or amorphous carbon as an explanation of mantle conductivity and have shown their effect in laboratory measurements. Amounts of graphite of the order of 100 ppm is required to account for the conductivity anomaly. Measurements by Mathev et al. (1984) indicate that these concentrations occur in the mantle and that carbon tends to occur along grain boundaries, which could provide a continuous conducting path. Mathev and Delaney (1981) and Mathev et al. (1984) suggested mechanisms whereby carbon could be tranported from the mantle to the crust via fracture zones.

The possible cause of the lowering of the bulk resistivity of the crust could be the effect of the presence of anomalously high temperature, presumably in the deeper parts of the crust, where temperature may be high enough that electrical conduction in

the solid rocks decreases resistivity to 10 Ohm-m. Adam (1978) and Shankland and Ander (1983) found a good correlation between depth and low electrical resistivity in the crust and high heat flow. Terrestrial heat flux in Tasmania is comparatively high. Wronski (1977) reported a thermal flux of 86.7 mW m^{-2} (2.07 HFU) and a thermal gradient of 40.4° C km^{-1} measured at Glenorchy, 17 kilometres northeast of the study area. If a constant thermal gradient is assumed then at depth of 25 kilometres a temperature of about 1000° C is obtained in the middle of the conductive layer. This temperature is sufficiently high to lower the resistivity at such depth and is in accord with the laboratory measurement results of Brace (1971) as reported by Jiracek et al. (1983) (see Figure VII.20).

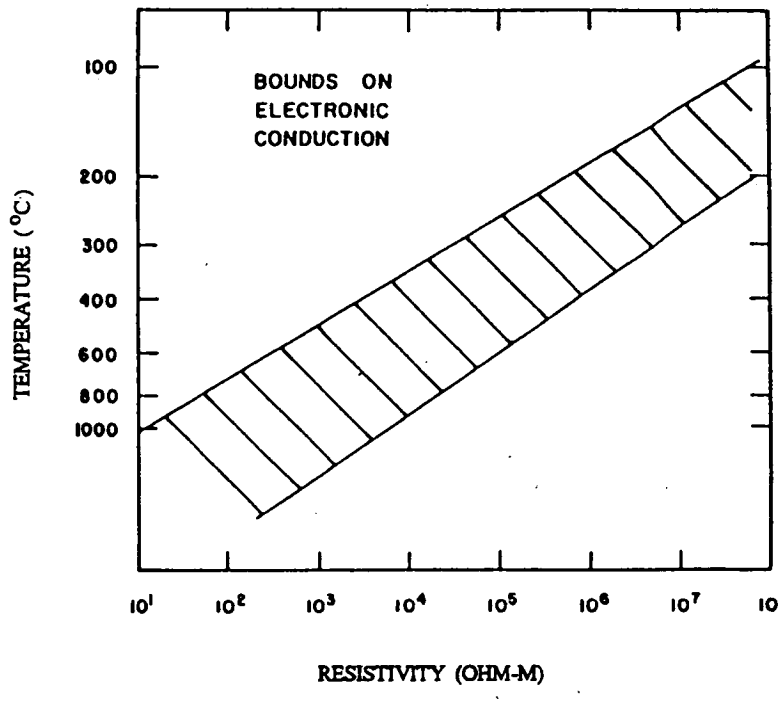

Figure VII.20. Minimum and maximum bounds on electronic semiconduction resistivity versus temperature for rocks samples (after Jiracek et al., 1983).

Chapter VIII.
CONCLUSIONS.

A variety of geophysical techniques including magnetotelluric, magnetovariational, potential field (gravity and magnetic) and transient electromagnetic techniques were used to investigate the subsurface electrical conductivity structure in southeast Tasmania. Measurements were taken at 14 magnetovariational and 9 magnetotelluric stations along two cross-sections. Results from these investigations have defined a trough-like structure and a lower-crustal conductive layer in this region.

Two-dimensional potential field modelling results indicate that the study area is blanketed by Permo-Triassic rocks intruded by Jurassic dolerite. The Permo-Triassic cover has a major unconformity at its base. This modelling process also delineated a northwest - southeast direction trough-like structure beneath the Permo-Triassic cover with the depth from the surface to the bottom of about 6 kilometres which is believed to be filled with Cambrian volcanics. Magnetotelluric results on northern cross-section indicate a trough with resistivity of 150 Ohm-m. In the southern cross-section this same trough has resistivity varying from 50 to 250 Ohm-m being more conductive on the flanks. Why this difference? Perhaps the northern cross-section has some mixture of 50 and 250 Ohm-m materials. The corrected induction vectors at WST and PPR indicate a central higher conductor, which is inconsistent with the magnetotelluric results. The reason for this discrepancy is not known. To the east is a large body of Precambrian Jubilee dolomitic sequences. This becomes narrower to the southern station and consistent with 100 Ohm-m body at both cross-sections.

The plot of induction vectors gained from magnetovariational data shows very strong ocean effects. Making use of Parkinson's et al. 1988 method and analogue model, correction of in-phase induction vectors at periods of 10 and 60 minutes was carried out to reduce ocean effect at shallow and deeper depths. At 10 minute periods inland and coastal anomalies were revealed. The inland anomaly has corrected in-phase induction vectors pointing in different directions. To the west of the Huon River they follow a northeasterly direction whereas to the east of the river they point northwest. This indicates a gradient anomaly zone along the Huon River. The significance of coastal effect is seen in the gradual swing in direction from southeast for observed vector, to east and almost perpendicular to the coast-line for corrected vector at the eastern-most station of southern cross-section. The probable explanation for this is high conductivity contrasts between the conducting ocean floor and the resistive block of eastern Tasmania.

The new simple method for derivation of rotation angle and dimensionality has been described and applied to different geometrical structures showing that this method works well and gives results very close to the conventional methods. This new method also gives almost the same rotation angle (θ) as Lilley's Mohr circle method when applied to the same station, but the Mohr circle method requires significant computer time. Based on the above facts, this new approach is a valid and useful method and it is also simpler and faster than other methods.

The magnetotelluric sounding results at cross-section I show the degree of anisotropy, indicated by the difference between the TE and TM mode resistivities, tends to increase at greater depth at all stations. The apparent resistivity value at all stations shows the existence of a low resistivity layer at greater depth. The skew and delta theta are small indicating a two-dimensional structure along this cross-section. At cross-section II the apparent resistivity curves exhibit large to moderate

anisotrophy. Two stations (OTC and THN) had very large skew and delta theta values which could be due to local three-dimensional structures.

To assess the electrical structure of the study area one-dimensional modelling was performed with the aid of gravity and magnetic and transient electromagnetic modelling results. This showed a trough-like structure underlain by a resistive layer. The thickness of this layer grades towards the western stations, i.e. to the centre of the island. The depth from the surface to the bottom varies from 21 kilometres to about 28 kilometres. This depth agrees with the depth of the Moho in Tasmania obtained from gravity modelling (Leaman et al., 1980). The one-dimensional modelling results also showed a lower-crustal conducting layer with uniform resistivity of 10 Ohm-m and an average thickness at all stations of about 2 kilometres.

A more realistic configuration for the electrical structure in this region is given by the two-dimensional modelling. The models were constructed based on the one-dimensional modelling results, however, in order to match the TE and TM apparent resistivity curves the conducting layer has to be thicker than is suggested by the one-dimensional results. The final model of cross-sections I and II shows that the calculated data fits better to the observed TE mode than the observed TM mode. A suggestion that the TM mode data may be affected by the fact that the deep conducting layer extends beneath the entire study area can be dismissed since confining the conductive layer under the trough-like structure only, gave no better fit with either the TE or TM modes. The final models, with the conductive layer beneath the entire study area, are thus considered as the preferred model to represent the electrical structure in this region. Based on these models the conductive layer now suggests a thickness of 7 kilometres with a resistivity of 10 Ohm-m, and uniform under the cross-sections.

Some hypotheses may be drawn to to explain the origin of the lower-crustal conducting layer in a tectonically in-active region such as southeast Tasmania. The

likely explanation is the presence of free carbon along grain boundaries or fractured rocks which provide a continuous conducting path. The mechanisms whereby carbon could be transported from the mantle to the crust via fracture zones have been suggested (Mathev et al. 1984). The possible cause is the effect of the presence of anomalously high temperature, presumably in the deeper part of the crust. The thermal flux of 86.7 mW m^{-2} (2.07 HFU) and thermal gradient of 40.4° C km^{-1} measured 17 kilometres northeast of the study area support this hypothesis.

Further resolution of the sub-surface resistivity structure in southeast Tasmania will need a three-dimensional modelling study to first determine accurately the effect of coastline and the ocean on the observed magnetotelluric parameters. However the present station distribution gives a quite limited coverage. Hence an increase in station distribution and the use of three-dimensional modelling techniques will lead to an even better understanding of electromagnetic induction in complicated structures such as those of southeast Tasmania.

The presence of the lower-crustal conductive in this area is of considerable interest as no comparable structure has been suggested by work in northern Tasmania (Hermanto, 1993). Clearly further work to define the extent of this feature and its relationship, if any, to other structure is critical to understanding the origin of the conductivity. For example, it may possibly correlated with the trough of Cambrian volcanics higher in the crust. Does this perhaps imply that it reflects changes in the crust in the Cambrian? Clearly a study of the other mayor Cambrian trough e.g. the Mount Read belt in western Tasmania is required to answer such questions. If such correlations with other Cambrian troughs do not exist then other possible relationships need to be considered e.g. the Cretaceous igneous activity at Cygnet.

REFERENCES :

Adam, A., 1978: Geothermal effects in the formation of electrically conducting zones and temperature distribution in the earth. Phys. Earth Planet. Inter., 17: 21-28.

Akasofu, S.I., 1974: A study of auroral displays photographed from the DMSP-2 satelite and from the Alaska meridian of stations. Space Sci. Rev., 16: 617-725.

Ashour, A.A., 1965: The coast effect on rapid geomagnetic variations. Geophys. J., 10: 147-161.

Bahr, K. and Groom, R.W., 1990: Correction for near surface effects. Tutorial presented at Ensenada, Mexico.

Bath, M., 1974: Spectral analysis in geophysics, developments in solid earth geophysics. 7, Elsevier, Oxford, 563 pp.

Berdichevsky, M.N., Vanyan, L.L and Dmitriev, V.I., 1989: Methods in the USSR to reduce near-surface inhomogeneity effects on deep magnetotelluric sounding. Phys. Earth Planet. Int., 53: 194-206.

Bindoff, N.L., 1983: A preliminary magnetotelluric survey of northeastern Tasmania. Honours thesis, Geology Department, University of Tasmania. Unpublished.

Boehl, J. E., Bostick, F. X., and Smith, H.W., 1977: An application of the Hilbert Transform to the magnetotelluric method : (Unpublished report). Electrical engineering and research laboratory, Austin, Texas, University of Texas, 98 pp.

Brace, W.F., 1971: Resistivity of saturated crustal rocks to 40 km. based on laboratory measurements, in Heacock, J.G. Ed., The structure and physical properties of the earth's crust. American Geophys. Union Monograph, 14: 243-256.

Breiner, S., 1981: Magnetometers for geophysical applications, in Weinstock, W. and Overton, W.C.,Jr., Eds., Squids application to geophysics, Tulsa, Ok. Society of Exploration Geophysics, 3 - 12.

Buselli, G., 1982: The effect of near surface superparamagnetic material on electromagnetic measurement. Geophysics, 47: 1315-1324.

Buyung, N., 1980: A geomagnetic induction study in the north-east of Tasmania. M.Sc. thesis, Geology Department, University of Tasmania. Unpublished.

Buselli, G. and O'Neill, B., 1977: SIROTEM, a new portable instrument for multichannel transient electromagnetic measurements. Bull. Aust. Soc. Explor. Geophys., 8: 82-87.

Buselli, G., McCracken, K.G. and Rutter, H., 1985: Manual for SIROTEM field procedures and data interpretation. CSIRO Div. of Mineral Phys. and Mineralogy, North Ryde. 340 pp.

Cagniard, L., 1953: Basic theory of the magnetotelluric method of geophysical prospecting. Geophysics, 18: 605-635.

Campbell, G.A. and Foster, R.M., 1948: Fourier integrals for practical applications. Van Nostrand, 177 pp.

Campbell, W.H., 1970: Rapid auroral luminosity fluctuations and geomagnetic field pulsations. J. Geophys. Res., 75: 6182-6208.

Campbell, W.H., 1976: An analysis of the spectra of geomagnetic variations having periods from 5 minutes to 4 hours. J. Geophys. Res., 81: 1369-1390.

Campbell, W.H., 1978: Induction of auroral zone electrical currents within the alaska pipeline. Pure Appl. Geophysics, 116: 1143-1173

Carr, J.M., 1984: Exploration Licence 20/80 Launceston. Final Report on area relinguished 22 August 1984. C.S.R. No. 84 / 2206.

Cerv, V. and Pek, J., 1990: Modelling and analysis of electromagnetic fields in 3D inhomogeneous media. Geophys. Survey, 11: 205-229.

Cheesman, S.J., 1989: A short baseline transient electromagnetic method for use on the sea-floor. Res. App. Geophys., 46, University of Toronto.

Cheesman, S.J., Edwards, R.N. and Chave, A.D., 1987: On the theory of the sea-floor conductivity mapping using transient electromagnetic systems. Geophysics, 52: 204-217.

Cheesman, S.J., Edwards, R.N. and Law, L.K., 1990: A test of a short-baseline sea-floor transient electromagnetic system. Geophys. J. Int., 103: 431-437.

Claerbout, J.F., 1976: Fundamentals of geophysical data processing with application to petroleum prospecting. McGraw-Hill, New York, 274 pp.

Cochrane, N.A. and Hyndman, R.D., 1970: A new analysis of geomagnetic depth sounding from Western Canada. Can. J. Earth Sci., 7: 1208-1281.

Connerney, J.E.P., Nekut, A. and Kuckes, A.F., 1980: Deep crustal electrical conductivity in the Adirondacks. J.Geophys.Res., 85: 2603-2614.

Cooley, J.W. and Tukey, J.E., 1965: An algorithm for the machine computation of complex Fourier series. Math. Comput., 19: 297-301.

Cull, J.P., 1989: Airborne Sirotem. Explor. Geophys., 20: 399-402.

Dosso, H.W., Nienaber, W. and Parkinson, W.D., 1985: An analogue model study of electromagnetic induction in the Tasmania region. Phys. Earth Plan. Int., 39: 118-133.

Duba A. and Shankland, T.J., 1982: Free carbon and electrical conductivity in the earth's mantle. Geophys. Res. Lett., 9: 1271-1274.

Everett, J.E. and Hyndman, R.D., 1967: Geomagnetic variations and electrical conductivity structure in southwestern Australia. Phys. Earth Plan. Int., 1: 24-34.

Farmer, N., 1985: Geological map of Kingborough area. Tas. Dept. of Mines. 105 pp.

Farmer, N. and Clarke, M.J., 1985: A diamond drill hole at Little Peppermint Bay, Woodbridge. Unpub. Rept. Dept. Mines Tas. 1985/24

Forbes, A.J., 1989: Geomagnetic field: Measurement, in James, D.E., Ed., The encyclopedia of solid earth geophysics. Van Nostrand Reinhold Co. New York. 498-507.

Fox, R.C., Hohmann, G.W., Killpack, T.J. and Rijo, L., 1980: Topographic effects in resistivity and induced polarization surveys. Geophysics., 45: 75-93

Frischknecht, F.C., Spies, B.R. and Labson, V., 1988: Electromagnetic sounding, in Nabighian, M.N. Ed., E.M. methods, theory and practice, Vol. 2: Soc. of Expl. Geophysicist.

Gamble, T.D., 1978: Remote reference magnetotellurics with SQUIDS. Ph.D thesis, University of California, Berkeley. Unpublished.

Gamble, T.D., Goubau, W.M. and Clarke, J., 1979: Magnetotellurics with a remote reference. Geophysics., 44: 53-68.

Gentleman, W.M. and Sande, G., 1966: Fast Fourier transforms for fun and profit. Proc. of Fall Joint Computer Conference., San Fransisco, 563-578.

GEOX SIROTEM: Transient electromagnetic system operation manual. Unley, S.A. 5041. Australia.

Goree, W.S., and Fuller, M., 1976: Magnetometers using RF-driven Squids and their applications in rock magnetism and palaeomagnetism. Rev. Geophysics Space Physics., 14: 591-608.

Gregory, G.P. and Lanzerotti, L.J., 1980: Geomagnetic depth sounding by induction arrow representation: A review. Rev. Geophys. Space Phys., 18: 203-209.

Hermance, J.F., 1973: Processing of magnetotelluric data. Phys. Earth Plan. Int., 7: 349-364.

Hermance, J.F., 1982: The asymptotic response of three-dimensional basin effects to magnetotelluric fields at long periods: The effects of current channeling. Geophysics., 47: 1562-1573.

Hermanto, M.R., 1985: Underground conductivity structure in Tasmania. M.Sc. thesis, Geology Department, University of Tasmania. Unpublished.

Hermanto, M.R., 1993: Magnetotelluric investigations of the Tamar lineament. Ph.D. thesis, Geology Department, University of Tasmania. Unpublished.

Honkura, Y., 1978: Electrical conductivity anomalies in the earth. Geophys. Survey., 3: 225-253.

Hughes, W.J. and Southwood, D.J., 1976: The screening of micropulsation signals by the atmosphere and ionosphere. J. Geophys. Res., 81: 3234-3240.

Hutton, V.R.S., 1969: Electromagnetic induction in the earth by the equatorial electrojet. Nature, 222: 363.

Hutton, V.R.S., 1972: Some problems of electromagnetic induction in the equatorial electrojet region - I Magnetotelluric relations. Geophys. J. R. astr. Soc., 28: 267-284.

Hyndman, R.D. and Cochrane, N.A., 1971: Electrical conductivity structure by geomagnetic induction at the continental margin of Atlantic Canada. Geophys. J.R. Astr. Soc., 25: 425-446.

Ingham, R., 1988: A MT and MV traverse across the New Zealand subduction zone. Geophys. J., 92: 495-504.

Irons, H.R., and Schwee, L.J., 1972: Magnetic thin film magnetometers for magnetic field measurements. IEEE Trans. Mag. 8: 61-65.

Jiracek, G.R., 1988: Near-surface and topographic distortions in electromagnetic induction. Review papaer, 9th IAGA workshop on Electromagnetic Induction in the Earth and Moon, Sochi, USSR.

Jiracek, G.R., 1990: Near-surface and topographic distortions in electromagnetic induction. Surv. in Geophys., 11: 163-203.

Jiracek, G.R., Ander, M.E., and Holcombe, H.T., 1979: Magnetotelluric soundings of crustal conductive zones in major continental rifts, in Rio Grande Rift: Tectonics and Magmatism, Riecker, R.E., Ed., AGU, Washington, D.C., 209-222.

Jiracek, G.R., and Holcombe, H.T., 1981: Evaluation of topographic effects in magnetotellurics using a modified Rayleigh technique: Technical Program Abstracts and Biographies, 51st Annual International meeting and exposition of the Society of Exploration Geophysicist. 24 pp.

Jiracek, G.R., Gustafson, E., and Mitchell, P.S., 1983: Magnetotelluric results opposing magma origin of crustal conductor in the Rio Grande rift, in Morgan, P., and Baker, B.H., Eds., Processes of continental rifting. Tectonophysics, 94: 299-326.

Johnson, B.D., 1972: Crustal structure studies in Tasmania. Ph.D thesis, Geology Department University of Tasmania. Unpblished.

Jones, A.G., 1988: Static shift of magnetotelluric data and its removal in a sedimentary basin environment. Geophysics, 53: 967-978.

Jones, F.W. and Pascoe. L.J., 1971: A general computer to determine the pertubation of alternating electric currents in a two-dimensional model of region of uniform conductivity with an embedded inhomogeneity. Geophys. J. R. Astr. Soc., 24: 3-30.

Jones, F.W. and Thomsons, D.J., 1974: A discussion of the finite difference method in computer modelling of electrical conductivity structures: A reply to the discussion by Williamson, Hewlett and Tammemangi. Geophys. J. R. Astr. Soc., 37: 537-544.

Jones, F.W., and Vozoff, K., 1978: The calculation of magnetotelluric quantities for three-dimensional conductivity inhomogeneities. Geophysics, 43: 1167-1175.

Jupp, D.L. and Vozoff, K., 1975: Stable iterative methods for the inversion of geophysical data. Geophys. J. Royal Astr. Soc., 42: 957-976.

Jupp, D.L. and Vozoff, K., 1976: Discussion on "The magnetotelluric method in the exploration of sedimentary basin". by Keeva Vozoff (1972). Geophysics, 41: 325-328.

Jupp, D.L.B. and Vozoff, K., 1989: Discussion on the magnatotelluric method in exploration of sedimentary basin. in Vozoff, K. (ed) Magnetotelluric method. Geophys. Reprint Series 5. Soc. of Expl. Geophys., 693-696.

Kanasewich, E.R., 1973: Time sequence analysis in geophysics. University of Alberta Press., Alberta.

Kato, Y. and Kikuchi, T., 1950: On the phase difference of earth current induced by the changes of the earth's magnetic field. Sci. Rep. Tohoku. Univ. Ser. V. Geophysics, 2: 139-145.

Kaufman, A.A. and Keller, G.V., 1981: The magnetotelluric sounding method. Elsevier Scientific Publishing Company. 595 pp.

Keary, P. and Brooks, M., 1984: An introduction to geophysical exploration. Blackwell Scientific Publications.

Keller, G.V., 1971: Natural-field and controlled-source methods in electromagnetic exploration. Geoexploration, 9: 99-147.

Keller, G.V. and Frischknecht, F.C., 1966: Electrical methods in geophysical prospecting. New York, Pergamon Press. 519 pp.

Ku, C.C., Hsieh, M.S., and Lim, S.H., 1973: The topographic effect on electromagnetic fields. Can. J. Earth Sci., 10: 645-656.

Kunetz, G., 1972: Processing and interpretation of magnetotelluric soundings. Geophysics, 37: 1005-1021.

Kurtz, R.D. and Garland, G.D., 1976: Magnetotelluric measurements in eastern Canada. Geophys. J. Roy. Astr. Soc., 45: 321-347.

Kurtz, R.D., Ostrowski, J.A. and Niblett, E.R., 1986: A magnetotelluric survey over the East Bull Lake Gabbro-Anorthosite complex. J. Geophys. Res., 91: 7403-7416.

Leaman, D.E., 1971: Geology and ground water resources of the Coal River Basin. Undergr. Wat. Supply Pap. Tasm. 7.

Leaman, D.E., 1972: Gravity survey of the Hobart District. Bull. Geol. Surv. Tas., 52

Leaman, D.E., 1973: Applied geophysics in Tasmania, Part 1. Summary of surveys and rock properties. Bull. Aust. Soc. Explor. Geophys., 4(2/3): 27-58.

Leaman, D.E., 1975 : Form, mechanism and control of dolerite intrusion near Hobart, Tasmania. J. Geol. Soc. Aust., 22: 175-186.

Leaman, D.E., 1977: Magnetic survey, Port Cygnet. Tech. Rept. Dept. Mines Tas., 20, 134.

Leaman, D.E., 1981: Interpretation of geophysical surveys, Catamaran area, Tasmania (El 6/79). Leaman Geophysics for Marathon Petroleum Aust. Appendix in 6 monthly report. Mines Department Open File. 81-1639, 1606, 1769.

Leaman, D.E., 1986a: Mt. Read volcanic project: preliminary interpretation report, 1985 west Tasmania aeromagnetic survey (Macquarie Harbour south to Elliot Bay). Tas. Dept. of Mines. (unpublished).

Leaman, D.E., 1986b: Mt. Read volcanic project: preliminary interpretation and evaluation report, 1981 west Tasmania aeromagnetic survey. Tas. Dept. of Mines. (unpublished).

Leaman, D.E., 1987: Review. Pre 1987 geophysical and structural data, D'Entrecasteaux Channel region, Tasmania. For Conga Oil Pty. Ltd. Report included in 1987 Annual Report to the Mines Department (Appendix 3).

Leaman, D.E., 1990: Inferences concerning the distribution and composition of Pre-carboniferous rocks in southeastern Tasmania. Roy. Soc. of Tasm., 124:1-12

Leaman, D.E., 1992a: Finding Cambrian keys: An essay in controversy, prospectivity and tectonic implications. Bull. Geol. Surv. Tasm., 70: 124-148.

Leaman, D.E., 1992b: Gold exploration and the use of the magnetic methods in northeast Tasmania. Bull. Geol. Surv. Tasm., 70: 149-160.

Leaman, D.E. and Naqvi, I.H., 1967: Geology and geophysics of the Cygnet District. Bull. Geol. Surv. Tasm., 49.

Leaman, D.E. and Richardson, R.G., 1989: Production of a residual gravity field map for Tasmania and some implications. Expl. Geophys., 20: 181-184.

Leaman, D.E. and Richardson, R.G., 1990: Tasmanian crustal features. Tenth Australian Geological Convention, Hobart 1990. (Abstract)

Leaman, D.E., Richardson, R.G. and Shirley, J.E., 1980: Tasmania - gravity field and its interpretation. Unpb. Rep. Dep. Mines Tasm. 1980/36.

Lee, C.D., Vine, F.J. and Ross, R.G., 1983: Electrical conductivity models for continental crust based on laboratory measurements on high grade metamorphic rocks. Geophys. J. R. Astr. Soc., 72: 353-372.

Lee, T., 1977: Estimation of depth to conductors by the use of electromagnetic transients. Geophys. Prosp., 25: 61-75.

Lee, T., 1984: The transient electromagnetic response of a magnetic or superparamagnetic ground. Geophysics, 49: 854-860.

Lee, T. and Lewis, R., 1974: Transient EM response of a large loop on a layered ground. Geophys. Prosp., 22: 430-444.

Lee, K. H., Labson, V., Wilt, M., and Goldstein, N., 1978: Catalogue of magnetotelluric apparent resistivity pseudo-sections over two dimensional models : (Unpublished report) Lawrence Barkely Laboratory Report 7057, 68 pp.

Lewis, R.J.G., 1965: Conductivity of the crust in Tasmania. Honours thesis, Geology Department University of Tasmania. Unpublished.

Lilley, F.E.M., 1976: A magnetometer array study across southern Victoria and the Bass Strait area, Australia. Geophys. J. R. Astr. Soc., 46: 165-184.

Lilley, F.E.M., 1992: Magnetotelluric analysis using Mohr circle. Geophysics, (in press)

Lilley, F.E.M. and Arora, B.R., 1982: The sign convention for quadrature Parkinson arrows in geomagnetic induction studies. Rev. Geophys. Space Phys., 20: 513-518.

Madden, T.R. and Swift, C.M., 1969: Magnetotelluric studies of the electrical conductivity structure of the crust and upper mantle. A.G.U. Monograph, 13: 469-479.

Marianiuk, J., Gnoinski, A., and Szymanski, A., 1978: Recording of geomagnetic field elements with a photo-electric magnetometer. Pol. Acad. Sci. Inst. Geophysics Pub. C-5 (125): 57-75.

Mathev, E.A. and Delaney, J.R., 1981: The nature and distribution of carbon in submarine basalts and peridotite nodules. Earth Planet. Sci. Lett., 56: 217-232.

Mathev, E.A., Dietrich, V.J. and Irving, A.J., 1984: The geochemistry of carbon in mantle peridotites. Geochem. Cosmochim. Acta, 48: 1849-1859.

McDougall, I., 1961 : Determination of the age of a basic intrusion by the potassium-argon method. Nature. 190: 1184-1186.

McDougall, I., 1962 : Differentiation of the Tasmanian dolerites; Red Hill dolerite-granophyre association. Bull. Geol. Soc. Am., 73: 278-315.

Morrison, H.F., Lee, K.H., Oppliger, G., and Dey, A., 1979: Magnetotelluric studies in Grass Valley, Nevada: (Unpublished report) Lawrence Barkely Laboratory Report 8646, 160 pp.

Orange, A.S., 1981: Notes on the interpretation of magnetotelluric data in complex areas (Unpublished report) Emerald Exploration Consultants, 33 pp.

Palacky, G.J., 1983: Tutorial: Research, applications, and publications in electrical and electromagnetic methods. Geophys. Prosp., 31: 861-872.

Papoulis, A., 1962: The Fourier integral and its applications. McGraw-Hill, New York, 318 pp.

Park, S.K., 1985: Distortion of magnetotelluric sounding curves by three-dimensional structures. Geophysics, 50: 785-797.

Parkinson, W.D., 1959: Directions of rapid geomagnetic fluctuations. Geophys. J. R. Astr. Soc., 2: 1-28.

Parkinson, W.D., 1962: The influence of continents and oceans on geomagnetic variations. Geophysics. J., 2: 1-14.

Parkinson, W.D., 1964: Conductivity anomaly in Australia and ocean effect. J. Geomag. Geoelectr., 15: 222-226.

Parkinson, W.D., 1983: Introduction to geomagnetism. Scottish Academic Press., 433 pp.

Parkinson, W.D. and Jones, F.W., 1979: The geomagnetic coast effect. Rev. of Geophys. and Space Phys., 17: 1999-2015.

Parkinson, W.D., Hermanto. R., Sayers, J., Bindoff, N.L., Dosso, H.W. and Nienabar, W., 1988: The Tamar coductivity anomaly. Phys. Earth Plan. Int., 52: 8-22.

Parkinson, W.D., Hermanto, R. and Dwipa, S., 1992: A simple method of determining rotation angle. J. Geomag. and Geoelect., special issue, (submitted).

Pascoe, L.J. and Jones, F.W., 1972: Boundary conditions and calculation of surface values for the general two-dimensional electromagnetic induction problem. Geophys. J. R. Astr. Soc., 27: 179-193.

Patra, H.P. and Mallick, K., 1980: Geosounding principles, 2. Elsevier Scientific Publishing Company. 419 pp.

Patrick, F.W. and Bostick, F.X., 1969: Magnetotelluric modelling techniques. Report No. 59, Electronic Research Centre, University of Texas, Austin.

Pellerin, L. and Hohmann, G.W., 1990: Transient electromagnetic inversion: a remedy for magnetotelluric static shifts. Geophysics, 55: 1242-1250.

Petiau, G. and Dupis, A., 1980: Noise, temperature coefficients and long time stability of electrodes for telluric observations. Geophys. Prospect., 24(15): 666-675

Pitcher, D.H., 1972: A study of geomagnetic variations in eastern Canada. M.Sc. thesis, Physics Department, University of Toronto. Unpublished.

Price, A.T., 1962: The theory of magnetotelluric methods when the source field is considered. J. Geophys. Res., 67: 1907-1918.

Primdahl, F., 1979: The fluxgate magnetometer. J. Physics. E: Soc. Instrum., 12: 241-253.

Raiche, A.P., 1984: The effect of ramp function turnoff on the TEM response of a layered earth. Expl. Geophys., 15: 37-41.

Raiche, A.P. and Spies, B.R., 1981: Coincident loop transient electromagnetic master curves for interpretation of two-layer earths. Geophysics, 46: 53-64.

Raiche, A.P., Jupp, D.L.B., Rutters, H. and Vozoff, K., 1985: The joint use of coincident loop transient electromagnetic and schlumberger sounding to resolve layered structures. Geophysics, 50: 1618-1627.

Rankin, D., 1962: The magnetotelluric effect on a dike. Geophysics, 27: 666-675.

Reddy, I.K. and Rankin,D., 1971: Magnetotelluric measurements in Central Alberta. Geophysics., 36: 739-753.

Reddy, I.K. and Rankin, D., 1974: Coherence functions for magnetotelluric analysis. Geophysics, 39: 312-320.

Reddy, I.K., Phyllips, R.J., Whitcomb, J.H., Cole, D.M. and Taylor, R.A., 1976: Monitoring of time dependent electrical resistivity by magnetotellurics. J. Geomag. Geoelectr., 28: 165-178.

Reddy, I.K., Rankin, D. and Phyllips, R.J., 1977: Three dimensional modelling in the magnetotelluric and magnetic variational sounding. Geophys. J. of Royal Astr. Soc., 51: 313-325.

Richardson, M., 1985: A magnetotelluric survey of the Fingal Valley. Honours thesis, Geology Department, University of Tasmania. Unpublished.

Rikitake, T., 1961: The effect of the ocean on rapid geomagnetic changes. Geophys. J., 5: 1-15.

Ritz, M. and Vassal, J., 1986: Geoelectrical structure of the northern part of the Senegal Basin from joint interpretation of magnetotelluric and geomagnetic data. J. of Geophys. Res., 91(B10) :443-456.

Roach, M.J., 1992: Geology and geophysics of the Lisle-Golconda goldfield, noertheast Tasmania. Bull. Geol. Surv. Tasm., 70: 189-198.

Robinson, E.A. and Treitel, S., 1976: The Robinson-Treitel reader. Seismograph Service Corp., Tulsa, 428 pp.

Roden, R.B., 1964: The effect of an ocean on magnetic diurnal variations. Geophys. J., 8: 375-388.

Roederer, J.G., 1977: Global problems in magnetospheric plasma physics and prospects for their solution., Space Sci. Rev., 21: 23-71.

Rokitiyansky, I.I., 1982: Geoelectromagnetic investigation of the earth's crust and mantle. Springer - Verlag. 381 pp.

Sayers, J., 1984: A magnetotelluric survey of the Midlands area. Honours thesis, Geology Department, University of Tasmania. Unpublished.

Schmucker, U., 1964: Anomalies of geomagnetic variations in the Southwestern United States. J. Geomag. Geoelect. Kyoto, 15: 193-221.

Schmucker, U., 1970: Anomalies of geomagnetic variations in the Southwestern United States. Scripps Inst. of Oceanography, La Jolla, California, Bulletin, 13: 1-165.

Schwarz, G., Haak, V., Martinez, E. and Bannister, J., 1984: The electrical conductivity of the Andean crust in northern Chile and southern Bolivia as inferred from magnetotelluric measurements. J. Geophys., 55: 169-178.

Shankland, T.J. and Ander, M.E., 1983: Electrical conductivity, temperatures and fluids in the lower crust. J. Geophys. Res., 88: 9475-9484.

Sims, W.F., Bostick, J.R. and Smith, H.W., 1971: The estimation of magnetotelluric impedance tensor elements from measured data. Geophysics, 36: 938-942.

Smith, B.D. and Ward, S.H., 1974: On the computation of polarization ellipse parameters. Geophysics, 39: 867-869.

Spichak, V.V., 1985: Differential boundary conditions for quasistationary electric and magnetic fields in a three-dimensional conducting medium. Elektr. Zond. Zemly, Moscow, IZMIRAN, 12-22.

Spies, B.R., 1980: The application of the transient electromagnetic method in Australian conditions - Field examples and model studies. Ph.D. thesis, Macquarie University, Sydney. Unpublished

Spies, B.R. and Raiche, A.P., 1980: Calculation of apparent conductivity for the transient electromagnetic (coincident loop) method using an HP-67 calculator. Geophysics, 45:1197-1204.

Stehfest, H., 1970: Algorithm 368: numerical inversion of Laplace transforms. Comm. ACM, 13: 47-49.

Sternberg, B.K, Washburne, J.C. and Pellerin, L., 1988: Correction for the static shift in magnetotellurics using transient electromagnetic soundings. Geophysics, 53: 1459-1468.

Strangway, D.W., Swift, C.M., Holmer, R.C., 1973: An application of audio frequency magnetotellurics (AMT) to mineral exploration. Geophysics, 38: 1159-1175.

Swift, C.M., 1967: A magnetotelluric investigation of an electrical conductivity anomaly in the Southwestern United States. (Ph.D thesis) : Cambridge, Massachusetts, Massachusetts Institute of Technology.

Talwani, M., 1965: Computation with the help of a digital computer of magnetic anomalies caused by bodies of arbitrary shape. Geophysics, 30:797-817

Talwani, M. and Ewing, M., 1960: Rapid computation of gravitational attraction of three-dimensional bodies of arbitrary shape. Geophysics, 25: 203-325

Telford, W.M., Geldart, L.P., Sheriff, R.E., and Keys, D.A., 1976: Applied Geophysics. Cambridge University Press. 860 pp

Thayer, R.E., 1975: Topographic distortion of telluric currents: A simple calculation. Geophysics, 40: 91-95

Tikhonov, A.N., 1950: Determination of the electrical characteristics of the deep strata of the earth's crust. Dokl. Akad. Nauk SSSR. 73: 295-297.

Tikhonov, A.N. and Lipskaya, N.V., 1952: Terrestrial electric field variations. Dok. Akad. Nauk. 87: 547-550.

Ting, S.C. and Hohmann, G.W., 1981: Integral equation modeling of three-dimensional magnetotelluric response. Geophysics, 46: 182-197.

Vozoff, K., 1972: The magnetotelluric method in the exploration of sedimentary basins. Geophysics, 37: 98-141.

Waeselynck, M., 1974: Magnetotellurics. Principle and outline of the recording technique, a case history. Geophys. Prospect., 22: 107-121.

Wait, J.R., 1954: On the relation between telluric currents and the earth's magnetic field. Geophysics, 19: 281-289.

Wait, J.R., 1958: Transmission and reflection of electromagnetic waves in the presence of stratified media. J. Res. Nat. Bur. Stand., 61: 205-232.

Wait, J.R., 1962: Theory of magne-totelluric fields. J. Res. Nat. Bur. Stand., 66D: 509-541.

Wannamaker, P. E., 1978: Magnetotelluric investigations at the Roosevelt Hot Springs KGRA and Mineral Mountains, Utah: University of Utah Topical Report, DOE/DGE/78-1701.a.6.1., 54 pp.

Wannamaker, P.E., Ward, S.H., Hohmann, G.H.,and Sill, W.R., 1980: Magnetotelluric models of the Roosevelt Hot Springs geothermal area, Utah. University of Utah Topical Report, DOE/ET/27002-8, 213 pp.

Wannamaker, P.E., Hohmann, G.W. and Ward, S.H., 1984: Magnetotelluric responses of three-dimensional bodies in layered earths, Geophysics, 49: 1517-1533.

Ward, S.H., 1959: AFMAG - airborne and ground. Geophysics, 24 : 761-789.

Ward, S.H., 1967: The electromagnetic method. Mining Geophysics, 11, Soc. Explor. Geophys., Tulsa, 224-327.

Williamson, K., Hewlett, C. and Tammemangi, H.Y., 1974: Computer modelling of electrical conductivity structure: Letter to the editors. Geophys. J. R. Astr. Soc., 37: 533-536.

Word, D.R., Smith, H.W. and Bostick, F.X., Jr., 1971: Crustal investigations by the magnetotelluric impedance method, in Heacock, J.G., Ed., The structure and physical properties of the earth's crust. American Geophys. Union Monograph, 14: 145-147.

Wronski, E.B., 1977: Two heat flow values for Tasmania. Geophys. J. R. Astr. Soc., 48: 131-133.

Zhdanov, M.S. and Spichak, V.V., 1989: Computer simulation of the Three-dimensional quasistationary electromagnetic fields in geoelectrics. Dokl. Akad. Nauk USSR, 309: 57-60.

APPENDIX II

GRAVITY AND MAGNETIC DATA.

APPENDIX II.1
GRAVITY AND MAGNETIC DATA: CROSS-SECTION I.

Gravity Data Cross-Section I: Southeast Tasmania.

Distance (m)	BA. Obs. (mGal)	Topograpny height (m)	Adjusted BA (mGal)
0	-3.0	320	-1.5
1000	-2.0	460	-1.0
2000	-1.0	680	-0.5
3000	0.0	840	0.3
4000	2.0	1000	2.0
5000	4.0	920	4.0
6000	6.0	680	6.0
7000	8.0	480	7.6
8000	9.0	300	8.8
9000	10.5	260	9.9
10000	11.0	160	10.9
11000	13.0	130	12.1
12000	14.0	240	13.2
13000	15.0	100	13.9
14000	16.0	260	14.7
15000	16.0	220	14.9
16000	16.0	120	14.6
17000	15.0	60	14.0
18000	14.0	100	13.3
19000	13.0	180	12.4
20000	11.0	260	11.3
21000	10.0	340	10.5
22000	10.2	260	10.4
23000	10.5	260	10.5
24000	11.0	260	10.8
25000	11.5	260	10.9
26000	11.0	100	10.7
27000	11.0	200	10.6
28000	10.5	380	10.3
29000	10.2	260	10.0
30000	10.0	300	9.7

Distance (m)	BA. Obs. (mGal)	Topograpny height (m)	Adjusted BA (mGal)
31000	9.5	420	9.3
32000	9.0	320	8.8
33000	8.5	110	8.2
34000	8.0	120	7.6
35000	7.0	140	6.9
36000	6.0	140	6.0
37000	5.0	120	5.2
38000	4.0	140	4.3
39000	3.0	140	3.5
40000	2.0	160	2.8
41000	1.5	300	2.2
42000	1.0	400	1.7
43000	1.0	360	1.8
44000	1.5	360	2.1
45000	2.0	300	2.9
46000	4.0	180	4.1
47000	6.0	200	5.3
48000	6.5	280	5.9
49000	6.5	280	6.0
50000	6.0	280	5.7
51000	5.0	140	5.4
52000	5.5	140	5.4
53000	6.0	100	5.6
54000	6.0	60	5.5
55000	6.0	20	5.1
56000	4.0	10	4.2
57000	3.0	0	3.4
58000	2.0	0	2.9
59000	2.0	0	2.7
60000	4.0	0	3.0

Magnetic Data Cross-Section 1: Southeast Tasmania.

Distance (m)	MA Obser. (nT)
0	-112.0
500	-112.0
1000	-115.0
1500	-85.0
2000	-72.0
2500	-72.0
3000	-60.0
3500	-40.0
4000	-25.0
4500	0.0
5000	-10.0
5500	-30.0
6000	-50.0
6500	-60.0
7000	-15.0
7500	0.0
8000	30.0
8500	25.0
8700	0.0
9000	-10.0
9500	-40.0
10000	-65.0
10500	-70.0
11000	-45.0
11500	0.0
12000	40.0
12500	65.0
13000	80.0
13500	83.0
14000	85.0
14500	83.0

Distance (m)	MA Obser. (nT)
15000	72.0
15500	65.0
16000	58.0
16500	62.0
17000	68.0
17500	70.0
18000	65.0
18500	30.0
18900	0.0
19500	-35.0
20000	-60.0
20500	-75.0
21000	-80.0
21500	-60.0
22000	-50.0
22600	-60.0
23000	-55.0
23500	-50.0
24000	-77.0
24500	-80.0
25000	-100.0
25500	-120.0
26000	-80.0
26500	0.0
27000	50.0
27500	90.0
28000	160.0
28500	180.0
29000	190.0
29500	175.0
30000	160.0

Distance (m)	MA Obser. (nT)
30500	155.0
31000	100.0
31400	0.0
32000	-65.0
32500	-150.0
33000	-185.0
33500	-175.0
34000	-165.0
34500	-165.0
35000	-155.0
35500	-140.0
36000	-130.0
36500	-120.0
37000	-90.0
37500	-80.0
38000	-80.0
38500	-100.0
39000	-110.0
39500	-110.0
40000	-110.0
40500	-110.0
41000	-100.0
41500	-80.0
42000	-55.0
42500	-45.0
43000	-25.0
43500	-30.0
44000	-60.0
44500	-100.0
45000	-100.0
45500	-110.0

Distance (m)	MA Obser. (nT)
46000	-90.0
46500	-40.0
47000	-15.0
47500	-15.0
48000	-35.0
48500	-60.0
49000	-70.0
49500	-70.0
50000	-55.0
50500	-20.0
51000	-5.0
51500	-8.0
52000	-45.0
52500	-65.0
53000	-72.0
53500	-75.0
54000	-80.0
54500	-87.0
55000	-95.0
55500	-97.0
56000	-95.0
56500	-95.0
57000	-100.0
57500	-105.0
58000	-105.0
58500	-95.0
59000	-90.0
59500	-75.0
60000	-40.0

APPENDIX II.1
GRAVITY AND MAGNETIC DATA: CROSS-SECTION II

Gravity Data Cross-section II : Southeast Tasmania

Distance (m)	BA Obs. (mGal)	Topography height (m)	Adjusted BA (mGal)
0	-7.0	1040	-7.0
1000	-6.7	930	-6.6
2000	-6.5	660	-5.9
3000	-6.2	400	-5.5
4000	-6.0	240	-5.1
5000	-5.8	240	-4.9
6000	-5.6	80	-4.5
7000	-5.4	240	-4.3
8000	-5.0	440	-3.9
9000	-3.0	600	-2.5
10000	0.0	420	-0.1
11000	2.0	220	1.6
12000	3.0	260	2.8
13000	4.5	120	3.8
14000	5.0	120	4.5
15000	5.5	180	5.1
16000	5.8	240	5.5
17000	6.0	220	5.9
18000	6.5	220	6.3
19000	7.0	270	6.9
20000	8.0	420	7.5
21000	8.0	280	7.7
22000	8.0	220	7.8
23000	8.0	240	8.1
24000	9.0	280	8.7
25000	10.0	280	9.3
26000	10.0	320	9.5
27000	10.0	280	9.5
28000	10.0	200	9.5
29000	10.0	240	9.5
30000	10.0	180	9.5

Distance (m)	BA Obs. (mGal)	Topography height (m)	Adjusted BA (mGal)
31000	10.0	10	9.2
32000	9.5	10	8.9
33000	9.0	60	8.4
34000	8.0	160	7.9
35000	7.5	260	7.4
36000	7.0	60	6.9
37000	6.2	140	6.4
38000	6.0	260	6.0
39000	5.5	440	5.6
40000	5.0	740	5.1
41000	5.0	560	5.1
42000	5.0	590	5.1
43000	5.0	610	5.1
44000	5.0	580	5.1
45000	5.5	620	5.5
46000	6.0	500	5.8
47000	6.5	440	6.2
48000	7.0	320	6.2
49000	6.5	360	5.9
50000	5.5	180	5.0
51000	4.0	0	4.1
52000	3.0	0	3.3
53000	2.0	0	2.7
54000	2.0	0	2.5
55000	2.0	0	2.4
56000	2.0	0	2.4
57000	3.0	160	2.8
58000	4.0	100	3.1
59000	4.0	0	2.8
60000	3.0	0	2.3

Magnetic Data Cross-Section II : Southeast Tasmania

Distance (m)	MA Obser. (nT)
0	-40.0
500	-50.0
750	-75.0
1000	-80.0
1500	-120.0
2000	-115.0
2500	-145.0
3000	-142.0
3500	-140.0
4000	-143.0
4500	-135.0
5000	-137.0
5500	-140.0
6000	-145.0
6500	-150.0
7000	-140.0
7500	-20.0
7750	0.0
8000	20.0
8500	70.0
9000	40.0
9500	10.0
9600	0.0
10000	-90.0
10500	-80.0
11000	-70.0
11500	-60.0
12000	-55.0
12500	-55.0
13000	-60.0
13500	-75.0
14000	-105.0

Distance (m)	MA Obser. (nT)
14500	-95.0
15000	-20.0
15500	20.0
16000	40.0
16500	60.0
17000	80.0
17500	130.0
18000	140.0
18500	170.0
19000	175.0
19500	150.0
20000	100.0
20500	30.0
20650	0.0
21000	-40.0
21500	-30.0
22000	-40.0
22500	-40.0
23000	-40.0
23500	-30.0
24000	-25.0
24500	5.0
25000	-15.0
25500	-15.0
26000	-10.0
26500	10.0
27000	10.0
27500	10.0
28000	-7.0
28500	0.0
29000	10.0
29500	10.0

Distance (m)	MA Obser. (nT)
30000	0.0
30500	-5.0
31000	-5.0
31500	0.0
32000	-10.0
32500	-5.0
33000	0.0
33500	-10.0
34000	0.0
34500	-25.0
35000	-40.0
35500	-55.0
36000	-70.0
36500	-60.0
37000	-60.0
38000	-50.0
38500	-10.0
38750	0.0
39000	20.0
39500	100.0
40000	220.0
40500	270.0
41000	250.0
41500	150.0
42000	25.0
42500	0.0
43000	120.0
43500	200.0
44000	230.0
44500	180.0
45000	180.0
45500	80.0

Distance (m)	MA Obser. (nT)
46000	40.0
46500	-50.0
47000	-100.0
47500	-150.0
48000	-105.0
48500	-10.0
48700	0.0
49000	100.0
49500	190.0
50000	150.0
50500	20.0
50700	0.0
51000	-100.0
51500	-160.0
52000	-155.0
52500	-140.0
53000	-130.0
53500	-120.0
54000	-115.0
54500	-112.0
55000	-112.0
56000	-117.0
56500	-100.0
57000	-97.0
57500	-85.0
58000	-85.0
58500	-72.0
59000	-70.0
59500	-85.0
60000	-105.0
60500	-117.0
61000	-115.0

APPENDIX V.

TEMPERATURE CORRECTION.

Apply temperature correction as shown below if detector head and control box temperatures are recorded on channel 4 and 5, otherwise use appropriate channel (CH) numbers.

MT Unit	Componen t	Channel	Coefficient	Datum Temp. (°C x 10)
I	X	4	-.06	200
		5	-.13	200
	Y	4	-.07	200
		5	.101	200
	Z	4	.156	200
		5	.041	200
II	X	4	-.009	200
		5	.073	200
	Y	4	.007	200
		5	0.0	200
	Z	4	.007	200
		5	-.10	200

APPENDIX VII.1.

1D TE MODEL RESULTS WITHOUT THE LOWER CRUSTAL CONDUCTIVE LAYER.

1D MAGNETOTELLURIC MODEL

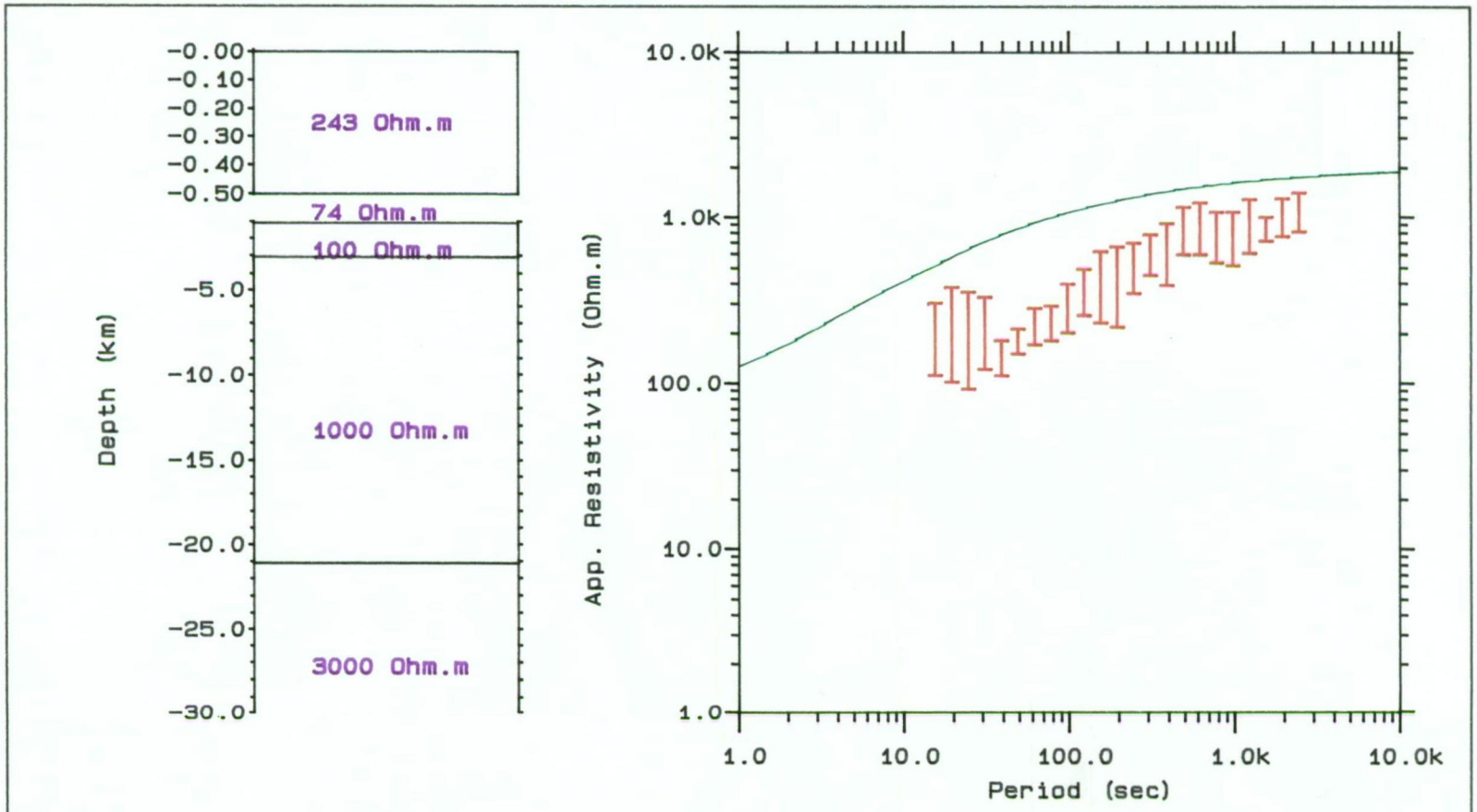

Figure AVII.1. 1D model results from Leslie Vale)
(red) -observed; (green) -calculated

1D MAGNETOTELLURIC MODEL

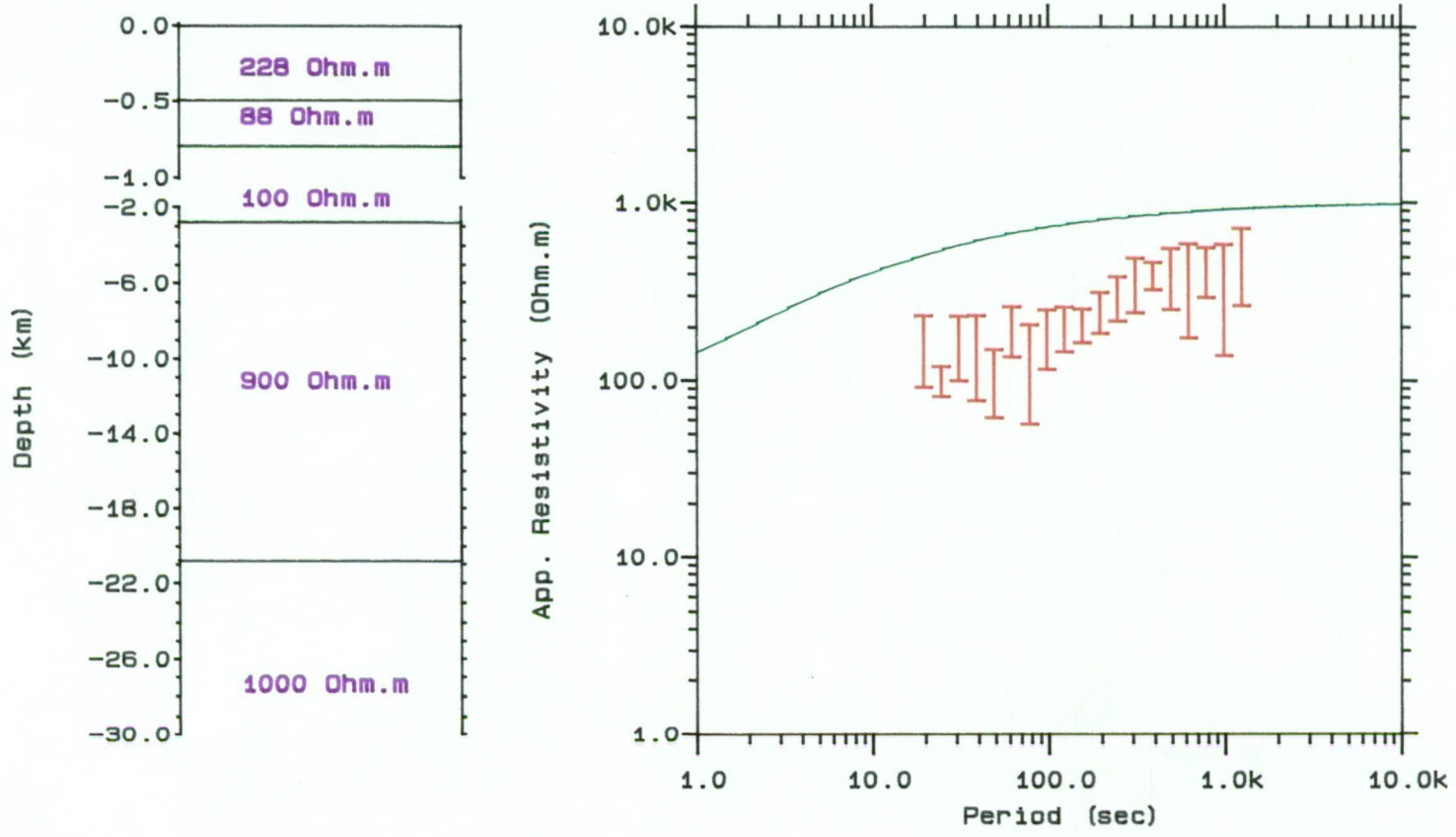

Figure AVII.2. 1D model results from Grove (GRV)
(red)-observed; (green)-calculated

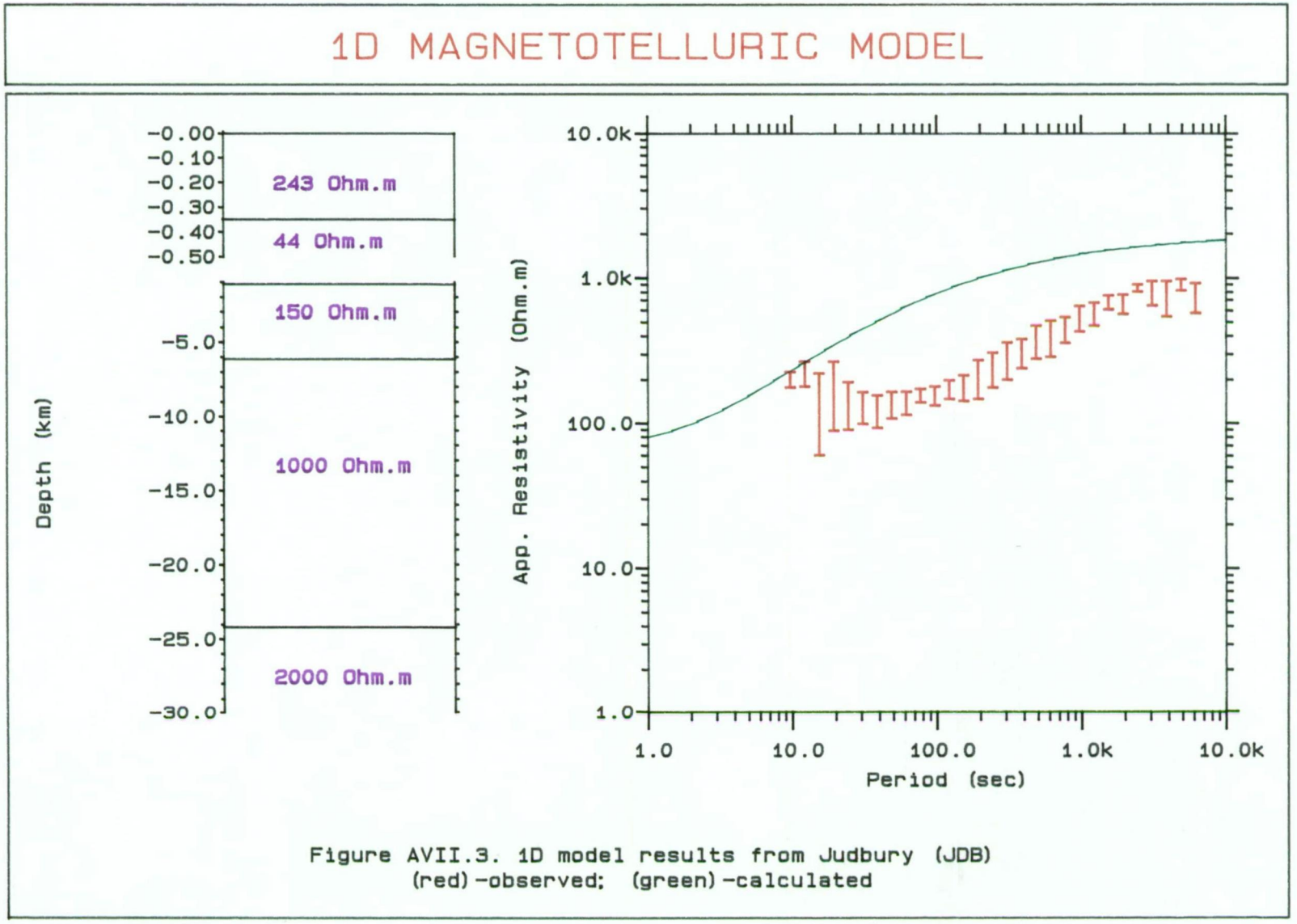

Figure AVII.3. 1D model results from Judbury (JDB)
(red)-observed; (green)-calculated

1D MAGNETOTELLURIC MODEL

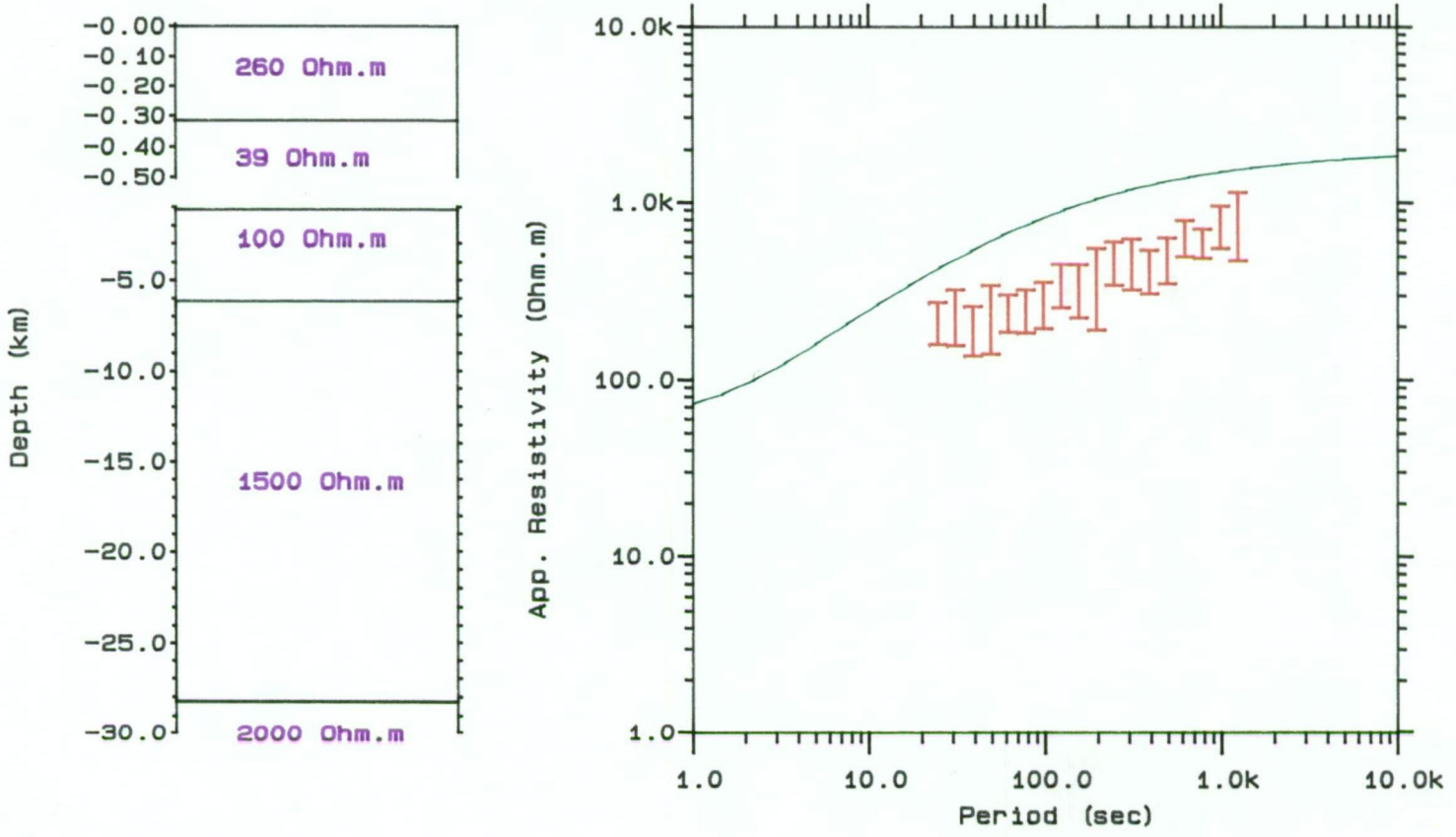

Figure AVII.4. 1D model results from Lonnavale (LNV)
(red)-observed; (green)-calculated

APPENDIX VII.2
STATIC SHIFT

The presence of charges on local surficial or near-surface, lateral inhomogeneities can distort magnetotelluric data thereby limiting interpretational accuracy. This phenomenon, generally referred to as near-surface distortions or static shift, have been studied in theoretical modelling studies, for example, by Wannamaker et al. (1984) and Park, (1985). It has been well demonstrated in a number of case histories and reported by Kurtz at al. (1986), Jones (1988), Sternberg et al. (1988) and others.

Jiracek (1990) stated that any resistivity contrast due to small-scale heterogeneities in the vicinity of the electric field measurements can give rise to a particular class of perturbation. The two measured electric fields (Ex, Ey) are perturbed from their regional values and a static (frequency independent) shift of the apparent resistivity sounding curve takes place. Sternberg eat al. (1988) identified the parallel shifts that occur in the dual logarithmic coordinates of apparent resistivity and frequency from two magnetotelluric results taken at very close distance, are identical but shifted along vertical axes. To remove the unwanted distortion from magnetotelluric data, some techniques have proposed and discussed by Jiracek (1988), Berdichevsky et al. (1989) and Bahr and Groom (1990). The independent inductive geophysical measurements, such as transient electromagnetic sounding have been used to measure the amount of static shift (Sternberg et al. 1988; Pellerin and Hohmann, 1990).

In this study, the theory described by Sternberg et al. (1988) was applied using the transient electromagnetic sounding measurements carried out with SIROTEM. Sternberg et al. (1988) showed that by dividing the transient time scale (in ms) by 200 allow direct comparation between transient electromagnetic and magnetotelluric. Appendixes VII.1 to VII.8 show apparent resistivity curves from magnetotelluric and one-dimensional interpretation along cross-section I and II. As can be seen from that Appendixes, insufficient of late delay time of transient electromagnetic data (see Chapter III) and lack of short period data in magnetotelluric, results in non overlapping of both data sets. However, both curves seem to match with the one-dimensional modelling results. The consistency between transient electromagnetic and magnetotelluric data suggests that there are no near-surface inhomogeneities present in the vicinity of those stations and therefore no static shift correction to the magnetotelluric data is required. Jones (1988) also stated that in two-dimensional surficial inhomogeneity the static shift problem can be avoided by considering the E-polarization results alone. In addition, the match of those two data sets found here may be due to the location for each magnetotelluric station and the placement of electrodes have been very carefully chosen by applying the method described in Chapter V.4.3.1.

1D MT AND SIROTEM MODEL

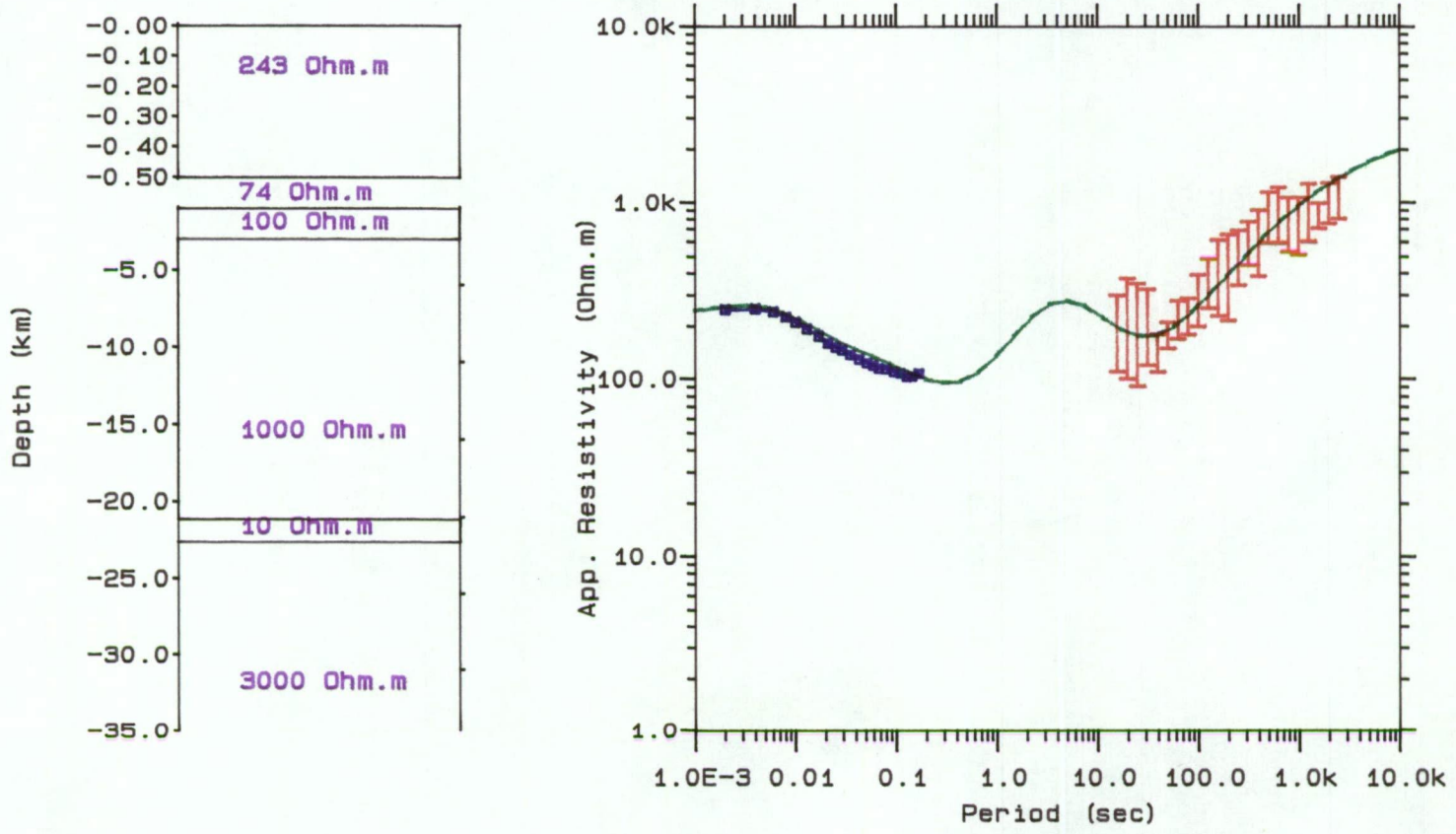

Figure BVII.1. 1D model based on MT and SIROTEM results from Leslie Vale (LSV) (red) -observed MT; (blue) -observed SIROTEM; (green) -calculated

1D MT AND SIROTEM MODEL

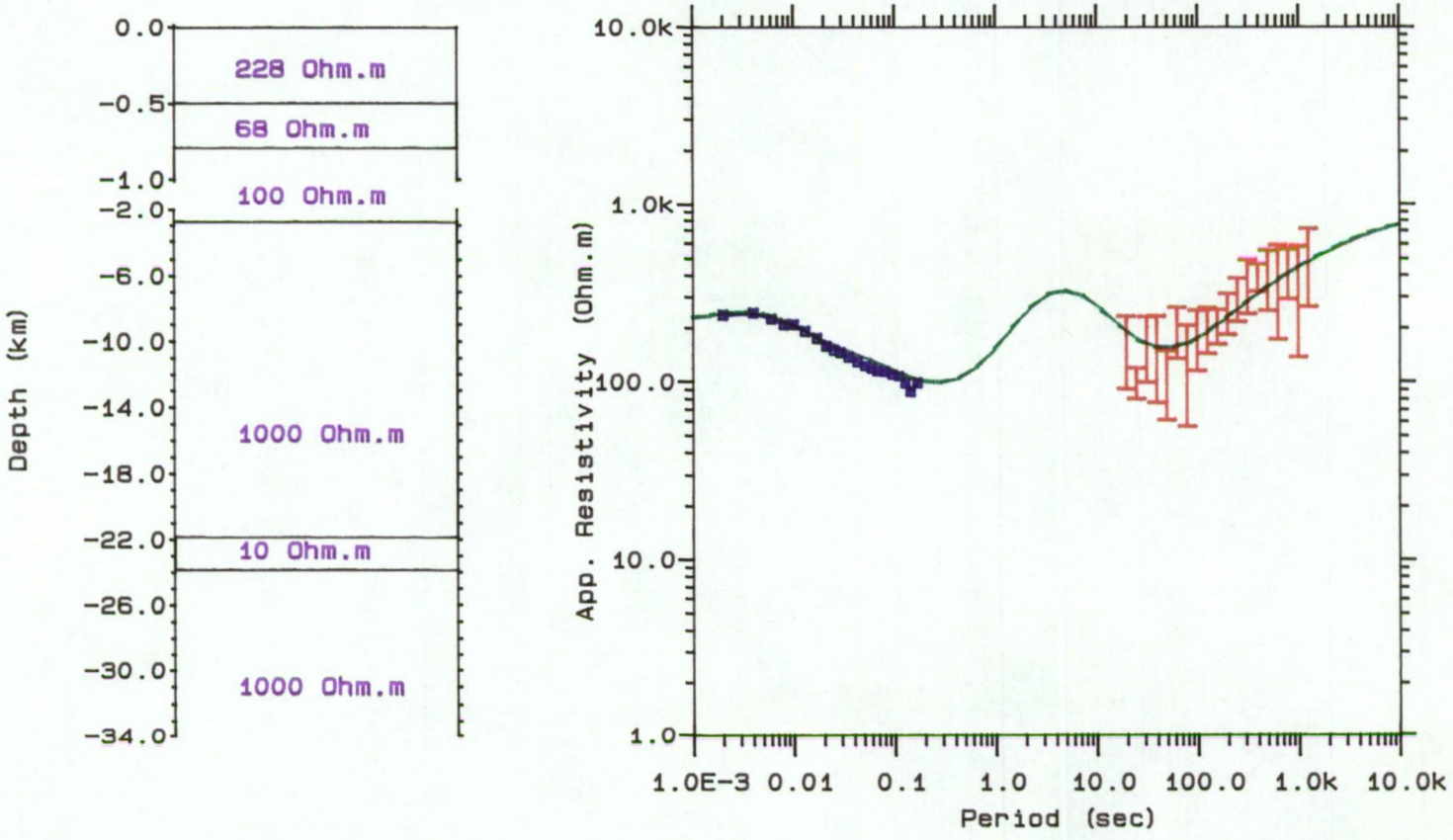

Figure BVII.2. 1D model based on MT and SIROTEM results from Grove (GRV) (red) -observed MT; (blue) -observed SIROTEM; (green) -calculated

1D MT AND SIROTEM MODEL

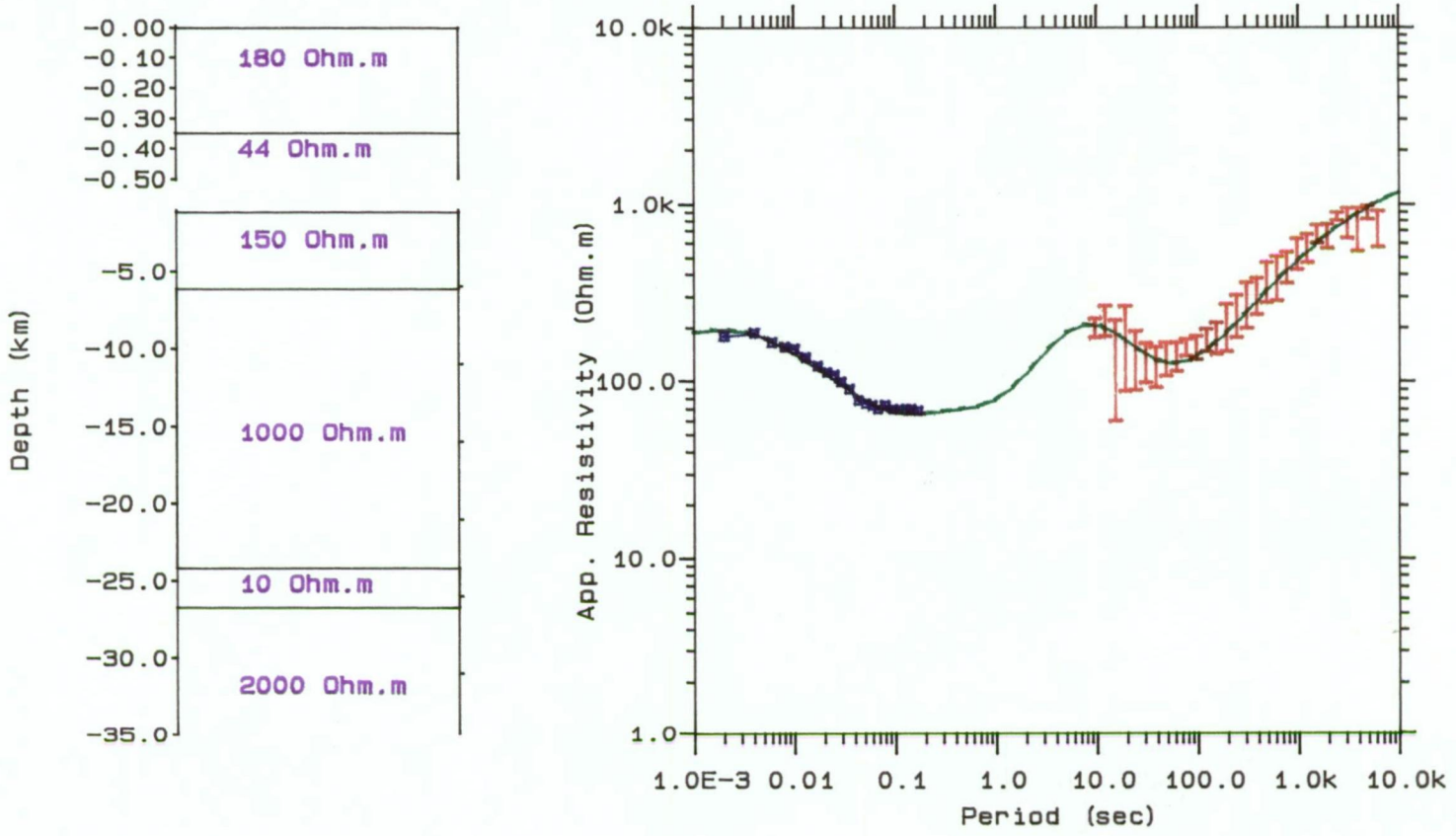

Figure **BVII.3.** 1D model based on MT and SIROTEM results from Judbury (JDB) (red) -observed MT; (blue) -observed SIROTEM; (green) -calculated

1D MT AND SIROTEM MODEL

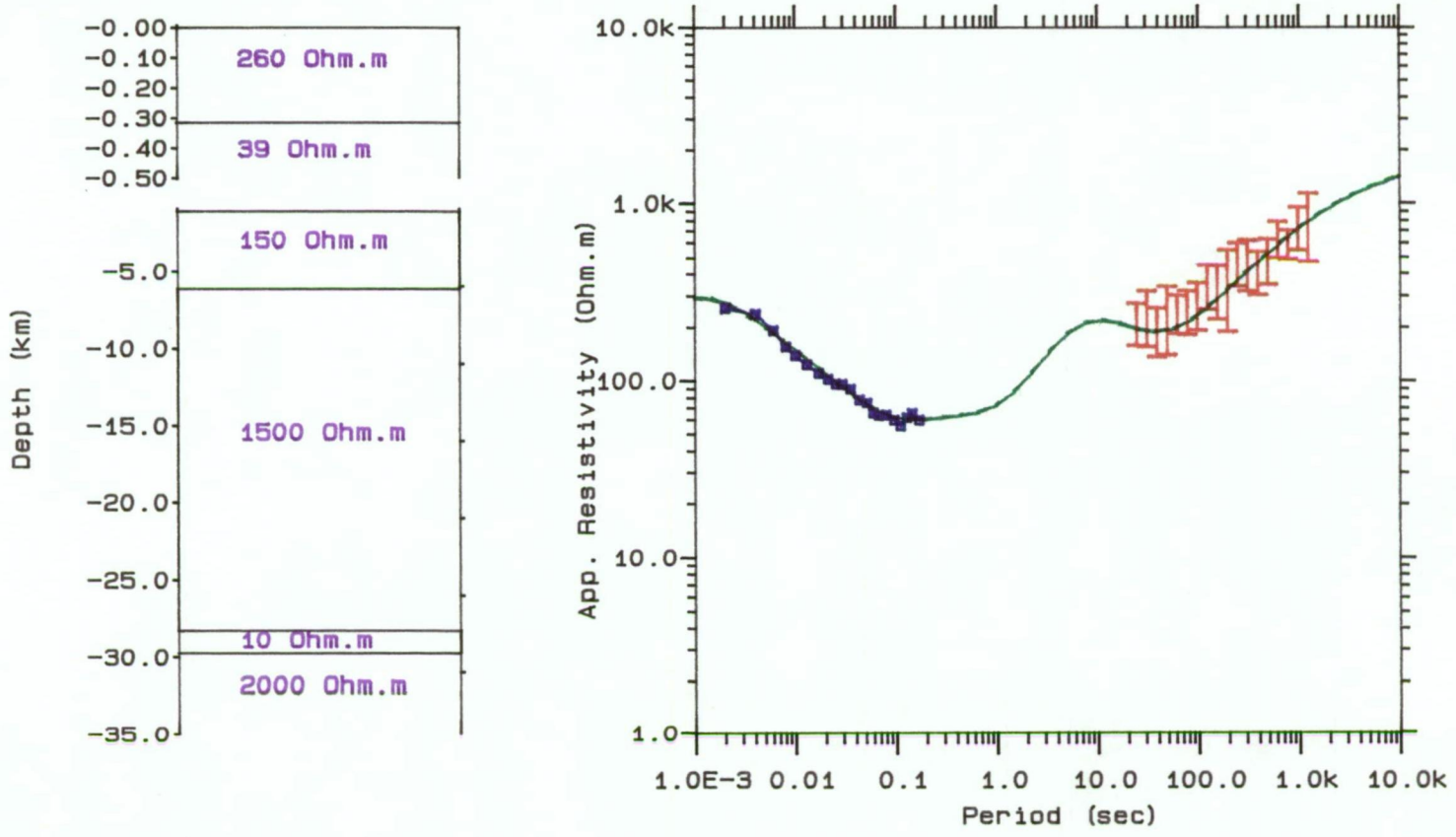

Figure BVII.4. 1D model based on MT and SIROTEM results from Lonnavale (LNV) (red) -observed MT; (blue) -observed SIROTEM; (green) -calculated

1D MT AND SIROTEM MODEL

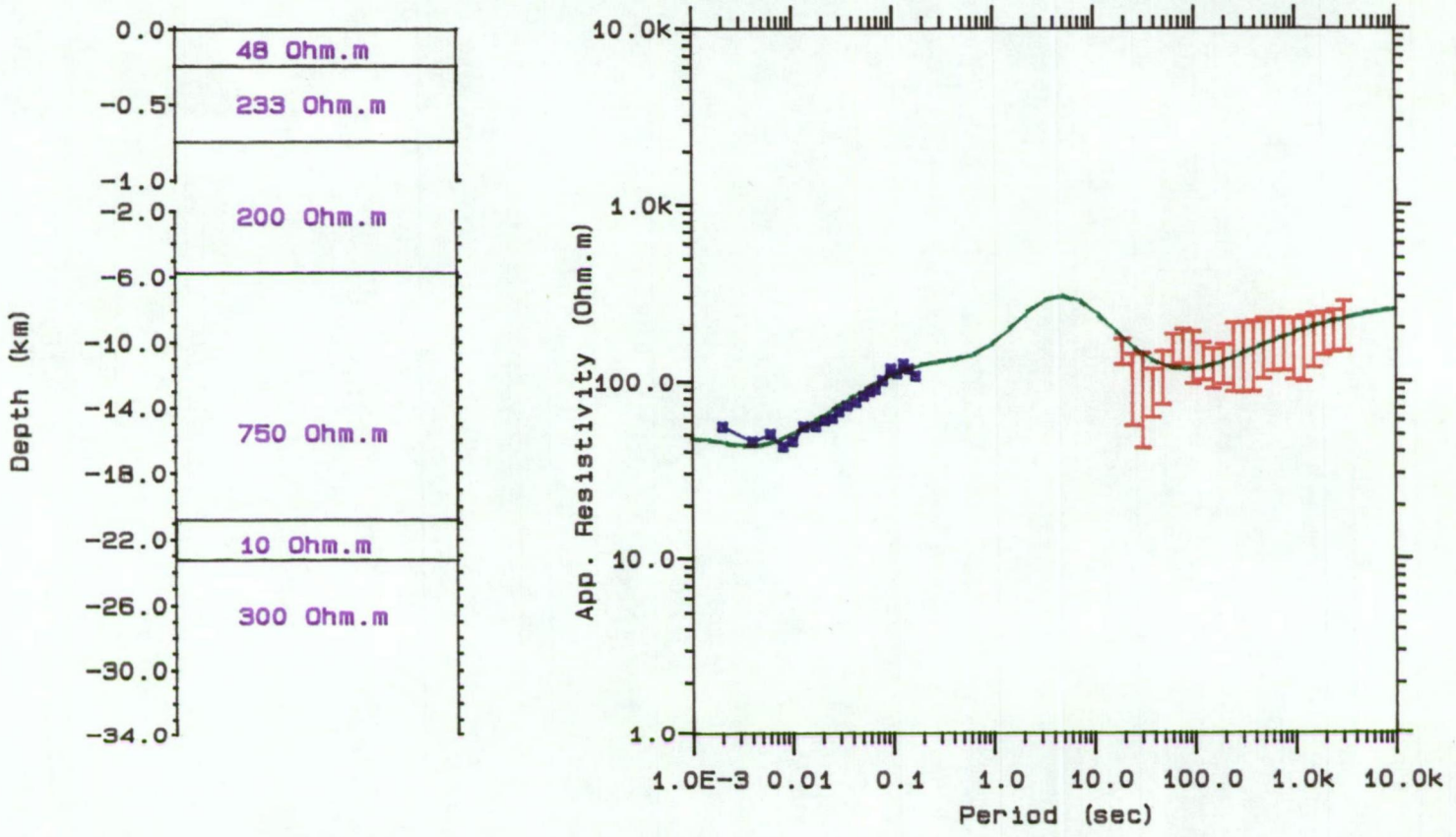

Figure BVII.5. 1D model based on MT and SIROTEM results from Woodstock (WST) (red) -observed MT; (blue) -observed SIROTEM; (green) -calculated

1D MT AND SIROTEM MODEL

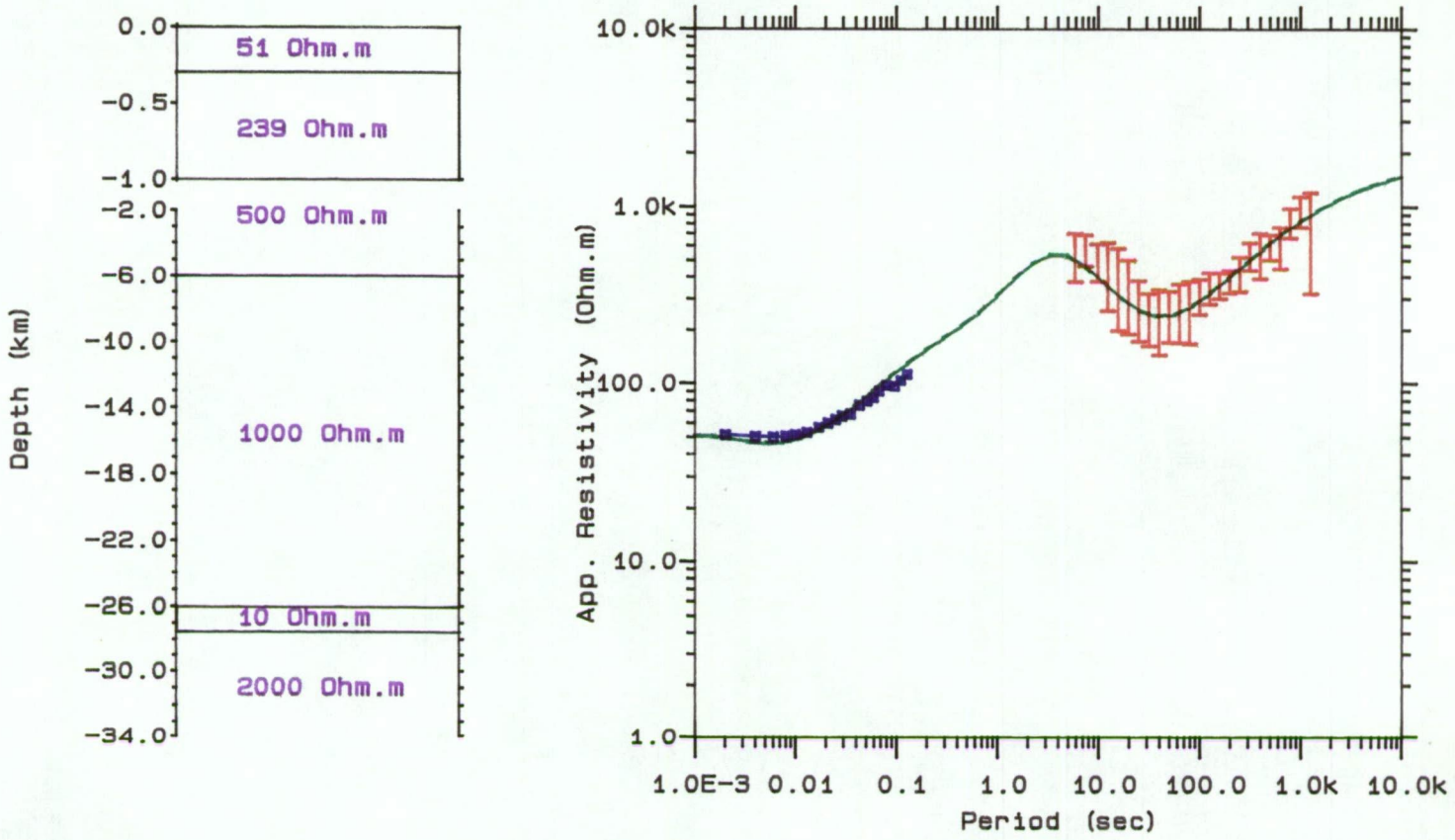

Figure BVII.6. 1D model based on MT and SIROTEM results from Franklin (FRN) (red) -observed MT; (blue) -observed SIROTEM; (green) -calculated

1D MT AND SIROTEM MODEL

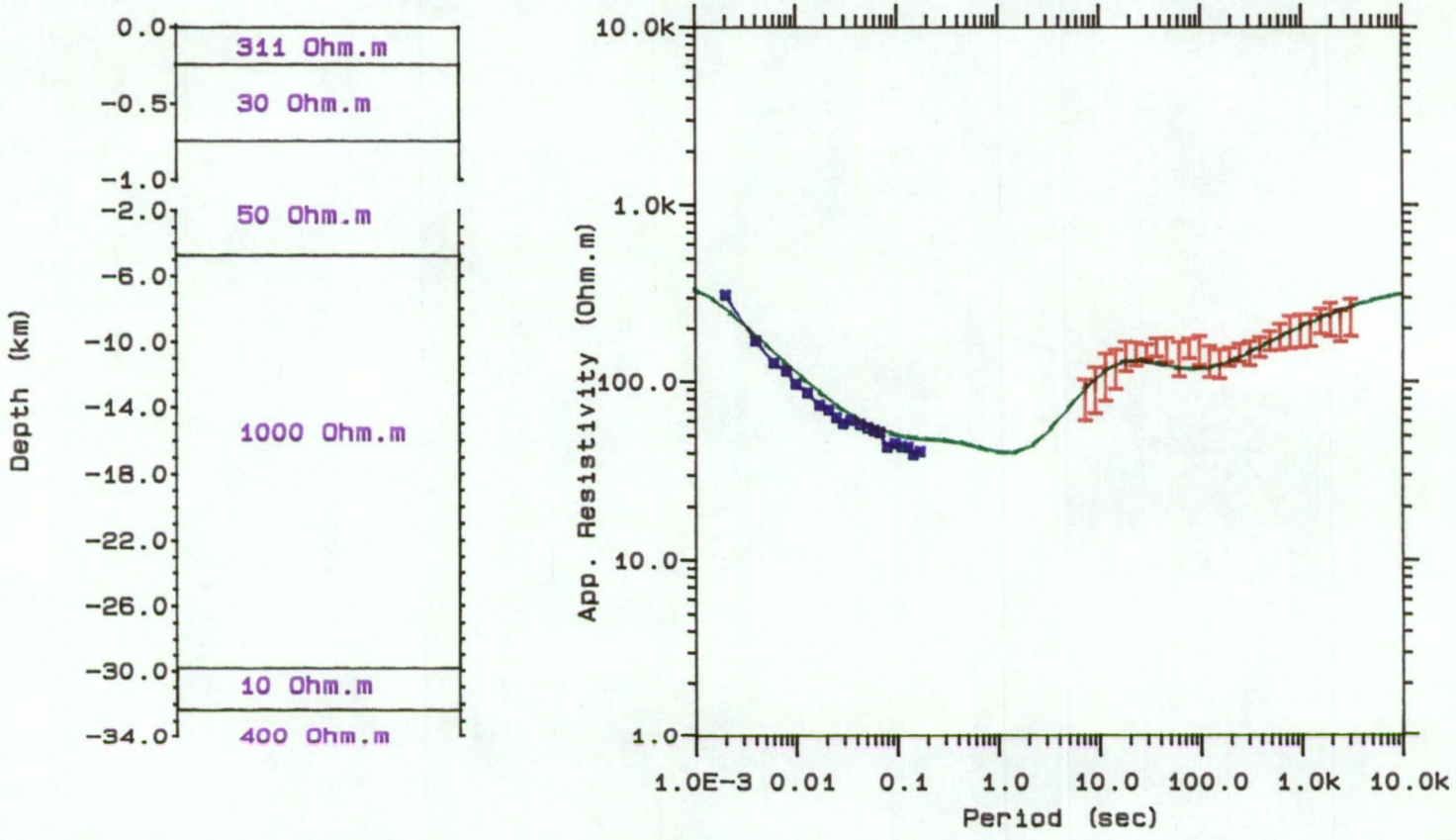

Figure BVII.7.1D model based on MT and SIROTEM results from Peppers Road (PPR) (red) -observed MT; (blue) -observed SIROTEM; (green) -calculated

1D MT AND SIROTEM MODEL

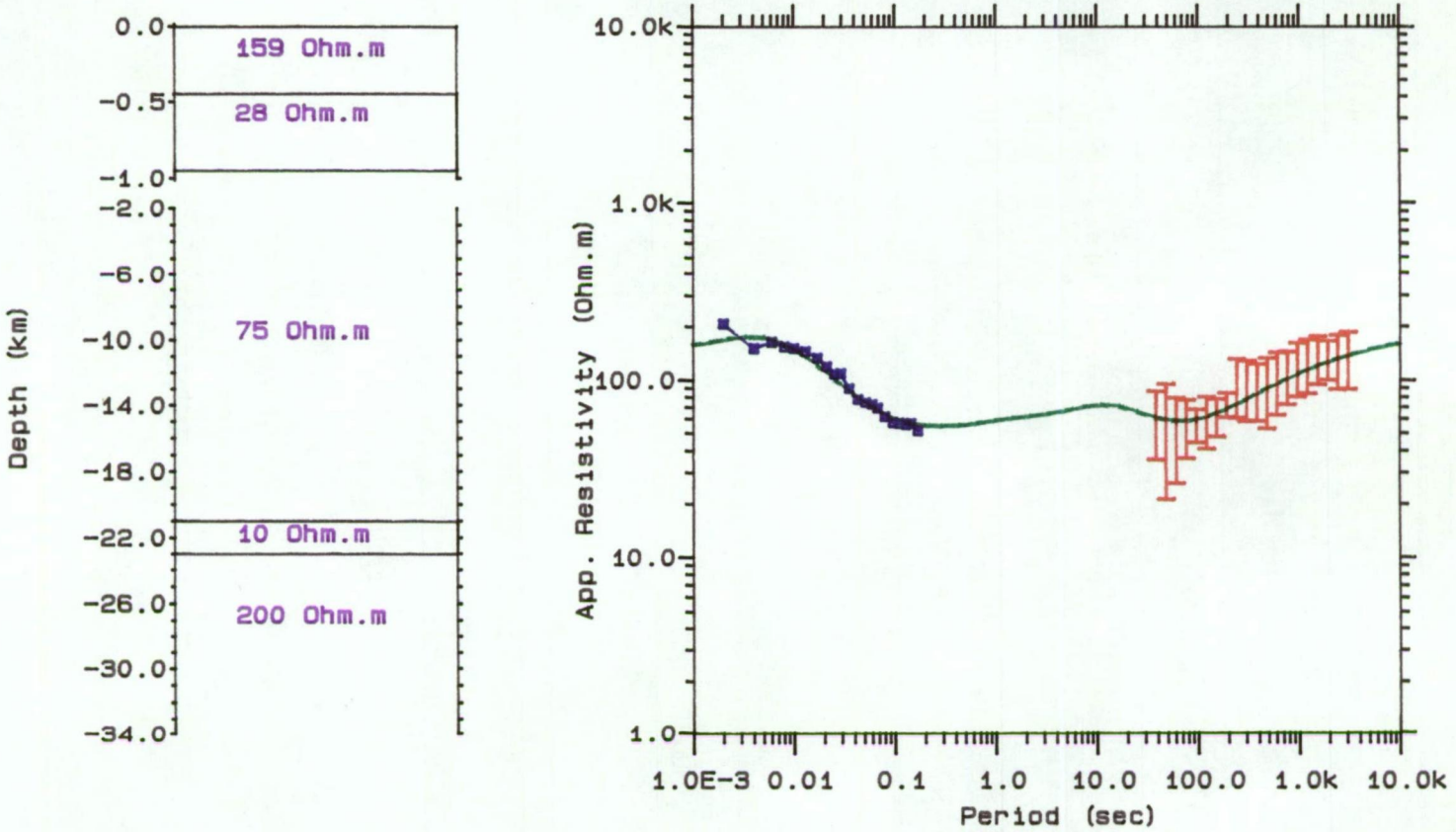

Figure BVII.8 1D model based on MT and SIROTEM results from Tahune (THN)
(red) -observed MT; (blue) -observed SIROTEM; (green) -calculated